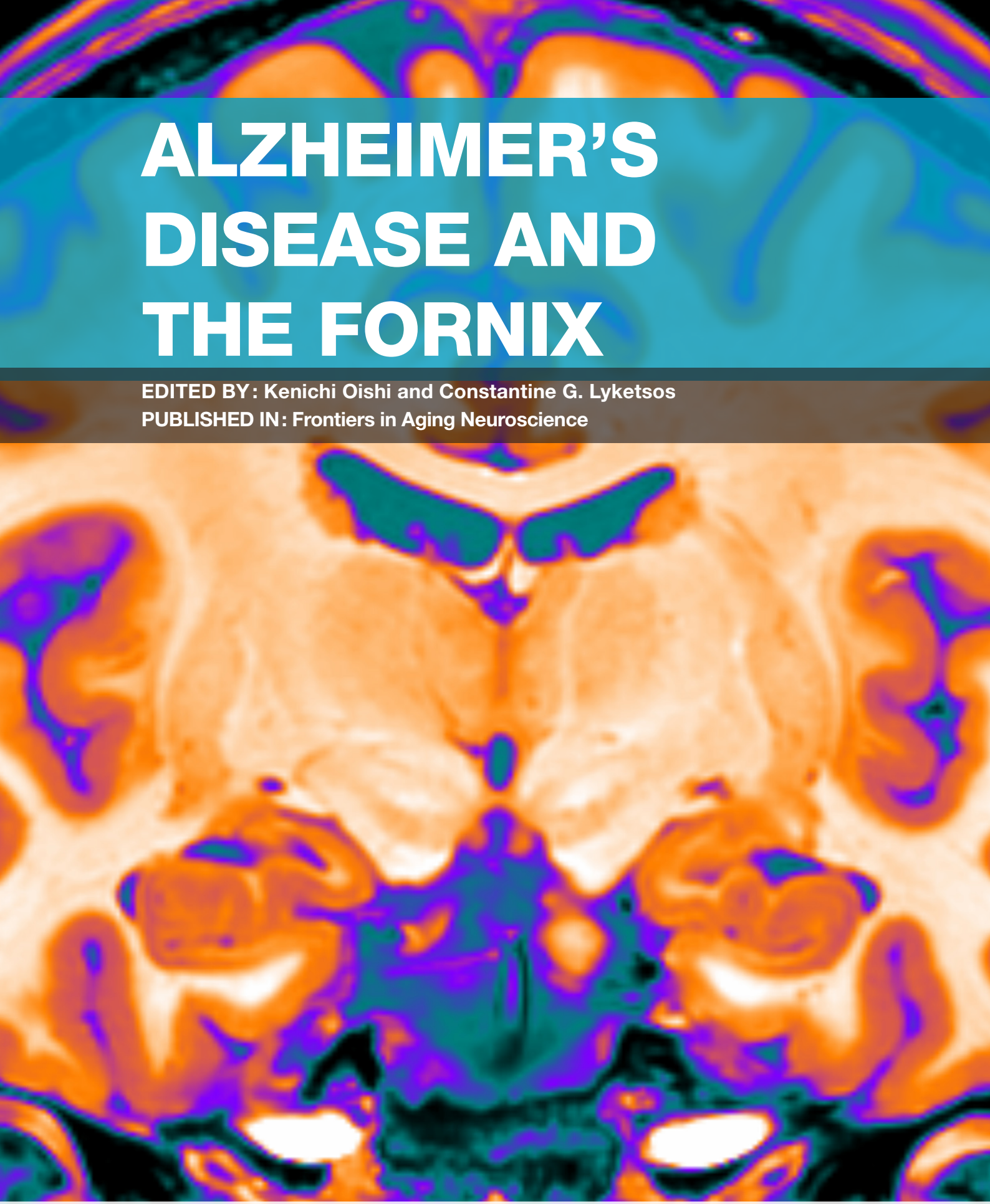

ALZHEIMER'S DISEASE AND THE FORNIX

EDITED BY: Kenichi Oishi and Constantine G. Lyketsos

PUBLISHED IN: Frontiers in Aging Neuroscience

frontiers Research Topics

ISSN 1664-8714
ISBN 978-2-88919-959-4
DOI 10.3389/978-2-88919-959-4

About Frontiers

Frontiers is more than just an open-access publisher of scholarly articles: it is a pioneering approach to the world of academia, radically improving the way scholarly research is managed. The grand vision of Frontiers is a world where all people have an equal opportunity to seek, share and generate knowledge. Frontiers provides immediate and permanent online open access to all its publications, but this alone is not enough to realize our grand goals.

Frontiers Journal Series

The Frontiers Journal Series is a multi-tier and interdisciplinary set of open-access, online journals, promising a paradigm shift from the current review, selection and dissemination processes in academic publishing. All Frontiers journals are driven by researchers for researchers; therefore, they constitute a service to the scholarly community. At the same time, the Frontiers Journal Series operates on a revolutionary invention, the tiered publishing system, initially addressing specific communities of scholars, and gradually climbing up to broader public understanding, thus serving the interests of the lay society, too.

Dedication to Quality

Each Frontiers article is a landmark of the highest quality, thanks to genuinely collaborative interactions between authors and review editors, who include some of the world's best academicians. Research must be certified by peers before entering a stream of knowledge that may eventually reach the public - and shape society; therefore, Frontiers only applies the most rigorous and unbiased reviews.
Frontiers revolutionizes research publishing by freely delivering the most outstanding research, evaluated with no bias from both the academic and social point of view.
By applying the most advanced information technologies, Frontiers is catapulting scholarly publishing into a new generation.

What are Frontiers Research Topics?

Frontiers Research Topics are very popular trademarks of the Frontiers Journals Series: they are collections of at least ten articles, all centered on a particular subject. With their unique mix of varied contributions from Original Research to Review Articles, Frontiers Research Topics unify the most influential researchers, the latest key findings and historical advances in a hot research area! Find out more on how to host your own Frontiers Research Topic or contribute to one as an author by contacting the Frontiers Editorial Office: **researchtopics@frontiersin.org**

ALZHEIMER'S DISEASE AND THE FORNIX

Topic Editors:
Kenichi Oishi, Johns Hopkins University, USA
Constantine G. Lyketsos, Johns Hopkins University, USA

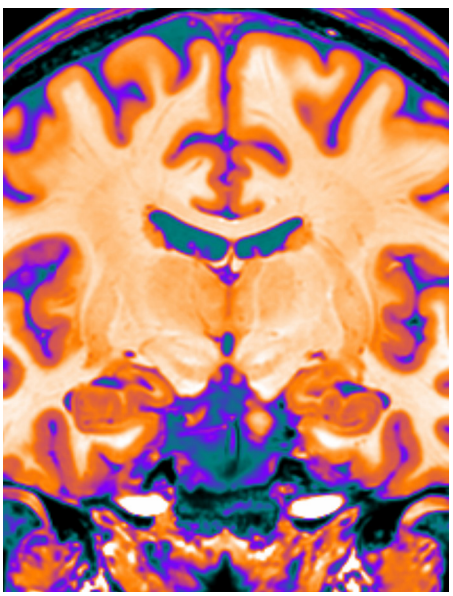

Coronal view of the human brain.
Image by Kenichi Oishi

This e-book focuses primarily on the role of the fornix as a functional, prognostic, and diagnostic marker of Alzheimer's disease (AD), and the application of such a marker in clinical practice.

Researchers have long been focused on the cortical pathology of AD, since the most important pathologic features are the senile plaques found in the cortex, and the neurofibrillary tangles and neuronal loss that start from the entorhinal cortex and the hippocampus. In addition to gray matter structures, histopathological studies indicate that the white matter is also altered in AD. The fornix is a white matter bundle that constitutes a core element of the limbic circuits, and is one of the most important anatomical structures related to memory. The fornices originate from the bilateral hippocampi, merge at the midline of the brain, again divide into the left and right side, and then into the precommissural and the postcommissural fibers, and terminate at the septal nuclei, nucleus accumbens (precommissural fornix), and hypothalamus (postcommissural fornix). These functional and anatomical features of the fornix have naturally captured researchers' attention as possible diagnostic and prognostic markers of AD. Growing evidence indicates that the alterations seen in the fornix are potentially a good marker with which to predict future conversion from mild cognitive impairment to AD, and even from a cognitively normal state to AD. The degree of alteration is correlated with the degree of memory impairment, indicating the potential for the use of the fornix as a functional marker. Moreover, there have been attempts to stimulate the fornix to recover the cognitive function lost with AD. Our goal is to provide information about the status of current research and to facilitate further scientific and clinical advancement in this topic.

Citation: Oishi, K., Lyketsos, C. G., eds. (2016). Alzheimer's Disease and the Fornix. Lausanne: Frontiers Media. doi: 10.3389/978-2-88919-959-4

Table of Contents

frontiers in Aging Neuroscience

EDITORIAL
published: 23 June 2016
doi: 10.3389/fnagi.2016.00149

Editorial: Alzheimer's Disease and the Fornix

Kenichi Oishi[1]* *and Constantine G. Lyketsos*[2]

[1] The Russell H. Morgan Department of Radiology and Radiological Sciences, Johns Hopkins University, Baltimore, MD, USA, [2] Department of Psychiatry and Behavioral Sciences, Johns Hopkins University, Baltimore, MD, USA

Keywords: Alzheimer's disease, fornix, limbic, diffusion tensor imaging, normal aging, memory, cognition, mild cognitive impairment

The Editorial on the Research Topic

Alzheimer's Disease and the Fornix

The fornix is a white matter bundle that connects the hippocampus with other limbic structures. It appears in the literature as early as 1543 in a historical publication of *De Humani Corporis Fabrica* by Andreas Vesalius (Swanson, 2014). The fornix is important for episodic memory recall (Tsivilis et al., 2008), which is impaired in Alzheimer's disease (AD). Alterations in the fornix were first observed in post-mortem AD brains (Hopper and Vogel, 1976). This volume focuses on the role of the fornix, and other limbic fibers, in the disease mechanisms of AD with some attention to how this might be applied in clinical practice.

The observation of limbic fibers *in vivo* forms a basis for understanding normal anatomy and alterations caused by various diseases. Mori and Aggarwal were able to observe the fornix, cingulum, and stria terminalis in mice and humans, using T1-weighted and diffusion tensor imaging.

In adult human brains, the limbic fibers are known to connect the structures of the default mode network (DMN), but the development of these fibers is less well understood. Yu et al. demonstrated that the developmental curve of DTI-derived measures of fornix integrity appear logarithmic, with rapid changes until 2 years of age followed by slow changes until 25 years. Development of the cingulate cingulum is disproportionally rapid during this period, but development of the hippocampal cingulum and the fornix is proportional. Notably, the functional and anatomic connectivity of the DMN is already established in the early postnatal period.

The fornix is among the white matter structures that mature early during development. Douet and Chang reviewed changes in DTI measures in the fornix during development and aging. Development of the fornix peaks in late adolescence, followed by pruning and then degeneration. Fractional anisotropy (FA) values correlate with cognitive performance in various age groups, including children, young adults, and the elderly. Correlations are seen in various brain diseases including schizophrenia, multiple sclerosis, Parkinson's, and epilepsy.

Normal aging affects the anatomy of the fornix. Kantarci proposed a hippocampus-fornix axis in which microstructural alterations in both hippocampus and fornix affect each other. In AD, it is likely that neuronal damage in hippocampus and axonal damage in fornix affect each other, but alterations in the fornix in normal aging are likely the consequence of age-related, non-specific axonal and myelin damage.

Less is known about the relationship between alterations in fornix and functional connectivity. Kehoe et al. investigated whether diffusivity in fornix is related to functional connectivity between thalamus and hippocampus. Several diffusivity measures were correlated with functional connectivity among cognitively normal elderly, but this correlation was not seen in individuals with amnestic mild cognitive impairment (MCI). This suggests that the pathological processes of amnestic MCI mitigate the structural-functional relationship that is normally seen.

Edited and reviewed by:
Rodrigo Orlando Kuljiš, University of Miami School of Medicine, USA

***Correspondence:**
Kenichi Oishi
koishi@mri.jhu.edu

Received: *01 April 2016*
Accepted: *10 June 2016*
Published: *23 June 2016*

Citation:
Oishi K and Lyketsos CG (2016) Editorial: Alzheimer's Disease and the Fornix. Front. Aging Neurosci. 8:149. doi: 10.3389/fnagi.2016.00149

Tract-based spatial statistics (TBSS) are commonly used to analyze neuroanatomical alterations related to AD. Acosta-Cabronero and Nestor reviewed AD studies that applied TBSS. In early AD, increases in the first eigenvalue were identified in fornix, parahippocampal white matter, and anterior thalamus. The authors emphasized the importance of technological factors that affect results of clinical DTI studies. These include the basis of diffusion-weighted signals and tensor calculation, the imaging parameters, the post-processing methodology, the subject cohort, multi-center study designs, and inclusion criteria. This review is quite helpful to investigators who plan to study DTI of AD or other diseases.

Nowrangi and Rosenberg summarized DTI-derived scalar measures as correlates of cognitive functions or Aβ deposition in AD, as predictors of future conversion from MCI to AD, and as potential targets for deep brain stimulation. Fletcher et al. applied these markers to a cohort of cognitively normal elderly to predict later occurrence of brain atrophy. Reduced FA was used as a marker for white matter alterations in various structures, including fornix, genu, splenium of the corpus callosum, and anterior and posterior cingulum. Volume reduction was used to evaluate neurodegeneration in the hippocampus and in the ventral and dorsal entorhinal cortices. Fornix FA was the most sensitive marker among structures investigated in predicting future brain atrophy typically seen in AD.

One direction for the future in neuroimaging studies is the application of research to the clinical arena, in which prediction is an important theme. Oishi and Lyketsos reviewed DTI analysis methods reported to detect anatomical abnormalities in the AD brain, especially fornix, and discussed the potential for the early diagnosis, prediction of cognitive worsening, and therapeutic targets.

Disease specificity is often an issue in clinical image reading. Although alterations in the fornix are often seen in AD, such alterations are also seen in other diseases, such as temporal lobe epilepsy. Alexander et al. investigated the relationship between limbic fiber integrity and cognitive function using DTI in patients with temporal lobe epilepsy. They identified a correlation between FA of the left fornix and processing speed, but not between T2 of the hippocampus and processing speed. This suggested that the relation between fornix injury and functional decline is not disease-specific, but rather, the result of injury in a neuronal network with specific neuronal functions.

In summary, the 10 articles included in this volume cover anatomy, development, aging, disease, and functional correlations or clinical significance, which are informative for readers who plan to investigate the fornix in AD or other diseases.

AUTHOR CONTRIBUTIONS

KO wrote preliminary draft and CL finalized the manuscript.

ACKNOWLEDGMENTS

This publication was made possible by grants P50AG005146 and R01AG042165 from the National Institutes of Health, and in Health Pilot Project grant from the Johns Hopkins Individualized Health Initiative. The contents of this paper are solely the responsibility of the authors and do not necessarily represent the official view of NIH or the Johns Hopkins Individualized Health Initiative. We thank Ms. Mary McAllister for her manuscript editing.

REFERENCES

Hopper, M. W., and Vogel, F. S. (1976). The limbic system in Alzheimer's disease. A neuropathologic investigation. *Am. J. Pathol.* 85, 1–20.

Swanson, L. (2014). *Neuroanatomical Terminology: A Lexicon of Classical Origins and Historical Foundations*. Oxford, UK: Oxford University Press.

Tsivilis, D., Vann, S. D., Denby, C., Roberts, N., Mayes, A. R., Montaldi, D., et al. (2008). A disproportionate role for the fornix and mammillary bodies in recall versus recognition memory. *Nat. Neurosci.* 11, 834–842. doi: 10.1038/nn.2149

Conflict of Interest Statement: The authors declare that the research was conducted in the absence of any commercial or financial relationships that could be construed as a potential conflict of interest.

frontiers in
AGING NEUROSCIENCE

REVIEW ARTICLE
published: 27 November 2014
doi: 10.3389/fnagi.2014.00321

In vivo magnetic resonance imaging of the human limbic white matter

***Susumu Mori*[1,2]* and *Manisha Aggarwal*[1]**

[1] *Russell H. Morgan Department of Radiology and Radiological Science, Johns Hopkins University School of Medicine, Baltimore, MD, USA*
[2] *F.M. Kirby Research Center for Functional Brain Imaging, Kennedy Krieger Institute, Baltimore, MD, USA*

Edited by:
P. Hemachandra Reddy, Texas Tech University, USA

Reviewed by:
Koteswara Rao Valasani, The University of Kansas, USA
Ramesh Kandimalla, Texas Tech University, USA

***Correspondence:**
Susumu Mori, Russell H. Morgan Department of Radiology and Radiological Science, Johns Hopkins University School of Medicine, 330 Traylor Building, 720 Rutland Avenue, Baltimore, MD 21205, USA
e-mail: susumu@mri.jhu.edu

The limbic system mediates memory, behavior, and emotional output in the human brain, and is implicated in the pathology of Alzheimer's disease and a wide spectrum of related neurological disorders. *In vivo* magnetic resonance imaging (MRI) of structural components comprising the limbic system and their interconnections via white matter pathways in the human brain has helped define current understanding of the limbic model based on the classical circuit proposed by Papez. MRI techniques, including diffusion MR imaging, provide a non-invasive method to characterize white matter tracts of the limbic system, and investigate pathological changes that affect these pathways in clinical settings. This review focuses on delineation of the anatomy of major limbic tracts in the human brain, namely, the cingulum, the fornix and fimbria, and the stria terminalis, based on *in vivo* MRI contrasts. The detailed morphology and intricate trajectories of these pathways that can be identified using relaxometry-based and diffusion-weighted MRI provide an important anatomical reference for evaluation of clinical disorders commonly associated with limbic pathology.

Keywords: limbic system, MRI, diffusion, human, white matter, *in vivo*

INTRODUCTION

The limbic system consists of a group of interconnected nuclei and cortical structures in the brain that mediate emotion, memory, and behavior (Patestas and Gartner, 2006). The classical circuit described by Papez includes important white matter pathways interlinking the hippocampus, mammillary bodies, anterior thalamic nuclei, cingulate gyrus (Cg), and the parahippocampal gyrus, that form a closed loop in each hemisphere (Papez, 1995). The complex connections of the limbic system are implicated in a wide array of neurological disorders including Alzheimer's disease, mild cognitive impairment, temporal lobe epilepsy, and schizophrenia, and continue to be defined using functional neuroimaging and magnetic resonance imaging (MRI) studies (Naidich et al., 1987a,b; Mark et al., 1995; Concha et al., 2010; Catani et al., 2013). This purpose of this review is to focus on the use of MRI methods for delineation of some of the major white matter tracts that are associated with the limbic system.

White matter tracts in the human brain can be broadly classified into three categories; association, projection, and commissural tracts (Nieuwenhuys et al., 2008). Association tracts establish connections across different cortical regions within the same hemisphere. Short association fibers form connections between different gyri within the same lobe, while long association fibers form intra-hemispheric connections across different lobes. Commissural tracts also establish connections between different cortical areas, but these specifically refer to inter-hemispheric connections. The projection tracts connect the cortex to other parts of the brain, such as deep nuclei, brain stem, cerebellum, and spinal cord. The tracts that interconnect the gray matter structures of the limbic system could be mainly categorized as projection or association tracts under this system of classification.

Advanced MRI techniques, particularly diffusion MRI, have afforded significant insights into the anatomy of the limbic system in the human brain, by enabling non-invasive and three-dimensional mapping of structural connectivity *in vivo*. Both gray and white matter components of the limbic system have been studied by using relaxation-based (T1- or T2-weighted) MRI in Alzheimer's disease (Smith et al., 1999; Callen et al., 2001) as well as other neurological disorders affecting the limbic system (Atlas et al., 1986; Ng et al., 1997; Kuzniecky et al., 1999; Oikawa et al., 2001; Tsivilis et al., 2008; Lövblad et al., 2014). Diffusion MRI, which is based on sensitization to the directional-dependence of NMR signal attenuation arising from restricted diffusion of water molecules in brain tissue (Moseley et al., 1990; Le Bihan, 2003), has been used to investigate the structural connectivity of white matter tracts in the limbic system (Yamada et al., 1998; Wakana et al., 2004; Concha et al., 2005; Kalus et al., 2006; Malykhin et al., 2008; Zeineh et al., 2012), as well as to examine limbic pathways under pathologic conditions (Haznedar et al., 2000; Hattingen et al., 2007; Dineen et al., 2009; Wilde et al., 2010). Diffusion MRI employs a pair of diffusion-weighting gradients in the MR pulse sequence to impart sensitization to water diffusion in the brain which is influenced by surrounding tissue microstructure. Diffusion tensor imaging (DTI) uses a Gaussian

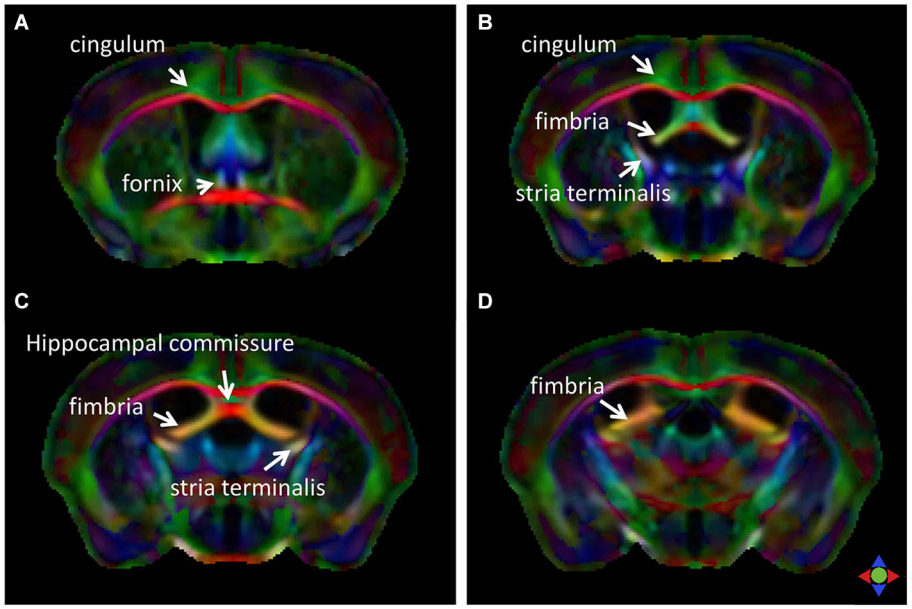

FIGURE 1 | Major limbic tracts in the mouse brain identified with diffusion tensor imaging (DTI). Direction-encoded color (DEC) maps derived from DTI in four coronal sections (**A–D**, from rostral to caudal) demonstrate the limbic tracts delineated on the basis of the primary orientation of diffusion anisotropy. Red, green, and blue in the color maps denote diffusion along the medial-lateral, anterior-posterior, and dorsal-ventral axes, respectively.

approximation of diffusion and is based on fitting the resulting signal decay to a six-element tensor model to estimate the degree and orientation of diffusion anisotropy, which can provide *in vivo* estimates and specific quantitative measures of white matter fiber structure and orientation (Basser and Jones, 2002; Tournier et al., 2011).

The limbic tracts in the human brain are relatively small in comparison to other mammalian species. For instance, major limbic tracts that can be identified with DTI in a mouse brain are demonstrated in **Figure 1**. It can be seen that these limbic tracts are large and well-defined, with the exception of the cingulum, which is relatively diffuse and characterized by an ambiguously defined boundary. As will be examined in detail in the following sections, many of these tracts are comparatively difficult to identify in the human brain. Interestingly, one exception is the cingulum, which is one of the most readily identifiable tracts in the human white matter (Burgel et al., 2006). **Figure 2** illustrates a connectivity diagram of the three major limbic tracts that are identifiable, albeit partially, in the human brain; namely, the cingulum, the stria terminalis, and the fornix. The Cg, which constitutes a part of the limbic system, receives sensory inputs from the neocortex (frontal, parietal, occipital, and temporal lobes) and projects to the hippocampal complex via the cingulum bundle. Anatomically, the cingulum forms a large outer C-shaped loop. The fornix also has a C-shaped trajectory that is nested within the cingulum, which is known to contain bidirectional connections between the septal area and the hippocampus. The stria terminalis forms the inner-most C-shaped trajectory connecting the septal area and the amygdala. The three-dimensional reconstruction of these tracts based on deterministic fiber tractography from a human DTI study is shown in

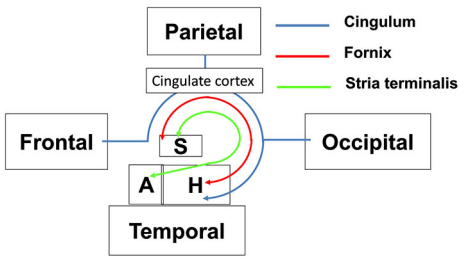

FIGURE 2 | Schematic diagram illustrating the structural connectivity in the limbic system via major limbic tracts in the human brain. Structural abbreviations are: A: amygdala, H: hippocampal formation, S: septum.

Figure 3. The cingulum can be delineated coursing along the ventral surface of the hippocampal formation, while the fornix and stria terminalis project primarily along its dorsal surface (**Figure 3**).

MR IMAGING OF LIMBIC TRACTS IN THE HUMAN BRAIN

Relaxometry-based and diffusion-weighted MR acquisitions generate complementary tissue contrasts for examination of limbic white matter anatomy, as will be shown in the following sections. T1-weighted imaging generally offers higher spatial resolution due to its relatively high signal-to-noise efficiency within clinically viable scan times. This can be specifically advantageous for visualizing the detailed morphology of the often highly convoluted limbic structures, such as the Cg and the hippocampal formation. One drawback of relaxation-based MRI is the lack of

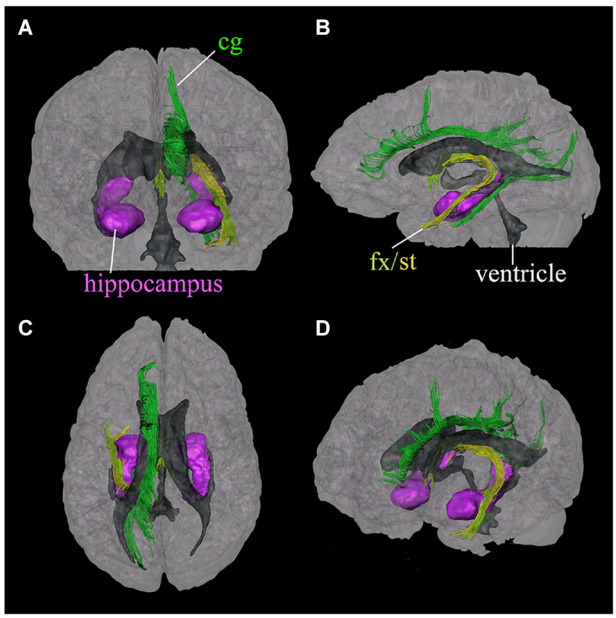

FIGURE 3 | Three-dimensional reconstruction of limbic system tracts in the human brain based on DTI. Reconstructed tracts in four different viewing angles through the brain are shown; **(A)** anterior view, **(B)** left lateral view, **(C)** superior view, and **(D)** oblique view from a right anterior angle. Reconstructed fibers are; cingulum (cg, dark green), fornix (fx, light green), and stria terminalis (st, yellow). The hippocampus and amygdala (purple) and the ventricles (gray) are shown for anatomical reference. (Reproduced with permission from Wakana et al. (2004)).

high anatomical contrast to decipher the architecture of white matter structures and tracts in the limbic system. On the other hand, DTI can provide rich tissue contrast for visualizing white matter axonal architecture, based on the orientation of structural barriers (e.g., axonal membranes and myelin sheaths) that restrict water diffusion preferentially along directions orthogonal to the long axis of the axons. DTI, however, is limited in terms of the achievable spatial resolution *in vivo*. The inherent limitation on the spatial resolution for DTI stems from its high sensitivity to physiological motion and the ensuing necessity to use single-shot rapid imaging—constraints which can be circumvented to some extent for *ex vivo* DTI studies, thereby allowing higher spatial resolution acquisitions as shown in **Figure 1**. In the following sections, the anatomy of major limbic tracts delineated with MR studies of the human brain *in vivo* will be described in detail.

CINGULUM BUNDLE

Figure 4 shows a series of coronal sections from high-resolution T1-weighted imaging and DTI of the human brain. The T1-weighted images shown are acquired on a 7T MR scanner, using a magnetization-prepared rapidly-acquired gradient echo (MPRAGE) sequence with whole brain coverage and a matrix size of 368 × 368 × 261, resulting in an isotropic spatial resolution of 0.625 mm. The DTI data are acquired at 3T using a single-shot echo planer imaging (EPI) sequence, with matrix size of 128 × 128 × 72 and isotropic spatial resolution of 1.8 mm. The *b*-value for DTI was 1000 s/mm^2, with diffusion encoding applied along 32 non-collinear gradient directions.

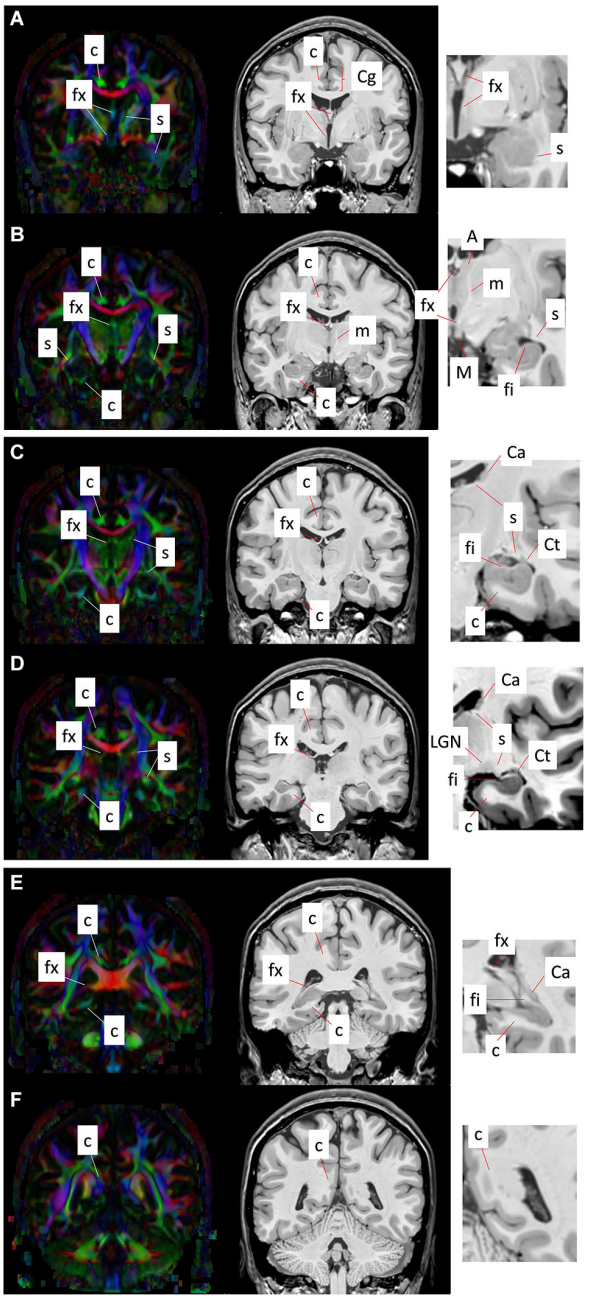

FIGURE 4 | Coronal T1-weighted images (right panel) and corresponding DEC maps derived from DTI (left panel) showing major limbic structures and tracts delineated with MRI contrasts. Images **(A–F)** show six coronal sections from the anterior to the posterior direction. Red, green, and blue in the DEC maps represent the primary orientation of diffusion along the medial-lateral, anterior-posterior, and superior-inferior axes, respectively. High-magnification views of select regions from T1-weighted contrasts are shown at the right, indicating the gray and white matter limbic structures that can be identified using MRI. Structural abbreviations are; c: cingulum, Ca: caudate, Cg: cingulate gyrus, Ct: tail of the caudate, fi: fimbria, fx: fornix, LGN: lateral geniculate nucleus, m: mammillothalamic tract, M: mammillary body, s: stria terminalis.

The cingulum constitutes a compact bundle of both long and short association fibers that connect the cingulate cortex to the parahippocampal gyrus, prefrontal cortex, and cortical association areas in the parietal and occipital lobes (Schmahmann et al., 2007; Nieuwenhuys et al., 2008; Nezamzadeh et al., 2010). Delineation of the cingulum bundle based on MR contrasts across coronal sections from anterior to posterior (**Figures 4A–F**) can be seen in **Figure 4**. The cingulum can be readily identified in the direction-encoded color (DEC) maps in **Figures 4A–D**, marked by a distinct anterior-posterior orientation (green in DEC maps) adjacent to the cortical gray matter in the Cg and the corpus callosum. It makes an almost 180° U-turn ventrally around the splenium of the corpus callosum toward the temporal lobe, and as it turns to the superior-inferior direction, its color changes to blue in DEC contrasts (**Figure 4F**). After curving around the splenium, it projects along the inferior surface of the hippocampus and becomes smaller and more diffuse towards the anterior pole of the hippocampus (**Figures 4A–D**). The projection in the temporal lobe can also be appreciated in DEC maps in **Figures 4B–D**. The location of the cingulum can be estimated from corresponding T1-weighted images in coronal views (**Figures 4A–F**), however its boundary is less obvious and cannot be clearly distinguished from neighboring white matter tracts in T1-weighted contrasts.

FORNIX

The fornix is a projection tract that constitutes the major efferent fiber pathway from the hippocampal region, connecting it with the mammillary body, and then to the anterior thalamic nuclei through the mammillothalamic tract (Nolte, 1998; Nieuwenhuys et al., 2008; Thomas et al., 2011). This part of the Papez circuit, as well as the participating gray matter structures, can be precisely reconstructed from the high-resolution T1-weighted MR images as shown in **Figure 5**. The anatomical locations of these structures can also be appreciated in the coronal sections of T1-weighted images shown in **Figures 4A–F**. Fibers in the fornix arise from the hippocampus in each hemisphere, continue into the fimbria (delineated in T1-weighted contrasts in **Figures 4C,D**) and form the crus of the ipsilateral fornix. The crura continue forward and converge under the splenium of the corpus callosum to form the body of the fornix. Fimbrial fibers that continue medially across the midline to the contralateral hemisphere form the commissural component of the fornix known as the hippocampal commissure, which projects to the contralateral hippocampus, and is relatively less distinct in MR contrasts in the human brain in contrast to its large size and prominent delineation in mouse brains (**Figure 1**). Because of the relatively small size of this fine white matter tract, DTI contrasts can reveal only parts of the fornix in the brain *in vivo* (DEC maps in **Figure 4**). Several studies have examined pathological changes in the fornix associated with Alzheimer's disease (Oishi et al., 2012; Fletcher et al., 2013, 2014) and related disorders (Ng et al., 1997; Kuzniecky et al., 1999) using MRI. While the body and crus of the fornix are more apparent in T1-weighted and DEC contrasts, the anterior portion of the fornix as it approaches the septal and hypothalamic regions becomes more diffuse and narrow. Although there are several different anatomical targets of fibers in the fornix in this region, only the projection towards the mammillary body can be clearly delineated in high-quality T1-weighted images (**Figure 4**).

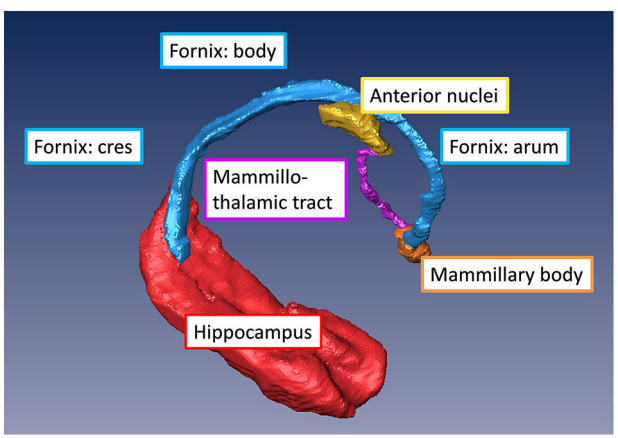

FIGURE 5 | Major gray and white matter limbic structures showing efferent connections of the hippocampal formation to the mammillary body (via the fornix) and to the anterior thalamic nuclei (via the mammillothalamic tract) reconstructed from *in vivo* T1-weighted MRI of the human brain.

STRIA TERMINALIS/FIMBRIA

The stria terminalis is a limbic pathway that constitutes the major efferent connection from the amygdala to the septal nuclei and the hypothalamus (Parent, 1996). Because of its small size, the stria terminalis is relatively difficult to recognize in both T1-weighted and DTI contrasts, but can be identified sporadically at several locations. Along the majority of its trajectory, it travels adjacent to the medial surface of the caudate nucleus, all the way to the tip of the tail of the caudate as can be clearly seen in DTI contrasts in **Figures 4C–E**. Here again, T1-weighted images provide an estimate of the location of the stria terminalis in coronal sections, but its precise boundary cannot be demarcated due to the lack of clear tissue contrast within the white matter in T1-weighted MRI. The ventral portion of the stria terminalis is relatively difficult to observe with MRI. Interestingly, as the stria terminalis travels dorsally, along the roof of the inferior horn of the lateral ventricles, there is a region where the DTI contrast intensifies with a marked increase in fractional anisotropy (**Figure 4D**). Because this region is adjacent to the lateral geniculate nucleus (LGN), it is possible that fibers in this region are mixed with adjacent fibers from the optic radiation. The fimbria travels primarily along the dorsal surface of the hippocampus, which can be clearly identified in the high-resolution T1-weighted images (**Figures 4B–D**). Although the stria terminalis and the fimbria are anatomically separated along opposite banks of the inferior horn of the ventricles, it is difficult to distinguish them in this region with DTI, owing to limited spatial resolution and resulting partial volume effects in *in vivo* diffusion-weighted images. The stria terminalis continues to travel anteriorly, finally reaching the amygdaloid complex (**Figures 4A,B**). Although small, this section of the stria

terminalis, not contaminated by adjacent fibers from the fimbria and optic radiation, can be clearly identified in high-quality DTI data (**Figures 4A,B**).

CONCLUSION AND FUTURE DIRECTIONS

In this mini review, we have described major tracts of the limbic system that can be delineated based on *in vivo* MRI of the human brain at clinical gradient strengths. The intricate three-dimensional morphologies of gray and white matter structures and interconnecting pathways of the limbic circuitry that can be resolved using non-invasive MR methods are important for clinical studies and for evaluation of various neurologic disorders that affect the limbic system. Functional and structural neuroimaging studies continue to refine existing conception of the limbic system and its disorders. Advances in both MR hardware, including higher field strengths (7T–9.4T) and high-performance gradient systems (e.g., 300 mT/m) for human scanners, as well as diffusion MR acquisition and modeling techniques, will be instrumental in pushing the envelope of the achievable resolution and the level of structural detail for *in vivo* studies of the human brain, which can potentially afford additional insights into deciphering the complex circuitry of the limbic system.

REFERENCES

Atlas, S. W., Zimmerman, R. A., Bilaniuk, L. T., Rorke, L., Hackney, D. B., Goldberg, H. I., et al. (1986). Corpus callosum and limbic system: neuroanatomic MR evaluation of developmental anomalies. *Radiology* 160, 355–362. doi: 10.1148/radiology.160.2.3726113

Basser, P. J., and Jones, D. K. (2002). Diffusion-tensor MRI: theory, experimental design and data analysis–a technical review. *NMR Biomed.* 15, 456–467. doi: 10.1002/nbm.783

Burgel, U., Amunts, K., Hoemke, L., Mohlberg, H., Gilsbach, J. M., and Zilles, K. (2006). White matter fiber tracts of the human brain: three-dimensional mapping at microscopic resolution, topography and intersubject variability. *Neuroimage* 29, 1092–1105. doi: 10.1016/j.neuroimage.2005.08.040

Callen, D. J., Black, S. E., Gao, F., Caldwell, C. B., and Szalai, J. P. (2001). Beyond the hippocampus: MRI volumetry confirms widespread limbic atrophy in AD. *Neurology* 57, 1669–1674. doi: 10.1212/wnl.57.9.1669

Catani, M., Dell'acqua, F., and Thiebaut De Schotten, M. (2013). A revised limbic system model for memory, emotion and behaviour. *Neurosci. Biobehav. Rev.* 37, 1724–1737. doi: 10.1016/j.neubiorev.2013.07.001

Concha, L., Gross, D. W., and Beaulieu, C. (2005). Diffusion tensor tractography of the limbic system. *AJNR Am. J. Neuroradiol.* 26, 2267–2274.

Concha, L., Livy, D. J., Beaulieu, C., Wheatley, B. M., and Gross, D. W. (2010). In vivo diffusion tensor imaging and histopathology of the fimbria-fornix in temporal lobe epilepsy. *J. Neurosci.* 30, 996–1002. doi: 10.1523/jneurosci.1619-09.2010

Dineen, R. A., Vilisaar, J., Hlinka, J., Bradshaw, C. M., Morgan, P. S., Constantinescu, C. S., et al. (2009). Disconnection as a mechanism for cognitive dysfunction in multiple sclerosis. *Brain* 132, 239–249. doi: 10.1093/brain/awn275

Fletcher, E., Carmichael, O., Pasternak, O., Maier-Hein, K. H., and Decarli, C. (2014). Early brain loss in circuits affected by Alzheimer's disease is predicted by fornix microstructure but may be independent of gray matter. *Front. Aging Neurosci.* 6:106. doi: 10.3389/fnagi.2014.00106

Fletcher, E., Raman, M., Huebner, P., Liu, A., Mungas, D., Carmichael, O., et al. (2013). Loss of fornix white matter volume as a predictor of cognitive impairment in cognitively normal elderly individuals. *JAMA Neurol.* 70, 1389–1395. doi: 10.1001/jamaneurol.2013.3263

Hattingen, E., Rathert, J., Raabe, A., Anjorin, A., Lanfermann, H., and Weidauer, S. (2007). Diffusion tensor tracking of fornix infarction. *J. Neurol. Neurosurg. Psychiatry* 78, 655–656. doi: 10.1136/jnnp.2006.109801

Haznedar, M. M., Buchsbaum, M. S., Wei, T. C., Hof, P. R., Cartwright, C., Bienstock, C. A., et al. (2000). Limbic circuitry in patients with autism spectrum disorders studied with positron emission tomography and magnetic resonance imaging. *Am. J. Psychiatry* 157, 1994–2001. doi: 10.1176/appi.ajp.157.12.1994

Kalus, P., Slotboom, J., Gallinat, J., Mahlberg, R., Cattapan-Ludewig, K., Wiest, R., et al. (2006). Examining the gateway to the limbic system with diffusion tensor imaging: the perforant pathway in dementia. *Neuroimage* 30, 713–720. doi: 10.1016/j.neuroimage.2005.10.035

Kuzniecky, R., Bilir, E., Gilliam, F., Faught, E., Martin, R., and Hugg, J. (1999). Quantitative MRI in temporal lobe epilepsy: evidence for fornix atrophy. *Neurology* 53, 496–501. doi: 10.1212/wnl.53.3.496

Le Bihan, D. (2003). Looking into the functional architecture of the brain with diffusion MRI. *Nat. Rev. Neurosci.* 4, 469–480. doi: 10.1038/nrn1119

Lövblad, K.-O., Schaller, K., and Isabel Vargas, M. (2014). The fornix and limbic system. *Semin. Ultrasound CT MR* 35, 459–473. doi: 10.1053/j.sult.2014.06.005

Malykhin, N., Concha, L., Seres, P., Beaulieu, C., and Coupland, N. J. (2008). Diffusion tensor imaging tractography and reliability analysis for limbic and paralimbic white matter tracts. *Psychiatry Res.* 164, 132–142. doi: 10.1016/j.pscychresns.2007.11.007

Mark, L. P., Daniels, D. L., Naidich, T. P., and Hendrix, L. E. (1995). Limbic connections. *AJNR Am. J. Neuroradiol.* 16, 1303–1306.

Moseley, M. E., Cohen, Y., Kucharczyk, J., Mintorovitch, J., Asgari, H. S., Wendland, M. F., et al. (1990). Diffusion-weighted MR imaging of anisotropic water diffusion in cat central nervous system. *Radiology* 176, 439–445. doi: 10.1148/radiology.176.2.2367658

Naidich, T. P., Daniels, D. L., Haughton, V. M., Pech, P., Williams, A., Pojunas, K., et al. (1987a). Hippocampal formation and related structures of the limbic lobe: anatomic-MR correlation. Part II. Sagittal sections. *Radiology* 162, 755–761. doi: 10.1148/radiology.162.3.3809490

Naidich, T. P., Daniels, D. L., Haughton, V. M., Williams, A., Pojunas, K., and Palacios, E. (1987b). Hippocampal formation and related structures of the limbic lobe: anatomic-MR correlation. Part I. Surface features and coronal sections. *Radiology* 162, 747–754. doi: 10.1148/radiology.162.3.3809489

Nezamzadeh, M., Wedeen, V. J., Wang, R., Zhang, Y., Zhan, W., Young, K., et al. (2010). In-vivo investigation of the human cingulum bundle using the optimization of MR diffusion spectrum imaging. *Eur. J. Radiol.* 75, e29–36. doi: 10.1016/j.ejrad.2009.06.019

Ng, S. E., Lau, T. N., Hui, F. K., Chua, G. E., Lee, W. L., Chee, M. W., et al. (1997). MRI of the fornix and mamillary body in temporal lobe epilepsy. *Neuroradiology* 39, 551–555. doi: 10.1007/s002340050465

Nieuwenhuys, R., Voogd, J., and Van Huijzen, C. (2008). *The Human Central Nervous System.* New York: Springer, Berlin.

Nolte, J. (1998). *The Human Brain: An Introduction to Its Functional Anatomy.* 4th Edn. St. Louis, MO: Mosby-Year Book.

Oikawa, H., Sasaki, M., Tamakawa, Y., and Kamei, A. (2001). The circuit of Papez in mesial temporal sclerosis: MRI. *Neuroradiology* 43, 205–210. doi: 10.1007/s002340000463

Oishi, K., Mielke, M. M., Albert, M., Lyketsos, C. G., and Mori, S. (2012). The fornix sign: a potential sign for Alzheimer's disease based on diffusion tensor imaging. *J. Neuroimaging* 22, 365–374. doi: 10.1111/j.1552-6569.2011.00633.x

Papez, J. W. (1995). A proposed mechanism of emotion. 1937. *J. Neuropsychiatry Clin. Neurosci.* 7, 103–112.

Parent, A. (1996). "The limbic system," in *Carpenter's Human Neuroanatomy.*, eds A. Parent and M. Carpenter (Philadelphia: Williams and Wilkins), 744–786.

Patestas, M. A., and Gartner, L. P. (2006). "Limbic system," in *A Textbook of Neuroanatomy.* (Oxford, England: Blackwell), 344–359.

Schmahmann, J. D., Pandya, D. N., Wang, R., Dai, G., D'arceuil, H. E., De Crespigny, A. J., et al. (2007). Association fibre pathways of the brain: parallel observations from diffusion spectrum imaging and autoradiography. *Brain* 130, 630–653. doi: 10.1093/brain/awl359

Smith, C. D., Malcein, M., Meurer, K., Schmitt, F. A., Markesbery, W. R., and Pettigrew, L. C. (1999). MRI temporal lobe volume measures and neuropsychologic function in Alzheimer's disease. *J. Neuroimaging* 9, 2–9.

Thomas, A. G., Koumellis, P., and Dineen, R. A. (2011). The fornix in health and disease: an imaging review. *Radiographics* 31, 1107–1121. doi: 10.1148/rg.314105729

Tournier, J. D., Mori, S., and Leemans, A. (2011). Diffusion tensor imaging and beyond. *Magn. Reson. Med.* 65, 1532–1556. doi: 10.1002/mrm.22924

Tsivilis, D., Vann, S. D., Denby, C., Roberts, N., Mayes, A. R., Montaldi, D., et al. (2008). A disproportionate role for the fornix and mammillary bodies in recall versus recognition memory. *Nat. Neurosci.* 11, 834–842. doi: 10.1038/nn.2149

Wakana, S., Jiang, H., Nagae-Poetscher, L. M., Van Zijl, P. C., and Mori, S. (2004). Fiber tract-based atlas of human white matter anatomy. *Radiology* 230, 77–87. doi: 10.1148/radiol.2301021640

Wilde, E. A., Ramos, M. A., Yallampalli, R., Bigler, E. D., Mccauley, S. R., Chu, Z., et al. (2010). Diffusion tensor imaging of the cingulum bundle in children after traumatic brain injury. *Dev. Neuropsychol.* 35, 333–351. doi: 10.1080/87565641003696940

Yamada, K., Shrier, D. A., Rubio, A., Yoshiura, T., Iwanaga, S., Shibata, D. K., et al. (1998). MR imaging of the mamillothalamic tract. *Radiology* 207, 593–598. doi: 10.1148/radiology.207.3.9609878

Zeineh, M. M., Holdsworth, S., Skare, S., Atlas, S. W., and Bammer, R. (2012). Ultra-high resolution diffusion tensor imaging of the microscopic pathways of the medial temporal lobe. *Neuroimage* 62, 2065–2082. doi: 10.1016/j.neuroimage.2012.05.065

Conflict of Interest Statement: The authors declare that the research was conducted in the absence of any commercial or financial relationships that could be construed as a potential conflict of interest.

Received: 08 August 2014; accepted: 04 November 2014; published online: 27 November 2014.

*Citation: Mori S and Aggarwal M (2014) In vivo magnetic resonance imaging of the human limbic white matter. Front. Aging Neurosci. **6**:321. doi: 10.3389/fnagi.2014.00321*

This article was submitted to the journal Frontiers in Aging Neuroscience.

frontiers in
AGING NEUROSCIENCE

ORIGINAL RESEARCH ARTICLE
published: 28 August 2014
doi: 10.3389/fnagi.2014.00228

Microstructure, length, and connection of limbic tracts in normal human brain development

Qiaowen Yu[1,2†], Yun Peng[3†], Virendra Mishra[2], Austin Ouyang[2], Hang Li[3], Hong Zhang[3], Min Chen[4], Shuwei Liu[1]* and Hao Huang[2,5]*

[1] *Shandong Provincial Key Laboratory of Mental Disorders, Research Center for Sectional and Imaging Anatomy, Shandong University School of Medicine, Jinan, China*
[2] *Advanced Imaging Research Center, University of Texas Southwestern Medical Center, Dallas, TX, USA*
[3] *Department of Radiology, Beijing Children's Hospital Affiliated to Capital Medical University, Beijing, China*
[4] *Department of Mathematical Sciences, University of Texas at Dallas, Richardson, TX, USA*
[5] *Department of Radiology, University of Texas Southwestern Medical Center, Dallas, TX, USA*

Edited by:
Kenichi Oishi, Johns Hopkins University, USA

Reviewed by:
Daniel Ortuño-Sahagun, Centro Universitario de Ciencias de la Salud, Mexico
Guo-Yuan Yang, Shanghai Jiao Tong University, China

****Correspondence:***
Shuwei Liu, Shandong Provincial Key Laboratory of Mental Disorders, Research Center for Sectional and Imaging Anatomy, Shandong University School of Medicine, No. 44 West Wenhua Road, Jinan, Shandong 250012, China
e-mail: liusw@sdu.edu.cn;
Hao Huang, Advanced Imaging Research Center, University of Texas Southwestern Medical Center, 5323 Harry Hines Blvd, Dallas, TX 75390-8542, USA
e-mail: hao.huang@utsouthwestern.edu

[†] Qiaowen Yu and Yun Peng have contributed equally to this work.

The cingulum and fornix play an important role in memory, attention, spatial orientation, and feeling functions. Both microstructure and length of these limbic tracts can be affected by mental disorders such as Alzheimer's disease, depression, autism, anxiety, and schizophrenia. To date, there has been little systematic characterization of their microstructure, length, and functional connectivity in normally developing brains. In this study, diffusion tensor imaging (DTI) and resting state functional MRI (rs-fMRI) data from 65 normally developing right-handed subjects from birth to young adulthood was acquired. After cingulate gyrus part of the cingulum (cgc), hippocampal part of the cingulum (cgh) and fornix (fx) were traced with DTI tractography, absolute and normalized tract lengths and DTI-derived metrics including fractional anisotropy, mean, axial, and radial diffusivity were measured for traced limbic tracts. Free water elimination (FWE) algorithm was adopted to improve accuracy of the measurements of DTI-derived metrics. The role of these limbic tracts in the functional network at birth and adulthood was explored. We found a logarithmic age-dependent trajectory for FWE-corrected DTI metric changes with fast increase of microstructural integrity from birth to 2 years old followed by a slow increase to 25 years old. Normalized tract length of cgc increases with age, while no significant relationship with age was found for normalized tract lengths of cgh and fx. Stronger microstructural integrity on the left side compared to that of the right side was found. With integrated DTI and rs-fMRI, the key connectional role of cgc and cgh in the default mode network was confirmed as early as birth. Systematic characterization of length and DTI metrics after FWE correction of limbic tracts offers insight into their morphological and microstructural developmental trajectories. These trajectories may serve as a normal reference for pediatric patients with mental disorders.

Keywords: limbic tract, development, trajectory, length, microstructure, DTI, connectivity, free water elimination

INTRODUCTION

The limbic system is a group of interconnected cortical and subcortical structures dedicated to linking visceral states and emotion to cognition and behavior (Mesulam, 2000). The limbic system plays a key role in a variety of psychiatric and neuropsychological disorders including schizophrenia (e.g., Torrey and Peterson, 1974; Reynolds, 1983; White et al., 2008; Leech and Sharp, 2014), major depressive disorder (e.g., Monkul et al., 2007; DeRubeis et al., 2008; Duman and Voleti, 2012), autism (e.g., Amaral et al., 2008), Alzheimer's disease (e.g., Braak and Braak, 1991), and obsessive-compulsive disorder (e.g., Fitzgerald et al., 2005; Abramowitz et al., 2009). As major white matter tracts underlying connectivity of the limbic system, cingulum bundle (including cingulum cingulate gyrus part or cgc and cingulum hippocampal part or cgh) and fornix (fx) could be affected in the pathological state. Moreover, structural changes of the limbic tracts could serve as an important biomarker for early detection of these disorders as previous studies suggest that disruption of limbic tracts precedes the clinical symptoms. For example, disruption of cgc was found in healthy subjects with high risk of major depressive disorder (e.g., Huang et al., 2011). Microstructural changes of fx, a major fiber bundle connecting to hippocampus, was found in subjects of mild cognitive impairment (MCI), a disorder that has been associated with risk for dementia (e.g., Oishi et al., 2011, 2012; Huang et al., 2012). Besides their important role in aging-related diseases such as dementia, disruption of limbic tracts was also found to be associated with psychiatric disorders of developing brain, such as schizophrenia (e.g., White et al., 2007) and autism (e.g., Weinstein et al., 2011). Quantitative characterization of these limbic tracts systematically during development thus offers a normal reference for mental disorders. Furthermore, understanding maturation of the limbic tracts may also provide insights on vulnerability of these

tracts in dementia of aging brains. Although the uncinate fasciculus and anterior thalamic projections could also be considered as part of the limbic system white matter tracts (e.g., Catani et al., 2013), cgc/cgh and fx were focused in this study.

In the developing human brain, water molecules tend to diffuse more freely along the limbic tract, instead of perpendicular to it. This diffusion property can be measured non-invasively with diffusion MRI, a modality of MRI. Diffusion tensor imaging (DTI) (Basser et al., 1994) characterizes water diffusion properties with a tensor model. DTI-derived metrics are highly sensitive to white matter microstructural changes. Fractional anisotropy (FA) (Pierpaoli and Basser, 1996; Beaulieu, 2002), derived from DTI and quantifying the shape of diffusion tensor, has been widely used to characterize microstructural integrity. Radial diffusivity (RD) and axial diffusivity (AD), also derived from diffusion tensor, convey unique information related to myelination and axonal integrity, respectively (Song et al., 2002). Mean diffusivity (MD) is the linear combination of AD and RD. Limbic tracts can be non-invasively traced with tractography based on diffusion MRI (e.g., Conturo et al., 1999; Jones et al., 1999a; Mori et al., 1999; Basser et al., 2000; Catani et al., 2002).

With traced limbic tracts as binary masks for DTI-derived metric maps, the microstructural properties of the limbic tracts can be quantified. Characterization of structural development of limbic tracts has been included in recent studies on white matter development (e.g., Hermoye et al., 2006; Lebel and Beaulieu, 2011). With different developmental period focused in these studies, different curves for trajectories of limbic tract microstructural changes were reported. Thus, far systematic microstructural measurements of limbic tracts with age coverage from birth to 25 years old has not been found in the literature. Moreover, corrections of bias of DTI metric measurements caused by partial volume effects (PVE) have not been reported either. As limbic tracts are relatively thin bundles compared to other major tracts such as corpus callosum and pathways of cgh and fx are close to the ventricle, contamination of cerebrospinal fluid (CSF) on DTI metric measurements could be severe. Such contamination may not be consistent during development as more water content was found in the younger brains such as neonate brain (e.g., Neil et al., 1998; Mukherjee et al., 2001, 2008). Corrections need to be made for a more accurate estimate of developmental trajectories of limbic tract DTI metrics. To the best of our knowledge, morphology of limbic tracts has not been quantitatively characterized. As coherent fiber bundles, it is possible to measure geodesic lengths of limbic tracts based on tractography results.

The limbic tracts are also involved in functional connectivity. It has been reported that cgc and cgh play a vital role in adult brain default mode network (DMN) (van den Heuvel et al., 2008, 2009; Greicius et al., 2009; Uddin et al., 2009). Specifically, cgc connects medial prefrontal cortex (MPFC) and posterior cingulate cortex (PCC) and cgh connects PCC and medial temporal lobes (MTL). Functional connectivity in DMN is related to episodic memory, theory of mind, and the ability to "mentalize" (Fair et al., 2008). Appearance of functional connectivity in DMN has been reported as early in development as the neonate stage (Doria et al., 2010). But weak relationship between functional and structural connectivity within the DMN exists during childhood (Supekar et al., 2010). To understand the relationship between structure and function, it is important to confirm involvement of limbic tracts in connecting functional regions in the DMN as early as birth.

In this study, DTI from 65 normally developing right-handed subjects at cross-sectional ages from birth to young adulthood and resting state functional MRI (rs-fMRI) from 15 of the subjects were acquired. After cgc, cgh, and fx were traced with DTI tractography, absolute and normalized tract lengths and DTI-derived metrics including FA, MD, AD, and RD were measured for traced limbic tracts. Free water elimination (FWE) algorithm (Pasternak et al., 2009) was adopted to enhance accuracy of the measurements of DTI-derived metrics. The role of these limbic tracts in the functional network at birth and adulthood was explored. Systematic characterization of tract geodesic length and DTI metrics after FWE correction of limbic tracts offers insight into their morphological and microstructural developmental trajectories. These trajectories may serve as a normal reference for pediatric patients with mental disorders.

MATERIALS AND METHODS

HUMAN SUBJECTS

Sixty-five healthy human subjects (41 M/24 F) with age range from 0 month (birth) to 25 years participated in this study. The age range covered the important developmental periods of early childhood, childhood, adolescence, and young adulthood. **Figure 1** shows a histogram of the age and gender distribution of all subjects. Included neonates were part of the cohort for studying normal perinatal and prenatal brain development and were selected after rigorous screening procedures (Huang et al., 2014). Neonates were well fed before scanning. All included children, adolescents and young adults were healthy subjects free of current and past neurological or psychiatric disorders. Right-handed were reported for all children who showed clear handedness. For young children, besides earplugs and earphones, extra foam padding was applied to reduce the sound of the scanner while they were asleep. Due to difficulty of acquiring MRI from human subjects with such a comprehensive developmental period from 0 month to

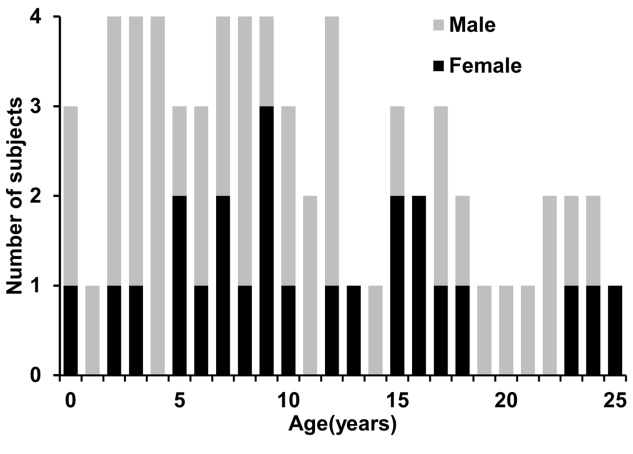

FIGURE 1 | Age and gender distribution of the 65 normal developing human subjects.

25 years in one site, the presented data were acquired from the same type of MR scanner with common MRI protocol in two sites, Children's Medical Center at Dallas and Children's Hospital in Beijing. All subjects gave informed written consent approved by the Institutional Review Board of those two institutions.

DATA ACQUISITION OF DTI AND fMRI

MRI of 3 neonates (2 M/1 F) at 40 weeks of gestation and 10 adolescents (12–17 years old; 4 M/6 F) was acquired from Children's Medical Center at Dallas. MRI of all other subjects was acquired from Children's Hospital in Beijing. A Philips 3 T Achieva MR scanner at both sites was used. A single-shot echo planar imaging (EPI) with SENSE (SENSitivity Encoding, reduction factor = 2.5) parallel imaging scheme was adopted for DTI acquisition. Eight-channel SENSE head coil and consoles installed with R2.6.3 software were used for both sites. The DTI imaging parameters were: TR (repetition time) = 6850 ms, TE (echo time) = 78 ms, in-plane field of view = 168 mm × 168 mm for neonates and 224 mm × 224 mm for all others, in-plane imaging resolution = 1.5 mm × 1.5 mm for neonates and 2 mm × 2 mm for all others, slice thickness = 1.5 mm for neonate to 2 mm for all others, slice number = 60–65 depending on the height of the subject brains, 30 independent diffusion-weighted directions (Jones et al., 1999b) uniformly distributed in space, *b*-value = 1000 s/mm^2, and repetition = 2. The axial image dimension was 256 × 256 after reconstruction. The total acquisition time of DTI was 11 min. With 30 diffusion weighted image (DWI) volumes and 2 repetitions, we accepted only those scanned datasets with less than 5 DWI volumes affected by motion more commonly seen in scan of neonates and young children. The affected volumes were replaced by the good volumes of another DTI repetition during postprocessing. rs-fMRI was also acquired from 15 out of 65 subjects, including 3 neonates and 3 young adults. A T2* weighted gradient echo EPI sequence was used. A total of 210 T2* weighted whole brain volumes were acquired with the following parameters: TR = 1500 ms for neonates and 2000 ms for young adults, TE = 27 ms for neonates and 30 ms for young adults, flip angle = 80°, in-plane imaging resolution = 2.4 mm × 2.4 mm for neonates and 3.4 mm × 3.4 mm for young adults, and slice thickness = 3mm with no gap for neonates and 4 mm with no gap for young adults; slice number = 30 for neonates and 37 for young adults. Scan time of rs-fMRI was 5–6 min. Rs-fMRI and DTI images were acquired in the same session.

TENSOR FITTING AND DTI-BASED TRACTOGRAPHY

Diffusion weighted images for each subject were corrected for motion and eddy current by registering all DWIs to the b0 image using a 12-parameter (affine) linear registration with automated image registration (AIR) algorithm (Woods et al., 1998). After the registration, six independent elements of the 3 × 3 diffusion tensor (Basser et al., 1994) were determined by multivariate least-square fitting of DWIs. The tensor was diagonalized to obtain three eigenvalues (λ_{1-3}) and eigenvectors (v_{1-3}). FA, MD, AD, and RD, derived from DTI and used to quantify white matter microstructure, were obtained for all the subjects using the equations of eigenvalues described in details previously (e.g., Mishra et al., 2013).

Fiber assignment of continuous tractography (FACT) (Mori et al., 1999) was used to trace limbic tracts for all subjects. The limbic tracts include cgc, cgh, and fx. FA threshold of 0.2 and a principal eigenvector turning angle threshold of 50 were used for FACT tractography. cgc and cgh were traced following the fiber tracking protocol (Wakana et al., 2007) with a multiple-ROI approach (Huang et al., 2004). The ROI placement protocol for tracing fx was as follows. The first ROI was drawn to include main body of fx identifiable on an axial slice of DTI color-encoded map. The second ROI was placed on the coronal slice where hippocampus was identifiable using "AND" operation. All other fibers were removed carefully to retain only the fx. The above-mentioned tensor fitting and fiber tracking was conducted by using DTIStudio (Jiang et al., 2006).

MEASUREMENTS OF LENGTHS AND DTI METRICS OF LIMBIC TRACTS

After tractography of cgc, cgh, and fx, the lengths and DTI metrics of each tract were measured for all subjects and plotted against age. These limbic tracts were visualized in 3D with Amira software (FEI, Berlington, MA, USA).

Measurement of tract length

The absolute and normalized limbic tract length were measured based on the tractography results. Specifically, geodesic length of each fiber in cgc, cgh, and fx was measured. A histogram was established for each limbic tract to show the distribution of fiber length. Note that a tract contains fibers with different lengths. In order to reduce the bias caused by a large number of short fibers, we defined the tract length by averaging 10% longest fibers of each tract. As shorter fibers could only cover part of the tract, reconstruction of the top 10% longest fibers showed that morphology of these fibers was in good agreement with that of the entire tract of all fibers. Tract length was further normalized by the size of the brain represented by the length between most anterior to most posterior edge to quantify relative tract length change during development.

Measurements of uncorrected and corrected DTI-based metrics

The binary masks of the individually traced limbic system tracts were used to compute the tract-level FA, MD, AD, and RD without correction of PVE of free water, defined as uncorrected DTI metrics. Young brains contain a large amount of free water. The uncorrected DTI metrics reflect the weighted average of all compartments including free water. In order to minimize the influence of CSF, FWE (Pasternak et al., 2009) was applied to correct the DTI metrics of cgc, cgh, and fx by using the following model: $S = S_0\left(f_{\text{iso}}e^{-bD_{\text{iso}}} + (1-f_{\text{iso}})e^{-b\bar{D}}\right)$, where S is the measured signal in the voxel, f_{iso} is the volume fraction of the isotropic compartment, b is the applied b-value, S_0 is the signal with no diffusion weighting, D_{iso} is the diffusion coefficient of the isotropic compartment, and $\bar{\bar{D}}$ is the corrected tensor representing the fiber bundle in the voxel. This is a two-compartment model with one compartment representing the fiber bundle and the other compartment representing the isotropic free water compartment in the voxel. We estimated the six elements of $\bar{\bar{D}}$ and f_{iso} by solving the non-linear equation in the model. The initial values of $\bar{\bar{D}}$ for iteration are those from single tensor model without isotropic

component. The diffusivity of the isotropic compartment D_{iso} was 3×10^{-3} mm^2/s (Pasternak et al., 2009). Note that with measurements from 30 diffusion gradients, an over-determined system was used to fit the six independent elements of tensor $\bar{\bar{D}}$ and f_{iso}.

Rs-fMRI DATA PROCESSING

The DMNs of three neonates and three young adults were identified with independent component analysis (ICA) of the rs-fMRI data. ICA was conducted with MELODIC tool (Multivariate Exploratory Linear Decomposition into Independent Components, a part of FSL)[1]. Pre-processing procedures included removing the first 10 volumes for stabilization of the magnetic field, motion correction, spatial smoothing with a Gaussian kernel of FWHM 5 mm, intensity normalization, and high-pass temporal filtering. Volumes with translational movement greater than 5 mm were removed from the dataset. The DMN cluster components in the fMRI space were transformed into the DTI space by registering the resampled fMRI image to b0 image in the DTI space using SPM8 (Statistical Parametric Mapping 8)[2]. Amira software (FEI, Berlington, MA) was used for reconstructing the DMN clusters and limbic tracts connecting them.

CURVE FITTING AND STATISTICAL ANALYSIS

The following equation was used for fitting a model between measurement y (including uncorrected/corrected DTI metrics and absolute/normalized tract length) and age t, $y = f(t) + c \cdot \text{sex} + \varepsilon$, where $f(t)$ was linear, logarithmic, or polynomial function of t and ε was an error term. F-test was used to find the best fitting curve. We first tested if the measurement y was age dependent, if so, we further tested which of the following curves, linear, logarithmic, or polynomial curves, fitted the data best.

With age and gender as covariates, generalized linear model (GLM) was used to test (1) if FWE correction significantly changed DTI metric measurements and (2) if lateralization (i.e., measurement in left or right hemisphere) was a significant factor for all measurements. The null hypothesis for FWE correction is that there is no difference of DTI metric measurement before and after the correction. The null hypothesis for lateralization is that there is no difference of length or DTI metric measurement of corresponding limbic tracts in the left and right hemisphere. The Bonferroni correction was used to control the spurious positives when rejecting the null hypotheses.

RESULTS

3D RECONSTRUCTED LIMBIC TRACTS AT DIFFERENT DEVELOPMENTAL STAGES

As shown in **Figure 2**, overall consistent 3D reconstructed limbic tracts, cgc, cgh, and fx, can be observed at five time points throughout the developmental period from 0 month to 25 years. cgc appears to be more extended to prefrontal regions and has more branches during development, while morphology of cgh and fx remains relatively stable.

DEVELOPMENT OF MICROSTRUCTURES OF LIMBIC TRACTS

The plots of uncorrected and corrected DTI metrics, namely, FA, MD, AD, and RD, of all limbic tracts at different ages are shown in **Figures 3–6**, respectively. As shown in **Tables 1–4**, significant age dependence was found in almost all DTI metrics of all limbic tracts, except measurements of MD, AD, and RD of fx. Among logarithmic, linear, and polynomial fitting between uncorrected/corrected DTI metrics and age, logarithmic model fits best to most of DTI

[1]www.fmrib.ox.ac.uk/fsl/melodic2/index.html
[2]http://www.fil.ion.ucl.ac.uk/spm/

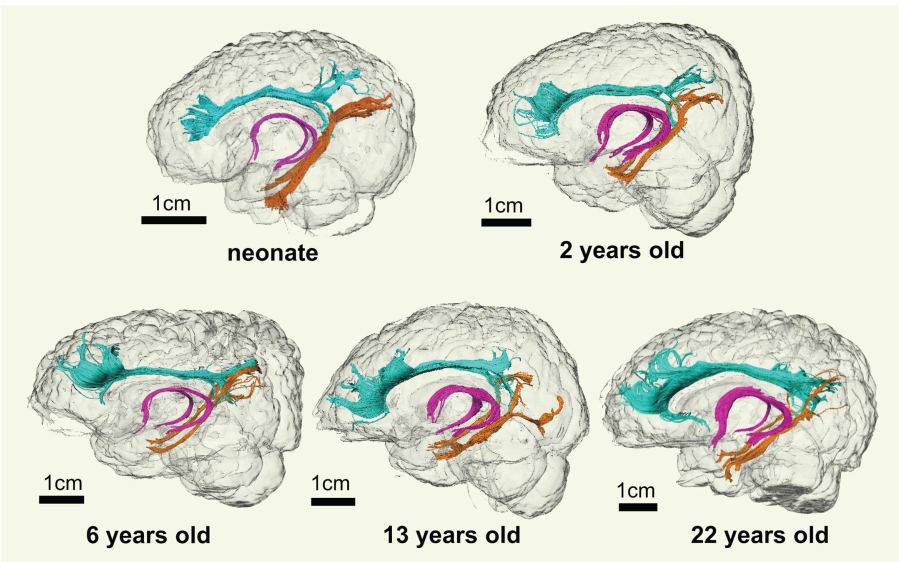

FIGURE 2 | 3D visualization of the traced limbic tracts of representative subjects at following developing stages, at birth (0 month), early childhood (2 years old), childhood (6 years old), adolescence (13 years old), and young adulthood (22 years old). Cingulate gyrus part of cingulum (cgc), cingulum hippocampal part (cgh), and fornix (fx) were painted with cyan, orange, and pink color, respectively.

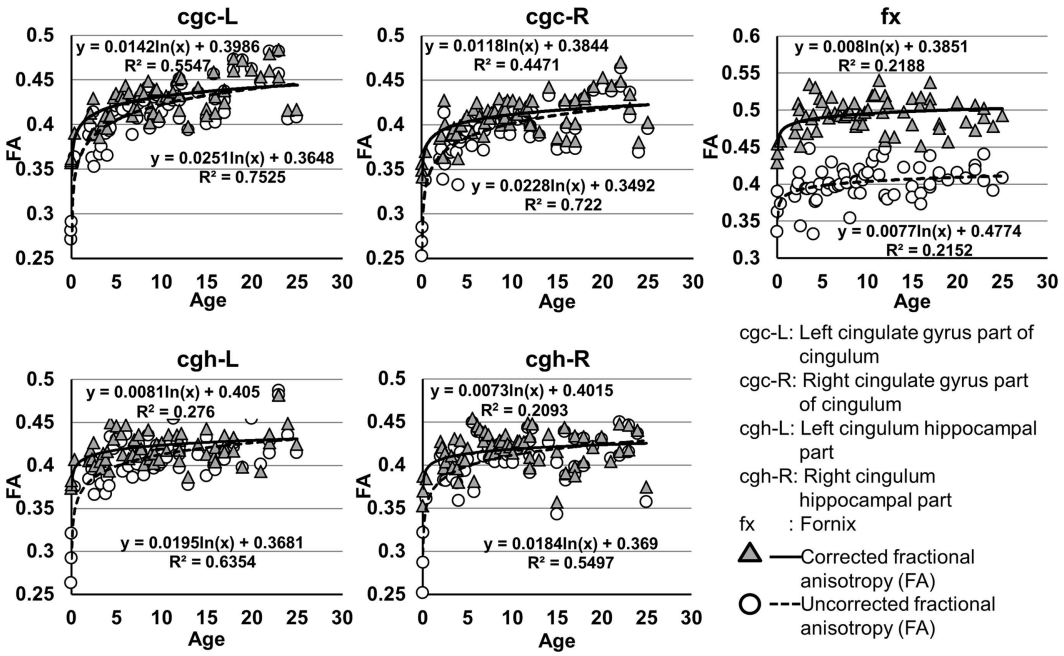

FIGURE 3 | Age-dependent changes of uncorrected and corrected fractional anisotropy (FA) measurements of limbic tracts. R^2 and fitting equations are listed in each panel.

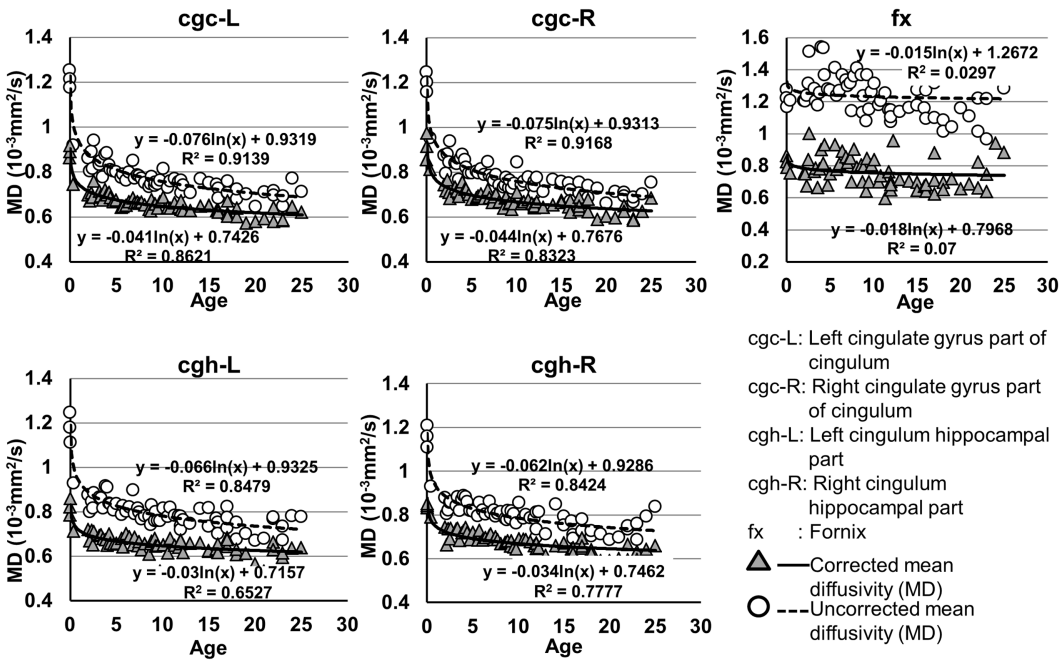

FIGURE 4 | Age-dependent changes of uncorrected and corrected mean diffusivity (MD) measurements of limbic tracts. R^2 and fitting equations are listed in each panel.

metric measurements of the limbic tract, also shown in **Tables 1**–**4**. For rest of the fittings, there is no statistical difference between linear and logarithmic fitting. No significant difference between linear and logarithmic fitting is especially apparent for corrected FA measurements of all limbic tracts (**Table 1**). Lowest R^2 was obtained with the polynomial fitting.

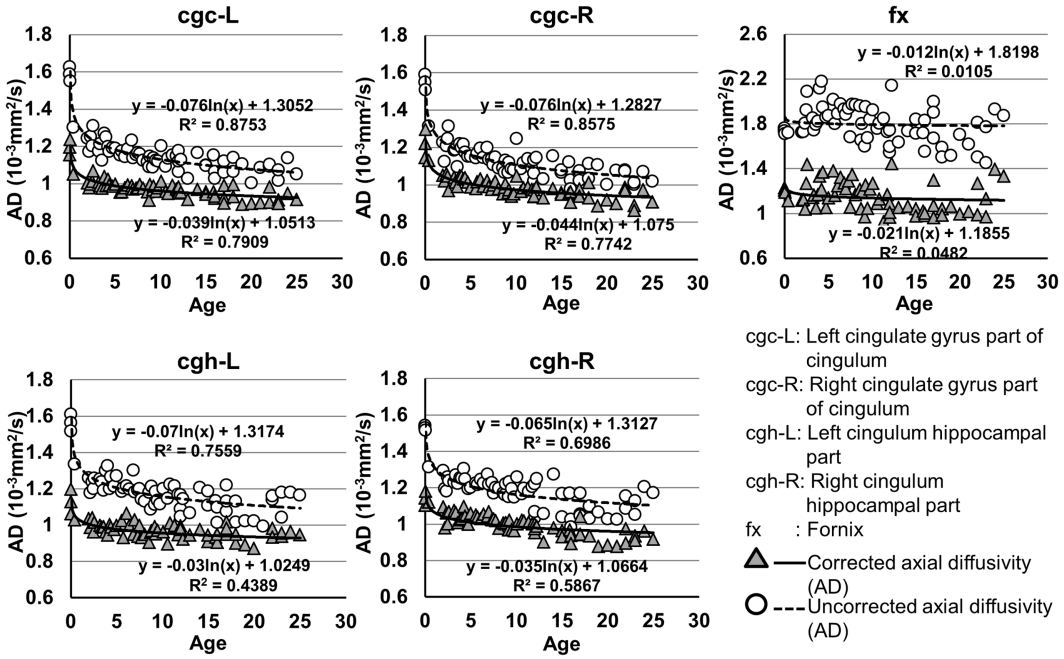

FIGURE 5 | Age-dependent changes of uncorrected and corrected axial diffusivity (AD) measurements of limbic tracts. R^2 and fitting equations are listed in each panel.

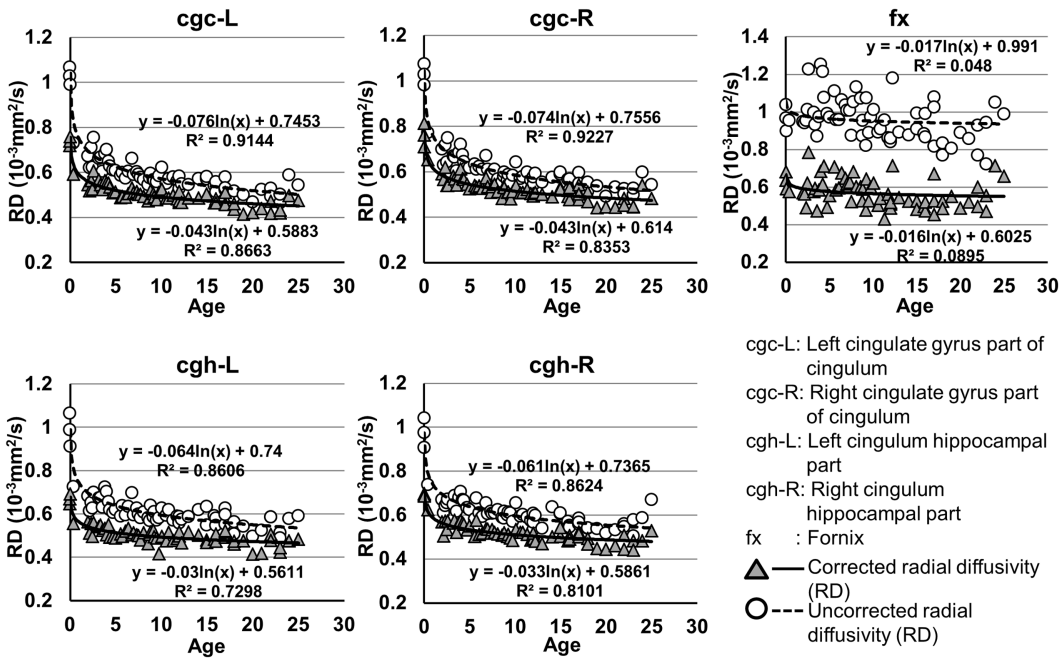

FIGURE 6 | Age-dependent changes of uncorrected and corrected radial diffusivity (RD) measurements of limbic tracts. R^2 and fitting equations are listed in each panel.

As shown in **Table 5**, DTI metrics of all limbic tracts were significantly altered after FWE correction. FA increases due to FWE correction for fx is apparent in **Figure 3**, while uncorrected and corrected FA of cgc-L/R and cgh-L/R overlap with no visible changes. Decrease of MD, AD, and RD of all limbic tracts can be clearly observed in **Figures 3–6**. Statistical results in **Table 5**

Table 1 | Relationship between fractional anisotropy (FA) of limbic tracts and age.

Limbic tracts	Age dependence	*F*-test between linear and logarithmic model		Best-fitting curve
		F value	*p* value	
cgc-L (UC)	***	2.11	**	Logarithmic
cgc-R (UC)	***	2.23	**	Logarithmic
cgh-L (UC)	***	1.87	*	Logarithmic
cgh-R (UC)	***	1.9	*	Logarithmic
fx (UC)	**	1.1	NS	Logarithmic/linear
cgc-L (C)	***	1.21	NS	Logarithmic/linear
cgc-R (C)	***	1.24	NS	Logarithmic/linear
cgh-L (C)	***	1.1	NS	Logarithmic/linear
cgh-R (C)	***	1.21	NS	Logarithmic/linear
fx (C)	**	1.24	NS	Logarithmic/linear

*Statistical significance $p < 0.05$, $p < 0.01$, and $p < 0.0001$ are indicated by bold *, **, and ***, respectively. cgc, right cingulate gyrus part of cingulum; cgh, hippocampal part of cingulum; fx, fornix; UC, uncorrected; C, corrected; L, left; R, right; NS, not significant.*

Table 2 | Relationship between mean diffusivity (MD) of limbic tracts and age.

Limbic tracts	Age dependence	*F*-test between linear and logarithmic model		Best-fitting curve
		F value	*p* value	
cgc-L (UC)	***	6.12	***	Logarithmic
cgc-R (UC)	***	6.16	***	Logarithmic
cgh-L (UC)	***	3.75	***	Logarithmic
cgh-R (UC)	***	3.49	***	Logarithmic
fx (UC)	NS	–	–	–
cgc-L (C)	***	3.5	***	Logarithmic
cgc-R (C)	***	2.83	***	Logarithmic
cgh-L (C)	***	1.75	*	Logarithmic
cgh-R (C)	***	1.67	**	Logarithmic
fx (C)	NS	–	–	–

*Statistical significance $p < 0.05$, $p < 0.01$, and $p < 0.0001$ are indicated by bold *, **, and ***, respectively. cgc, right cingulate gyrus part of cingulum; cgh, hippocampal part of cingulum; fx, fornix; UC, uncorrected; C, corrected; L, left; R, right; NS, not significant.*

Table 3 | Relationship between axial diffusivity (AD) of limbic tracts and age.

Limbic tracts	Age dependence	*F*-test between linear and logarithmic model		Best-fitting curve
		F value	*p* value	
cgc-L (UC)	***	4.37	***	Logarithmic
cgc-R (UC)	***	3.57	***	Logarithmic
cgh-L (UC)	***	2.34	**	Logarithmic
cgh-R (UC)	***	1.7	NS	Logarithmic/linear
fx (UC)	NS	–	–	–
cgc-L (C)	***	2.6	**	Logarithmic
cgc-R (C)	***	2.15	**	Logarithmic
cgh-L (C)	***	1.28	NS	Logarithmic
cgh-R (C)	***	0.78	NS	Logarithmic/linear
fx (C)	NS	–	–	–

*Statistical significance $p < 0.05$, $p < 0.01$, and $p < 0.0001$ are indicated by bold *, **, and ***, respectively. cgc, right cingulate gyrus part of cingulum; cgh, hippocampal part of cingulum; fx, fornix; UC, uncorrected; C, corrected; L, left; R, right; NS, not significant.*

Table 4 | Relationship between radial diffusivity (RD) of limbic tracts and age.

Limbic tracts	Age dependence	*F*-test between linear and logarithmic model		Best-fitting curve
		F value	*p* value	
cgc-L (UC)	***	6.16	***	Logarithmic
cgc-R (UC)	***	6.81	***	Logarithmic
cgh-L (UC)	***	4.25	***	Logarithmic
cgh-R (UC)	***	4.41	***	Logarithmic
fx (UC)	NS	–	–	–
cgc-L (C)	***	3.55	***	Logarithmic
cgc-R (C)	***	2.93	***	Logarithmic
cgh-L (C)	***	2.14	**	Logarithmic
cgh-R (C)	***	2.49	**	Logarithmic
fx (C)	*	0.99	NS	Logarithmic/linear

*Statistical significance $p < 0.05$, $p < 0.01$, and $p < 0.0001$ are indicated by bold *, **, and ***, respectively. cgc, right cingulate gyrus part of cingulum; cgh, hippocampal part of cingulum; fx, fornix; UC, uncorrected; C, corrected; L, left; R, right; NS, not significant.*

indicate that there are statistically significant changes for all DTI metrics of all limbic tracts with FWE correction.

DEVELOPMENT OF LENGTHS OF LIMBIC TRACTS

The plots of absolute and normalized lengths of all limbic tracts at different ages are shown in **Figure 7**. As shown in **Table 6**, significant age dependence was found in absolute lengths of all limbic tracts and normalized lengths of cgc-L/R. Among logarithmic, linear, and polynomial fitting between measured length and age, polynomial model was first rejected due to lowest R^2. After *F*-test, significant difference between logarithmic and linear model was found only for absolute length of cgc-L (**Table 6**). Logarithmic curves were fitted with highest R^2 for absolute and normalized lengths of all limbic tracts, as shown in dashed and solid curves in **Figure 7**, respectively. **Figure 7** and **Table 6** suggest that increases of absolute tract lengths of cgh-L, cgh-R, and fx results from overall brain size increases during development, while increases of absolute tract length of cgc-L and cgc-R are due to both overall brain size increases and relative increases of lengths of these two tracts in the brain.

Table 5 | Comparisons of DTI metrics of limbic tract before and after FWE correction with age and gender as covariates.

Limbic tracts	FA		AD		RD		MD	
	***t* value**	***p* value**	***t* value**	***p* value**	***t* value**	***p* value**	***t* value**	***p* value**
cgc-L	88.28	***	341.8	***	287	***	324	***
cgc-R	73.44	***	264.9	***	281	***	298.1	***
cgh-L	40.82	***	207.1	***	208.3	***	229.2	***
cgh-R	28.63	***	191.3	***	232.4	***	254.5	***
fx	214.5	***	214.3	***	191.8	***	206.5	***

*Statistical significance after Bonferroni correction is indicated by bold. cgc, right cingulate gyrus part of cingulum; cgh, hippocampal part of cingulum; fx, fornix; L, left; R, right; ***p < 0.001.*

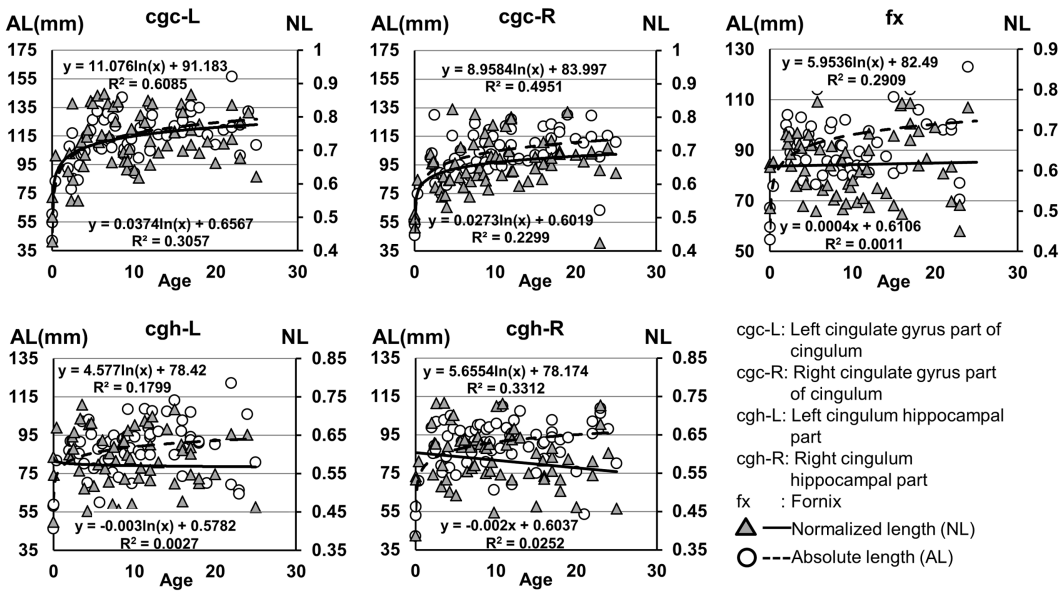

FIGURE 7 | Age-dependent changes of absolute and normalized fiber length of limbic tracts. R^2 and fitting equations are listed in each panel.

LATERALIZATION

Higher FA and lower AD, RD, and MD in the left cgc/cgh can be observed in **Figures 3–6**. In addition, longer normalized tract length of cgc on the left side compared to that on the right side can be observed in **Figure 7**. Statistical comparisons of normalized tract length and corrected DTI metrics on the left and right side are listed in **Table 7**. Significant differences were found in all DTI metrics between the left and right cgc and between the left and right cgh (**Table 7**). Statistically significant difference of normalized tract length was found between cgc-L and cgc-R, but not between cgh-L and cgh-R (**Table 7**).

STRUCTURAL CONNECTIVITY OF DMN REGIONS THROUGH LIMBIC TRACTS FOR NEONATE AND ADULT BRAIN

Figure 8 shows the functional connectivity maps in the DMN and structural limbic tracts connecting the DMN regions for a neonate and an adult brain. Consistency of DMN regions (MPFC, PCC, and MTL) and limbic tracts connecting these regions is clear between the neonate (**Figure 8A**) and adult (**Figure 8B**) brain. Specifically, cgc connects MPFC and PCC; cgh connects PCC and MTL for both neonate and adult brain.

DISCUSSION

With DTI from 65 subjects of cross-sectional age from 0 month to 25 years and rs-fMRI from 15 of them, we have quantitatively characterized development of microstructure, length, and connection of limbic tracts that play a key role in emotion, memories, and behavior. Limbic tracts were traced with DTI tractography. As limbic tracts are relatively thin and discrete compared to other major white matter tracts such as corpus callosum, the contamination of CSF to DTI metric measurements cannot be ignored. Correction of DTI metric measurement with FWE was conducted to achieve more accurate measurements of limbic tract microstructure. Together with the tract length measurement, microstructure and length of limbic tracts from birth to adulthood were quantitatively characterized. In addition, consistent role of limbic tracts connecting major DMN regions at birth and adulthood has been confirmed and demonstrated. Comparisons between DTI metrics

and lengths of the left and right limbic tracts suggest significant lateralization with longer and better myelinated cgc on the left side compared to that on the right side.

Despite that the overall shape of limbic tracts is relatively consistent throughout the developmental period from birth to young adulthood (**Figure 2**), **Figures 3–6** demonstrate rapid increase of FA and decrease of AD, RD, and MD within the first 2 years and relatively slow changes of these DTI metrics after 2 years until a plateau is reached during adolescence. Age-dependent increase of FA could be caused by larger decrease of RD compared to that of AD as FA is roughly the ratio between AD and RD. Rapid FA changes of cingulum within first 2 years could be caused by myelination, the majority of which begins within the first 2 years of life (Yakovlev and Andre-Roch, 1967). The asynchronous myelination of white matter tracts has been reported in neuropathology (Kinney et al., 1988) and MRI study (e.g., Deoni et al., 2011). Memory, emotion, and motivation functions are related to limbic tracts and important for survival. It is vital for limbic tracts to become well myelined earlier than other tracts, especially those projected from frontal and temporal lobes (Baumann and Pham-Dinh, 2001).

Including cross-sectional ages from birth to 25 years with a consistent group of dataset could offer more complete insight into structural maturation of limbic tracts. After test of three models including linear, logarithmic, and polynomial, **Tables 1–4** show that logarithmic model is overall best fitted to most limbic tract microstructural trajectories. Microstructural measurements of developing limbic tracts were found in previous literature (e.g., Hermoye et al., 2006; Grieve et al., 2011; Lebel and Beaulieu, 2011), which includes less comprehensive developmental periods. Depending on the early or late developing time window focused in these previous studies, different curves for developmental trajectories of limbic tracts were reported. For example, a non-linear trend of DTI metrics of white matter tracts was reported in a longitudinal DTI study with age range from 5 to 32 years (Lebel and Beaulieu, 2011). In that study, a large number of subjects were enrolled with 2 scans for most of the subjects, but early childhood period from 0 to 5 years was absent. During the early stage of development from birth to 54 months, non-linear trends could also be observed from measurements of FA and averaged apparent diffusion coefficient of cingulum (Hermoye et al., 2006), showing rapid DTI metric change in the first 3–6 months. A linear model was reported to be more suitable for very early development of limbic tracts of infants with shorter age range from 3.9 to 18.4 weeks (Dubois et al., 2008). In another study with later stage of limbic tract development from childhood to adulthood, polynomial curve was reported (Grieve et al., 2011). These previous findings are generally in agreement with the results presented in this study, since segmented developmental trajectory of DTI metrics at different developmental time window from birth to childhood could be quite different. For example, it can be observed from **Figures 3–6** that limbic tract metric changes before 2 years demonstrate clear linear behavior.

cgc-L/R, cgh-L/R, and fx are relatively thin and discrete white matter tracts. Contamination of brain CSF to DTI metric measurements of the limbic tracts could be severe. We adopted FWE (Pasternak et al., 2009) to achieve a more accurate characterization of developmental trajectories of microstructural measures. It

Table 6 | Relationship between limbic tract length (absolute and normalized) and age.

Tract length	Age dependence	*F*-test between linear and logarithmic		Best-fitting curve
		***F* value**	***p* value**	
cgc-L (absolute)	***	1.79	*	Logarithmic
cgc-R (absolute)	***	1.46	NS	Logarithmic
cgh-L (absolute)	***	1.19	NS	Logarithmic/linear
cgh-R (absolute)	***	1.39	NS	Logarithmic/linear
fx (absolute)	***	1.17	NS	Logarithmic/linear
cgc-L (normalized)	***	1.32	NS	Logarithmic
cgc-R (normalized)	***	1.2	NS	Logarithmic
cgh-L (normalized)	NS	–	–	–
cgh-R (normalized)	NS	–	–	–
fx (normalized)	NS	–	–	–

*Statistical significance is indicated by bold. cgc, right cingulate gyrus part of cingulum; cgh, hippocampal part of cingulum; fx, fornix; L, left; R, right; *p < 0.05; ***p < 0.001; NS, not significant.*

Table 7 | Comparisons of normalized tract length and corrected DTI metrics between the left and right cingulate gyrus part of cingulum (cgc) and between the left and right hippocampal part of cingulum (cgh), with age and gender as covariates.

Corrected DTI metrics	Fractional anisotropy		Axial diffusivity		Radial diffusivity		Mean diffusivity	
	***t* value**	***p* value**	***t* value**	***p* value**	***t* value**	***p* value**	***t* value**	***p* value**
cgc-L vs cgc-R	68.8	***	150.8	***	253.4	***	238.5	***
cgh-L vs cgh-R	14.2	***	50.94	***	149.2	***	115.2	***
Normalized tract length	***t* value**				***p* value**			
cgc-L vs cgc-R	30.1				***			
cgh-L vs cgh-R	0.75				NS			

*Statistical significance p < 0.001 after Bonferroni correction is indicated by bold ***. L, left; R, right; NS, not significant.*

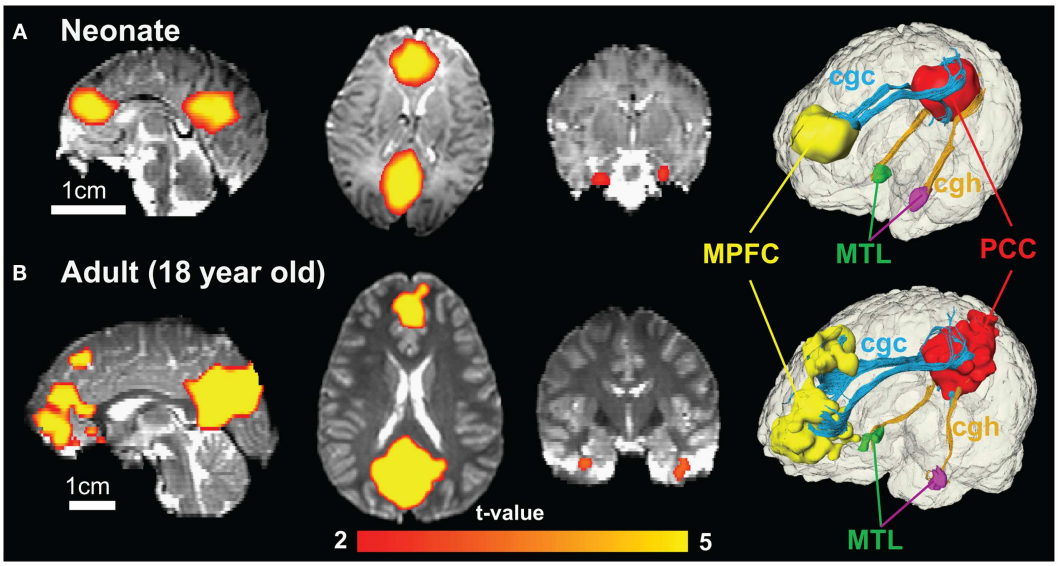

FIGURE 8 | Functional connectivity maps of DMN in sagittal, axial, and coronal slices from the left to right show similar connectivity pattern in neonate (A) and adult (B) brain. The color of connected brain clusters encodes *t* values. 3D visualization on the most right panels reveals clearly that cingulate gyrus part of cingulum (cgc) connects MPFC and PCC and cingulum hippocampal part (cgh) connects PCC and MTL for both neonate and adult brain. The 3D reconstruction of clusters at MPFC, PCC, and MTL was directly extracted from rs-fMRI analysis.

is clear that FA is increased and AD, RD, and MD are decreased after FWE correction, causing clear shift of DTI metric trajectories in **Figures 3–6**. Results in **Table 5** confirmed statistical significance of the shift after FWE correction. The amount of correction of DTI metric measurement is more dramatic for fx compared to that of cgc or cgh, as fibers of fx course closely around the ventricle and metric measurements of fx could be affected by severe CSF contamination. FA trajectories of cgc-L/R and cgh-L/R (**Figure 3**) are less affected by FWE correction than those of MD, AD, and RD (**Figures 3–6**) as FA can be considered approximately as a ratio of AD and RD and shift of AD and shift of RD offset each other. The shifts between uncorrected and corrected curves in **Figures 3–6** were heterogeneous. Specifically, DTI metric measurements of cgc-L/R and cgh-L/R were more severely affected by free water contamination in early childhood (**Figures 3–6**). Nevertheless, these shifts did not change the fitting models for most limbic tracts (**Tables 1–4**). Only for corrected FA of cgc-L/R and cgh-L/R, developmental trajectories of them could also be fitted with linear model as well as logarithmic model (**Table 1**) after FWE correction. To the best of our knowledge, no FWE correction has been reported for previous DTI metric measurements of developing limbic tracts. It is possible that FWE correction could help restore the real underlying microstructural maturation process of limbic tracts. Nevertheless, further cross-validation from a larger sample dataset is still needed to ensure accuracy of DTI metric measures after FWE correction.

Lengths of all limbic tracts increase during development, as shown in **Figure 7** and **Table 6**. Specifically, the length increases of cgh-L/R and fx follow the overall brain size development and no significant age dependence has been found after these lengths were normalized by the brain size. Significant age dependence has been found only for normalized lengths of cgc-L/R, indicating that there are extra length increases of cgc-L/R besides following growth of entire brain. Although the overall shape of cgc is relatively stable throughout development, extra cgc growth can be observed in its anterior part close to prefrontal cortex (**Figure 2**). Relative increase of cgc length is probably related to its growth in the prefrontal region. Functions of prefrontal areas are involved in planning, decision making, and moderating social behavior that develop during late childhood and adolescence (e.g., Gogtay et al., 2004). Connection of anterior cgc to late-developed prefrontal cortex may explain extra length growth of cgc from birth to young adulthood, but no extra length growth of cgh or fx.

Significant lateralization has been found for all DTI metrics of cgc-L/R and cgh-L/R with age and gender as covariates, as shown in **Table 7**. Higher FA and lower AD, RD, and MD of cgc and cgh can be observed on the left side than right side (**Figures 3–6**). This lateralization was associated with higher microstructural integrity on the left side of limbic tracts. Lateralization of DTI metrics of cgc and cgh may be related to unique functions of the left side of human brain such as language (van Veen et al., 2001). Exclusive right-handedness of the recruited subjects may also play a role. These findings are consistent to previous DTI metric measurements of cingulum (Gong et al., 2005; Verhoeven et al., 2010). Strengthened left limbic tracts were also demonstrated by longer length of cgc-L compared to that of cgc-R (**Table 7**). However, no significant length difference could be found for the left and right cgh.

In functional connectivity, brain regions where spontaneous blood oxygen level-dependent (BOLD) signal oscillations are temporally correlated can be either directly connected by white matter tracts or connected through a relay. The adult brain regions of PCC, MPFC, and MTL in DMN are connected by limbic tracts (Greicius et al., 2009). **Figure 8** clearly demonstrates consistent

connectivity roles of limbic tracts in connecting DMN regions for both the neonate and adult brain. Immature DMN functional connectivity has been reported with rs-fMRI of neonate brains recently (Fransson et al., 2007, 2009; Doria et al., 2010; Smyser et al., 2010). Unlike other major white matter tracts such as arcuate fasciculus, limbic tracts are well formed at birth, as shown in **Figure 2**. However, the role of limbic tracts in connecting DMN regions as early as birth time has not been confirmed previously. With myelination of cgc and cgh during development indicated by **Figures 3–6**, it can be speculated that enhanced myelination of cgc and cgh provide structural basis for maturation of DMN during development.

It is difficult to acquire all DTI data from birth to young adulthood in one site. We combined datasets acquired in two sites, but with the same imaging protocol and same Philips 3 T Achieva scanners. Rigorous quality control is conducted routinely for both scanners. We performed quantitative analysis based on DTI tractography and metric measurements to evaluate the effects of these two scanners in our previous study (Huang et al., 2014), and it was concluded that the scanner effects are negligible. Multiple factors could contribute to variations of MRI data, including variability caused by thermal variations of the same scanner itself, physiological variability of the participant and differences of two scanners. In an earlier experiment, DTI was acquired from the same young adult human volunteer scanned at two Philips 3 T Achieva scanners. FA measurement differences caused by scanner difference were tested to be within the range of variability of scanning the same subject twice with one scanner (Saxena et al., 2012). These previous experiments suggest that scanner difference will not cause significant differences of reported results. It also should be noted that this study is not a real longitudinal one as the subjects at each cross-sectional age were not the same. It will be very difficult to follow a same cohort of subjects from birth to 25 years old. However, multiple scans from same subjects during their development could be helpful to characterize real longitudinal development of limbic tracts.

In conclusion, with DTI and rs-fMRI from developing brains at cross-sectional ages from 0 month to 25 years, we have quantitatively characterized development of microstructure, length, and connection of limbic tracts that play a key role in emotion, memories, and behavior. Logarithmic developmental trajectories were found for most age-dependent changes of limbic tract microstructures and lengths from birth to young adulthood. Correction of CSF contamination has significantly increased FA and reduced MD, AD, and RD of developing limbic tracts, but has not changed the age-dependent trajectories of these metrics. Stronger microstructural integrity and longer tract lengths were found for limbic tracts on the left side compared to those on the right side. Consistent role of limbic tracts connecting major DMN regions at birth and adulthood has been confirmed and demonstrated.

ACKNOWLEDGMENTS

This study is sponsored by NIH (MH092535 and MH092535-S1), Natural Science Foundation of China (Grant Nos. 31271161 and 31071050), and Specialized Research Fund for the Doctoral Program of Higher Education of China (No. 20120131130008).

SUPPLEMENTARY MATERIAL

The Supplementary Material for this article can be found online at http://www.frontiersin.org/Journal/10.3389/fnagi.2014.00228/abstract

REFERENCES

Abramowitz, J. S., Taylor, S., and McKay, D. (2009). Obsessive-compulsive disorder. *Lancet* 374, 491–499. doi:10.1016/S0140-6736(09)60240-3

Amaral, D. G., Schumann, C. M., and Nordahl, C. W. (2008). Neuroanatomy of autism. *Trends Neurosci.* 31, 137–145. doi:10.1016/j.tins.2007.12.005

Basser, P. J., Mattiello, J., and LeBihan, D. (1994). Estimation of the effective self-diffusion tensor from the NMR spin echo. *J. Magn. Reson.* B 103, 247–254. doi:10.1006/jmrb.1994.1037

Basser, P. J., Pajevic, S., Piepaoli, C., Duda, J., and Aldroubi, A. (2000). *In vitro* fiber tractography using DT-MRI data. *Magn. Reson. Med.* 44, 625–632. doi:10.1002/1522-2594(200010)44:4<625::AID-MRM17>3.0.CO;2-O

Baumann, N., and Pham-Dinh, D. (2001). Biology of oligodendrocyte and myelin in the mammalian central nervous system. *Physiol. Rev.* 81, 871–927.

Beaulieu, C. (2002). The basis of anisotropic water diffusion in the nervous system – a technical review. *NMR. Biomed.* 15, 435–455. doi:10.1002/nbm.782

Braak, H., and Braak, E. (1991). Neuropathological stageing of Alzheimer-related changes. *Acta Neuropathol.* 82, 239–259. doi:10.1007/BF00308809

Catani, M., Dell'Acqua, F., and Thiebaut de Schotten, M. (2013). A revised limbic system model for memory, emotion and behaviour. *Neurosci. Biobehav. Rev.* 37, 1724–1737. doi:10.1016/j.neubiorev.2013.07.001

Catani, M., Howard, R. J., Pajevic, S., and Jones, D. K. (2002). Virtual *in vivo* interactive dissection of white matter fasciculi in the human brain. *Neuroimage* 17, 77–94. doi:10.1006/nimg.2002.1136

Conturo, T. E., Lori, N. F., Cull, T. S., Akbudak, E., Snyder, A. Z., Shimony, J. S., et al. (1999). Tracking neuronal fiber pathways in the living human brain. *Proc. Natl. Acad. Sci. U.S.A.* 96, 10422–10427. doi:10.1073/pnas.96.18.10422

Deoni, S. C., Mercure, E., Blasi, A., Gasston, D., Thomson, A., Johnson, M., et al. (2011). Mapping infant brain myelination with magnetic resonance imaging. *J. Neurosci.* 31, 784–791. doi:10.1523/JNEUROSCI.2106-10.2011

DeRubeis, R. J., Siegle, G. J., and Hollon, S. D. (2008). Cognitive therapy versus medication for depression: treatment outcomes and neural mechanisms. *Nat. Rev. Neurosci.* 9, 788–796. doi:10.1038/nrn2345

Doria, V., Beckmann, C. F., Arichi, T., Merchant, N., Groppo, M., Turkheimer, F. E., et al. (2010). Emergence of resting state networks in the preterm human brain. *Proc. Natl. Acad. Sci. U.S.A.* 107, 20015–20020. doi:10.1073/pnas.1007921107

Dubois, J., Dehaene-Lambertz, G., Perrin, M., Mangin, J. F., Cpintepas, Y., Duchesnay, E., et al. (2008). Asynchrony of the early maturation of white matter bundles in healthy infants: quantitative landmarks revealed noninvasively by diffusion tensor imaging. *Hum. Brain Mapp.* 29, 14–27. doi:10.1002/hbm.20363

Duman, R. S., and Voleti, B. (2012). Signaling pathways underlying the pathophysiology and treatment of depression: novel mechanisms for rapid acting agents. *Trends Neurosci.* 35, 47–56. doi:10.1016/j.tins.2011.11.004

Fair, D. A., Cohen, A. L., Dosenbach, N. U., Church, J. A., Miezin, F. M., Barch, D. M., et al. (2008). The maturing architecture of the brain's default network. *Proc. Natl. Acad. Sci. U.S.A.* 105, 4028–4032. doi:10.1073/pnas.0800376105

Fitzgerald, K. D., Welsh, R. C., Gehring, W. J., Abelson, J. L., Himle, J. A., Liberzon, I., et al. (2005). Error-related hyperactivity of the anterior cingulate cortex in obsessive-compulsive disorder. *Biol. Psychiatry* 57, 287–294. doi:10.1016/j.biopsych.2004.10.038

Fransson, P., Skiold, B., Engstrom, M., Hallberg, B., Mosskin, M., Aden, U., et al. (2009). Spontaneous brain activity in the newborn brain during natural sleep – an fMRI study in infants born at full term. *Pediatr. Res.* 66, 301–305. doi:10.1203/PDR.0b013e3181b1bd84

Fransson, P., Skiold, B., Horsch, S., Nordell, A., Blennow, M., and Lagercrantz, H. (2007). Resting-state networks in the infant brain. *Proc. Natl. Acad. Sci. U.S.A.* 104, 15531–15536. doi:10.1073/pnas.0704380104

Gogtay, N., Giedd, J. N., Lusk, L., Hayashi, K. M., Greenstein, D., Vaituzis, A. C., et al. (2004). Dynamic mapping of human cortical development during childhood through early adulthood. *Proc. Natl. Acad. Sci. U.S.A.* 101, 8174–8179. doi:10.1073/pnas.0402680101

Gong, G., Jiang, T., Zhu, C., Zang, Y., Wang, F., Xie, S., et al. (2005). Asymmetry analysis of cingulum based on scale-invariant parameterization by diffusion tensor image. *Hum. Brain Mapp.* 24, 92–98. doi:10.1002/hbm.20072

Greicius, M. D., Supekar, K., Menon, V., and Dougherty, R. F. (2009). Resting-state functional connectivity reflects structural connectivity in the default mode network. *Cereb. Cortex* 19, 72–78. doi:10.1093/cercor/bhn059

Grieve, S. M., Korgaonkar, C. R., Clark, C. R., and Willian, L. M. (2011). Regional heterogeneity in limbic maturational changes: evidence from integrating cortical thickness, volumetric and diffusion tensor imaging measures. *Neuroimage* 55, 868–879. doi:10.1016/j.neuroimage.2010.12.087

Hermoye, L., Saint-Martin, C., Cosnard, G., Lee, S. K., Kim, J., Nassogne, M. C., et al. (2006). Pediatric diffusion tensor imaging: normal database and observation of the white matter maturation in early childhood. *Neuroimage* 29, 493–504. doi:10.1016/j.neuroimage.2005.08.017

Huang, H., Fan, X., Weiner, M., Martin-Cook, K., Xiao, G., Davis, J., et al. (2012). Distinctive disruption patterns of white matter tracts in Alzheimer's disease with full diffusion tensor characterization. *Neurobiol. Aging* 33, 2029–2045. doi:10.1016/j.neurobiolaging.2011.06.027

Huang, H., Fan, X., Williamson, D. E., and Rao, U. (2011). White matter changes in healthy adolescents at familial risk for unipolar depression: a diffusion tensor imaging study. *Neuropsychopharmacology* 36, 684–691. doi:10.1038/npp.2010.199

Huang, H., Shu, N., Mishra, V., Jeon, T., Chalak, L., Zhang, Z., et al. (2014). Development of human structural brain networks through infancy and childhood. *Cereb. Cortex* doi:10.1093/cercor/bht335

Huang, H., Zhang, J., van Zijl, P. C., and Mori, S. (2004). Analysis of noise effects on DTI-based tractography using the brute-force and multi-ROI approach. *Magn. Reson. Med.* 52, 559–565. doi:10.1002/mrm.20147

Jiang, H., van Zijl, P. C., Kim, J., Pearlson, G. D., and Mori, S. (2006). DtiStudio: resource program for diffusion tensor computation and fiber bundle tracking. *Comput. Methods Programs Biomed.* 81, 106–116. doi:10.1016/j.cmpb.2005.08.004

Jones, D. K., Simmons, A., Williams, S. C., and Horsfield, M. A. (1999a). Non-invasive assessment of axonal fiber connectivity in the human brain via diffusion tensor MRI. *Magn. Reson. Med.* 42, 37–41.

Jones, D. K., Horsfield, M. A., and Simmons, A. (1999b). Optimal strategies for measuring diffusion in anisotropic systems by magnetic resonance imaging. *Magn. Reson. Med.* 42, 515–525. doi:10.1002/(SICI)1522-2594(199909)42:3<515::AID-MRM14>3.3.CO;2-H

Kinney, H. C., Brody, B. A., Kloman, A. S., and Gilles, F. H. (1988). Sequence of central nervous system myelination in human infancy. II. Patterns of myelination in autopsied infants. *J. Neuropathol. Exp. Neurol.* 47, 217–234.

Lebel, C., and Beaulieu, C. (2011). Longitudinal development of human brain wiring continues from childhood into adulthood. *J. Neurosci.* 31, 10937–10947. doi:10.1523/JNEUROSCI.5302-10.2011

Leech, R., and Sharp, D. J. (2014). The role of the posterior cingulate cortex in cognition and disease. *Brain* 137, 12–32. doi:10.1093/brain/awt162

Mesulam, M. (2000). "Behavioral neuroanatomy: large-scale networks, association cortex, frontal syndromes, the limbic system, and the hemispheric specializations," in *Principles of Behavioral and Cognitive Neurology*, ed. M. Mesulam (New York: Oxford University Press), 1–120.

Mishra, V., Cheng, H., Gong, G., He, Y., Dong, Q., and Huang, H. (2013). Differences of inter-tract correlations between neonates and children around puberty: a study based on microstructural measurements with DTI. *Front. Hum. Neurosci.* 7:721. doi:10.3389/fnhum.2013.00721

Monkul, E. S., Hatch, J. P., Nicoletti, M. A., Spence, S., Brambilla, P., Lacerda, A. L., et al. (2007). Fronto-limbic brain structures in suicidal and non-suicidal female patients with major depressive disorder. *Mol. Psychiatry* 12, 360–366. doi:10.1038/sj.mp.4001919

Mori, S., Crain, B. J., Chacko, V. P., and van Zijl, P. C. (1999). Three-dimensional tracking of axonal projections in the brain by magnetic resonance imaging. *Ann. Neurol.* 45, 265–269. doi:10.1002/1531-8249(199902)45:2<265::AID-ANA21>3.0.CO;2-3

Mukherjee, P., Chung, S. W., Berman, J. I., Hess, C. P., and Henry, R. G. (2008). Diffusion tensor MR imaging and fiber tractography: technical considerations. *AJNR Am. J. Neuroradiol.* 29, 843–852. doi:10.3174/ajnr.A1052

Mukherjee, P., Miller, J. H., Shimony, J. S., Conturo, T. E., Lee, B. C., Almli, C. R., et al. (2001). Normal brain maturation during childhood: developmental trends characterized with diffusion-tensor MR imaging. *Radiology* 221, 349–358. doi:10.1148/radiol.2212001702

Neil, J. J., Shiran, S. I., McKinstry, R. C., Schefft, G. L., Snyder, A. Z., Almli, C. R., et al. (1998). Normal brain in human newborns: apparent diffusion coefficient and diffusion anisotropy measured by using diffusion tensor MR imaging. *Radiology* 209, 57–66. doi:10.1148/radiology.209.1.9769812

Oishi, K., Akhter, K., Mielke, M., Ceritoglu, C., Zhang, J., Jiang, H., et al. (2011). Multi-modal MR analysis with disease-specific spatial filtering: initial testing to predict mild cognitive impairment patients who convert to Alzheimer's disease. *Front. Neurol.* 2:54. doi:10.3389/fneur.2011.00054

Oishi, K., Mielke, M. M., Albert, M., Lyketsos, C. G., and Mori, S. (2012). The fornix sign: a potential sign of Alzheimer's disease based on diffusion tensor imaging. *J. Neuroimaging* 22, 365–374. doi:10.1111/j.1552-6569.2011.00633.x

Pasternak, O., Sochen, N., Gur, Y., Intrator, N., and Assaf, Y. (2009). Free water elimination and mapping from diffusion MRI. *Magn. Reson. Med.* 62, 717–730. doi:10.1002/mrm.22055

Pierpaoli, C., and Basser, P. J. (1996). Toward a quantitative assessment to diffusion anisotropy. *Magn. Reson. Med.* 36, 893–906. doi:10.1002/mrm.1910360612

Reynolds, G. P. (1983). Increased concentrations and lateral asymmetry of amygdala dopamine in schizophrenia. *Nature* 305, 527–529. doi:10.1038/305527a0

Saxena, K., Tamm, L., Walley, A., Simmons, A., Rollins, N., Chia, J., et al. (2012). A preliminary investigation of corpus callosum and anterior commissure aberrations in aggressive youth with bipolar disorders. *J. Child Adolesc. Psychopharmacol.* 22, 112–119. doi:10.1089/cap.2011.0063

Smyser, C. D., Inder, T. E., Shimony, J. S., Hill, J. E., Degnan, A. J., Snyder, Z. A., et al. (2010). Longitudinal analysis of the neural development in preterm infants. *Cereb. Cortex* 20, 2852–2862. doi:10.1093/cercor/bhq035

Song, S. K., Sun, S. W., Ramsbottom, M. J., Chang, C., Russell, J., and Cross, A. H. (2002). Dysmelination revealed through MRI as increased radial (but unchanged axial) diffusion of water. *Neuroimage* 17, 1429–1436. doi:10.1006/nimg.2002.1267

Supekar, K., Uddin, L. Q., Prater, K., Amin, H., Greicius, M. D., and Menon, V. (2010). Development of functional and structural connectivity within the default mode network in young children. *Neuroimage* 52, 290–301. doi:10.1016/j.neuroimage.2010.04.009

Torrey, E. F., and Peterson, M. R. (1974). Schizophrenia and the limbic system. *Lancet* 2, 942–946. doi:10.1016/S0140-6736(74)91143-X

Uddin, L. Q., Kelly, A. M., Biswal, B. B., Castellanos, F. X., and Milham, M. P. (2009). Functional connectivity or default network components: correlation, anticorrelation, and causality. *Hum. Brain Mapp.* 30, 625–637. doi:10.1002/hbm.20531

van den Heuvel, M., Mandl, R., Luiqjes, J., and Hulshoff Pol, H. (2008). Microstructural organization of the cingulum tract and the level of default mode functional connectivity. *J. Neurosci.* 28, 10844–10851. doi:10.1523/JNEUROSCI.2964-08.2008

van den Heuvel, M., Mandl, R. C., Kahn, R. S., and Hulshoff Pol, H. (2009). Functionally linked resting-state networks reflect the underlying structural connectivity architecture of the human brain. *Hum. Brain Mapp.* 30, 3127–3141. doi:10.1002/hbm.20737

van Veen, V., Cohen, J. D., Botvinick, M. M., Stenger, V. A., and Carter, C. S. (2001). Anterior cingulate cortex, conflict monitoring, and levels of processing. *Neuroimage* 14, 1302–1308. doi:10.1006/nimg.2001.0923

Verhoeven, J. S., Sage, C. A., Leemans, A., Van Hecke, W., Callaert, D., Peeters, R., et al. (2010). Construction of a stereotaxic DTI atlas with full diffusion tensor information for studying white matter maturation from childhood to adolescence using tractography-based segmentations. *Hum. Brain Mapp.* 31, 470–486. doi:10.1002/hbm.20880

Wakana, S., Caprihan, A., Panzenboeck, M. M., Fallon, J. H., Perry, M., Gollub, R. L., et al. (2007). Reproducibility of quantitative tratography methods applied to cerebral white matter. *Neuroimage* 36, 630–644. doi:10.1016/j.neuroimage.2007.02.049

Weinstein, M., Ben-Sira, L., Levy, Y., Zachor, D. A., Ben Itzhak, E., Artzi, M., et al. (2011). Abnormal white matter integrity in young children with autism. *Hum. Brain Mapp.* 32, 534–543. doi:10.1002/hbm.21042

White, T., Cullen, K., Rohrer, L. M., Karatekin, C., Luciana, M., Schmidt, M., et al. (2008). Limbic structures and networks in children and adolescents with schizophrenia. *Schizophr. Bull.* 34, 18–29. doi:10.1093/schbul/sbm110

White, T., Kendi, A. T., Lehericy, S., Kendi, M., Karatekin, C., Guimaraes, A., et al. (2007). Disruption of hippocampal connectivity in children and adolescents with schizophrenia – a voxel-based diffusion tensor imaging study. *Schizophr. Res.* 90, 302–307. doi:10.1016/j.schres.2006.09.032

Woods, R. P., Grafton, S. T., Holmes, C. J., Cherry, S. R., and Mazziotta, J. C. (1998). Automated image registration: I. General methods and intrasubject,

intramodality validation. *J. Comput. Assist. Tomogr.* 22, 139–152. doi:10.1097/00004728-199801000-00028

Yakovlev, P. I., and Andre-Roch, L. (1967). "The myelogenetic cycles of regional maturation of the brain," in *Regional Development of the Brain in Early Life*, ed. A. Minkowski (Oxford: Blackwell Scientific), 3–70.

Conflict of Interest Statement: The authors declare that the research was conducted in the absence of any commercial or financial relationships that could be construed as a potential conflict of interest.

Received: 10 May 2014; accepted: 08 August 2014; published online: 28 August 2014.

Citation: Yu Q, Peng Y, Mishra V, Ouyang A, Li H, Zhang H, Chen M, Liu S and Huang H (2014) Microstructure, length, and connection of limbic tracts in normal human brain development. Front. Aging Neurosci. ***6****:228. doi: 10.3389/fnagi.2014.00228*

This article was submitted to the journal Frontiers in Aging Neuroscience.

frontiers in
AGING NEUROSCIENCE

REVIEW ARTICLE
published: 14 January 2015
doi: 10.3389/fnagi.2014.00343

Fornix as an imaging marker for episodic memory deficits in healthy aging and in various neurological disorders

Vanessa Douet* and Linda Chang*

Department of Medicine, John A. Burns School of Medicine, University of Hawaii, Honolulu, HI, USA

Edited by:
Jean Mariani, Universite Pierre et Marie Curie, France

Reviewed by:
Olivier Piguet, Neuroscience Research Australia, Australia
Claudia Metzler-Baddeley, Cardiff University, UK

****Correspondence:***
Vanessa Douet and Linda Chang, Department of Medicine, John A. Burns School of Medicine, The Queen's Medical Center, 1356 Lusitana Street, UH Tower, Room 716, Honolulu, HI 96813, USA
e-mail: douet@hawaii.edu; lchang@hawaii.edu

The fornix is a part of the limbic system and constitutes the major efferent and afferent white matter tracts from the hippocampi. The underdevelopment of or injuries to the fornix are strongly associated with memory deficits. Its role in memory impairments was suggested long ago with cases of surgical forniceal transections. However, recent advances in brain imaging techniques, such as diffusion tensor imaging, have revealed that macrostructural and microstructural abnormalities of the fornix correlated highly with declarative and episodic memory performance. This structure appears to provide a robust and early imaging predictor for memory deficits not only in neurodegenerative and neuroinflammatory diseases, such as Alzheimer's disease and multiple sclerosis, but also in schizophrenia and psychiatric disorders, and during neurodevelopment and "typical" aging. The objective of the manuscript is to present a systematic review regarding published brain imaging research on the fornix, including the development of its tracts, its role in various neurological diseases, and its relationship to neurocognitive performance in human studies.

Keywords: fornix, development, aging, episodic memory, neuropsychiatric disorders, DTI

INTRODUCTION

The fornix is part of the limbic system that comprises cortical and subcortical structures. The cortical structures include cingulate and parahippocampal gyri, as well as the entorhinal cortex. The subcortical structures comprise the amygdalae, septal nuclei, nucleus accumbens, mammillary bodies, hypothalamus, anterior nucleus of the thalami, hippocampi and fornix.

The limbic system was first described by Pierre Paul Broca [1827–1880] (Broca, 1890) and was proposed to be the circuit of emotional experience and behavior by James W. Papez [1883–1958] (Papez, 1937). Later, its functions were linked to pleasure and reward, as well as memory and integration of memories (Rajmohan and Mohandas, 2007). Episodic memory belongs to the long-term memory system, and refers to conscious recollection of specific events (episodes) and contexts (time and place). Episodic memory frequently declines with aging and often becomes deficient in neurodegenerative diseases (Samson and Barnes, 2013) and psychiatric disorders (White et al., 2008). The critical subcortical structure for memory functions is the hippocampus (Penfield and Milner, 1958). As the major efferent white matter tract from the hippocampus, the fornix was frequently evaluated in relation to hippocampi and to memory impairments, especially to deficits in episodic memory (Yanike and Ferrera, 2014). Cumulative data from structural and diffusion tensor imaging (DTI) studies suggest that forniceal measures correlate with episodic memory performance in various neuropathological conditions, as well as during "typical" brain development and brain aging. The fornix appears to be a robust imaging predictor of episodic memory performance, independent of age and the etiology that may affect the integrity of the fornix.

In this review, we will focus on the findings from imaging studies of the fornix including its development, its implication in cognitive performance, and the structural changes associated with typical aging and neurodegenerative disorders. After a brief description of its anatomy, we will summarize the studies conducted on the forniceal formation across the lifespan, particularly those assessed by DTI which provided much new knowledge in our understanding of the fornix. We will then concentrate on diseases that may lead to an impaired or underdeveloped fornix and its likely consequences on cognitive performance, particularly in episodic memory.

MATERIALS AND METHODS

We searched in the PubMed® database for relevant publications during the last decade (last update on 2014 November 15th). Our search terms included "MRI," "DTI," diseases of interest, "aging," "development," "cognition," "memory" in combination with "fornix." 482 results were obtained. We screened the abstracts and included only the papers that were original, published in English and referred to human research. However, the most important selection criterion was that the studies explicitly reported imaging findings of the fornix. Conference abstracts and case reports were excluded. After screening all relevant studies and excluding those papers not fulfilling the inclusion criteria, we evaluated 143 studies in further detail.

ANATOMY OF THE FORNIX (FIGURE 1)

The fornix of the brain is a C-shaped structure that projects from the posterior hippocampus to the septal area and hypothalamus. As the hippocampus terminates near the splenium of the corpus callosum, the fimbria becomes a detached bundle, the crus of the fornix. The two crura merge medially to form the body of the fornix. At the interventricular foramen, the body of the fornix diverges into the two adjacent columns that pass through the middle of the hypothalamus toward the mammillary bodies (**Figure 1A**).

The fornix is the largest efferent pathway from the hippocampus, and belongs to the "Papez circuit," which is also referred to as the limbic system. Forniceal fibers from the forebrain project to the anterior nucleus of the thalami, the mammillary bodies, hypothalamus, the septal nuclei and the ventral striata. Some fibers of the precommissural fornix spread beyond the septal nuclei and the ventral striata, and reach the orbital and anterior cingulate cortices. Forniceal fibers also contact the entorhinal cortex, amygdalae and back-project to the posterior cingulate gyrus (Nolte, 2009). The Papez circuit, or the limbic system, is involved in learning, memory, emotion and social behavior (King et al., 2013).

NORMAL DEVELOPMENT AND AGING OF THE FORNIX (TABLE 1)

On T1-weighted MRI, the left and right columns of the fornix are difficult to delineate, and are mainly treated as a single central structure that diverges into both cerebral hemispheres. Forniceal changes are often associated with abnormalities in surrounding structures, resulting in structural distortions that are difficult to assess. However, DTI can differentiate more easily the fornix from surrounding structures, and can quantify microstructural changes within the fornix. DTI characterizes the three-dimensional diffusion of water molecules and provides information on the integrity of tissue microstructures. The fractional anisotropy (FA) value indicates the architectural degree of the tissue, which may be influenced by the amount of myelination, the coherence of axonal fibers, or a combination of both, while the mean diffusivity (MD) value is a measure of the overall averaged water diffusion within a volume of tissue. For instance, a lower than typical FA observed during development of healthy children might indicate hypomyelination or slower growth of the axons, while a decline in FA might reflect either demyelination or a decline in the number of myelinated axonal fibers, or both. An increase in MD is associated with either neuronal damage or degeneration of microstructural barriers such as cell membranes. Loss of myelin typically increases radial diffusivity (RD), whereas axial diffusivity (AxD) may be a more specific marker of axonal damage (Song et al., 2002, 2003).

Recently, the development of the fornix across the lifespan has become an active area of investigation because of the quality of visualization which is possible with DTI. However, only a small minority of these studies was conducted longitudinally (**Table 1**).

On the post-mortem human fetal brain, the fornix can be identified on MRI as early as 10 weeks of gestation (Rados et al., 2006). DTI techniques showed that the fornix is one of the most prominent tracts in the fetal brain and its entire tract is fully formed by 13 gestational weeks (Huang et al., 2006, 2009).

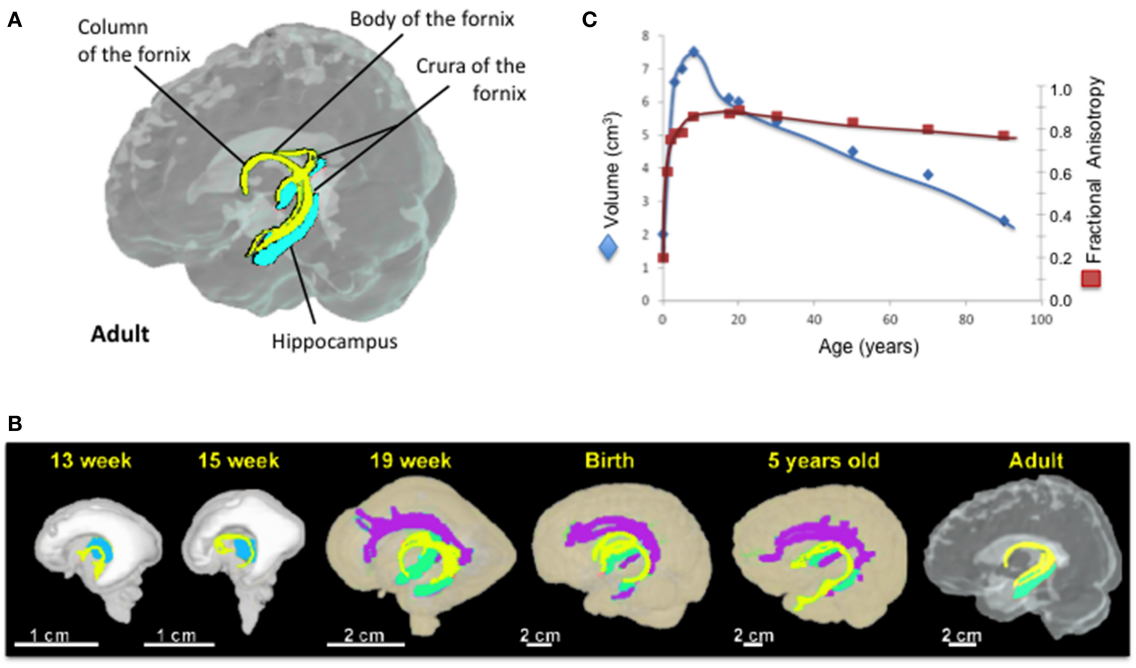

FIGURE 1 | The fornix across lifespan. (A) Anatomy of the fornix in the adult brain. Courtesy of Dr. Kenichi Oishi. **(B)** 3D reconstruction of the developmental tract of the fornix from 13 weeks of gestational age to adulthood. **(C)** Developmental trajectories of forniceal volume (blue) and FA (red) from birth to 90 years old. (Adapted from Huang et al., 2006 and Huang et al., 2009). Yellow, the fornix; Green, the hippocampus; Purple, cingulum; Blue, Thalamus.

Table 1 | Fornix metrics across the lifespan.

Authors	Subjects [age, M(male), F(female)]	Imaging Parameters	Image Analysis	Fornix-related Findings
Rados et al., 2006	16 post-mortem fetal brains (10–30 weeks gestation)	T1 and T2 weighted MRI Nissl-staining	Visualization	Fornix at 10 weeks of gestational age.
Huang et al., 2006	3 post-mortem fetal brains (19–20 weeks gestation) 3 female newborns 3 children (5–6 years, 2M, 1F)	4.7 T (postmortem fœtus), 7 directions 1.5 T (living subjects), 30 directions, 1.88 mm slice (newborns) and 2.3 mm slice (children)	Tractography, 4 tracts, 7 ROIs	Fornix such as cingulum already prominent during fetal stage, as early as 19 weeks of gestational age.
Huang et al., 2009	30 post-mortem fetal brains (13–22 weeks gestation); 3 brains per week	11.7 T (13–16 weeks), 200–400 μm slice 4.7 T (≥17 weeks), 300–600 μm slice, 6 directions	4 tracts and 7 ROIs	Fornix is the major tract at 13 weeks of gestational age although it is a small tract in adults
Dubois et al., 2008	23 term born infants [10.3 ± 3.8 (3.9–18.4) maturational age; 12M, 11F]	1.5 T, 14–30 directions, 2.5 mm slice	Tractography (12 ROIs)	↑FA during first week of infancy ↓MD and RD during first week of infancy
Hermoye et al., 2006	30 children [16 ± 16 months (0–4.5 years), 17M, 13F]	1.5 T, 32 directions, 1.9 mm slice (newborns) and 2.3 mm slice (children)	12 ROIs	Fornix present at birth and prominent compared to other brain structures
Douet et al., 2014	972 children [12.03 ± 3.6 (3–20) years, 509 boys, 463 girls]	3 T scanners ($n = 10$), 30 directions, 2.5 mm slice	5 ROIs	↑FA with age (max at 14.8 years) then plateau ↑volume with age (max at 12.6 years) then decrease slightly ↑volume α ↑episodic memory ↑FA and ↓volume α ↓episodic memory in children with *NRG1*-TT-risk alleles for schizophrenia and psychosis
Simmonds et al., 2014	128 young adults [14.9 ± 4.2 (8–29) years, 61M, 67F]	3 T, 6 directions, 1.56 mm slice	42 ROIs	↔FA for the body portion, ↑AxD and RD (+1–2% per year) after age 20 years ↑FA with age (13.1–16.4 years, +1–2% per year) for the crescent portion
Rudebeck et al., 2009	25 Healthy Controls [25.3 ± 2.9 (22–31) years, 14M, 9F]	3 T, Diffusion-weighted imaging	TBSS, VBM, 1 ROI	↑FA α ↑episodic memory (recollection) Spatial recognition FA
Lebel et al., 2012	403 [31.3 ± 21.5 (5–83) years, 195M, 208F]	1.5 T, 6 directions, 3 mm slice	Tractography	Inverted U-shaped curve of FA with age (max at 19.5 years old); U-shaped curve for diffusivities (MD, RD, AxD) with age (min ∼17.5 years old); Inverted U-shaped curve for volume (max 21.3 years)
Sala et al., 2012	84 Healthy controls [44 (13–70) years, 36M, 48F]	1.5 T, 12 directions, 4 mm slice	Automated atlas-based ROIs	Inverted U-shaped curve of FA with age; U-shaped curve for MD ↑AxD and RD and ↓volume with age
Giorgio et al., 2010	66 adults [31M, 35F]- 35 young [23–40 years, 16M, 21F], 19 middle-age [41–60 years, 9M, 10F], 10 older [60–82 years, 6M, 4F]-	1.5 T, 60 directions, 2.5 mm	TBSS, VBM	↓volume in older adults compared to young and mid-adults
Michielse et al., 2010	69 adults [46.9 ± 17.8 (22–84) years, 17M, 52F]	1.5 T, 6 directions, 2 mm slice	9 ROIs Tractography (crus only)	Linear ↓volume and FA with age Linear ↓AxD and MD with age and RD ↔ No asymmetry with age

(Continued)

Table 1 | Continued

Authors	Subjects [age, M(male), F(female)]	Imaging Parameters	Image Analysis	Fornix-related Findings
Lee et al., 2009	31 adults [36 (19–62) years, 15M, 16F]	3 T, 32 directions, 2.5 mm slice	14 Manual ROIs	No age-related changes in FA and ADC. No sex-difference
Stadlbauer et al., 2008	38 adults [49.6 ± 20.1 (18–88) years, 18M, 20F]	3 T, 6 directions, 1.9 mm slice	Tractography	↓FA with age (−2.1% per decade), ↓number of tract ↑MD (4.2% per decade)
Pagani et al., 2008	84 adults [44 (13–70) years, 36M, 48F]	1.5 T, 12 directions, 4 mm slice	VBM 11 clusters	↓volume with age
Zahr et al., 2009	24 adults- 12 young [25.5 ± 4.34 (29–33) years, 12 older adults [77.67 ± 4.94 (67–84) years-	3 T, 15 directions, 2.5 mm slice	Tractography 8 ROIs	↓FA and ↑ADC, RD and AxD in older adults compared to young. ↑FA and ↓ADC correlate with ↑working memory, motor, problem solving scores
Sullivan et al., 2010	120 adults [48.3 ± 14.4 (20–81) years, 55M, 65F]	1.5 T, 6 directions, 4 mm slice	Tractography	↑ADC, RD, and AxD with age No changes in FA
Burzynska et al., 2010	143 adults—80 young [25.7 ± 3.2 (20–32) years, 45M, 35F], 63 older [64.8 ± 2.9 (60–71) years, 34M, 29F]-	1.5 T, 12 directions, 2.5 mm slice	TBSS, VBM (body/colum and crus)	Body/column: ↓FA and ↑ diffusivities (MD, RD, and AxD) in older adults compared to young Crus: ↓FA and ↑RD and AxD in older adults compared to young
Jang et al., 2011	60 adults [49.2 (20–78) years, 30M, 30F]- young adults: 20–39 years, mid-adults: 40–59 years, older adults: 60–79 years-	1.5 T, 32 directions, 2.3 mm slice	Tractography 3 ROIs (body, column and crus = 3parts)	↓FA and ↑ADC with age ↓number of tract
Sasson et al., 2013	52 adults [51 (25–82 years), 20M, 32F]	3 T, 19 directions, 2.5 mm slice	Tractography, VBA	↓FA and ↑AxD with age
Pelletier et al., 2013	129 Healthy controls [73.9 years, ≥65 years, 68M, 61F]	3 T, 21 directions, 2.5 mm slice	TBSS and 2 ROIs	↓FA with age; FA as a predictor of age ↑FA α ↑ hippocampal volume
Vernooij et al., 2008	832 Healthy controls [73.9 ± 4.8 years, ≥55 years, 413M, 419F]	1.5 T, 25 directions, 2.5 mm slice	TBSS	↓ Volume, ↓FA, ↑AxD and RD with age
Metzler-Baddeley et al., 2011	46 adults [67.9 ± 8.6 (53–93) years, 21M, 25F]	3 T, 30 directions, 2.4 mm slice	Tractography 4 ROIs	↓FA with age ↑FA α ↑episodic memory
Fletcher et al., 2013	102 [73 ± 6.4 years, 20 converters to MCI, and 82 non converters]	1.5 T, 6 directions, 1.5 mm slice	1 manual ROI (body only)	↓FA and volume with age
Yasmin et al., 2009	100 adults [58 ± 11 (40–84) years, 50M, 50F]	3 T, 13 directions, 2.5 mm slice	8 ROIs	↓FA and ↑MD with age

α, correlate; T, Tesla; ROI, Region of Interest; FA, fractional anisotropy; MD, Mean Diffusivity; AxD, Axial diffusivity; RD, Radial diffusivity. VBM, voxel based morphometry; TBSS, Tract based spatial statistics.

At birth, the fornix is more prominent compared to the other brain fiber tracts and this phenotype is retained during infancy (Hermoye et al., 2006; Dubois et al., 2008). The development of fornix is thought to be completed by age 5 years (Hermoye et al., 2006; Dubois et al., 2008; Lebel et al., 2012) (**Figure 1B**). However, three cross-sectional (Lebel et al., 2012; Sala et al., 2012; Douet et al., 2014) and two longitudinal (Simmonds et al., 2014) DTI studies that investigated the volume and/or white matter integrity and density of the fornix showed its development through adolescence, and further age-related changes of the fornix throughout the lifespan (**Figure 1C**). Forniceal (body/column and crescent) FA exhibits an inverted U-shaped curve while the MD shows

a U-shaped curve, and both peak at late adolescence (maximum at 19.5 years for FA and minimum at 17.8 years for MD) (Lebel et al., 2012; Sala et al., 2012). A recent longitudinal study reported no significant changes in the developmental trajectory of FA of the forniceal body/column, while FA in its crescent portion continues to increase during adolescence [13–16 years] (Simmonds et al., 2014). These findings suggest that the age-related changes of FA observed in the cross-sectional studies were primarily due to changes in the crescent rather than in the body/column of the fornix. Before peaking at late adolescence, the fornix has the steepest age-dependent increase in MD amongst all major tracts (Lebel et al., 2012; Sala et al., 2012), with AxD and RD showing more than 2% change per year (Simmonds et al., 2014). Interestingly, age-related increase of AxD, i.e., accelerated prunning, was found in the left hemisphere but not in the right hemisphere during childhood and adolescence (Simmonds et al., 2014). Similarly, asymmetric atrophy of the hippocampus and fornix were reported in several neurological disorders such as schizophrenia (Crow et al., 1989; DeLisi et al., 1997; McDonald et al., 2000; Chance et al., 2005; Mitchell and Crow, 2005; Mitelman et al., 2005), bipolar disorders (Brisch et al., 2008), temporal lobe epilepsy (Baldwin et al., 1994; Hori, 1995; Kim et al., 1995; Kuzniecky et al., 1999), and in some patients with traumatic brain injury (Tate and Bigler, 2000; Tomaiuolo et al., 2004). Therefore, finding a more sensitive neuroimaging marker to assess the forniceal lateralization, such as AxD of the fornix, may be useful for early diagnosis of these disorders.

Prior to adulthood, the forniceal volume also exhibits an inverted U-shaped curve with age, and thereafter an age-dependent decrease in the volume in both longitudinal and cross-sectional studies (Pagani et al., 2008; Giorgio et al., 2010; Michielse et al., 2010; Lebel et al., 2012; Sala et al., 2012; Fletcher et al., 2013).

During adulthood, the white matter integrity and density of the fornix typically decrease with age across DTI studies (Stadlbauer et al., 2008; Lee et al., 2009; Yasmin et al., 2009; Michielse et al., 2010; Sullivan et al., 2010; Lebel et al., 2012; Sala et al., 2012; Fletcher et al., 2013; Sasson et al., 2013). The majority of the studies found age-related decreases of the forniceal FA (Stadlbauer et al., 2008; Yasmin et al., 2009; Zahr et al., 2009; Burzynska et al., 2010; Michielse et al., 2010; Jang et al., 2011; Metzler-Baddeley et al., 2011; Lebel et al., 2012; Sala et al., 2012; Fletcher et al., 2013; Pelletier et al., 2013; Sasson et al., 2013), and only two studies showed no changes with age (Lee et al., 2009; Sullivan et al., 2010). Findings on the diffusivities (MD, AxD and RD) are less consistent and varied depending on the region of interest (crus, body/column or the entire fornix). While the majority of the studies found diffusivities (MD, AxD and RD) of the fornix increase with age (Stadlbauer et al., 2008; Yasmin et al., 2009; Zahr et al., 2009; Burzynska et al., 2010; Sullivan et al., 2010; Jang et al., 2011; Lebel et al., 2012; Sala et al., 2012; Sasson et al., 2013; Simmonds et al., 2014), several studies reported either age-related decrease of MD and AxD (Michielse et al., 2010) or no changes in the fornix with age for MD (Lee et al., 2009) and RD (Michielse et al., 2010) across the age span of 10 to 80 years. White matter maturation follows sex-specific differential trajectories (Westerhausen et al., 2004; Schmithorst et al., 2008; Asato et al., 2010). Girls showed maturation of white matter integrity earlier than boys (Asato et al., 2010). In particular, girls showed greater age-dependent increase of MD in associative regions compared to boys. Furthermore, tendencies for age-related increase of FA were found in the right hemisphere for girls but in the left hemisphere for boys. These sex-specific brain differences parallel the pubertal changes that occur during adolescence, suggesting that hormonal changes might influence white matter maturity. However, the few studies that examined the relationships between physical pubertal maturity and circulating hormones on white matter maturation were underpowered by sample size(Peper et al., 2008, 2009). Nevertheless, discrepancies on diffusivities between DTI studies are not due to differences in age range and sex distribution, since they are similar across all of these studies. The image processing methods for these studies are also similar between those that showed conflicting results. Therefore, sample size or inter-subject variations might have contributed to the different findings regarding the age-related changes in FA and MD.

Overall, the fornix is one of the earliest white matter tracts to mature. After its maturation peaks during late adolescence, the fornix begins to "atrophy" throughout the remainder of the lifespan. However, "pruning" rather than degenerative processes likely contribute to the early decreases in forniceal volume. More detail anatomical assessments of the fornix (column, body, and crus) and more systematic evaluations across a larger age range, followed longitudinally, are needed to better characterize the developmental trajectories of the fornix.

Relationship with cognition

Fibers from the fornix comprise the main cholinergic input to the hippocampi and major efferent pathways from the hippocampi to the anterior thalamic nuclei, mammillary bodies, striata, and prefrontal cortices. These anatomical connections are involved in memory networks, which demonstrate that the fornix plays a critical and central role in memory tasks, particularly episodic memory. However, few studies investigated the relationships between forniceal metrics and memory tasks during typical development and aging. During childhood [3–20 years], larger forniceal volume was correlated with better episodic memory scores in healthy children. But this relationship was reversed in those carrying the *NRG1*-T-risk alleles for schizophrenia and psychosis (Douet et al., 2014). During young adulthood [22–31 years], greater FA in the fornix was associated with better episodic memory scores, especially with spatial recognition (Rudebeck et al., 2009). Similarly, across studies of young adults and older adults, forniceal FA correlated positively with working memory (Zahr et al., 2009), episodic memory (Rudebeck et al., 2009), and with both verbal and visual recall tasks (Rudebeck et al., 2009; Zahr et al., 2009; Metzler-Baddeley et al., 2011). A 4-year longitudinal follow-up study of healthy older adults found that lower forniceal volume and higher AxD at baseline predicted conversion to cognitive impairments (mild cognitive impairment or dementia) (Fletcher et al., 2013). Therefore, volumetric and white matter changes of the fornix appear to be effective biomarkers to validate or corroborate with memory performance across the lifespan, and to predict hippocampal function (Aggleton et al.,

2000; Rudebeck et al., 2009; Fletcher et al., 2013; Pelletier et al., 2013).

FORNIX AS A PREDICTOR OF MEMORY DEFICITS

Early studies in humans did not report associated memory deficits after lesion of the fornix (Garcia-Bengochea and Friedman, 1987). More recent studies, however, consistently reported deficits in several cognitive abilities, especially in episodic memory, in patients with injuries to the fornix (Gaffan et al., 1991; Squire and Zola-Morgan, 1991; Aggleton et al., 2000). Moreover, as part of the limbic system, fornix degeneration may precede hippocampal dysfunction, and may predict conversion to cognitive impairment better than hippocampal atrophy (Fletcher et al., 2013). Hence, assessments of the fornix have recently become a major research focus in determining its role in neurological disorders that are associated with memory impairments.

Alzheimer disease and dementia syndromes (Table 2)

Alzheimer disease (AD) and mild cognitive impairment (MCI) can be distinguished from normal aging by the different clinical syndromes (Petersen et al., 2001). MCI includes amnestic MCI (aMCI) and non-amnestic MCI (naMCI) (Petersen, 2004), depending on the memory impairment features. While naMCI patients tend to develop frontotemporal dementia or other types of dementias with broader cognitive deficits, aMCI patients are at risk for Alzheimer's disease (Mielke et al., 2014). In the US population, the prevalence of MCI ranges from 3 to 19% depending on the studies. About 40% of MCI patients will develop AD or other dementias, while most of MCI patients stay stable, and some even revert to a healthy control diagnosis (Mielke et al., 2014). Therefore, understanding prodromal AD and predicting accurately when MCI will convert to dementia can lead to early diagnosis and prevention of dementia when effective preventive strategies become available.

The neuropathology of AD is characterized by the presence of extracellular beta-amyloid plaques and intracellular neurofibrillary tangles that both lead to neuronal dysfunction and apoptosis (Bossy-Wetzel et al., 2004). Neurofibrillary tangles result from the intracellular oligomerization of the microtubule-associated protein Tau. The deposition of neurofibrillary tangles begins primarily in the limbic system structures, initially in the entorhinal cortex and the medial temporal regions, then progressively spread across the cerebral cortex. Hippocampal and entorhinal cortical atrophy assessed with MRI is well documented in patients with AD (Teipel et al., 2013), and in many with MCI (Pihlajamaki et al., 2009). Furthermore, this observation has extended the investigation of all limbic structures in relation to disease progression and cognitive performance.

The fornix is atrophied in MCI and AD patients compared to healthy controls, (Callen et al., 2001; Copenhaver et al., 2006; Ringman et al., 2007; Hattori et al., 2012) as confirmed by a longitudinal follow-up study (Douaud et al., 2013). Furthermore, in a large cohort of 79 aMCI and 204 healthy controls (HC), the volume of the crus of the fornix more specifically discriminated between MCI and HC (Cui et al., 2012).

Decreased FA of the fornix, on DTI, was found to be more sensitive than decreases in volume and/or area, on structural MRI, for predicting AD progression, since decreased FA preceded the atrophy more than two years prior to conversion from MCI to AD (Douaud et al., 2013). AD patients had lower FA (Liu et al., 2011b; Metzler-Baddeley et al., 2012) and higher MD and RD in the fornix compared to healthy controls (Mielke et al., 2009; Stricker et al., 2009; Liu et al., 2011b; Hattori et al., 2012; Huang et al., 2012; Oishi et al., 2012; Nowrangi et al., 2013; Zhuang et al., 2013), and at disease onset as defined by comparison between MCI and/or early onset AD patients (Mielke et al., 2009; Zhuang et al., 2010; Liu et al., 2011b; Oishi et al., 2012; Canu et al., 2013; Douaud et al., 2013; Nowrangi et al., 2013). A similar phenotype of lower FA in the fornix was found also in patients with genetically inherited dementias in comparison to controls (Ringman et al., 2007). Longitudinal studies showed that the magnitude of age-related changes of DTI metrics is similar between AD, MCI and healthy controls (Mielke et al., 2009, 2012; Oishi et al., 2012), suggesting that abnormal forniceal FA and MD are likely to predict convertion from MCI to AD.

Lower FA and higher diffusivity metrics in the fornix were associated also with worse performance on short- and long-term memory tasks and with clinical dementia evaluations in AD and MCI patients (Ringman et al., 2007; Mielke et al., 2009, 2012; Kantarci et al., 2011; Zhuang et al., 2013), as well as in healthy controls (Sexton et al., 2011; Oishi et al., 2012; Nowrangi et al., 2013). These cognitive measures showed deficits in verbal memory (i.e., California Verbal Learning Test, Hopkins Verbal Learning Test) and visual memory (Rey-Osterrieth Complex Figure Test), as well as in more global measures (MMSE and Clinical Dementia Rating).

Therefore, measurements of macro- and micro-structural changes in the fornix may provide preclinical surrogate markers to predict the development of Alzheimer disease and allow early treatment in these patients.

Schizophrenia (SCZ) (Table 3)

Clinical signs, brain imaging and genetic studies all contributed to the hypothesis that schizophrenia and psychiatric diseases are neurodevelopmental disorders (Rapoport et al., 2012) with neurodegenerative components (Vita et al., 2012). In addition, findings from postmortem and neuroimaging studies suggest that white matter maturation and myelination processes are disrupted in schizophrenia, which might trigger its symptoms (Heckers et al., 1991; Arnold et al., 1995) or lead to age-related white matter loss and cognitive decline (Chang et al., 2007; Kochunov and Hong, 2014). Brain abnormalities in SCZ patients occur in the paralimbic and temporolimbic regions (Kasai et al., 2003), which are involved in episodic memory. Incidentally, episodic memory impairment is one of the most consistent phenotype for schizophrenia (Schaefer et al., 2013). Since the fornix is part of the limbic system, and is involved in episodic memory, it has been evaluated with histopathology and brain imaging in SCZ patients.

Histopathologic studies showed that SCZ men, but not women, had greater than normal fiber density in the left fornix, suggesting sex and hemisphere specific alterations in the myelination of the fornix in schizophrenia (Chance et al., 1999). However, the fornix volume and cross-sectional area were found to be similar between SCZ patients and healthy adult controls in

Table 2 | Forniceal macro- and micro-structure alterations in patients with Alzheimer's disease and mild cognitive impairments.

Authors	Subjects [Mean age ± *SD* (age range), Male, Female]	Image Acquisition	Image Analysis	Fornix-related Findings
STRUCTURAL MRI STUDIES				
Callen et al., 2001	40 AD [69.1 ± 7.3 (54.5–80) years, 20M, 20F] 40 HC [70.4 ± 6.3 (55.8–80.6) years, 20M, 20F]	1.5 T, T1-weighted MRI, 1.5 mm slice	ROI	Volume: AD < HC
Copenhaver et al., 2006	16 AD [75.6 ± 6.9 (63–86) years, 7M, 9F] 20 CC [73.9 ± 6.6 (63–86) years, 6M, 14F] 20 MCI [69.6 ± 6.2 (63–86) years, 10M, 10F] 20 HC [71.3 ± 5.7 (63–86) years, 6M, 14F]	1.5 T, T1-weighted MRI, 1.5 mm slice	ROI (crus)	Volume: AD < HC ↓volume with age in all groups
DIFFUSION TENSOR STUDIES				
Ringman et al., 2007	12 FADmc [35 ± 6.4 years, 2M, 10F] 8 FADnc [36 ± 6.2 years, 1M, 7F]	1.5 T, 6 directions	ROI	Area: FADmc < FADnc FA: FADmc < FADnc ↓ FA ∝ ↓all NPTs and ↑ AD severity
Stricker et al., 2009	16 AD [77.3 ± 9.0 years, 8M, 8F] 14 HC [77.4 ± 8.1 years, 5M, 9F]	3 T, 15 directions, 3 mm slice	TBSS	FA: AD < HC
Mielke et al., 2009	25 AD [75.6 ± 7.0 years, 18M, 7F] 25 MCI [75.8 ± 5.3 years, 18M, 7F] 25 HC [74.3 ± 7.1 years, 11M, 14F]	3 T, 30 directions 2.2 mm slice	ROI (body) 3-month follow-up	No difference longitudinally (3 months) Cross-sectionally FA: MCI > AD < HC In MCI and AD: ↓FA ∝ ↓ memory scores (on CVLT) and ↓CDR
Sexton et al., 2010	7AD [68.1 ± 9.6 years, 5M, 2F] 8 MCI [73.0 ± 7.5 years, 3M, 5F] 8HC [77.1 ± 4.6 years, 3M, 5F]	1.5 T, 51 directions, 2.8 mm slice	TBSS and ROIs (Body and crus)	↑FA (Left_crus), ↓AxD (Left_crus), ↓MD (crus) and RD (crus) α ↑episodic memory factor (CVLT-R, HVLT-R, RCFT)
Zhuang et al., 2010	96 aMCI [79.57 ± 4.71 (70–90) years, 57M, 39F] 69 naMCI [77.62 ± 4.49 (70–90) years, 21M, 48F] 252 HC [77.87 ± 4.52 (70–90) years, 106M, 146F]	3 T, 6 directions 3.5 mm slice	TBSS	FA: aMCI < HC FA discriminated ∼70% (aMCI vs. HC)
Kantarci et al., 2011	149 MCI/71 HC [median 79 (52–95) years]	3 T, 21 directions 3.3 mm slice	ROIs and VBM	↑FA ∝ ↑language function, ↑visual-spatial processing
Liu et al., 2011b	17 AD [76 ± 7 years, 6M, 11F] 27 MCI [75 ± 6 years, 15M, 12F] 19 HC [75 ± 6 years, 11M, 8F]	1.5 T, 30 directions 5 mm slice	TBSS	FA: AD < HC FA: AD < MCI in the right fornix
Cui et al., 2012	79 aMCI [79.42 ± 4.71 years, 49M, 30F] 204 HC [77.65 ± 4.37(67–90) years, 85M, 119F]	3 T, 6 directions 3.5 mm	ROI	Crus discriminates between MCI and HC
Hattori et al., 2012	20 AD [74.6 ± 5.7 years, 10M, 10F] 22 iNPH [77.3 ± 4.9 years, 10M, 12F 20 HC [73.9 ± 6.0years, 7M, 13F]	1.5 T, 13 directions 3 mm slice	Tractography	Volume: iNPH < AD < lHC FA: iNPH < HC; AD < HC fornix differentiated iNPH from AD
Huang et al., 2012	26AD [70.8 ± 8.2 years, 15M. 11F] 11aMCI [69.1 ± 7.3 years, 5M, 6F] 24HC [69.5 ± 7.1 years, 10M, 14F]	3 T, 30 directions 2. mm slice	ROI	FA: AD < HC MD and RD: AD > HC; No group difference in AxD

(Continued)

Table 2 | Continued

Authors	Subjects [Mean age ± *SD* (age range), Male, Female]	Image Acquisition	Image Analysis	Fornix-related Findings
Metzler-Baddeley et al., 2012	25 MCI [76.8 ± 7.3 years, 14M, 11F] 20 HC [74 ± 6.5years, 10M, 10F]	3 T, 30 directions 2.4 mm slice	Tractography ROI	No correlation between FA and episodic memory; ↓FA with age
Mielke et al., 2012	23 aMCI [75.6 ± 5.5 years, 16M, 7F]	3 T, 32 directions 2.2 mm slice	ROI(body) 3-, 6-, 12-month and 2.5 yrs follow-ups	↓ FA correlated with↓ memory (CVLT) and ↓CDR ↑ MD, AxD, RD correlate with ↓ memory FA and MD predicted AD progression Longitudinally: no difference in FA or diffusivities
Oishi et al., 2012	25 AD [75.6 ± 6.9 years, 18M, 7F] 25 aMCI [75.8 ± 5.2 years 18M, 7F] 25 HC [74.3 ± 7.1 years, 11M, 14F]	3 T, 30 directions 2.2 mm slice	ROI 6- and 12 month follow-ups	Cross-sectionally: FA: AD < MCI or HC ↓ FA ∝↓memory performance (WMS delayed recall, CVLT) FA preded conversion from HC to aMCI, and from aMCI to AD Longitudinally: no difference in FA or diffusivities
Douaud et al., 2013	22 sMCI [69 ± 9 years, 11M, 11F] 13 pMCI [76 ± 6 years, 3M, 10F]	3 T, 30 directions 3 mm slice	TBSS	Volume: pMCI < sMCI FA: pMCI < sMCI; MD: pMCI > sMCI ↓FA ∝ ↑ MD ∝ ↓vol
Nowrangi et al., 2013	25 AD [75.6 ± 6.9 years, 18M, 7F] 25 aMCI [75.8 ± 5.2 years 18M, 7F] 25 HC [74.3 ± 7.1 years, 11M, 14F]	3 T, 32 directions 2.2 mm slice	ROI 6- and 12 month follow-ups	FA: AD < HC/MCI MD: AD > HC/MCI ↑ MD in all subjects over 12 month (greater ↑ MD over 6 month in MCI compared to HC)
Fletcher et al., 2013	102 [73 ± 6.4 years, 20 converters to MCI, and 82 non–converters]	1.5 T, 6 directions, 1.5 mm slice	1 manual ROI (body only)	↓FA and volume with age
Canu et al., 2013	22 EOAD [59.4 ± 4.6 (48–68)years, 11M, 11F] 24 Younger HC [59.1 ± 2.7 (51–64) years, 12M, 12F] 35 LOAD [75.4 ± 4.6 (68–84)years, 12M, 23F] 16 Older HC 73.1 ± 4.3 (67–81) years, 6M, 10F]	3 T, 35 directions 2.3 mm slice	ROI VBM	FA: EOAD < Younger HC MD and RD: EOAD > Younger HC
Zhuang et al., 2013	27 "late" aMCI [81.0 ± 4.6 (74.0–88.8) years, 18M, 9F] 39 "early" aMCI [74 ± 5.3 (72.9–90.7) years, 24M, 15F] 155 HC [79.1 ± 4.4 (72.5–90.5) years, 61M, 94F]	3 T, 32 directions 2.5 mm slice	TBSS ROI	FA: late aMCI < HC(in left fornix) AxD, RD and MD:late or late aMCI > HC (entire fornix) ↓FA and ↑MD ∝ ↓ episodic memory

MRI, Magnetic Resonance Imaging; T, Tesla; TBSS, Tract-based spatial statistic; VBA, Voxel-based analysis; ROI, Region of Interest; FA, Fractional Anisotropy; MD, Mean Diffusivity, AxD, Axial Diffusivity; RD, Radial Diffusivity.

EOAD, early-onset Alzheimer's disease; LOAD, late-onset Alzheimer's disease; HC, Healthy controls; naMCI, non-amnesic; MCI;AD, Alzheimer disease; iNPH, idiopathic normal pressure hydrocephalus; FAD, familial Alzheimer's disease; FADmc, familial Alzheimer's disease mutation carriers, FADnc, familial Alzheimer's disease non-carriers; pMCI, amnestic MCI patients who progressed to probable AD no earlier than 2 years after their baseline scan; sMCI, amnestic MCI patients who were clinically stable i.e., did not develop AD for at least 3 years following their first evaluation.

WMS–R, Wechsler Memory Scale–Revised; CDR, Clinical Dementia Rating; RCFT, Rey Complex Fig Test; HVLT-R, Hopkins Verbal Learning Test-Revised.

Table 3 | Forniceal macro- and micro-structure alterations in schizophrenia and psychiatric disorders.

Authors	Subjects [Mean age ± *SD*, range, (Male/Female)]	Image Acquisition	Image Analysis	Fornix-related Findings
Chance et al., 1999	29 SCZ [70 ± 13.8 years, 16M, 13F] 33 HC [69.45 ± 12.7 years, 19M, 14F]	Post mortem brain Parrafin wax 5 μm section	Palmgren's silver stain for nerve fibers	Fiber density: men < women Fiber density in men: SCZ > HC in the left fornix only No group difference in the numbers of fibers
Brisch et al., 2008	19 SCZ [51.37 ± 7.85 years, 11M, 8F] 9 bDep [51.78 ± 11.90 years, 6M, 3F] 7 uDep [46.71 ± 14.31 years, 2M, 5F] 14 HC [53.64 ± 9.61 years, 8M, 4F]	Post mortem brain 20 μm section	Nissl and myelin-stained	No differences in volume and mean cross-sectional areas
Davies et al., 2001	17 SCZ [16.9 ± 0.4 (14.83–20.5) years, 11M, 6F] 9 PsyC [16.25 ± 0.5 (12.7–17.8) years, 6M, 38F] 8 HC [16.9 ± 0.58 (14–18.3) years, 4M, 4F]	1.5 T MRI 1.5 mm slice	ROI (body)	Area: SCZ > HC (+39.69%) Area: SCZ > PsyC (+26.23%) Area: HC = PsyC
Zahajszky et al., 2001	15 SCZ [37.6 ± 9.3 (20–54) years] 15 matched HC [37.9 ± 8.8 (23–54) years] Only men	1.5 T MRI 6 directions 3 mm slice	ROI (body and crus)	No difference in volume between groups. No association between volume and illness or between volume and cognitive/clinical measures.
Abdul-Rahman et al., 2011	33 SCZ [39.4 ± 8.82 years, 24M, 7F] 31 HC [35.4 ± 8.82 years, 25M, 8F]	3 T 15 directions 3 mm slice	ROI Tractography	FA: SCZ < HC RD: SCZ > HC, no difference in AxD Specific loci of FA reduction within the fornix in SCZ, ↓FA α ↑psychopathology
Davenport et al., 2010	15 SCZ_onset [10–20 years, 8M, 7F] 14 ADHD [10–20 years, 12M, 2F] 26 HC [10–20 years, 16M, 12F]	3 T 12 directions 2 mm slice	VBA	In left posterior fornix: FA: SCZ_onset < HC and ADHD < HC
Fitzsimmons et al., 2009	36 SCZ [39.89 ± 9.06 years] 36 HC [39.59 ± 9.32 years] Only men	1.5 T 6 directions 4 mm slice	Tractography ROI	FA: SCZ < HC In HC: ↑FA α ↑ visual and verbal memory tasks, recall and recognition. In SCZ: no correlations
Fitzsimmons et al., 2014	21 FES [21.71 ± 4.86 years, 16M, 5F] 22 HC [21.23 ± 3.29 years, 13M, 9F)	3 T 51 directions Slice not reported	Tractography ROI	FA: FES < HC MD, RD and AxD: FES > HC MD (left) < MD (right) in FES only No correlation between DTI metrics and clinical characteristics
Kendi et al., 2008	15 SCZ [14.5 ± 2.6 (8–19 years), 7M, 8F)] 15HC [15.1 ± 2.5 (8–19 years), (8M, 7F]	3 T 12 directions 2 mm	ROI	Volume: SCZ < HC (-11%) No changes in FA
Kuroki et al., 2006	24SCZ [40.3 ± 8.5 years (24–52 years)] 31HC [40.6 ± 8.7 years (23–54 years)] Only men	1.5 T 6 directions 4 mm slice	ROI	FA: SCZ < HC (-7.5%) MD: SCZ > HC (+6.7%) Volume: SCZ < HC (-15.5%) ↓FA α ↑medication dosage ↓cross-sectional area α ↓global attention scores ↓cross-sectional area α ↓hippocampal volume

(Continued)

Table 3 | Continued

Authors	Subjects [Mean age ± *SD*, range, (Male/Female)]	Image Acquisition	Image Analysis	Fornix-related Findings
Lee et al., 2013	17 FES [21.5 ± 4.8 (18–30 years), 13M, 4F] 17 HC [23.1 ± 3.5 (18–30 years), 12M, 5F]	3 T 51 directions 1.7 mm	TBSS ROI	FA: FES < HC In the right fornix only, ↓FA α ↓reading scores No effect of medication on FA in FES group
Luck et al., 2010	32 FES [23.6 ± 0.7 years, 22M, 10F)] 25 HC [24.5 ± 0.8 years, (13M, 12F]	1.5 T 60 directions 4.4 mm slice	Tractography	FA: FES < HC
Nestor et al., 2007	21 SCZ [39.79 ± 9.16 (18–55 years)] 24 HC [40.64 ± 9.38 (18–55 years)] Only men	1.5 T 6 directions 4 mm slice	ROI	In SCZ: ↓FA α ↓scores for memory(↓DPT) In HC: ↑FA α ↑scores for memory (↑DPT, verbal memory and recall)
Takei et al., 2008	31SCZ [33.8 ± 9.0 (22–55 years), 12M, 19F)] 65 HC [34.7 ± 9.7 (21–54 years), 24M, 41F]	1.5 T 6 directions Slice not reported	Tractography ROI	FA: SCZ < HC MD: SCZ > HC No lateralization. In SCZ only: ↑MD_left α ↓verbal learning scores and ↑MD_right α ↓category fluency test performance
Smith et al., 2006	33 SCZ, 15 MS, Not reported	1.5 T 10 directions 2.5 mm	TBSS	FA: SCZ < HC
Maier-Hein et al., 2014	20 BPD [16.7 ± 1.6 (14–18 years)] 20 mixed psychosis diagnoses (CC) [16.0 ± 1.3 (14–18 years)] 20 HC [16.8 ± 1.2 (14–18 years)] Only women	3 T 12 directions 2.5 mm slice	TBSS ROI	FA: BPD < HC = CC

α: correlate.

MRI, Magnetic Resonance Imaging; T, Tesla; TBSS, Tract-based spatial statistic; VBA, Voxel-based analysis; ROI, Region of Interest; FA, Fractional Anisotropy; MD, Mean Diffusivity, AxD, Axial Diffusivity; RD, Radial Diffusivity.

HC, Healthy controls; SCZ, schizophrenic patients; PsyC, psychiatric controls non–schizophrenics: ADHD, Attention deficit hyperactivity disorder; uDep, unipolar Depression, bDep, bipolar depression; BPD, bipolar disorder; FES, first episode schizophrenia.

DPT, Doors and People Test.

postmortem brain tissues (Brisch et al., 2008), and in an *in vivo* MRI study (Zahajszky et al., 2001). In contrast, larger fornices were found on MRI of adolescent SCZ (ages 16–17 years, both males and females) compared to healthy controls and to patients with other serious psychiatric disorders (Davies et al., 2001). These variable findings regarding the forniceal volume might have resulted from the different subject populations and the less well defined fornix structures on these earlier structural MRI studies.

Findings on the fornix measurement have been more consistent across DTI studies. Using tractography, forniceal bundle volume in SCZ adolescents and adults were smaller [−11–16%] than in healthy controls (Kuroki et al., 2006; Kendi et al., 2008). The various DTI studies and approaches, using tractography, regions of interest (ROI) and tract-based spatial statistics (TBSS), consistently showed that FA of the fornix is lower in SCZ patient compared to healthy control. The lower than normal FA appears early at the onset of SCZ, which typically occurs just before adolescence (Davenport et al., 2010). This phenotype was reported in adolescent patients with their first episode of SCZ (Lee et al., 2009), in SCZ young adults (Luck et al., 2010; Fitzsimmons et al., 2014) and in mid-life SCZadults (Kuroki et al., 2006; Takei et al., 2008; Fitzsimmons et al., 2009; Abdul-Rahman et al., 2011), suggesting that lower than "normal" FA is a stable marker for SCZ that is retained throughout the lifespan. Lower FA in SCZ patients is frequently accompanied by either higher MD (Kuroki et al., 2006; Takei et al., 2008), RD (Abdul-Rahman et al., 2011) or both (Fitzsimmons et al., 2014). Findings on AxD are less consistent. Two studies showed no changes in AxD between SCZ patients and healthy controls (Kendi et al., 2008; Abdul-Rahman et al., 2011), whereas another study found higher AxD along with higher MD and RD in young adults with first episode schizophrenia (Fitzsimmons et al., 2014). The higher RD was suggested to be a marker of myelin disruption, higher MD a marker of

atrophy, while AxD may reflect axonal disruption (Song et al., 2005). Therefore, the lower FA and higher diffusivities involving all three measures (MD, RD and AxD) possibly reflect alterations in both myelin and axons. These alterations are notable in the fornix already at illness onset, but the causative mechanism is not yet defined. Moreover, the functionality of the forniceal changes and their impacts on the limbic network is still unclear. Some studies found no association between forniceal metrics and either cognitive or clinical measures (Zahajszky et al., 2001; Fitzsimmons et al., 2009, 2014; Lee et al., 2013), while others reported that lower FA correlated with greater psychopathology (Abdul-Rahman et al., 2011) and higher medication dosage in SCZ patients (Kuroki et al., 2006). Lower FA and/or higher MD was further associated with greater episodic memory impairments (verbal and visual memory tests) in SCZ patients (Nestor et al., 2007; Takei et al., 2008; Lee et al., 2013). In healthy controls, these correlations between FA and visual and verbal memory tasks were also observed (Nestor et al., 2007; Fitzsimmons et al., 2009).

In conclusion, abnormalities in the fornix are found in SCZ patients and are most likely due to degeneration, involving both axonal injury and demyelination, of the fornix. To some extent, these microstructural abnormalities in the fornix may serve as an imaging marker for disease severity in schizophrenia, although it remains unclear whether these changes in the fornix contribute to disruption of the limbic networks and to hippocampal atrophy. In addition, DTI metrics (FA and MD) appear to be sensitive indicators of injury to the fornix and subsequent memory deficits in SCZ patients. Further investigations using these metrics, in addition to other imaging modalities (e.g., evaluating brain network connectivities), are needed to follow patients longitudinally from the prodromal period to the first episodes to understand further the evolution of the neuropathology of schizophrenia.

Multiple Sclerosis and other neurodegenerative diseases (Table 4)

Multiple Sclerosis (MS) is an autoimmune demyelinating disease that is characterized by the infiltration of macrophages and T-cells that activate glia and microglia, which lead to fulminant neuroinflammation and intense demyelination of nerve fibers (Pivneva, 2008). About half of the MS patients develop cognitive deficits and most frequently, episodic memory deficits (Brissart et al., 2011). As parts of the limbic system, both the hippocampus and the fornix were often found affected in MS patients. Compared to healthy controls, MS patients had lower magnetization transfer ratio (MTR) in the right fornix, but this abnormality in the fornix did not correlate with cognitive performance (Ranjeva et al., 2005). Using TBSS, tractography or ROI, MS patients consistently showed lower FA with higher MD and RD in the fornix than healthy controls across studies and during adulthood (Smith et al., 2006; Dineen et al., 2009, 2012; Roosendaal et al., 2009; Fink et al., 2010; Kern et al., 2012; Koenig et al., 2013; Syc et al., 2013). Findings on AxD in the fornix were less consistent and less systematically investigated. Forniceal AxD showed either no group differences (Dineen et al., 2012) or higher values in MS compared to healthy controls (Roosendaal et al., 2009; Syc et al., 2013). In most of these studies, MS patients with lower FA and higher diffusivity metrics in the fornix had poorer performance in verbal and visual memory or recall and greater episodic memory impairments (Brief Visual Memory Test-Revised) (Dineen et al., 2009, 2012; Koenig et al., 2013, 2014; Syc et al., 2013). Moreover, these forniceal DTI metrics correlated with Expanded Disability Status Scale (EDSS) and disease duration in these MS patients (Syc et al., 2013; Koenig et al., 2014).

Altogether, these findings showed that DTI metrics in the fornix are consistently abnormal in MS patients. Since DTI measures in the fornix can assess disease severity, they may be useful for monitoring MS disease progression. Furthermore, forniceal DTI metrics correlated with hippocampal volume in patients with MS, and DTI measures in the fornix had an even stronger association with visual and episodic memory than the hippocampal volume (Koenig et al., 2014). Therefore, similar to patients who convert from MCI to AD, longitudinal forniceal DTI measures may be useful in predicting hippocampal abnormalities and memory deficits in MS patients.

Parkinson's disease. Parkinson's disease (PD) is most commonly regarded as a movement disorder (Gelb et al., 1999), since degeneration of the nigrostriatal dopaminergic system leads to dysfunction of the motor system with the four cardinal signs of tremors, bradykinesia, rigidity and postural instability. However, dopamine also mediates attention and working memory, which are requried for most higher level cognitive function, Therefore, PD patients commonly develop dementia and cognitive deficits including deficits in executive function, attention, language and memory (Zgaljardic et al., 2003; McKinlay et al., 2010). Few studies investigated the fornix in PD patients using DTI. Similar to AD patients, MD of the fornix was higher in PD patients than in healthy adults (Kim et al., 2013), and higher MD correlated with worse short-term non-verbal memory (Zheng et al., 2014). However, since many dementia patients have co-occurrence of AD and PD, it remains unclear whether the fornix abnormalities are related specifically to PD. Depression is also common amongst PD patients, and those with depression showed lower FA in the frontal white matter than PD patients without depression; although the fornix was not specifically evaluated in this study, and the temporal white matter showed no group difference (Matsui et al., 2007). Another DTI study found that PD patients with excessive daytime sleepiness (Epsworth Sleepiness Scale $\geq$ 10) had significantly lower FA in their fornix compared to controls (Matsui et al., 2006). Therefore, abnormalities in the fornix appear to contribute to the co-morbid symptoms beyond the extrapyramidal system, such as memory deficits and excessive daytime sleepiness in patients with PD.

Epilepsy. Since a large number of etiologies exist for epilepsy, the fornix may or may not be affected depending on whether this major efferent white matter tract from the hippocampi is affected by the lesion or condition that caused the epilepsy. For instance, mesial temporal sclerosis (MTS) causes temporal lobe epilepsy (TLE), and is frequently accompanied by forniceal atrophy and lower FA when the fornix of these patients are compared to non-epileptic controls (Baldwin et al., 1994; Kim et al., 1995). Decreased fornix volumes and lower FA were often associated with ipsilateral hippocampal sclerosis, both quantitatively and qualitatively (Baldwin et al., 1994; Kuzniecky et al.,

Table 4 | Forniceal macro- and micro-structure alterations in multiple sclerosis and other neurodegenerative diseases.

Authors	Subjects [Mean age ± *SD* (range), M (male), F (female)]	Image Acquisition	Image Analysis	Fornix-related Findings
MULTIPLE SCLEROSIS (MS)				
Ranjeva et al., 2005	18 CISSMS [29.3 ± 7 years, 2M, 16F] 18 Healthy controls [25.27 ± 6.3 years, 2M, 16F]	1.5 T 5 mm slice	MTR	MTR (right fornix): MS < HC
Dineen et al., 2009	37 MS [43.5 (31.1–56.3) years, 11M, 26F] 25 HC [36.4 (28.2–55.3) years, 9M, 16F]	3 T 15 directions 2.5 mm slice	TBSS	FA: MS < HC ↓FA in the left fornix α ↓episodic memory scores (CVLT and BVRT)
Dineen et al., 2012	34 relapsing-remitting MS [42.6 (31.1–56.1) years, 11M, 13F] 24 HC [38.7 (28.3–55.3) years, 9M, 15F]	3 T 15 directions 2.5 mm slice	ROI	FA: MS < HC RD: MS > HC; no group difference in AxD ↓FA α ↓episodic memory scores (CVLT and BVRT)
Fink et al., 2010	50 MS [43.3 ± 9.3 (20–65) years, 10M, 40F] 20 HC (41.3 ± 10.1 (20–56) years]	1.5 T 30 directions 1 mm slice	Tracto-graphy ROI	FA: MS < HC RD: MS > HC in left fornix only In MS, ↑ RD (Right fornix) α ↓episodic long-term memory (CVLT_recognition)
Kern et al., 2012	18 MS [42.1 (23–54.5 years), 14M, 4F] 16 HC [35.2 (24–50.3 years), 14M, 2F]	3 T 12 directions 3 mm slice	TBSS	FA: MS < HC In MS: ↓FA α ↓verbal memory performance
Koenig et al., 2013	40 MS [42.55 ± 9.1 (32–52 years), 11M, 29F] 20 HC [41.35 ± 9.7 (32–52 years), 7M, 13]	3 T 71 directions 1 mm slice	ROI	FA: MS < HC RD and MD: MS > HC In MS: ↑RD, MD and ↓FA(Left-fornix) α ↓episodic memory (BVMT-R scores) No group difference in volume
Koenig et al., 2014	52 MS [44.27 ± 8.9 (32–52 years), 16M, 36F] 20 HC [41.35 ± 9.7 (32–52 years), 7M, 13F]	3 T 71 directions 1 mm slice	ROI	Volume: MS < HC In MS: ↓FA and volume (Left-fornix)and ↑MD, AxD and RD α ↓episodic memory (BVMT-R and SDMT) ↑MD, RD, and AxD (Right-fornix) and ↓volume α ↑EDSS In MS: ↑FA and ↓MD, RD, AxD α ↑hippocampal volume No correlation in HC
Roosendaal et al., 2009	30 MS [40.6 ± 9.1, 11M, 19F] 31 HC [40.6 ± 9.9 years, 10M, 21F)]	1.5 T 61 directions 3 mm slice	TBSS ROI	FA: MS < HC RD and AxD: MS >HC No correlation between FA and EDSS
Syc et al., 2013	64 RRMS [39 ± 11 (32–52 years), 23M, 41F] 24 SPMS [55 ± 8 (32–52 years), 7M, 17F] 13 PPMS [56 ± 7 (32–52 years), 7M, 6F] 16 HC [40 ± 9 (32–52 years), 5M, 11F]	3 T MTR 1.5 mm slice	Tractography ROI	FA: MS < HC (-19%) MD, RD and AxD: MS > HC (+13%) ↓FA and ↑MD, RD, AxD α ↑EDSS and ↑disease duration ↓FA and ↑MD, RD α ↓PASAT-3 scores ↓FA and ↑MD, RD and AxD α ↑9-HPT times
PARKINSON'S DISEASE (PD)				
Matsui et al., 2006	11 PD with EDS (ESS > 10) [72.2 ± 7.2 years, 8M, 3M] 26 PD without EDS [71.2 2419.2 years, 23F, 3M] 10 controls [72.4 ± 6.4 years, 7M/3F]	1.5 T 6 directions 4 mm slice	5 manual ROIs	FA: PD with EDS < PD without EDS or controls FA α with Epworth Sleepiness Scale (ESS)

(Continued)

Table 4 | Continued

Authors	Subjects [Mean age ± *SD* (range), M (male), F (female)]	Image Acquisition	Image Analysis	Fornix-related Findings
Matsui et al., 2007	14 PD with depression [71.1 ± 9.9 years, 12F, 2M] 14 PD without depression [69.3 ± 8.1 years, 10F, 4M]	1.5 T 6 directions 4 mm slice	14 manual ROIs	FA: PD with depression < PD without depression only in frontal white matter (anterior cingulum); fornix not evaluated but no group difference in temporal white matter.
Kim et al., 2013	64 PD [63.0 ± 8.9 years, 22M, 42F] 64 HC [62.9 ± 9.0 years, 22M, 44F]	3 T 15 directions 2 mm slice	TBSS	MD: PD > HC
Zheng et al., 2014	16 PD [62.2 ± 9.6 years, 11M, 5F]	3 T 20 directions 2 mm slice	40 ROIs	↑ MD = ↓ Non-verbal memory scores (short-term)
EPILEPSY				
Liu et al., 2011a	15 JME patients [21 ± 4 (17–32 years), 3M, 12F] vs. 15 HC [21 ± 4 (17–31 years), 3M, 12F] 17 IGE-GTC [21 ± 4 (18–31 years), 7M, 3F] vs. 10 HC [21 ± 4 (18–30 years), 7M, 3F]	1.5 T 6 directions 1.5 mm slice	Tractography	FA: JME < HC FA: IGE-GTC = HC
Kuzniecky et al., 1999	35 MTS suspected (age, sex not reported) 50 MTLE [32 (17–42 years), 19M, 31F] 17 HC [35 (24–41 years), 8M, 9F]	1.5 T MRI 1.5 mm slice, no gap	Manual ROIs	Asymmetric size 86% of MTLE patients had atrophy ipsilateral to hippocampal atrophy
Ozturk et al., 2008	35 MTS suspected (age, sex not reported) 353 HC [49.2 (7–87 years), 134M, 219F]	3 T MTR 1.5 mm slice	Visual evaluation (Blinded to Grouping)	Asymmetric size MTS: 34.3% (12/35) HC: 7.9% (28/353)
Kim et al., 1995	33 preHS [31.5 (13–57 years), 19M, 14F] 7 postHS [27 917–40 years), 3M, 4F] 34 HC [33.8 (14–56 years), 17M, 17F]	1.5 T MRI 3 mm slice	Visual evaluation (Blinded to Grouping)	Asymmetric size preHS: 42% postHS: 74% HC: 6%
TRAUMATIC BRAIN INJURY (TBI)				
Gale et al., 1993	27 TBI 18 HC Only women	MRI	Fornix-to-brain ratios (FBR)	FBR: TBI < HC Atrophy in TBI No correlation between FBR and neuropsychological outcome.
Tate and Bigler, 2000	86 TBI [30 ± 11.73 (16–65 years), 58M, 28F] 46 HC [37.21 ± 13.08 (16–65 years), 31M, 15F]	1.5 T MRI 5 mm slice, 2 mm gap	ROI	Area: TBI< HC In TBI: ↓Area_fornix α ↓vol_hippocampus α ↑ injury severity No correlation in HC No correlation between area and memory performance (GMI and WMS-R)
Tomaiuolo et al., 2004	19 TBI [35.5 ± 14.71 (17–68 years), 12M, 7F] 19 HC [37.4 ± 15.18 (18–72 years), 12M, 7F]	1.5 T MRI 1 mm slice	ROI	Volume: TBI< HC ↓volume α ↓memory performance [Immediate and delayed recall of both RCFT and WMS (word list)]
Kinnunen et al., 2011	28 TBI [38.9 ± 12.2 years, 21M, 7F] 26 HC [35.4 ± 11.1 years, 12M, 14F]	3 T 16 directions 2 mm slice	TBSS	In TBI and HC, ↓ FA α ↓associative memory and learning performance (Immediate recall DPT)

(Continued)

Table 4 | Continued

Authors	Subjects [Mean age ± *SD* (range), M (male), F (female)]	Image Acquisition	Image Analysis	Fornix-related Findings
Palacios et al., 2011	15 TBI [23.6 ± 4.79 (18–32 years), 11M, 4F] 16 HC [23.7 ± 4.8 (18–32 years), 9M, 7F]	1.5 T 25 directions 5 mm slice	TBSS ROI	FA: TBI < HC In TBI: ↓FA in fornix α with worse declarative memory but not with working memory; ↓FA in SLF α with working memory
Adnan et al., 2013	29 TBI [5 and 30 months post-injury]		ROI	FA: TBI < HC

α: correlate.

MRI, Magnetic Resonance Imaging; T, Tesla; MTR, magnetization transfer ratio; TBSS, Tract-based spatial statistic; VBA, Voxel-based analysis; ROI, Region of Interest; MO, mode of anisotropy; FA, fractional anisotropy; MD, Mean Diffusivity, AxD, Axial diffusivity; RD, Radial diffusivity.

MS, Multiple sclerosis; PD, Parkinson's disease; RRMS, relapsing-remitting multiple sclerosis; SPMS, secondary progressive multiple sclerosis; PPMS, primary progressive multiple sclerosis; CISSMS, clinically isolated syndrome suggestive of multiple sclerosis; JME, juvenile myoclonic epilepsy; IGE-GTC, generalized tonic–clonic seizures; MTLE, Mesial temporal lobe epilepsy; MS, Mesial Temporal Sclerosis; preHS, pre-surgical hippocampal sclerosis; postHS, post-surgical hippocampal sclerosis; TBI, Traumatic brain injury.

EDSS, Expanded Disability Status Scale; 9-HPT, 9-Hole Peg Test; PASAT-3, Paced Auditory serial Addition Task-3, second version; GMI, General Memory Index score; WMS–R, Wechsler Memory Scale–Revised; RCFT, Rey Complex Fig Test; BVMT-R, Brief Visuospatial Memory Test-Revised; SDMT, Symbol Digit Modalities Test.

1999), and appear to be a good predictor of TLE with accurate lateralization. Therefore, evaluating the fornix and its asymmetry, even with visual interpretations, may be useful in support of presurgical planning (i.e., for surgical resection) for patients with medically intractable TLE. In addition, low frequency depth electrode stimulation of the fornix led to hippocampal and posterior cingulum responses, demonstrating these functional connections, and reduced interictal epileptiform discharges and seizures in patients with intractable mesial temporal lobe epilepsy, without affecting their memory (Koubeissi et al., 2013). Depth electrode stimulation of the fornix also led to either ipsilateral or contralateral hippocampal responses, which again confirmed these neural pathway connections and explained how seizure discharge might spread between homotopic mesial temporal structures without neocortical involvement (Lacuey et al., 2014).

Lastly, a recent DTI study, using tractography, found that patients with juvenile myoclonic epilepsy (JME) had lower FA in the crus of the fornix, body of the corpus callosum and many other major white matter tracts, but not in those with only generalized tonic-clonic seizures, suggesting different neuroanatomical substrates in these two different types of idiopathic generalized epilepsies (Liu et al., 2011a). Taken together, these studies demonstrate that the fornix may play a role in mediating seizure spreads across the cerebral hemispheres both in patients with temporal lobe epilepsy as well as in generalized epilepsies. However, it may also be a treatment target for deep brain stimulation or surgical approaches in these patients.

Traumatic Brain Injury (TBI) results from physical forces that damage the brain, which may cause cognitive impairments such as memory and attention deficits. TBI is also associated with atrophy of the fornix (Gale et al., 1993; Tate and Bigler, 2000; Tomaiuolo et al., 2004). The fornix is particularly susceptible to physical shearing forces (Tate and Bigler, 2000), probably due to its delicate fiber tracts that straddle both cerebral hemispheres. The effects of TBI on the fornix volume have been examined in relation to memory. However, only one of the three studies (Tate and Bigler, 2000; Gale et al., 1993; Tomaiuolo et al., 2004) found a correlation between forniceal atrophy and memory performance (Tomaiuolo et al., 2004). However, using DTI with TBSS, white matter abnormalities were observed in several regions of the brain in TBI patients, but only lower FA in the fornix correlated with worse performance in associative memory and learning in both the TBI and healthy control groups (Kinnunen et al., 2011). In another study, patients with diffuse TBI, which leads to diffuse axonal injury, had globally decreased FA in the brain. However, regional analyses showed that lower FA in the superior longitudinal fasciculus was associated with working memory deficits, while lower forniceal FA was associated with poorer declarative memory in these TBI patients with diffuse injuries (Palacios et al., 2011). Lower forniceal FA and memory deficits were consistently found in TBI patients compared to healthy controls (Palacios et al., 2011; Adnan et al., 2013), suggesting a critical role of the fornix integrity in the development of memory impairments after TBI.

DISCUSSION

LIMITATIONS AND FUTURE STUDIES

Several factors have limited the study of the fornix. First, the anatomy of the fornix makes it difficult to evaluate the abnormalities in this brain structure. Specific regions of the fornix (i.e., column, crus or pre-commissural fornix) are even more difficult to visualize or quantify. DTI has improved the visualization of the fornix, which has led to many more studies of this structure in several neurological disorders. However, the forniceal DTI measures in the published studies are often affected by the fornix's close proximity to the ventricles, which can lead to partial volume effects from the CSF in the ventricles. While CSF suppression (using inversion recovery pulses on MRI) would suppress the signals from CSF, most of the DTI studies did not apply such CSF signal suppression during the image acquisition. Partial volume

effect from adjacent CSF signal may generate biased (higher) diffusivity and (lower) FA values of the fornix although this structure is generally well delineated on DTI. Nevertheless, refined methods have been developed to minimize the CSF partial volume effect on DTI and obtain higher resolution images. These improved DTI acquisition methods include reducing the repetition time and using non-zero minimum diffusion weighting (Baron and Beaulieu, 2014), or increased the image resolution of DTI (Herbst et al., 2014) by combining multiplexed sensitivity encoding (Chen et al., 2013) and prospective motion correction (Zaitsev et al., 2006; Herbst et al., 2012; Gumus et al., 2014). Others have developed novel criteria for DTI metric selection (Pasternak et al., 2010) using relationships between distribution and distance of the measured diffusion quantities or the use of multi-contrast MRI (Tang et al., 2014) with an automated parcellation atlas, which may further delineate and accurately assess how the fornix might be affected in various brain disorders. Second, the various methods (e.g., manual or automated ROIs, TBSS, tractography) used to measure the diffusivities and FA in the fornix do not always yield the same results. Systematic comparisons or the use of more than one approach to measure the fornix in the same datasets could provide validation to the abnormal findings in the various brain disorders. Third, the majority of the studies reviewed utilized a cross-sectional design, longitudinal follow-up studies would minimize the potential confounding effects of inter-subject variability (e.g., due to differences in disease severity or illness duration) or premorbid group differences. Intra-subject measurements in longitudinal evaluations are more sensitive in detecting, predicting and monitoring neurodegeneration compared to cross-sectional measures. Despite these limitations, the studies reviewed consistently showed correlations between DTI metrics in the fornix and memory performance of typically aging individuals and in patients with various neurodegenerative and neuropsychiatric disorders. These findings strengthen the role of the fornix as a useful imaging marker to predict memory deficits or impairments.

CONCLUSION

The fornix is clearly a critical component of the limbic system and is closely linked to memory performance. Alterations of the fornix are related to cognitive functions in childhood and in later life. In addition, forniceal changes were found in schizophrenia and other psychiatric disorders. Therefore, the fornix appears to be more than a clinical surrogate marker of memory impairments for neurodegenerative and neuroinflammatory diseases, such as Alzheimer's disease and multiple sclerosis. Although the fornix is one of the less heritable brain structures (Jahanshad et al., 2013), few studies reported how genes might influence the typical development or aging of the fornix. Imaging genetics might be useful to further elucidate the role of the fornix in various brain disorders as well as during healthy neurodevelopment and brain aging.

ACKNOWLEDGMENTS

We thank Eric Cunningham and Kristin Lee for carefully editing this manuscript. NIH grant supports: K24 DA016170 & G12-MD007601.

REFERENCES

Abdul-Rahman, M. F., Qiu, A., and Sim, K. (2011). Regionally specific white matter disruptions of fornix and cingulum in schizophrenia. *PLoS ONE* 6:e18652. doi: 10.1371/journal.pone.0018652

Adnan, A., Crawley, A., Mikulis, D., Moscovitch, M., Colella, B., and Green, R. (2013). Moderate-severe traumatic brain injury causes delayed loss of white matter integrity: evidence of fornix deterioration in the chronic stage of injury. *Brain Inj.* 27, 1415–1422. doi: 10.3109/02699052.2013.823659

Aggleton, J. P., Vann, S. D., Oswald, C. J., and Good, M. (2000). Identifying cortical inputs to the rat hippocampus that subserve allocentric spatial processes: a simple problem with a complex answer. *Hippocampus* 10, 466–474. doi: 10.1002/1098-1063(2000)10:4<466::AID-HIPO13>3.0.CO;2-Y

Arnold, S. E., Franz, B. R., Gur, R. C., Gur, R. E., Shapiro, R. M., Moberg, P. J., et al. (1995). Smaller neuron size in schizophrenia in hippocampal subfields that mediate cortical-hippocampal interactions. *Am. J. Psychiatry* 152, 738–748.

Asato, M. R., Terwilliger, R., Woo, J., and Luna, B. (2010). White matter development in adolescence: a DTI study. *Cereb. Cortex* 20, 2122–2131. doi: 10.1093/cercor/bhp282

Baldwin, G. N., Tsuruda, J. S., Maravilla, K. R., Hamill, G. S., and Hayes, C. E. (1994). The fornix in patients with seizures caused by unilateral hippocampal sclerosis: detection of unilateral volume loss on MR images. *AJR Am. J. Roentgenol.* 162, 1185–1189. doi: 10.2214/ajr.162.5.8166008

Baron, C. A., and Beaulieu, C. (2014). Acquisition strategy to reduce cerebrospinal fluid partial volume effects for improved DTI tractography. *Magn. Reson. Med.* doi: 10.1002/mrm.25226. [Epub ahead of print].

Bossy-Wetzel, E., Schwarzenbacher, R., and Lipton, S. A. (2004). Molecular pathways to neurodegeneration. *Nat. Med.* 10, S2–S9. doi: 10.1038/nm1067

Brisch, R., Bernstein, H. G., Stauch, R., Dobrowolny, H., Krell, D., Truebner, K.,et al. (2008). The volumes of the fornix in schizophrenia and affective disorders: a post-mortem study. *Psychiatry Res.* 164, 265–273. doi: 10.1016/j.pscychresns.2007.12.007

Brissart, H., Daniel, F., Morele, E., Leroy, M., Debouverie, M., and Defer, G. L. (2011). [Cognitive rehabilitation in multiple sclerosis: a review of the literature]. *Rev. Neurol. (Paris)* 167, 280–290. doi: 10.1016/j.neurol.2010.07.039

Broca, P. P. (1890). "Anatomie comparée des circonvolutions cérébrales," in *Extrait de la "Revue d'Anthropologie,"* ed Masson (Paris: Elsevier-France), Sér.2,. T. 1, 385–498.

Burzynska, A. Z., Preuschhof, C., Backman, L., Nyberg, L., Li, S. C., Lindenberger, U., et al. (2010). Age-related differences in white matter microstructure: region-specific patterns of diffusivity. *Neuroimage* 49, 2104–2112. doi: 10.1016/j.neuroimage.2009.09.041

Callen, D. J., Black, S. E., Gao, F., Caldwell, C. B., and Szalai, J. P. (2001). Beyond the hippocampus: MRI volumetry confirms widespread limbic atrophy in AD. *Neurology* 57, 1669–1674. doi: 10.1212/WNL.57.9.1669

Canu, E., Agosta, F., Spinelli, E. G., Magnani, G., Marcone, A., Scola, E., et al. (2013). White matter microstructural damage in Alzheimer's disease at different ages of onset. *Neurobiol. Aging* 34, 2331–2340. doi: 10.1016/j.neurobiolaging.2013.03.026

Chance, S. A., Esiri, M. M., and Crow, T. J. (2005). Macroscopic brain asymmetry is changed along the antero-posterior axis in schizophrenia. *Schizophr. Res.* 74, 163–170. doi: 10.1016/j.schres.2004.09.001

Chance, S. A., Highley, J. R., Esiri, M. M., and Crow, T. J. (1999). Fiber content of the fornix in schizophrenia: lack of evidence for a primary limbic encephalopathy. *Am. J. Psychiatry* 156, 1720–1724.

Chang, L., Friedman, J., Ernst, T., Zhong, K., Tsopelas, N. D., and Davis, K. (2007). Brain metabolite abnormalities in the white matter of elderly schizophrenic subjects: implication for glial dysfunction. *Biol. Psychiatry* 62, 1396–1404. doi: 10.1016/j.biopsych.2007.05.025

Chen, N. K., Guidon, A., Chang, H. C., and Song, A. W. (2013). A robust multi-shot scan strategy for high-resolution diffusion weighted MRI enabled by multiplexed sensitivity-encoding (MUSE). *Neuroimage* 72, 41–7. doi: 10.1016/j.neuroimage.2013.01.038

Copenhaver, B. R., Rabin, L. A., Saykin, A. J., Roth, R. M., Wishart, H. A., Flashman, L. A., et al. (2006). The fornix and mammillary bodies in older adults with Alzheimer's disease, mild cognitive impairment, and cognitive complaints: a volumetric MRI study. *Psychiatry Res.* 147, 93–103. doi: 10.1016/j.pscychresns.2006.01.015

Crow, T. J., Colter, N., Frith, C. D., Johnstone, E. C., and Owens, D. G. (1989). Developmental arrest of cerebral asymmetries in early onset schizophrenia. *Psychiatry Res*. 29, 247–253.

Cui, Y., Sachdev, P. S., Lipnicki, D. M., Jin, J. S., Luo, S., Zhu, W., et al. (2012). Predicting the development of mild cognitive impairment: a new use of pattern recognition. *Neuroimage* 60, 894–901. doi: 10.1016/j.neuroimage.2012.01.084

Davenport, N. D., Karatekin, C., White, T., and Lim, K. O. (2010). Differential fractional anisotropy abnormalities in adolescents with ADHD or schizophrenia. *Psychiatry Res*. 181, 193–198. doi: 10.1016/j.pscychresns.2009.10.012

Davies, D. C., Wardell, A. M., Woolsey, R., and James, A. C. (2001). Enlargement of the fornix in early-onset schizophrenia: a quantitative MRI study. *Neurosci. Lett*. 301, 163–166. doi: 10.1016/S0304-3940(01)01637-8

DeLisi, L. E., Sakuma, M., Kushner, M., Finer, D. L., Hoff, A. L., and Crow, T. J. (1997). Anomalous cerebral asymmetry and language processing in schizophrenia. *Schizophr. Bull*. 23, 255–271.

Dineen, R. A., Bradshaw, C. M., Constantinescu, C. S., and Auer, D. P. (2012). Extra-hippocampal subcortical limbic involvement predicts episodic recall performance in multiple sclerosis. *PLoS ONE* 7:e44942. doi: 10.1371/journal.pone.0044942

Dineen, R. A., Vilisaar, J., Hlinka, J., Bradshaw, C. M., Morgan, P. S., Constantinescu, C. S., et al. (2009). Disconnection as a mechanism for cognitive dysfunction in multiple sclerosis. *Brain* 132(Pt 1), 239–249. doi: 10.1093/brain/awn275

Douaud, G., Menke, R. A., Gass, A., Monsch, A. U., Rao, A., Whitcher, B., et al. (2013). Brain microstructure reveals early abnormalities more than two years prior to clinical progression from mild cognitive impairment to Alzheimer's disease. *J. Neurosci.* 33, 2147–2155. doi: 10.1523/JNEUROSCI.4437-12.2013

Douet, V., Chang, L., Pritchett, A., Lee, K., Keating, B., Bartsch, H., et al. (2014). Schizophrenia-risk variant rs6994992 in the neuregulin-1 gene on brain developmental trajectories in typically-developing children. *Transl. Psychiatry* doi: 10.1038/tp.2014.41

Dubois, J., Dehaene-Lambertz, G., Soares, C., Cointepas, Y., Le Bihan, D., and Hertz-Pannier, L. (2008). Microstructural correlates of infant functional development: example of the visual pathways. *J. Neurosci*. 28, 1943–1948. doi: 10.1523/JNEUROSCI.5145-07.2008

Fink, F., Eling, P., Rischkau, E., Beyer, N., Tomandl, B., Klein, J., et al. (2010). The association between California verbal learning test performance and fibre impairment in multiple sclerosis: evidence from diffusion tensor imaging. *Mult. Scler*. 16, 332–341. doi: 10.1177/1352458509356367

Fitzsimmons, J., Hamoda, H. M., Swisher, T., Terry, D., Rosenberger, G., Seidman, L. J., et al. (2014). Diffusion tensor imaging study of the fornix in first episode schizophrenia and in healthy controls. *Schizophr. Res*. 156, 157–160. doi: 10.1016/j.schres.2014.04.022

Fitzsimmons, J., Kubicki, M., Smith, K., Bushell, G., Estepar, R. S., Westin, C. F., et al. (2009). Diffusion tractography of the fornix in schizophrenia. *Schizophr. Res*. 107, 39–46. doi: 10.1016/j.schres.2008.10.022

Fletcher, E., Raman, M., Huebner, P., Liu, A., Mungas, D., Carmichael, O., et al. (2013). Loss of fornix white matter volume as a predictor of cognitive impairment in cognitively normal elderly individuals. *JAMA Neurol*. 70, 1389–1395. doi: 10.1001/jamaneurol.2013.3263

Gaffan, E. A., Gaffan, D., and Hodges, J. R. (1991). Amnesia following damage to the left fornix and to other sites. A comparative study. *Brain* 114(Pt 3), 1297–1313.

Gale, S. D., Burr, R. B., Bigler, E. D., and Blatter., D. (1993). Fornix degeneration and memory in traumatic brain injury. *Brain Res. Bull*. 32, 345–349.

Garcia-Bengochea, F., and Friedman, W. A. (1987). Persistent memory loss following section of the anterior fornix in humans. A historical review. *Surg. Neurol*. 27, 361–364.

Gelb, D. J., Oliver, E., and Gilman, S. (1999). Diagnostic criteria for Parkinson disease. *Arch. Neurol*. 56, 33–39.

Giorgio, A., Santelli, L., Tomassini, V., Bosnell, R., Smith, S., De Stefano, N., et al. (2010). Age-related changes in grey and white matter structure throughout adulthood. *Neuroimage* 51, 943–951. doi: 10.1016/j.neuroimage.2010.03.004

Gumus, K., Keating, B., Poser, B. A., Armstrong, B., Chang, L., Maclaren, J., et al. (2014). Prevention of motion-induced signal loss in diffusion-weighted echo-planar imaging by dynamic restoration of gradient moments. *Magn. Reson. Med*. 71, 2006–2013. doi: 10.1002/mrm.24857

Hattori, T., Sato, R., Aoki, S., Yuasa, T., and Mizusawa, H. (2012). Different patterns of fornix damage in idiopathic normal pressure hydrocephalus and Alzheimer disease. *AJNR Am. J. Neuroradiol.* 33, 274–279. doi: 10.3174/ajnr.A2780

Heckers, S., Heinsen, H., Geiger, B., and Beckmann, H. (1991). Hippocampal neuron number in schizophrenia. A stereological study. *Arch. Gen. Psychiatry* 48, 1002–1008.

Herbst, M., Maclaren, J., Weigel, M., Korvink, J., Hennig, J., and Zaitsev, M. (2012). Prospective motion correction with continuous gradient updates in diffusion weighted imaging. *Magn. Reson. Med*. 67, 326–338. doi: 10.1002/mrm.23230

Herbst, M., Zahneisen, B., Knowes, B., Zaitsev, M., and Ernst, T. (2014). Prospective motion correction of segmented diffusion weighted EPI. *Mag. Reson. Med.* doi: 10.1002/mrm.25547. [Epub ahead of print].

Hermoye, L., Saint-Martin, C., Cosnard, G., Lee, S. K., Kim, J., Nassogne, M. C., et al. (2006). Pediatric diffusion tensor imaging: normal database and observation of the white matter maturation in early childhood. *Neuroimage* 29, 493–504. doi: 10.1016/j.neuroimage.2005.08.017

Hori, A. (1995). Unilateral volume loss of the fornix in patients with seizures caused by ipsilateral hippocampal sclerosis. *AJR Am. J. Roentgenol.* 164, 1304. doi: 10.2214/ajr.164.5.7717266

Huang, H., Fan, X., Weiner, M., Martin-Cook, K., Xiao, G., Davis, J., et al. (2012). Distinctive disruption patterns of white matter tracts in Alzheimer's disease with full diffusion tensor characterization. *Neurobiol. Aging* 33, 2029–2045. doi: 10.1016/j.neurobiolaging.2011.06.027

Huang, H., Xue, R., Zhang, J., Ren, T., Richards, L. J., Yarowsky, P., et al. (2009). Anatomical characterization of human fetal brain development with diffusion tensor magnetic resonance imaging. *J. Neurosci*. 29, 4263–4273. doi: 10.1523/JNEUROSCI.2769-08.2009

Huang, H., Zhang, J., Wakana, S., Zhang, W., Ren, T., Richards, L. J., et al. (2006). White and gray matter development in human fetal, newborn and pediatric brains. *Neuroimage* 33, 27–38. doi: 10.1016/j.neuroimage.2006.06.009

Jahanshad, N., Kochunov, P. V., Sprooten, E., Mandl, R. C., Nichols, T. E., Almasy, L., et al. (2013). Multi-site genetic analysis of diffusion images and voxelwise heritability analysis: a pilot project of the ENIGMA-DTI working group. *Neuroimage* 81, 455–469. doi: 10.1016/j.neuroimage.2013.04.061

Jang, S. H., Cho, S. H., and Chang, M. C. (2011). Age-related degeneration of the fornix in the human brain: a diffusion tensor imaging study. *Int. J. Neurosci.* 121, 94–100. doi: 10.3109/00207454.2010.531894

Kantarci, K., Senjem, M. L., Avula, R., Zhang, B., Samikoglu, A. R., Weigand, S. D., et al. (2011). Diffusion tensor imaging and cognitive function in older adults with no dementia. *Neurology* 77, 26–34. doi: 10.1212/WNL.0b013e31822313dc

Kasai, K., Shenton, M. E., Salisbury, D. F., Hirayasu, Y., Lee, C. U., Ciszewski, A. A., et al. (2003). Progressive decrease of left superior temporal gyrus gray matter volume in patients with first-episode schizophrenia. *Am. J. Psychiatry* 160, 156–164. doi: 10.1176/appi.ajp.160.1.156

Kendi, M., Kendi, A. T., Lehericy, S., Ducros, M., Lim, K. O., Ugurbil, K., et al. (2008). Structural and diffusion tensor imaging of the fornix in childhood- and adolescent-onset schizophrenia. *J. Am. Acad. Child Adolesc. Psychiatry* 47, 826–832. doi: 10.1097/CHI.Ob013e318172ef36

Kern, K. C., Ekstrom, A. D., Suthana, N. A., Giesser, B. S., Montag, M., Arshanapalli, A., et al. (2012). Fornix damage limits verbal memory functional compensation in multiple sclerosis. *Neuroimage* 59, 2932–2940. doi: 10.1016/j.neuroimage.2011.09.071

Kim, H. J., Kim, S. J., Kim, H. S., Choi, C. G., Kim, N., Han, S., et al. (2013). Alterations of mean diffusivity in brain white matter and deep gray matter in Parkinson's disease. *Neurosci. Lett*. 550, 64–68. doi: 10.1016/j.neulet.2013.06.050

Kim, J. H., Tien, R. D., Felsberg, G. J., Osumi, A. K., and Lee, N. (1995). Clinical significance of asymmetry of the fornix and mamillary body on MR in hippocampal sclerosis. *AJNR Am. J. Neuroradiol.* 16, 509–515.

King, E. C., Pattwell, S. S., Sun, A., Glatt, C. E., and Lee, F. S. (2013). Nonlinear developmental trajectory of fear learning and memory. *Ann. N.Y. Acad. Sci*. 1304, 62–69. doi: 10.1111/nyas.12280

Kinnunen, K. M., Greenwood, R., Powell, J. H., Leech, R., Hawkins, P. C., Bonnelle, V., et al. (2011). White matter damage and cognitive impairment after traumatic brain injury. *Brain* 134(Pt 2), 449–463. doi: 10.1093/brain/awq347

Kochunov, P., and Hong, L. E. (2014). Neurodevelopmental and neurodegenerative models of schizophrenia: white matter at the center stage. *Schizophr. Bull*. 40, 721–728. doi: 10.1093/schbul/sbu070

Koenig, K. A., Lowe, M. J., Lin, J., Sakaie, K. E., Stone, L., Bermel, R. A., et al. (2013). Sex differences in resting-state functional connectivity in multiple sclerosis. *AJNR Am. J. Neuroradiol.* 34, 2304–2311. doi: 10.3174/ajnr.A3630

Koenig, K. A., Sakaie, K. E., Lowe, M. J., Lin, J., Stone, L., Bermel, R. A., et al. (2014). Hippocampal volume is related to cognitive decline and fornicial diffusion measures in multiple sclerosis. *Magn. Reson. Imaging* 32, 354–358. doi: 10.1016/j.mri.2013.12.012

Koubeissi, M. Z., Kahriman, E., Syed, T. U., Miller, J., and Durand, D. M. (2013). Low-frequency electrical stimulation of a fiber tract in temporal lobe epilepsy. *Ann. Neurol.* 74, 223–231. doi: 10.1002/ana.23915

Kuroki, N., Kubicki, M., Nestor, P. G., Salisbury, D. F., Park, H. J., Levitt, J. J., et al. (2006). Fornix integrity and hippocampal volume in male schizophrenic patients. *Biol. Psychiatry* 60, 22–31. doi: 10.1016/j.biopsych.2005.09.021

Kuzniecky, R., Bilir, E., Gilliam, F., Faught, E., Martin, R., and Hugg, J. (1999). Quantitative MRI in temporal lobe epilepsy: evidence for fornix atrophy. *Neurology* 53, 496–501.

Lacuey, N., Zonjy, B., Kahriman, E. S., Kaffashi, F., Miller, J., and Luders, H. O. (2014). Functional connectivity between right and left mesial temporal structures. *Brain Struct. Funct.* doi: 10.1007/s00429-014-0810-0. [Epub ahead of print].

Lebel, C., Gee, M., Camicioli, R., Wieler, M., Martin, W., and Beaulieu, C. (2012). Diffusion tensor imaging of white matter tract evolution over the lifespan. *Neuroimage* 60, 340–352. doi: 10.1016/j.neuroimage.2011.11.094

Lee, C. E., Danielian, L. E., Thomasson, D., and Baker, E. H. (2009). Normal regional fractional anisotropy and apparent diffusion coefficient of the brain measured on a 3 T MR scanner. *Neuroradiology* 51, 3–9. doi: 10.1007/s00234-008-0441-3

Lee, S. H., Kubicki, M., Asami, T., Seidman, L. J., Goldstein, J. M., Mesholam-Gately, R. I., et al. (2013). Extensive white matter abnormalities in patients with first-episode schizophrenia: a diffusion tensor iimaging (DTI) study. *Schizophr. Res.* 143, 231–238. doi: 10.1016/j.schres.2012.11.029

Liu, M., Concha, L., Beaulieu, C., and Gross, D. W. (2011a). Distinct white matter abnormalities in different idiopathic generalized epilepsy syndromes. *Epilepsia* 52, 2267–2275. doi: 10.1111/j.1528-1167.2011.03313.x

Liu, Y., Spulber, G., Lehtimäki, K. K., Könönen, M., Hallikainen, I., Gröhn, H., et al. (2011b). Diffusion tensor imaging and tract-based spatial statistics in Alzheimer's disease and mild cognitive impairment. *Neurobiol. Aging* 32, 1558–1571. doi: 10.1016/j.neurobiolaging.2009.10.006

Luck, D., Malla, A. K., Joober, R., and Lepage, M. (2010). Disrupted integrity of the fornix in first-episode schizophrenia. *Schizophr. Res.* 119, 61–64. doi: 10.1016/j.schres.2010.03.027

Maier-Hein, K. H., Brunner, R., Lutz, K., Henze, R., Parzer, P., Feigl, N., et al. (2014). Disorder-specific white matter alterations in adolescent borderline personality disorder. [Research Support, Non-U.S. Gov't]. *Biol. Psychiatry* 75, 81–88. doi: 10.1016/j.biopsych.2013.03.031

Matsui, H., Nishinaka, K., Oda, M., Niikawa, H., Komatsu, K., Kubori, T., et al. (2006). Disruptions of the fornix fiber in Parkinsonian patients with excessive daytime sleepiness. *Parkinsonism Relat. Disord.* 12, 319–322. doi: 10.1016/j.parkreldis.2006.01.007

Matsui, H., Nishinaka, K., Oda, M., Niikawa, H., Komatsu, K., Kubori, T., et al. (2007). Depression in Parkinson's disease. Diffusion tensor imaging study. *J. Neurol.* 254, 1170–1173. doi: 10.1007/s00415-006-0236-6

McDonald, B., Highley, J. R., Walker, M. A., Herron, B. M., Cooper, S. J., Esiri, M. M., et al. (2000). Anomalous asymmetry of fusiform and parahippocampal gyrus gray matter in schizophrenia: a postmortem study. [Comparative Study Research Support, Non-U.S. Gov't]. *Am. J. Psychiatry* 157, 40–47. doi: 10.1176/ajp.157.1.40

McKinlay, A., Grace, R. C., Dalrymple-Alford, J. C., and Roger, D. (2010). Characteristics of executive function impairment in Parkinson's disease patients without dementia. *J. Int. Neuropsychol. Soc.* 16, 268–277. doi: 10.1017/S1355617709991299

Metzler-Baddeley, C., Hunt, S., Jones, D. K., Leemans, A., Aggleton, J. P., and O'Sullivan, M. J. (2012). Temporal association tracts and the breakdown of episodic memory in mild cognitive impairment. *Neurology* 79, 2233–2240. doi: 10.1212/WNL.0b013e31827689e8

Metzler-Baddeley, C., Jones, D. K., Belaroussi, B., Aggleton, J. P., and O'Sullivan, M. J. (2011). Frontotemporal connections in episodic memory and aging: a diffusion MRI tractography study. *J. Neurosci.* 31, 13236–13245. doi: 10.1523/JNEUROSCI.2317-11.2011

Michielse, S., Coupland, N., Camicioli, R., Carter, R., Seres, P., Sabino, J., et al. (2010). Selective effects of aging on brain white matter microstructure: a diffusion tensor imaging tractography study. *Neuroimage* 52, 1190–1201. doi: 10.1016/j.neuroimage.2010.05.019

Mielke, M. M., Kozauer, N. A., Chan, K. C., George, M., Toroney, J., Zerrate, M., et al. (2009). Regionally-specific diffusion tensor imaging in mild cognitive impairment and Alzheimer's disease. *Neuroimage* 46, 47–55. doi: 10.1016/j.neuroimage.2009.01.054

Mielke, M. M., Okonkwo, O. C., Oishi, K., Mori, S., Tighe, S., Miller, M. I., et al. (2012). Fornix integrity and hippocampal volume predict memory decline and progression to Alzheimer's disease. *Alzheimers Dement.* 8, 105–113. doi: 10.1016/j.jalz.2011.05.2416

Mielke, M. M., Vemuri, P., and Rocca, W. A. (2014). Clinical epidemiology of Alzheimer's disease: assessing sex and gender differences. *Clin. Epidemiol.* 6, 37–48. doi: 10.2147/CLEP.S37929

Mitchell, R. L., and Crow, T. J. (2005). Right hemisphere language functions and schizophrenia: the forgotten hemisphere? *Brain* 128(Pt 5), 963–978. doi: 10.1093/brain/awh466

Mitelman, S. A., Shihabuddin, L., Brickman, A. M., and Buchsbaum, M. S. (2005). Cortical intercorrelations of temporal area volumes in schizophrenia. *Schizophr. Res.* 76, 207–229. doi: 10.1016/j.schres.2005.01.010

Nestor, P. G., Kubicki, M., Kuroki, N., Gurrera, R. J., Niznikiewicz, M., Shenton, M. E., et al. (2007). Episodic memory and neuroimaging of hippocampus and fornix in chronic schizophrenia. *Psychiatry Res.* 155, 21–28. doi: 10.1016/j.pscychresns.2006.12.020

Nolte, J. (2009). *The Human Brain: An Introduction Ot Its Functional Anatomy*. Philadelphia, PA: Mosby Elsevier.

Nowrangi, M. A., Lyketsos, C. G., Leoutsakos, J. M., Oishi, K., Albert, M., Mori, S., et al. (2013). Longitudinal, region-specific course of diffusion tensor imaging measures in mild cognitive impairment and Alzheimer's disease. *Alzheimers Dement.* 9, 519–528. doi: 10.1016/j.jalz.2012.05.2186

Oishi, K., Mielke, M. M., Albert, M., Lyketsos, C. G., and Mori, S. (2012). The fornix sign: a potential sign for Alzheimer's disease based on diffusion tensor imaging. *J. Neuroimaging* 22, 365–374. doi: 10.1111/j.1552-6569.2011.00633.x

Ozturk, A., Yousem, D. M., Mahmood, A., and El Sayed, S. (2008). Prevalence of asymmetry of mamillary body and fornix size on MR imaging. *AJNR Am. J. Neuroradiol.* 29, 384–387. doi: 10.3174/ajnr.A0801

Pagani, E., Agosta, F., Rocca, M. A., Caputo, D., and Filippi, M. (2008). Voxel-based analysis derived from fractional anisotropy images of white matter volume changes with aging. *Neuroimage* 41, 657–667. doi: 10.1016/j.neuroimage.2008.03.021

Palacios, E. M., Fernandez-Espejo, D., Junque, C., Sanchez-Carrion, R., Roig, T., Tormos, J. M., et al. (2011). Diffusion tensor imaging differences relate to memory deficits in diffuse traumatic brain injury. *BMC Neurol.* 11:24. doi: 10.1186/1471-2377-11-24

Papez, J. W. (1937). A proposed mechanism of emotion. 1937. *J. Neuropsychiatry Clin. Neurosci.* 7, 103–112.

Pasternak, O., Sochen, N., and Basser, P. J. (2010). The effect of metric selection on the analysis of diffusion tensor MRI data. *Neuroimage* 49, 2190–2204. doi: 10.1016/j.neuroimage.2009.10.071

Pelletier, A., Periot, O., Dilharreguy, B., Hiba, B., Bordessoules, M., Peres, K., et al. (2013). Structural hippocampal network alterations during healthy aging: a multi-modal MRI study. *Front. Aging Neurosci.* 5:84. doi: 10.3389/fnagi.2013.00084

Penfield, W., and Milner, B. (1958). Memory deficit produced by bilateral lesions in the hippocampal zone. *AMA Arch. Neurol. Psychiatry* 79, 475–497.

Peper, J. S., Brouwer, R. M., Schnack, H. G., van Baal, G. C., van Leeuwen, M., van den Berg, S. M., et al. (2008). Cerebral white matter in early puberty is associated with luteinizing hormone concentrations. *Psychoneuroendocrinology* 33, 909–915. doi: 10.1016/j.psyneuen.2008.03.017

Peper, J. S., Brouwer, R. M., Schnack, H. G., van Baal, G. C., van Leeuwen, M., van den Berg, S. M., et al. (2009). Sex steroids and brain structure in pubertal boys and girls. *Psychoneuroendocrinology* 34, 332–342. doi: 10.1016/j.psyneuen.2008.09.012

Petersen, R. C. (2004). Mild cognitive impairment as a diagnostic entity. *J. Intern. Med.* 256, 183–194. doi: 10.1111/j.1365-2796.2004.01388.x

Petersen, R. C., Doody, R., Kurz, A., Mohs, R. C., Morris, J. C., Rabins, P. V., et al. (2001). Current concepts in mild cognitive impairment. *Arch. Neurol.* 58, 1985–1992. doi: 10.1001/archneur.58.12.1985

Pihlajamaki, M., Jauhiainen, A. M., and Soininen, H. (2009). Structural and functional MRI in mild cognitive impairment. *Curr. Alzheimer Res.* 6, 179–185. doi: 10.2174/156720509787602898

Pivneva, T. A. (2008). Microglia in normal condition and pathology. *Fiziol. Zh.* 54, 81–89.

Rados, M., Judas, M., and Kostovic, I. (2006). *In vitro* MRI of brain development. *Eur. J. Radiol.* 57, 187–198. doi: 10.1016/j.ejrad.2005.11.019

Rajmohan, V., and Mohandas, E. (2007). The limbic system. *Indian J. Psychiatry*, 49, 132–139. doi: 10.4103/0019-5545.33264

Ranjeva, J. P., Audoin, B., Au Duong, M. V., Ibarrola, D., Confort-Gouny, S., Malikova, I., et al. (2005). Local tissue damage assessed with statistical mapping analysis of brain magnetization transfer ratio: relationship with functional status of patients in the earliest stage of multiple sclerosis. *AJNR Am. J. Neuroradiol.* 26, 119–127.

Rapoport, J. L., Giedd, J. N., and Gogtay, N. (2012). Neurodevelopmental model of schizophrenia: update 2012. *Mol. Psychiatry* 17, 1228–1238. doi: 10.1038/mp.2012.23

Ringman, J. M., O'Neill, J., Geschwind, D., Medina, L., Apostolova, L. G., Rodriguez, Y., et al. (2007). Diffusion tensor imaging in preclinical and presymptomatic carriers of familial Alzheimer's disease mutations. *Brain* 130(Pt 7), 1767–1776. doi: 10.1093/brain/awm102

Roosendaal, S. D., Geurts, J. J., Vrenken, H., Hulst, H. E., Cover, K. S., Castelijns, J. A., et al. (2009). Regional DTI differences in multiple sclerosis patients. *Neuroimage* 44, 1397–1403. doi: 10.1016/j.neuroimage.2008.10.026

Rudebeck, S. R., Scholz, J., Millington, R., Rohenkohl, G., Johansen-Berg, H., and Lee, A. C. (2009). Fornix microstructure correlates with recollection but not familiarity memory. *J. Neurosci.* 29, 14987–14992. doi: 10.1523/JNEUROSCI.4707-09.2009

Sala, S., Agosta, F., Pagani, E., Copetti, M., Comi, G., and Filippi, M. (2012). Microstructural changes and atrophy in brain white matter tracts with aging. *Neurobiol. Aging* 33, 488–498. doi: 10.1016/j.neurobiolaging.2010.04.027

Samson, R. D., and Barnes, C. A. (2013). Impact of aging brain circuits on cognition. *Eur. J. Neurosci.* 37, 1903–1915. doi: 10.1111/ejn.12183

Sasson, E., Doniger, G. M., Pasternak, O., Tarrasch, R., and Assaf, Y. (2013). White matter correlates of cognitive domains in normal aging with diffusion tensor imaging. *Front. Neurosci.* 7:32. doi: 10.3389/fnins.2013.00032

Schaefer, J., Giangrande, E., Weinberger, D. R., and Dickinson, D. (2013). The global cognitive impairment in schizophrenia: consistent over decades and around the world. *Schizophr. Res.* 150, 42–50. doi: 10.1016/j.schres.2013.07.009

Schmithorst, V. J., Holland, S. K., and Dardzinski, B. J. (2008). Developmental differences in white matter architecture between boys and girls. *Hum. Brain Mapp.* 29, 696–710. doi: 10.1002/hbm.20431

Sexton, C. E., Kalu, U. G., Filippini, N., Mackay, C. E., and Ebmeier, K. P. (2011). A meta-analysis of diffusion tensor imaging in mild cognitive impairment and Alzheimer's disease. *Neurobiol. Aging* 32, 2322. doi: 10.1016/j.neurobiolaging.2010.05.019

Sexton, C. E., Mackay, C. E., Lonie, J. A., Bastin, M. E., Terriére, E., O'Carroll, R. E., et al. (2010). MRI correlates of episodic memory in Alzheimer's disease, mild cognitive impairment, and healthy aging. [Research Support, Non-U.S. Gov't]. *Psychiatry Res.* 184, 57–62. doi: 10.1016/j.pscychresns.2010.07.005

Simmonds, D. J., Hallquist, M. N., Asato, M., and Luna, B. (2014). Developmental stages and sex differences of white matter and behavioral development through adolescence: a longitudinal diffusion tensor imaging (DTI) study. *Neuroimage* 92, 356–368. doi: 10.1016/j.neuroimage.2013.12.044

Smith, S. M., Jenkinson, M., Johansen-Berg, H., Rueckert, D., Nichols, T. E., Mackay, C. E., et al. (2006). Tract-based spatial statistics: voxelwise analysis of multi-subject diffusion data. [Research Support, Non-U.S. Gov't]. *Neuroimage* 31, 1487–1505. doi: 10.1016/j.neuroimage.2006.02.024

Song, S. K., Sun, S. W., Ju, W. K., Lin, S. J., Cross, A. H., and Neufeld, A. H. (2003). Diffusion tensor imaging detects and differentiates axon and myelin degeneration in mouse optic nerve after retinal ischemia. *Neuroimage* 20, 1714–1722. doi: 10.1016/j.neuroimage.2003.07.005

Song, S. K., Sun, S. W., Ramsbottom, M. J., Chang, C., Russell, J., and Cross, A. H. (2002). Dysmyelination revealed through MRI as increased radial (but unchanged axial) diffusion of water. *Neuroimage* 17, 1429–1436. doi: 10.1006/nimg.2002.1267

Song, S. K., Yoshino, J., Le, T. Q., Lin, S. J., Sun, S. W., Cross, A. H., et al. (2005). Demyelination increases radial diffusivity in corpus callosum of mouse brain. *Neuroimage* 26, 132–40. doi: 10.1016/j.neuroimage.2005.01.028

Squire, L. R., and Zola-Morgan, S. (1991). The medial temporal lobe memory system. *Science* 253, 1380–1386.

Stadlbauer, A., Salomonowitz, E., Strunk, G., Hammen, T., and Ganslandt, O. (2008). Quantitative diffusion tensor fiber tracking of age-related changes in the limbic system. *Eur. Radiol.* 18, 130–137. doi: 10.1007/s00330-007-0733-8

Stricker, N. H., Schweinsburg, B. C., Delano-Wood, L., Wierenga, C. E., Bangen, K. J., Haaland, K. Y., et al. (2009). Decreased white matter integrity in late-myelinating fiber pathways in Alzheimer's disease supports retrogenesis. *Neuroimage* 45, 10–16. doi: 10.1016/j.neuroimage.2008.11.027

Sullivan, E. V., Rohlfing, T., and Pfefferbaum, A. (2010). Quantitative fiber tracking of lateral and interhemispheric white matter systems in normal aging: relations to timed performance. *Neurobiol. Aging* 31, 464–481. doi: 10.1016/j.neurobiolaging.2008.04.007

Syc, S. B., Harrison, D. M., Saidha, S., Seigo, M., Calabresi, P. A., and Reich, D. S. (2013). Quantitative MRI demonstrates abnormality of the fornix and cingulum in multiple sclerosis. *Mult. Scler. Int.* 2013:838719. doi: 10.1155/2013/838719

Takei, K., Yamasue, H., Abe, O., Yamada, H., Inoue, H., Suga, M., et al. (2008). Disrupted integrity of the fornix is associated with impaired memory organization in schizophrenia. *Schizophr. Res.* 103, 52–61. doi: 10.1016/j.schres.2008.03.008

Tang, X., Yoshida, S., Hsu, J., Huisman, T. A., Faria, A. V., Oishi, K., et al. (2014). Multi-contrast multi-atlas parcellation of diffusion tensor imaging of the human brain. *PLoS ONE* 9:e96985. doi: 10.1371/journal.pone.0096985

Tate, D. F., and Bigler, E. D. (2000). Fornix and hippocampal atrophy in traumatic brain injury. *Learn. Mem.* 7, 442–446. doi: 10.1101/lm.33000

Teipel, S. J., Grothe, M., Lista, S., Toschi, N., Garaci, F. G., and Hampel, H. (2013). Relevance of magnetic resonance imaging for early detection and diagnosis of Alzheimer disease. *Med. Clin. North Am.* 97, 399–424. doi: 10.1016/j.mcna.2012.12.013

Tomaiuolo, F., Carlesimo, G. A., Di Paola, M., Petrides, M., Fera, F., Bonanni, R., et al. (2004). Gross morphology and morphometric sequelae in the hippocampus, fornix, and corpus callosum of patients with severe non-missile traumatic brain injury without macroscopically detectable lesions: a T1 weighted MRI study. *J. Neurol. Neurosurg. Psychiatry* 75, 1314–1322. doi: 10.1136/jnnp.2003.017046

Vernooij, M. W., de Groot, M., van der Lugt, A., Ikram, M. A., Krestin, G. P., Hofman, A., et al. (2008). White matter atrophy and lesion formation explain the loss of structural integrity of white matter in aging. [Research Support, Non-U.S. Gov't]. *Neuroimage* 43, 470–477. doi: 10.1016/j.neuroimage.2008.07.052

Vita, A., De Peri, L., Deste, G., and Sacchetti, E. (2012). Progressive loss of cortical gray matter in schizophrenia: a meta-analysis and meta-regression of longitudinal MRI studies. *Transl. Psychiatry* 2, e190 doi: 10.1038/tp.2012.116

Westerhausen, R., Kreuder, F., Dos Santos Sequeira, S., Walter, C., Woerner, W., Wittling, R. A., et al. (2004). Effects of handedness and gender on macro- and microstructure of the corpus callosum and its subregions: a combined high-resolution and diffusion-tensor MRI study. *Brain Res. Cogn. Brain Res.* 21, 418–426. doi: 10.1016/j.cogbrainres.2004.07.002

White, T., Nelson, M., and Lim, K. O. (2008). Diffusion tensor imaging in psychiatric disorders. *Top Magn. Reson. Imaging* 19 97–109. doi: 10.1097/RMR.0b013e3181809f1e

Yanike, M., and Ferrera, V. P. (2014). Representation of outcome risk and action in the anterior caudate nucleus. *J. Neurosci.* 34, 3279–3290. doi: 10.1523/JNEUROSCI.3818-13.2014

Yasmin, H., Aoki, S., Abe, O., Nakata, Y., Hayashi, N., Masutani, Y., et al. (2009). Tract-specific analysis of white matter pathways in healthy subjects: a pilot study using diffusion tensor MRI. *Neuroradiology* 51, 831–840. doi: 10.1007/s00234-009-0580-1

Zahajszky, J., Dickey, C. C., McCarley, R. W., Fischer, I. A., Nestor, P., Kikinis, R., et al. (2001). A quantitative MR measure of the fornix in schizophrenia. *Schizophr. Res.* 47, 87–97. doi: 10.1016/S0920-9964(00)00051-7

Zahr, N. M., Rohlfing, T., Pfefferbaum, A., and Sullivan, E. V. (2009). Problem solving, working memory, and motor correlates of association and commissural fiber bundles in normal aging: a quantitative fiber tracking study. *Neuroimage* 44, 1050–1062. doi: 10.1016/j.neuroimage.2008.09.046

Zaitsev, M., Dold, C., Sakas, G., Hennig, J., and Speck, O. (2006). Magnetic resonance imaging of freely moving objects: prospective real-time motion

correction using an external optical motion tracking system. *Neuroimage* 31, 1038–1050. doi: 10.1016/j.neuroimage.2006.01.039

Zgaljardic, D. J., Borod, J. C., Foldi, N. S., and Mattis, P. (2003). A review of the cognitive and behavioral sequelae of Parkinson's disease: relationship to frontostriatal circuitry. *Cogn. Behav. Neurol.* 16, 193–210. doi: 10.1097/00146965-200312000-00001

Zheng, Z., Shemmassian, S., Wijekoon, C., Kim, W., Bookheimer, S. Y., and Pouratian, N. (2014). DTI correlates of distinct cognitive impairments in Parkinson's disease. *Hum. Brain Mapp*. 35, 1325–1333. doi: 10.1002/hbm.22256

Zhuang, L., Sachdev, P. S., Trollor, J. N., Reppermund, S., Kochan, N. A., Brodaty, H., et al. (2013). Microstructural white matter changes, not hippocampal atrophy, detect early amnestic mild cognitive impairment. *PLoS ONE* 8:e58887. doi: 10.1371/journal.pone.0058887

Zhuang, L., Wen, W., Zhu, W., Trollor, J., Kochan, N., Crawford, J., et al. (2010). White matter integrity in mild cognitive impairment: a tract-based spatial statistics study. *Neuroimage* 53, 16–25. doi: 10.1016/j.neuroimage.2010.05.068

Conflict of Interest Statement: The authors declare that the research was conducted in the absence of any commercial or financial relationships that could be construed as a potential conflict of interest.

Received: 18 July 2014; accepted: 14 December 2014; published online: 14 January 2015.

*Citation: Douet V and Chang L (2015) Fornix as an imaging marker for episodic memory deficits in healthy aging and in various neurological disorders. Front. Aging Neurosci. **6**:343. doi: 10.3389/fnagi.2014.00343*

This article was submitted to the journal Frontiers in Aging Neuroscience.

frontiers in
AGING NEUROSCIENCE

ORIGINAL RESEARCH ARTICLE
published: 05 February 2015
doi: 10.3389/fnagi.2015.00010

Fornix white matter is correlated with resting-state functional connectivity of the thalamus and hippocampus in healthy aging but not in mild cognitive impairment – a preliminary study

Elizabeth G. Kehoe[1]*, Dervla Farrell[1], Claudia Metzler-Baddeley[2], Brian A. Lawlor[3], Rose Anne Kenny[4], Declan Lyons[5], Jonathan P. McNulty[6], Paul G. Mullins[7], Damien Coyle[8] and Arun L. Bokde[1]

[1] *Trinity College Institute of Neuroscience and Cognitive Systems Group, Discipline of Psychiatry, School of Medicine, Trinity College Dublin, Dublin, Ireland*
[2] *Cardiff University Brain Research Imaging Centre (CUBRIC), Neuroscience and Mental Health Research Institute (NMHRI), School of Psychology, Cardiff University, Cardiff, UK*
[3] *Department of Psychiatry, Jonathan Swift Clinic, St. James Hospital, Trinity College Institute of Neuroscience, Trinity College Dublin, Dublin, Ireland*
[4] *Mercer's Institute for Successful Ageing, St. James Hospital, Trinity College Institute of Neuroscience, Trinity College Dublin, Dublin, Ireland*
[5] *St. Patrick's Hospital, Dublin, Ireland*
[6] *School of Medicine and Medical Science, University College Dublin, Dublin, Ireland*
[7] *School of Psychology, Bangor University, Bangor, UK*
[8] *Intelligent Systems Research Centre, University of Ulster, Derry, UK*

Edited by:
Kenichi Oishi, Johns Hopkins University, USA

Reviewed by:
Kenichi Oishi, Johns Hopkins University, USA
Andreia Vadconcellos Faria, Johns Hopkins University, USA
Kentaro Akazawa, Kyoto Prefectural University of Medicine, Japan

****Correspondence:***
Elizabeth G. Kehoe, Trinity College Institute of Neuroscience, Lloyd Institute, Room 3.36b, Trinity College Dublin, Dublin 2, Ireland
e-mail: elkehoe@tcd.ie

In this study, we wished to examine the relationship between the structural connectivity of the fornix, a white matter (WM) tract in the limbic system, which is affected in amnestic mild cognitive impairment (aMCI) and Alzheimer's disease, and the resting-state functional connectivity (FC) of two key related subcortical structures, the thalamus, and hippocampus. Twenty-two older healthy controls (HC) and 18 older adults with aMCI underwent multi-modal MRI scanning. The fornix was reconstructed using constrained-spherical deconvolution-based tractography. The FC between the thalamus and hippocampus was calculated using a region-of-interest approach from which the mean time series were exacted and correlated. Diffusion tensor imaging measures of the WM microstructure of the fornix were correlated against the Fisher *Z* correlation values from the FC analysis. There was no difference between the groups in the fornix WM measures, nor in the resting-state FC of the thalamus and hippocampus. We did however find that the relationship between functional and structural connectivity differed significantly between the groups. In the HCs, there was a significant positive association between linear diffusion (CL) in the fornix and the FC of the thalamus and hippocampus, however, there was no relationship between these measures in the aMCI group. These preliminary findings suggest that in aMCI, the relationship between the functional and structural connectivity of regions of the limbic system may be significantly altered compared to healthy ageing. The combined use of diffusion weighted imaging and functional MRI may advance our understanding of neural network changes in aMCI, and elucidate subtle changes in the relationship between structural and functional brain networks.

Keywords: diffusion MRI, tractography, functional connectivity, fornix, mild cognitive impairment (MCI), hippocampus, thalamus

INTRODUCTION

Alzheimer's disease (AD) is the most common cause of neurodegenerative dementia and is often preceded by a stage known as amnestic mild cognitive impairment (aMCI) (Petersen et al., 1999; Petersen, 2004), which confers an increased risk of developing AD (Stephan et al., 2012). With the prevalence of AD predicted to rise substantially over the coming years (Barnes and Yaffe, 2011), there has been increasing interest in using neuroimaging to understand early brain changes associated with preclinical groups such as aMCI (Jack et al., 2010; Sperling et al., 2011), which may represent the earliest stages of the disease. Early neuroimaging studies of aMCI and AD predominantly focused on localized brain changes such as hippocampal atrophy (Hua et al., 2010; Jack et al., 2010), however there is now a large body of evidence suggesting that the brain's inherent structural and functional connectivity (FC) is disrupted in aMCI and AD (Seeley et al., 2009; Teipel et al., 2014; Vidal-Pineiro et al., 2014).

Functional connectivity studies have found reduced connectivity in resting-state networks in aMCI and AD, including the default mode network (DMN) (Greicius et al., 2004; Beason-Held, 2011; Brier et al., 2012; Jacobs et al., 2013; Sheline and Raichle, 2013), and have found that altered FC is also linked to memory

dysfunction in these populations (Wu et al., 2013; Dunn et al., 2014). Studies using diffusion weighted imaging (DWI) and tractography to measure white matter (WM) connectivity in aMCI and AD have found significant alterations in tracts essential for memory function such as the fornix, uncinate fasciculus, and cingulum (Naggara et al., 2006; Muller et al., 2007; Stahl et al., 2007; Catheline et al., 2010; Fellgiebel and Yakushev, 2011; Metzler-Baddeley et al., 2012a,b).

The fornix is the main efferent pathway of the hippocampus, connecting it with regions including the mammillary bodies of the hypothalamus and the thalamus (Schmahmann and Pandya, 2006; Aggleton et al., 2010). A number of studies have found changes in the fornix in aMCI and AD (Mielke et al., 2009; Zhuang et al., 2010; Bozoki et al., 2012; Lee et al., 2012), such as lower fractional anisotropy (FA – thought to reflect fiber tract density and myelination). Furthermore, in a prospective study in healthy older adults, lower FA in the fornix at baseline predicted conversion to aMCI after 2 years (Zhuang et al., 2012a).

Although memory dysfunction in aMCI has been linked with both hippocampal atrophy (Convit et al., 1997; Grundman et al., 2003; Stoub et al., 2006) and WM degeneration in the fornix (Zhuang et al., 2012b), however, the role of the thalamus in aMCI is less well-defined, even though this structure is closely associated with the fornix and hippocampus. The thalamus plays a major role in generating the many rhythms in electroencephalography (EEG), which change substantively during neurodegeneration (Cantero et al., 2009); yet little is known about the role of the thalamus in neurodegeneration, and whether or not thalamus atrophy is a primary or secondary phenomenon to hippocampal or cortical atrophy in AD.

Several volumetric studies have found that the thalamus does undergo neurodegeneration in aMCI and AD (Chetelat et al., 2005; Shiino et al., 2006; de Jong et al., 2008; Cherubini et al., 2010; Roh et al., 2011; Zhang et al., 2013), and in a study that combined shape analysis of the thalamus and diffusion tensor imaging (DTI) (Zarei et al., 2010), thalamic regions most highly connected to the hippocampus showed the most severe atrophy in aMCI. Changes in the FC of the thalamus have been reported in aMCI (Zhou et al., 2013) albeit less frequently than changes in hippocampal FC, and in one study of healthy elders (Ystad et al., 2010), a negative correlation was found between thalamic FC and verbal free recall. This suggested that higher performers displayed more de-synchronization of thalamic signals, and that the FC of the thalamus may be linked to memory function. Yoon et al. (2012) found a positive correlation between perfusion in the left thalamus and performance on the Rey complex figure test in MCI, suggesting a role for the thalamus in cognitive decline.

In the current study, we used DWI and resting-state functional MRI (fMRI) to examine the connectivity of the fornix, thalamus, and hippocampus in aMCI, putatively viewed as a set of connected brain structures, which together form part of a limbic episodic memory network that malfunctions if one or more components are impaired. In particular, we wished to examine whether there was a correspondence between the structural and FC measures, and whether this was altered in aMCI. This is the first study to our knowledge to examine the link between structural and FC of the thalamus and hippocampus in aMCI. Previous studies have suggested that functional and structural connectivity are closely related, particularly in healthy participants (Damoiseaux and Greicius, 2009; Greicius et al., 2009), however the link between the two is not well-defined (Sporns, 2014), especially in the context of ageing and aMCI. Disruption of anatomical connections may influence the organization of FC, and combining MRI modalities should provide greater insight into the neural network connectivity changes in aMCI.

We performed constrained-spherical deconvolution (CSD)-based fiber tractography of the fornix in a cohort of older adults with aMCI and healthy age-matched controls, and examined the resting-state FC of the thalamus and hippocampus. Taken together, these MRI measures should provide a fuller picture of the changes that occur in the fornix in aMCI, as well as about the relationships between microstructural WM changes and alterations in FC. We predicted that the aMCIs would show decreased FA (thought to reflect fiber tract density and myelination; Mori and Zhang, 2006), and increased mean diffusivity values (MD – which tends to be low in highly intact, organized tracts and which usually increases in disease states and neurodegeneration; Mori and Zhang, 2006) in the fornix relative to controls, in line with previous studies (Mielke et al., 2009; Zhuang et al., 2010; Bozoki et al., 2012; Lee et al., 2012). We also predicted that there would be reduced resting-state FC of the thalamus and hippocampus, similar to previous findings (Zhou et al., 2008, 2013), which may be related to WM microstructural alterations in the fornix.

MATERIALS AND METHODS

PARTICIPANTS

Twenty-two older healthy control (HC) participants and 19 older participants with aMCI took part in the study. The tractography analysis was unsuccessful for one aMCI participant, in whom the tracts were almost completely absent. An examination of their T1-weighted anatomical scan revealed quite advanced levels of atrophy and gross enlargement of the lateral ventricles. Therefore, 18 aMCI were included in the final sample.

The HCs were community-dwelling older adults recruited from the greater Dublin area *via* newspaper advertisements. They underwent a health screening questionnaire and a neuropsychological assessment, the Consortium to Establish a Registry for Alzheimer's Disease (CERAD , Morris et al., 1988), in order to rule out possible cognitive impairment before inclusion in the study. The CERAD battery has been shown to be sensitive to the presence of age-related cognitive decline (Welsh et al., 1991, 1992). All of the older participants included in the study scored no more than 1.5 SD below the standardized mean scores for subjects of a similar age and education level on any of the sub-tests.

The aMCI participants were recruited from memory clinics in St. James Hospital and St. Patrick's Hospital in Dublin, and were diagnosed by a clinician according to the Peterson criteria (Petersen et al., 1999) – i.e., abnormal memory scores for age and education level with no dementia. Four were single amnestic MCI (aMCI), and 14 were multi-domain aMCI (Petersen, 2004). Neuropsychological measures were administered or supervised by an experienced neuropsychologist and included the mini-mental state examination (MMSE; Folstein et al., 1975) and Cambridge cognitive examination (CAMCOG; Huppert et al., 1995).

All of the participants were right-handed with no history of head trauma, neurological disease, stroke, transient ischemic attack, heart attack, or psychiatric illness. They completed the Geriatric Depression Scale (GDS; Yesavage, 1988), the Eysenck Personality Questionnaire Revised Edition Short Scale (EPQ-R; Eysenck and Eysenck, 1991), and a Cognitive Reserve Questionnaire (Rami et al., 2011) before the MRI scan. The groups did not differ in terms of age, gender, education level, or levels of cognitive reserve as assessed by the self-report Cognitive Reserve Questionnaire. The aMCI group had lower MMSE scores, higher GDS scores, and scored lower on the EPQ measure of extraversion than the HC group. See **Table 1** for a summary of the participant demographics.

The study had full ethical approval from the St. James Hospital and the Adelaide and Meath Hospital, incorporating the National Children's Hospital Research Ethics Committee. All participants gave written informed consent before taking part in the study.

MRI DATA ACQUISITION

Whole-brain high angular resolution diffusion imaging (HARDI) data were acquired on a 3.0 Tesla Philips Intera MR system (Best, The Netherlands) equipped with an eight channel head coil. A parallel sensitivity encoding (SENSE) approach (Pruessmann et al., 1999) with a reduction factor of two was used during the DWI acquisition. Single-shot spin echo-planar imaging was used to acquire the DWI data with following parameters: Echo time (TE) 79 ms, repetition time (TR) 20,000 ms, field of view (FOV) 248 mm, matrix 112×112, isotropic voxel of $2.3\,\text{mm} \times 2.3\,\text{mm} \times 2.3\,\text{mm}$, and 65 slices with 2.3 mm thickness with no gap between the slices. Diffusion gradients were applied in 61 isotropically distributed orientations with $b = 3000\,\text{s/mm}^2$, and four images with $b = 0\,\text{s/mm}^2$ were also acquired. The total scan time was 17 min.

A high-resolution 3D T1-weighted anatomical image was acquired for each participant with the following parameters: TE = 3.9 ms, TR = 8.5 ms, FOV = 230 mm, slice thickness = 0.9 mm, voxel size = $0.9\,\text{mm} \times 0.9\,\text{mm} \times 0.9\,\text{mm}$. These images were used for the correction of EPI-induced geometrical distortions in the DWI data.

Resting-state fMRI data were also acquired during the scanning session. The scan lasted for 7 min during which time the participants were asked to keep their eyes open and fixate on a cross hairs in the center of a screen behind the MR scanner, visible *via* a mirror. The blood oxygenation dependent (BOLD) signal changes were measured using a T2*-weighted echo-planar imaging sequence with TE = 30 ms and TR = 2000 ms. Each volume of data covered the entire brain with 39 slices, and the slices were acquired in interleaved sequence from inferior to superior direction. Two hundred ten volumes of data were acquired, with voxel dimensions of $3.5\,\text{mm} \times 3.5\,\text{mm} \times 3.85\,\text{mm}$ and a 0.35 mm gap between the slices.

Table 1 | Demographic details of the participants.

	HC ($n = 22$)	aMCI ($n = 18$)	p^* ($df = 38$)
Gender	12 M, 10 F	9 M, 9 F	1.00
Age	68.86 ± 6.47	68.83 ± 7.71	0.99
Education	14.36 ± 3.17	14.50 ± 3.00	0.89
MMSE	28.82 ± 0.96	27.22 ± 2.10	**0.003**
GDS	0.77 ± 1.11	2.67 ± 2.30	**0.002**
EPQ E	8.27 ± 2.64	5.33 ± 3.36	**0.004**
EPQ N	2.14 ± 0.96	3.89 ± 3.46	0.52
CR	17.82 ± 3.02	16.89 ± 4.92	0.47

MMSE, mini-mental state exam; GDS, geriatric depression scale; EPQ E, Eysenck personality questionnaire extraversion scale; EPQ N, Eysenck personality questionnaire neuroticism scale; CR, cognitive reserve scale. Standard deviations are indicated in parentheses.

**Results of independent samples t-tests, except for gender which was compared with a Fischer's exact test. Statistically significant differences are indicated in bold font.*

DWI ANALYSIS

The DWI data were analyzed using ExploreDTI v4.8.3 (Leemans et al., 2009)[1]. The images were corrected for distortion due to head motion, eddy currents and for EPI-induced geometrical distortions by co-registration and resampling to the high-resolution T1-weighted anatomical images. This was implemented in ExploreDTI according to the method described by Irfanoglu et al. (2012) and the encoding vectors were reoriented appropriately (Leemans and Jones, 2009). Since ageing and neurodegeneration are related to brain atrophy and the fornix is extremely susceptible to contamination from cerebrospinal fluid (CSF) and atrophy-based partial volume artefacts, the free water elimination approach (Pasternak et al., 2009) was applied to correct for partial volume effects prior to fitting the tensor model to the data in each voxel. The free water elimination method has been used successfully in several previous tractography studies of ageing and aMCI, particularly in relation to the fornix (Metzler-Baddeley et al., 2012a,b; Fletcher et al., 2014).

Tractography of the fornix

For the analysis of the fornix a hybrid analysis approach was used, whereby reconstruction of the tracts was completed using CSD-based tractography (Jeurissen et al., 2011) and DTI-based WM indices were extracted for statistical analyses. CSD rather than DTI-based tractography was chosen as it can account for complex WM orientation such as crossing fibers (Tournier et al., 2008, 2011), and this approach has recently been successful at detecting changes in tracts with complex WM architecture in MCI and AD (Metzler-Baddeley et al., 2012b; Reijmer et al., 2012). In the case of the fornix for instance, DTI-based tractography cannot resolve complex fiber architecture in regions where the anterior columns of the fornix cross with fibers of the anterior commissure (Metzler-Baddeley et al., 2012a). Several previous studies have successfully used deterministic tractography based on the CSD method to segment the fornix (Metzler-Baddeley et al., 2011, 2013).

After the pre-processing steps whole-brain tractography was performed using every voxel as a seed point. The principle diffusion orientation at each point was estimated by the CSD tractography algorithm, which propagated in 0.5 mm steps along this

[1]http://www.exploredti.com/

direction. At each new location the fiber orientation(s) was estimated before the tracking moved a further 0.5 mm along the direction that subtended the smallest angle to the current trajectory. A trajectory was followed through the data until the scaled height of the fiber orientation density function peak dropped below 0.1, or the direction of the pathway changed through an angle of more than 60°.

Following whole-brain tractography, the fornix was extracted by drawing several regions of interest (ROIs) defined according to previously published methods (Metzler-Baddeley et al., 2011, 2013). The ROIs were drawn manually for one subject and then applied to all of the other subjects using an "atlas-based" tractography (ABT) approach, by spatial transformation of the ROIs to the other subjects' native space. This ensured consistency in the placement of the ROIs. See **Figure 1** for an example of the ROIs in the template subject, which was a HC participant. For several subjects this ABT approach was unsuccessful, most often due to inter-subject anatomical variability, such as neurodegeneration and encroachment of the lateral ventricles in some of the aMCI participants. In these cases, the ROIs for the tractography were drawn manually, with some adjustment and/or extra ROIs typically needed.

Statistical analysis of the tractography data

From the reconstructions of the fornix WM microstructural indices were extracted for statistical analyses in IBM SPSS Statistics for Windows, Version 22.0 (Armonk, NY: IBM Corp). These included free water corrected FA, corrected MD and the corrected Westin measures of linear diffusion coefficient (CL), and planar diffusion coefficient (CP) (Westin et al., 2002). The Westin measures describe the geometrical shape of the diffusion tensor, with a high value of CL implying only one dominant fiber orientation within a voxel (Vos et al., 2012), and a high value of CP indicating the presence of crossing fiber configurations (Vos et al., 2012).

The diffusion tensor metrics in the left and right fornix were compared within the two groups using a series of paired t-tests and no statistically significant differences were found. The values in the left and right fornix were therefore averaged to give a single fornix measure for each subject. This also reduced the number of multiple comparisons in the statistical tests, reducing the possibility of Type I errors. The diffusion metrics were compared between the groups using four paired t-tests, which were corrected for multiple comparisons using a Bonferroni-corrected p-level of $p < 0.0125$.

RESTING-STATE FUNCTIONAL CONNECTIVITY OF THE THALAMUS AND HIPPOCAMPUS

The fMRI data were processed using the DPARSF V2.3 toolbox (Data Processing Assistant for Resting-State fMRI, Yan and Zang, 2010)[2], which utilizes SPM8[3] for the pre-processing steps and the REST V1.8 toolbox (Song et al., 2011) for the resting-state analysis. Data pre-processing involved slice timing correction, realignment to correct for head motion, normalization to MNI152 space by T1-image unified segmentation, smoothing with a 4 mm full-width-at-half-maximum Gaussian kernel, and detrending and filtering (0.01–0.08 Hz). The normalized voxel size was 3 mm × 3 mm × 3 mm. Several nuisance covariates were regressed out, including six head motion parameters and signals from the WM and CSF.

The resting-state FC of the thalamus and hippocampus was measured using a ROI FC approach. The ROIs were created using probabilistic atlases included in FSL[4] and were defined in the MNI152 template space. The left and right hippocampus ROIs were based on the Harvard-Oxford subcortical atlas structures. For the thalamus ROIs, the Oxford thalamic connectivity atlas (Behrens et al., 2003a,b), a probabilistic atlas of seven sub-thalamic regions, segmented according to their WM connectivity to cortical areas, was used to delineate the temporal region of the thalamus. The temporal region was chosen because, anatomically, this region is most likely to be structurally connected to the cortex nearest the hippocampus, and so the temporal thalamic-hippocampus resting-state measure was devised to mirror as closely as possible the regions structurally connected by the fornix. See **Figure 2**. The

[2]http://rfmri.org/DPARSF
[3]http://www.fil.ion.ucl.ac.uk/spm
[4]http://fsl.fmrib.ox.ac.uk/fsl/fsl4.0/fslview/atlas-descriptions.html

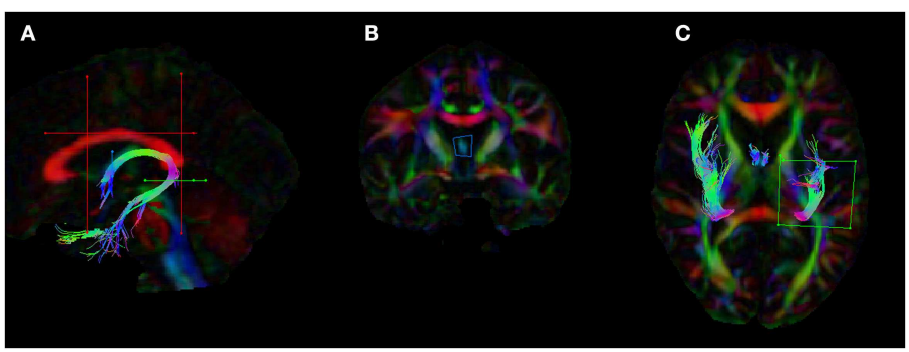

FIGURE 1 | Placement of the regions of interests (ROIs) for the dissection of the fornix in ExploreDTI. (A) The five ROIs used to segment the fornix **(B)** coronal view of the seed ROI **(C)** ROI used to split the tracts and isolate the left fornix. The blue ROI is a SEED/OR gate, the green ROI is an AND gate, whilst the red ROIs are NOT gates. These ROIs were drawn for one subject and once deemed to be accurate and robust they were applied to all other subjects using an "atlas-based" tract segmentation method. The atlas in this case was the FA image of this subject.

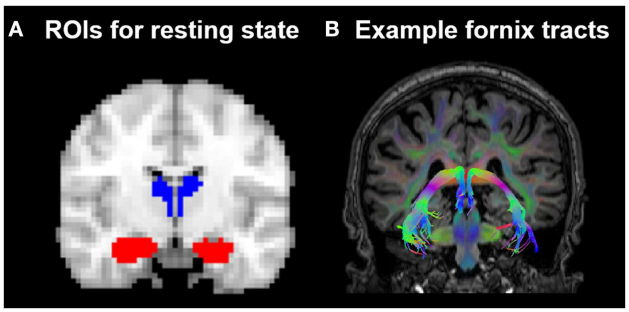

FIGURE 2 | (A) Position of the resting-state regions of interest (ROIs) in relation to **(B)** the fornix in one HC subject. ROIs for the resting-state analysis were placed in the hippocampus (indicated in red) and the thalamic region probabilistically connected to the temporal lobe (indicated in blue), as defined by the Oxford thalamic connectivity atlas (Behrens et al., 2003a,b).

four subcortical ROIs were thresholded at a minimum probability level of 20%, binarized, and re-sampled to 3 mm × 3 mm × 3 mm.

The average fMRI time series from the four ROIs were extracted and correlated to determine the FC of the regions at rest. Fisher-Z score transformations of these values were exported to IBM SPSS v.22 for second-level statistical analysis. The FC Fischer Z-scores between the left thalamus and left hippocampus, and between the right thalamus and right hippocampus, were compared within groups, and there was found to be no statistically significant difference. An average thalamus–hippocampus FC measure was therefore calculated for each subject, which was correlated against the fornix WM measures. For each group, four correlations were run and a Bonferroni-corrected p-value of 0.0125 was applied.

Several of the correlation coefficients were compared between the groups. To do this, the Pearson r values were first converted to Fisher Z scores. The Z statistic was then calculated using:

$Z = (\text{Fisher } Z1 - \text{Fisher } Z2)/\sqrt{(\text{variance})}$, where variance is equal to: $\frac{1}{N1} + \frac{1}{N2}$.

RESULTS

COMPARISON OF FORNIX WHITE MATTER MICROSTRUCTURE IN HC AND aMCI GROUPS

The analyses of WM microstructural indices in the fornix revealed no statistically significant differences between the HC and aMCI groups. There was a trend towards higher CL and lower CP in the HCs versus aMCIs, however these results did not meet the Bonferroni-corrected threshold of $p < 0.0125$. See **Table 2** for a summary of these results and **Figure 3** for examples of the fornix tracts in one HC and one aMCI participant.

RESTING-STATE FUNCTIONAL CONNECTIVITY OF THE THALAMUS AND HIPPOCAMPUS AND RELATION TO FORNIX WM MICROSTRUCTURE

The average FC of the temporal thalamic regions and the hippocampus indicated a high degree of resting-state FC in both the HCs (Fisher's $Z = 0.48 \pm 0.23$) and aMCIs (Fisher's $Z = 0.50 \pm 0.21$). There was no statistically significant difference in FC between the groups [$t\ (38) = -0.32$, $p = 0.75$].

The correlational analysis of the functional and structural connectivity measures revealed a significant positive association in the HC group between the linear diffusion coefficient in the fornix and the FC of the thalamus–hippocampus ($r = 0.55$, $p = 0.008$), which was absent in the aMCI group ($r = -0.08$, $p = 0.81$). These correlation coefficients differed significantly from one another ($Z = 5.17$, $p < 0.0001$). Scatterplots of these correlational results are shown in **Figure 4**. One of the datasets had a CL value of <0.2, which upon examination was found to be a statistical outlier ($p < 0.05$). This dataset was removed from the correlational analyses, thus in **Figure 4** there are 22 HCs and 17 aMCI datasets plotted.

Table 2 | Mean DWI measures for fornix in the HC and aMCI groups.

Fornix	HC	aMCI	*t*-statistic	*p*-value
FA	0.25 ± 0.02	0.24 ± 0.03	1.22	0.23
MD	0.0009 ± 0.00006	0.0009 ± 0.00007	−0.88	0.38
CL	0.29 ± 0.02	0.26 ± 0.04	2.21	0.033
CP	0.0698 ± 0.012	0.0863 ± 0.032	−2.21	0.034

FA, fractional anisotropy; MD, mean diffusivity; CL, linear diffusion coefficient; CP, planar diffusion coefficient.

DISCUSSION

In this study, we examined the structural integrity of the fornix, an important limbic WM tract, and the resting-state FC of two associated subcortical structures, the thalamus, and hippocampus. This is the first study to our knowledge to examine the relationship between the structural and FC of the thalamus and hippocampus, and whether this is altered in aMCI, a condition which is known to affect fornix WM and resting-state connectivity of intrinsic brain networks.

RELATIONSHIP BETWEEN FUNCTIONAL AND STRUCTURAL CONNECTIVITY

Although, contrary to our predictions, we found no evidence of reduced FC between the thalamus and hippocampus in aMCI, we did find that the correspondence between the FC and fornix WM was altered in this group. There was a significant positive relationship in the HCs between CL in the fornix and the FC of the thalamus–hippocampus, however this relationship was absent in the aMCIs.

Elucidating the relationship between structural and FC is not trivial, and is an area of growing interest within the neuroimaging community (van den Heuvel and Sporns, 2013; Sporns, 2014). Previous combined fMRI–DTI studies have found that resting-state FC does in general reflect the brain's structurally connected WM networks (Damoiseaux and Greicius, 2009; Greicius et al., 2009), and functional and structural connectivity measures have been found to correlate, particularly in healthy individuals (Skudlarski et al., 2008; van den Heuvel et al., 2008).

Several studies have indicated however, that the relationship between functional and structural connectivity can be altered in disease states. For example, in a study of major depressive disorder (de Kwaasteniet et al., 2013), patients had a negative correlation between FA in the uncinate fasciculus – another of the limbic WM tracts – and the FC between the subgenual anterior cingulate cortex and the hippocampus, which was not mirrored in the HC. Furthermore, in a study of schizophrenia (Skudlarski et al., 2010), patients

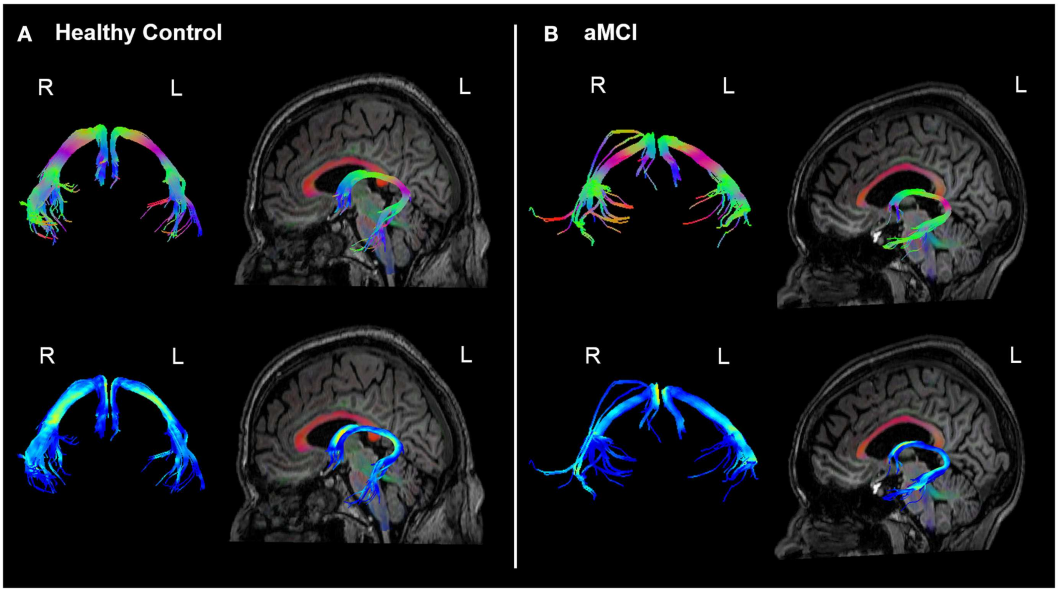

FIGURE 3 | Example fornix tracts in a (A) healthy control and (B) amnestic aMCI subject. The top panel in each case shows the tracts color-encoded with the first eigenvector (FE); the bottom panel shows the same tracts color-encoded with FA values. For each subject, the left and right fornix is shown in isolation on the left, and on the right the fornix can be seen overlaid on the subject's T1-weighted structural image, with the FE shown in semi-transparent color (note the corpus callosum in red for example). The DWI data were co-registered to the structural images during the processing to correct for EPI-induced geometric distortions, however as illustrated by these figures this also facilitates the inspection of the white tracts in reference to the high-resolution anatomical image of the brain.

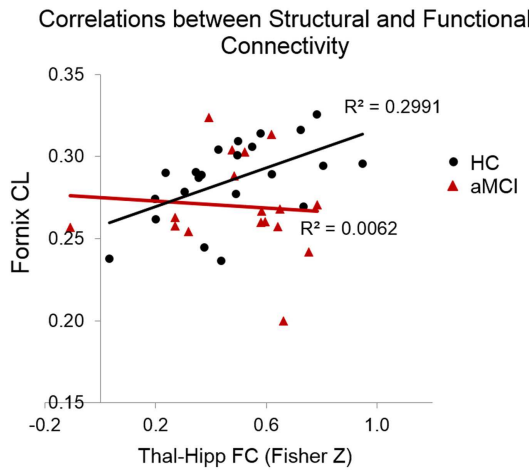

FIGURE 4 | Scatterplots indicating the correlations between functional and structural connectivity measures. In the HCs but not the MCIs there was a significant positive relationship between CL in the fornix and the resting-state connectivity of the thalamus and hippocampus.

compared to controls were found to show not only overall reduced global WM connectivity as derived from DTI, but also a lower coherence between WM connectivity and FC. The current study supports the idea that the correspondence between functional and structural connectivity may be altered in neuropathological states. This is an area of research which certainly warrants further investigation in future studies.

Functional connections in the brain also exist between regions, which are not directly structurally connected, likely mediated by indirect structural connections (Honey et al., 2009), however in the current study we focused our analysis on the connectivity of two subcortical structures, which are known to be directly linked *via* a WM tract. We found evidence that there is a close correspondence between functional and structural connectivity in these structures in healthy ageing, which appears to be disrupted in aMCI.

FORNIX RESULTS

A number of previous studies have found that the fornix is affected in aMCI, with changes such as lower FA and increased RD reported (Lee et al., 2012; Metzler-Baddeley et al., 2012a; Oishi et al., 2012; Zhuang et al., 2013). We had predicted that the aMCI group would show similar changes in fornix WM indices consistent with compromised WM, however we found no evidence of this in the current study, with no differences in fornix WM microstructural indices between the groups.

The lack of difference in the fornix WM microstructural indices between the HCs and aMCIs may be due to sparing of the fornix in this aMCI cohort, however several other factors may also have contributed. This study was limited by a relatively small sample size, which likely reduced the power to detect group differences. Furthermore, the aMCI cohort included both single and multi-domain aMCI. This increased heterogeneity of the sample may also have decreased the likelihood of detecting differences between the groups. Multi-domain aMCI also confers an increased risk of conversion to vascular dementia (VaD) (Petersen, 2004; Rasquin et al., 2005; Libon et al., 2010) and not just AD, which has typically

not been found to involve the same level of disruption to the limbic system as AD (Burton et al., 2009). However some previous studies of aMCI also failed to detect changes in FA (Nowrangi et al., 2013; Rowley et al., 2013), suggesting that FA may not always be a strong indicator of WM connectivity changes in this cohort.

LINEAR AND PLANAR DIFFUSION COEFFICIENTS

The WM indices of linear and planar diffusion coefficients (CL and CP) did show a trend towards being significantly different between the groups ($p < 0.035$ in each case, which did not survive Bonferroni correction), with higher CL and lower CP in the HCs. High CL values are thought to reflect the presence of one dominant fiber orientation within a voxel (Vos et al., 2012), while high CP values are thought to indicate the presence of crossing fiber configurations (Vos et al., 2012). The fornix is generally considered to be a largely single-fiber orientation tract, however differences in CL and CP may also reflect WM damage. For example, in a recent study, which investigated WM changes following a season of playing varsity football (Davenport et al., 2014), there was a strong association between the number of head impacts and reduced FA, as well as reduced CL and increased CP. In fact, the strongest statistical relationship was with changes in CL, with the authors suggested may reflect WM disconnection due to the focal disruption of axons caused by the traumatic head impacts. Changes in CL and CP may also reflect WM changes in aMCI, such as WM degeneration and disruption to axonal organization, however further investigation of how these indices change in ageing and aMCI is needed.

STRENGTHS AND LIMITATIONS OF THE CURRENT STUDY

The present study extends previous studies by examining how fornix WM microstructural is related to the resting-state FC of two closely related structures, the thalamus and hippocampus. It is becoming common for neuroimaging researchers to collect multi-modal MRI data, therefore it is important for more studies to integrate findings across these modalities. This is the first study to our knowledge to combine FC and diffusion tractography to examine the fornix in ageing and aMCI, and the first to find differences in the relationship between the functional and structural connectivity of the thalamus and hippocampus related to aMCI.

The DWI methods employed in this study were very robust, as CSD-based tractography methods are preferable to DTI-based approaches, particular for brain regions with complex WM architecture. Correcting for free water is also an important preprocessing step since it is well established that atrophy-related CSF partial volume can bias DTI-based indices (Metzler-Baddeley et al., 2012a; Vos et al., 2012; Baron and Beaulieu, 2014; Maier-Hein et al., 2014). A recent study has highlighted how signals from CSF can contribute to differences in WM microstructural measures in MCI (Berlot et al., 2014), highlighting the importance of controlling for this confound.

A possible methodological limitation of our study is that we did not examine possible non-linear relationships between WM measures and FC. Variability in these measures may also be better captured by using more advanced statistical approaches, such as joint ICA (Calhoun et al., 2009). This is something which could be explored in future studies.

CONCLUSION

In the current study, we used multi-modal MRI to examine the relationship between the functional and structural connectivity of two important subcortical structures, the thalamus and hippocampus, in healthy ageing and aMCI. We did not replicate previous findings of changes in DTI metrics in aMCI, which may indicate that the study was underpowered to properly test these differences. Thus the results should be taken as preliminary findings, which we believe warrant further investigation in a larger cohort. However, although there were no group differences in the WM measures of the fornix or in the FC of the thalamus–hippocampus at rest, there was a strong correspondence between the structural and FC measures in the HCs, which was absent in the aMCI group. The results suggest a disruption to the relationship between functional and structural connectivity in aMCI, which may be representative of early neuropathological connectivity changes in the limbic system. Both DWI and FC have offered new insights into brain network changes in aMCI. However, the complementary strengths of both of these methods combined may advance our understanding of neural network disconnection in this condition, and may increase the potential biomarker capabilities of MRI by elucidating subtle changes in the relationship between structural and functional brain networks.

ACKNOWLEDGMENTS

We wish to acknowledge the assistance of Mr. Sojo Josephs in acquiring the MRI data. We would like to thank Prof. Alexander Leemans for advice regarding the DTI analysis, and Dr. Nia Goulden for advice on the use of the DPARSFA toolbox. The MRI data were accessed from the Lonsdale cluster maintained by the Trinity Centre for High Performance Computing. This cluster was funded through grants from Science Foundation Ireland. This research was supported by funding from a Department of Education and Learning N. Ireland (DELNI) Cross Border project between the University of Ulster and Trinity College Dublin, and from the European Regional Development Fund *via* the Interregional 4A Ireland Wales Programme 2007–2013.

REFERENCES

Aggleton, J. P., O'mara, S. M., Vann, S. D., Wright, N. F., Tsanov, M., and Erichsen, J. T. (2010). Hippocampal-anterior thalamic pathways for memory: uncovering a network of direct and indirect actions. *Eur. J. Neurosci.* 31, 2292–2307. doi:10.1111/j.1460-9568.2010.07251.x

Barnes, D. E., and Yaffe, K. (2011). The projected effect of risk factor reduction on Alzheimer's disease prevalence. *Lancet Neurol.* 10, 819–828. doi:10.1016/s1474-4422(11)70072-2

Baron, C. A., and Beaulieu, C. (2014). Acquisition strategy to reduce cerebrospinal fluid partial volume effects for improved DTI tractography. *Magn. Reson. Med.* doi:10.1002/mrm.25226

Beason-Held, L. L. (2011). Dementia and the default mode. *Curr. Alzheimer Res.* 8, 361–365. doi:10.2174/156720511795745294

Behrens, T. E., Johansen-Berg, H., Woolrich, M. W., Smith, S. M., Wheeler-Kingshott, C. A., Boulby, P. A., et al. (2003a). Non-invasive mapping of connections between human thalamus and cortex using diffusion imaging. *Nat. Neurosci.* 6, 750–757. doi:10.1038/nn1075

Behrens, T. E., Woolrich, M. W., Jenkinson, M., Johansen-Berg, H., Nunes, R. G., Clare, S., et al. (2003b). Characterization and propagation of uncertainty in diffusion-weighted MR imaging. *Magn. Reson. Med.* 50, 1077–1088. doi:10.1002/mrm.10609

Berlot, R., Metzler-Baddeley, C., Jones, D. K., and O'sullivan, M. J. (2014). CSF contamination contributes to apparent microstructural alterations in mild cognitive impairment. *Neuroimage* 92, 27–35. doi:10.1016/j.neuroimage.2014.01.031

Bozoki, A. C., Korolev, I. O., Davis, N. C., Hoisington, L. A., and Berger, K. L. (2012). Disruption of limbic white matter pathways in mild cognitive impairment and Alzheimer's disease: a DTI/FDG-PET Study. *Hum. Brain Mapp.* 33, 1792–1802. doi:10.1002/hbm.21320

Brier, M. R., Thomas, J. B., Snyder, A. Z., Benzinger, T. L., Zhang, D., Raichle, M. E., et al. (2012). Loss of intranetwork and internetwork resting state functional connections with Alzheimer's disease progression. *J. Neurosci.* 32, 8890–8899. doi:10.1523/jneurosci.5698-11.2012

Burton, E. J., Barber, R., Mukaetova-Ladinska, E. B., Robson, J., Perry, R. H., Jaros, E., et al. (2009). Medial temporal lobe atrophy on MRI differentiates Alzheimer's disease from dementia with Lewy bodies and vascular cognitive impairment: a prospective study with pathological verification of diagnosis. *Brain* 132, 195–203. doi:10.1093/brain/awn298

Calhoun, V. D., Liu, J., and Adali, T. (2009). A review of group ICA for fMRI data and ICA for joint inference of imaging, genetic, and ERP data. *Neuroimage* 45, S163–S172. doi:10.1016/j.neuroimage.2008.10.057

Cantero, J. L., Atienza, M., Gomez-Herrero, G., Cruz-Vadell, A., Gil-Neciga, E., Rodriguez-Romero, R., et al. (2009). Functional integrity of thalamocortical circuits differentiates normal aging from mild cognitive impairment. *Hum. Brain Mapp.* 30, 3944–3957. doi:10.1002/hbm.20819

Catheline, G., Periot, O., Amirault, M., Braun, M., Dartigues, J. F., Auriacombe, S., et al. (2010). Distinctive alterations of the cingulum bundle during aging and Alzheimer's disease. *Neurobiol. Aging* 31, 1582–1592. doi:10.1016/j.neurobiolaging.2008.08.012

Cherubini, A., Peran, P., Spoletini, I., Di Paola, M., Di Iulio, F., Hagberg, G. E., et al. (2010). Combined volumetry and DTI in subcortical structures of mild cognitive impairment and Alzheimer's disease patients. *J. Alzheimers Dis.* 19, 1273–1282. doi:10.3233/jad-2010-091186

Chetelat, G., Landeau, B., Eustache, F., Mezenge, F., Viader, F., De La Sayette, V., et al. (2005). Using voxel-based morphometry to map the structural changes associated with rapid conversion in MCI: a longitudinal MRI study. *Neuroimage* 27, 934–946. doi:10.1016/j.neuroimage.2005.05.015

Convit, A., De Leon, M. J., Tarshish, C., De Santi, S., Tsui, W., Rusinek, H., et al. (1997). Specific hippocampal volume reductions in individuals at risk for Alzheimer's disease. *Neurobiol. Aging* 18, 131–138. doi:10.1016/S0197-4580(97)00001-8

Damoiseaux, J. S., and Greicius, M. D. (2009). Greater than the sum of its parts: a review of studies combining structural connectivity and resting-state functional connectivity. *Brain Struct. Funct.* 213, 525–533. doi:10.1007/s00429-009-0208-6

Davenport, E. M., Whitlow, C. T., Urban, J. E., Espeland, M. A., Jung, Y., Rosenbaum, D. A., et al. (2014). Abnormal white matter integrity related to head impact exposure in a season of high school varsity football. *J. Neurotrauma* 31, 1617–1624. doi:10.1089/neu.2013.3233

de Jong, L. W., Van Der Hiele, K., Veer, I. M., Houwing, J. J., Westendorp, R. G., Bollen, E. L., et al. (2008). Strongly reduced volumes of putamen and thalamus in Alzheimer's disease: an MRI study. *Brain* 131, 3277–3285. doi:10.1093/brain/awn278

de Kwaasteniet, B., Ruhe, E., Caan, M., Rive, M., Olabarriaga, S., Groefsema, M., et al. (2013). Relation between structural and functional connectivity in major depressive disorder. *Biol. Psychiatry* 74, 40–47. doi:10.1016/j.biopsych.2012.12.024

Dunn, C. J., Duffy, S. L., Hickie, I. B., Lagopoulos, J., Lewis, S. J., Naismith, S. L., et al. (2014). Deficits in episodic memory retrieval reveal impaired default mode network connectivity in amnestic mild cognitive impairment. *Neuroimage Clin.* 4, 473–480. doi:10.1016/j.nicl.2014.02.010

Eysenck, H. J. E., and Eysenck, S. B. G. (1991). *Manual of the Eysenck Personality Scales (EPS Adult)*. London: Hodder & Stoughton.

Fellgiebel, A., and Yakushev, I. (2011). Diffusion tensor imaging of the hippocampus in MCI and early Alzheimer's disease. *J. Alzheimers Dis.* 26(Suppl. 3), 257–262. doi:10.3233/jad-2011-0001

Fletcher, E., Carmichael, O., Pasternak, O., Maier-Hein, K. H., and Decarli, C. (2014). Early brain loss in circuits affected by Alzheimer's disease is predicted by fornix microstructure but may be independent of gray matter. *Front. Aging Neurosci.* 6:106. doi:10.3389/fnagi.2014.00106

Folstein, M. F., Folstein, S. E., and Mchugh, P. R. (1975). "Mini-mental state". A practical method for grading the cognitive state of patients for the clinician. *J. Psychiatr. Res.* 12, 189–198. doi:10.1016/0022-3956(75)90026-6

Greicius, M. D., Srivastava, G., Reiss, A. L., and Menon, V. (2004). Default-mode network activity distinguishes Alzheimer's disease from healthy aging: evidence from functional MRI. *Proc. Natl. Acad. Sci. U. S. A.* 101, 4637–4642. doi:10.1073/pnas.0308627101

Greicius, M. D., Supekar, K., Menon, V., and Dougherty, R. F. (2009). Resting-state functional connectivity reflects structural connectivity in the default mode network. *Cereb. Cortex* 19, 72–78. doi:10.1093/cercor/bhn059

Grundman, M., Jack, C. R. Jr., Petersen, R. C., Kim, H. T., Taylor, C., Datvian, M., et al. (2003). Hippocampal volume is associated with memory but not monmemory cognitive performance in patients with mild cognitive impairment. *J. Mol. Neurosci.* 20, 241–248. doi:10.1385/JMN:20:3:241

Honey, C. J., Sporns, O., Cammoun, L., Gigandet, X., Thiran, J. P., Meuli, R., et al. (2009). Predicting human resting-state functional connectivity from structural connectivity. *Proc. Natl. Acad. Sci. U. S. A.* 106, 2035–2040. doi:10.1073/pnas.0811168106

Hua, X., Lee, S., Hibar, D. P., Yanovsky, I., Leow, A. D., Toga, A. W., et al. (2010). Mapping Alzheimer's disease progression in 1309 MRI scans: power estimates for different inter-scan intervals. *Neuroimage* 51, 63–75. doi:10.1016/j.neuroimage.2010.01.104

Huppert, F. A., Brayne, C., Gill, C., Paykel, E. S., and Beardsall, L. (1995). CAMCOG – a concise neuropsychological test to assist dementia diagnosis: sociodemographic determinants in an elderly population sample. *Br. J. Clin. Psychol.* 34(Pt 4), 529–541. doi:10.1111/j.2044-8260.1995.tb01487.x

Irfanoglu, M. O., Walker, L., Sarlls, J., Marenco, S., and Pierpaoli, C. (2012). Effects of image distortions originating from susceptibility variations and concomitant fields on diffusion MRI tractography results. *Neuroimage* 61, 275–288. doi:10.1016/j.neuroimage.2012.02.054

Jack, C. R. Jr., Bernstein, M. A., Borowski, B. J., Gunter, J. L., Fox, N. C., Thompson, P. M., et al. (2010). Update on the magnetic resonance imaging core of the Alzheimer's disease neuroimaging initiative. *Alzheimers Dement.* 6, 212–220. doi:10.1016/j.jalz.2010.03.004

Jacobs, H. I., Radua, J., Luckmann, H. C., and Sack, A. T. (2013). Meta-analysis of functional network alterations in Alzheimer's disease: toward a network biomarker. *Neurosci. Biobehav. Rev.* 37, 753–765. doi:10.1016/j.neubiorev.2013.03.009

Jeurissen, B., Leemans, A., Jones, D. K., Tournier, J. D., and Sijbers, J. (2011). Probabilistic fiber tracking using the residual bootstrap with constrained spherical deconvolution. *Hum. Brain Mapp.* 32, 461–479. doi:10.1002/hbm.21032

Lee, D. Y., Fletcher, E., Carmichael, O. T., Singh, B., Mungas, D., Reed, B., et al. (2012). Sub-regional hippocampal injury is associated with fornix degeneration in Alzheimer's disease. *Front. Aging Neurosci.* 4:1. doi:10.3389/fnagi.2012.00001

Leemans, A., Jeurissen, B., Sijbers, J., and Jones, D. K. (2009). "ExploreDTI: a graphical toolbox for processing, analyzing, and visualizing diffusion MR data.," in *7th Annual Meeting of International Society for Magnetic Resonance in Medicine* (Hawaii).

Leemans, A., and Jones, D. K. (2009). The B-matrix must be rotated when correcting for subject motion in DTI data. *Magn. Reson. Med.* 61, 1336–1349. doi:10.1002/mrm.21890

Libon, D. J., Xie, S. X., Eppig, J., Wicas, G., Lamar, M., Lippa, C., et al. (2010). The heterogeneity of mild cognitive impairment: a neuropsychological analysis. *J. Int. Neuropsychol. Soc.* 16, 84–93. doi:10.1017/s1355617709990993

Maier-Hein, K. H., Westin, C. F., Shenton, M. E., Weiner, M. W., Raj, A., Thomann, P., et al. (2014). Widespread white matter degeneration preceding the onset of dementia. *Alzheimers Dement.* doi:10.1016/j.jalz.2014.04.518

Metzler-Baddeley, C., Baddeley, R. J., Jones, D. K., Aggleton, J. P., and O'sullivan, M. J. (2013). Individual differences in fornix microstructure and body mass index. *PLoS ONE* 8:e59849. doi:10.1371/journal.pone.0059849

Metzler-Baddeley, C., Hunt, S., Jones, D. K., Leemans, A., Aggleton, J. P., and O'sullivan, M. J. (2012a). Temporal association tracts and the breakdown of episodic memory in mild cognitive impairment. *Neurology* 79, 2233–2240. doi:10.1212/WNL.0b013e31827689e8

Metzler-Baddeley, C., Jones, D. K., Steventon, J., Westacott, L., Aggleton, J. P., and O'sullivan, M. J. (2012b). Cingulum microstructure predicts cognitive control in older age and mild cognitive impairment. *J. Neurosci.* 32, 17612–17619. doi:10.1523/jneurosci.3299-12.2012

Metzler-Baddeley, C., Jones, D. K., Belaroussi, B., Aggleton, J. P., and O'sullivan, M. J. (2011). Frontotemporal connections in episodic memory and aging: a diffusion MRI tractography study. *J. Neurosci.* 31, 13236–13245. doi:10.1523/jneurosci.2317-11.2011

Mielke, M. M., Kozauer, N. A., Chan, K. C., George, M., Toroney, J., Zerrate, M., et al. (2009). Regionally-specific diffusion tensor imaging in mild cognitive impairment and Alzheimer's disease. *Neuroimage* 46, 47–55. doi:10.1016/j.neuroimage.2009.01.054

Mori, S., and Zhang, J. (2006). Principles of diffusion tensor imaging and its applications to basic neuroscience research. *Neuron* 51, 527–539. doi:10.1016/j.neuron.2006.08.012

Morris, J. C., Mohs, R. C., Rogers, H., Fillenbaum, G., and Heyman, A. (1988). Consortium to establish a registry for Alzheimer's disease (CERAD) clinical and neuropsychological assessment of Alzheimer's disease. *Psychopharmacol. Bull.* 24, 641–652.

Muller, M. J., Greverus, D., Weibrich, C., Dellani, P. R., Scheurich, A., Stoeter, P., et al. (2007). Diagnostic utility of hippocampal size and mean diffusivity in amnestic MCI. *Neurobiol. Aging* 28, 398–403. doi:10.1016/j.neurobiolaging.2006.01.009

Naggara, O., Oppenheim, C., Rieu, D., Raoux, N., Rodrigo, S., Dalla Barba, G., et al. (2006). Diffusion tensor imaging in early Alzheimer's disease. *Psychiatry Res.* 146, 243–249. doi:10.1016/j.pscychresns.2006.01.005

Nowrangi, M. A., Lyketsos, C. G., Leoutsakos, J. M., Oishi, K., Albert, M., Mori, S., et al. (2013). Longitudinal, region-specific course of diffusion tensor imaging measures in mild cognitive impairment and Alzheimer's disease. *Alzheimers Dement.* 9, 519–528. doi:10.1016/j.jalz.2012.05.2186

Oishi, K., Mielke, M. M., Albert, M., Lyketsos, C. G., and Mori, S. (2012). The fornix sign: a potential sign for Alzheimer's disease based on diffusion tensor imaging. *J. Neuroimaging* 22, 365–374. doi:10.1111/j.1552-6569.2011.00633.x

Pasternak, O., Sochen, N., Gur, Y., Intrator, N., and Assaf, Y. (2009). Free water elimination and mapping from diffusion MRI. *Magn. Reson. Med.* 62, 717–730. doi:10.1002/mrm.22055

Petersen, R. C. (2004). Mild cognitive impairment as a diagnostic entity. *J. Intern. Med.* 256, 183–194. doi:10.1111/j.1365-2796.2004.01388.x

Petersen, R. C., Smith, G. E., Waring, S. C., Ivnik, R. J., Tangalos, E. G., and Kokmen, E. (1999). Mild cognitive impairment: clinical characterization and outcome. *Arch. Neurol.* 56, 303–308. doi:10.1001/archneur.56.3.303

Pruessmann, K. P., Weiger, M., Scheidegger, M. B., and Boesiger, P. (1999). SENSE: sensitivity encoding for fast MRI. *Magn. Reson. Med.* 42, 952–962. doi:10.1002/(SICI)1522-2594(199911)42:5<952::AID-MRM16>3.3.CO;2-J

Rami, L., Valls-Pedret, C., Bartres-Faz, D., Caprile, C., Sole-Padulles, C., Castellvi, M., et al. (2011). Cognitive reserve questionnaire. Scores obtained in a healthy elderly population and in one with Alzheimer's disease. *Rev. Neurol.* 52, 195–201.

Rasquin, S. M., Lodder, J., Visser, P. J., Lousberg, R., and Verhey, F. R. (2005). Predictive accuracy of MCI subtypes for Alzheimer's disease and vascular dementia in subjects with mild cognitive impairment: a 2-year follow-up study. *Dement. Geriatr. Cogn. Disord.* 19, 113–119. doi:10.1159/000082662

Reijmer, Y. D., Leemans, A., Heringa, S. M., Wielaard, I., Jeurissen, B., Koek, H. L., et al. (2012). Improved sensitivity to cerebral white matter abnormalities in Alzheimer's disease with spherical deconvolution based tractography. *PLoS ONE* 7:e44074. doi:10.1371/journal.pone.0044074

Roh, J. H., Qiu, A., Seo, S. W., Soon, H. W., Kim, J. H., Kim, G. H., et al. (2011). Volume reduction in subcortical regions according to severity of Alzheimer's disease. *J. Neurol.* 258, 1013–1020. doi:10.1007/s00415-010-5872-1

Rowley, J., Fonov, V., Wu, O., Eskildsen, S. F., Schoemaker, D., Wu, L., et al. (2013). White matter abnormalities and structural hippocampal disconnections in amnestic mild cognitive impairment and Alzheimer's disease. *PLoS ONE* 8, e74776. doi:10.1371/journal.pone.0074776

Schmahmann, J. D., and Pandya, D. N. (2006). *Fibre Pathways of the Brain.* New York NY: Oxford University Press.

Seeley, W. W., Crawford, R. K., Zhou, J., Miller, B. L., and Greicius, M. D. (2009). Neurodegenerative diseases target large-scale human brain networks. *Neuron* 62, 42–52. doi:10.1016/j.neuron.2009.03.024

Sheline, Y. I., and Raichle, M. E. (2013). Resting state functional connectivity in preclinical Alzheimer's disease. *Biol. Psychiatry* 74, 340–347. doi:10.1016/j.biopsych.2012.11.028

Shiino, A., Watanabe, T., Maeda, K., Kotani, E., Akiguchi, I., and Matsuda, M. (2006). Four subgroups of Alzheimer's disease based on patterns of atrophy using VBM and a unique pattern for early onset disease. *Neuroimage* 33, 17–26. doi:10.1016/j.neuroimage.2006.06.010

Skudlarski, P., Jagannathan, K., Anderson, K., Stevens, M. C., Calhoun, V. D., Skudlarska, B. A., et al. (2010). Brain connectivity is not only lower but different in schizophrenia: a combined anatomical and functional approach. *Biol. Psychiatry* 68, 61–69. doi:10.1016/j.biopsych.2010.03.035

Skudlarski, P., Jagannathan, K., Calhoun, V. D., Hampson, M., Skudlarska, B. A., and Pearlson, G. (2008). Measuring brain connectivity: diffusion tensor imaging validates resting state temporal correlations. *Neuroimage* 43, 554–561. doi:10.1016/j.neuroimage.2008.07.063

Song, X. W., Dong, Z. Y., Long, X. Y., Li, S. F., Zuo, X. N., Zhu, C. Z., et al. (2011). REST: a toolkit for resting-state functional magnetic resonance imaging data processing. *PLoS ONE* 6, e25031. doi:10.1371/journal.pone.0025031

Sperling, R. A., Aisen, P. S., Beckett, L. A., Bennett, D. A., Craft, S., Fagan, A. M., et al. (2011). Toward defining the preclinical stages of Alzheimer's disease: recommendations from the National Institute on Aging-Alzheimer's Association workgroups on diagnostic guidelines for Alzheimer's disease. *Alzheimers Dement.* 7, 280–292. doi:10.1016/j.jalz.2011.03.003

Sporns, O. (2014). Contributions and challenges for network models in cognitive neuroscience. *Nat. Neurosci.* 17, 652–660. doi:10.1038/nn.3690

Stahl, R., Dietrich, O., Teipel, S. J., Hampel, H., Reiser, M. F., and Schoenberg, S. O. (2007). White matter damage in Alzheimer disease and mild cognitive impairment: assessment with diffusion-tensor MR imaging and parallel imaging techniques. *Radiology* 243, 483–492. doi:10.1148/radiol.2432051714

Stephan, B. C., Hunter, S., Harris, D., Llewellyn, D. J., Siervo, M., Matthews, F. E., et al. (2012). The neuropathological profile of mild cognitive impairment (MCI): a systematic review. *Mol. Psychiatry* 17, 1056–1076. doi:10.1038/mp.2011.147

Stoub, T. R., Detoledo-Morrell, L., Stebbins, G. T., Leurgans, S., Bennett, D. A., and Shah, R. C. (2006). Hippocampal disconnection contributes to memory dysfunction in individuals at risk for Alzheimer's disease. *Proc. Natl. Acad. Sci. U. S. A.* 103, 10041–10045. doi:10.1073/pnas.0603414103

Teipel, S. J., Grothe, M. J., Filippi, M., Fellgiebel, A., Dyrba, M., Frisoni, G. B., et al. (2014). Fractional anisotropy changes in Alzheimer's disease depend on the underlying fiber tract architecture: a multiparametric DTI study using joint independent component analysis. *J. Alzheimers Dis.* 41, 69–83. doi:10.3233/jad-131829

Tournier, J. D., Mori, S., and Leemans, A. (2011). Diffusion tensor imaging and beyond. *Magn. Reson. Med.* 65, 1532–1556. doi:10.1002/mrm.22924

Tournier, J. D., Yeh, C. H., Calamante, F., Cho, K. H., Connelly, A., and Lin, C. P. (2008). Resolving crossing fibres using constrained spherical deconvolution: validation using diffusion-weighted imaging phantom data. *Neuroimage* 42, 617–625. doi:10.1016/j.neuroimage.2008.05.002

van den Heuvel, M., Mandl, R., Luigjes, J., and Hulshoff Pol, H. (2008). Microstructural organization of the cingulum tract and the level of default mode functional connectivity. *J. Neurosci.* 28, 10844–10851. doi:10.1523/jneurosci.2964-08.2008

van den Heuvel, M. P., and Sporns, O. (2013). An anatomical substrate for integration among functional networks in human cortex. *J. Neurosci.* 33, 14489–14500. doi:10.1523/jneurosci.2128-13.2013

Vidal-Pineiro, D., Valls-Pedret, C., Fernandez-Cabello, S., Arenaza-Urquijo, E. M., Sala-Llonch, R., Solana, E., et al. (2014). Decreased default mode network connectivity correlates with age-associated structural and cognitive changes. *Front. Aging Neurosci.* 6:256. doi:10.3389/fnagi.2014.00256

Vos, S. B., Jones, D. K., Jeurissen, B., Viergever, M. A., and Leemans, A. (2012). The influence of complex white matter architecture on the mean diffusivity in diffusion tensor MRI of the human brain. *Neuroimage* 59, 2208–2216. doi:10.1016/j.neuroimage.2011.09.086

Welsh, K., Butters, N., Hughes, J., Mohs, R., and Heyman, A. (1991). Detection of abnormal memory decline in mild cases of Alzheimer's disease using CERAD neuropsychological measures. *Arch. Neurol.* 48, 278–281. doi:10.1001/archneur.1991.00530150046016

Welsh, K. A., Butters, N., Hughes, J. P., Mohs, R. C., and Heyman, A. (1992). Detection and staging of dementia in Alzheimer's disease. Use of the neuropsychological measures developed for the consortium to establish a registry for Alzheimer's disease. *Arch. Neurol.* 49, 448–452. doi:10.1001/archneur.1992.00530290030008

Westin, C. F., Maier, S. E., Mamata, H., Nabavi, A., Jolesz, F. A., and Kikinis, R. (2002). Processing and visualization for diffusion tensor MRI. *Med. Image Anal.* 6, 93–108. doi:10.1016/S1361-8415(02)00053-1

Wu, Q. J., Guo, Z. J., Liu, S. E., Yu, H. Q., Chen, J., and Yang, H. M. (2013). Relationship between episodic memory and resting-state brain functional connectivity network in patients with Alzheimer's disease and mild cognition impairment. *Zhonghua Yi Xue Za Zhi* 93, 1795–1800.

Yan, C., and Zang, Y. (2010). DPARSF: a MATLAB toolbox for "pipeline" data analysis of resting-state fMRI. *Front. Syst. Neurosci.* 4, 13. doi:10.3389/fnsys.2010.00013

Yesavage, J. A. (1988). Geriatric depression scale. *Psychopharmacol. Bull.* 24, 709–711.

Yoon, H. J., Park, K. W., Jeong, Y. J., and Kang, D. Y. (2012). Correlation between neuropsychological tests and hypoperfusion in MCI patients: anatomical labeling using xjView and Talairach Daemon software. *Ann. Nucl. Med.* 26, 656–664. doi:10.1007/s12149-012-0625-0

Ystad, M., Eichele, T., Lundervold, A. J., and Lundervold, A. (2010). Subcortical functional connectivity and verbal episodic memory in healthy elderly – a resting state fMRI study. *Neuroimage* 52, 379–388. doi:10.1016/j.neuroimage.2010.03.062

Zarei, M., Patenaude, B., Damoiseaux, J., Morgese, C., Smith, S., Matthews, P. M., et al. (2010). Combining shape and connectivity analysis: an MRI study of thalamic degeneration in Alzheimer's disease. *Neuroimage* 49, 1–8. doi:10.1016/j.neuroimage.2009.09.001

Zhang, Y., Schuff, N., Camacho, M., Chao, L. L., Fletcher, T. P., Yaffe, K., et al. (2013). MRI markers for mild cognitive impairment: comparisons between white matter integrity and gray matter volume measurements. *PLoS ONE* 8:e66367. doi:10.1371/journal.pone.0066367

Zhou, B., Liu, Y., Zhang, Z., An, N., Yao, H., Wang, P., et al. (2013). Impaired functional connectivity of the thalamus in Alzheimer's disease and mild cognitive impairment: a resting-state fMRI study. *Curr. Alzheimer Res.* 10, 754–766. doi:10.2174/15672050113109990146

Zhou, Y., Dougherty, J. H. Jr., Hubner, K. F., Bai, B., Cannon, R. L., and Hutson, R. K. (2008). Abnormal connectivity in the posterior cingulate and hippocampus in early Alzheimer's disease and mild cognitive impairment. *Alzheimers Dement.* 4, 265–270. doi:10.1016/j.jalz.2008.04.006

Zhuang, L., Sachdev, P. S., Trollor, J. N., Kochan, N. A., Reppermund, S., Brodaty, H., et al. (2012a). Microstructural white matter changes in cognitively normal individuals at risk of amnestic MCI. *Neurology* 79, 748–754. doi:10.1212/WNL.0b013e3182661f4d

Zhuang, L., Wen, W., Trollor, J. N., Kochan, N. A., Reppermund, S., Brodaty, H., et al. (2012b). Abnormalities of the fornix in mild cognitive impairment are related to episodic memory loss. *J. Alzheimers Dis.* 29, 629–639. doi:10.3233/jad-2012-111766

Zhuang, L., Sachdev, P. S., Trollor, J. N., Reppermund, S., Kochan, N. A., Brodaty, H., et al. (2013). Microstructural white matter changes, not hippocampal atrophy, detect early amnestic mild cognitive impairment. *PLoS ONE* 8, e58887. doi:10.1371/journal.pone.0058887

Zhuang, L., Wen, W., Zhu, W., Trollor, J., Kochan, N., Crawford, J., et al. (2010). White matter integrity in mild cognitive impairment: a tract-based spatial statistics study. *Neuroimage* 53, 16–25. doi:10.1016/j.neuroimage.2010.05.068

Conflict of Interest Statement: The authors declare that the research was conducted in the absence of any commercial or financial relationships that could be construed as a potential conflict of interest.

*Received: 31 July 2014; accepted: 22 January 2015; published online: 05 February 2015. Citation: Kehoe EG, Farrell D, Metzler-Baddeley C, Lawlor BA, Kenny RA, Lyons D, McNulty JP, Mullins PG, Coyle D and Bokde AL (2015) Fornix white matter is correlated with resting-state functional connectivity of the thalamus and hippocampus in healthy aging but not in mild cognitive impairment – a preliminary study. Front. Aging Neurosci. **7**:10. doi: 10.3389/fnagi.2015.00010*

This article was submitted to the journal Frontiers in Aging Neuroscience.

frontiers in
AGING NEUROSCIENCE

ORIGINAL RESEARCH ARTICLE
published: 30 June 2014
doi: 10.3389/fnagi.2014.00142

Correlations between limbic white matter and cognitive function in temporal-lobe epilepsy, preliminary findings

Ryan P. D. Alexander[1], Luis Concha[2], Thomas J. Snyder[3], Christian Beaulieu[2] and Donald William Gross[1]*

[1] *Division of Neurology, University of Alberta, Edmonton, AB, Canada*
[2] *Department of Biomedical Engineering, University of Alberta, Edmonton, AB, Canada*
[3] *Department of Psychiatry, University of Alberta, Edmonton, AB, Canada*

Edited by:
Kenichi Oishi, Johns Hopkins University, USA

Reviewed by:
JackJ. Lin, University of California, Irvine, USA
Kenichi Oishi, Johns Hopkins University, USA

****Correspondence:***
Donald William Gross, Department of Medicine, Division of Neurology, 2E3.19 Walter C Mackenzie Health Sciences Centre, Edmonton, AB T6G 2B7, Canada
e-mail: donald.gross@ualberta.ca

The limbic system is presumed to have a central role in cognitive performance, in particular memory. The purpose of this study was to investigate the relationship between limbic white matter microstructure and neuropsychological function in temporal-lobe epilepsy (TLE) patients using diffusion tensor imaging (DTI). Twenty-one adult TLE patients, including 7 non-lesional (nlTLE) and 14 with unilateral mesial temporal sclerosis (uTLE), were studied with both DTI and hippocampal T2 relaxometry. Correlations were performed between fractional anisotropy (FA) of the bilateral fornix and cingulum, hippocampal T2, neuropsychological tests. Positive correlations were observed in the whole group for the left fornix and processing speed index. In contrast, memory tests did not show significant correlations with DTI findings. Subgroup analysis demonstrated an association between the left fornix and processing speed in nlTLE but not uTLE. No correlations were observed between hippocampal T2 and test scores in either the TLE group as a whole or after subgroup analysis. Our findings suggest that integrity of the left fornix specifically is an important anatomical correlate of cognitive function in TLE patients, in particular patients with nlTLE.

Keywords: mesial temporal sclerosis, temporal-lobe epilepsy, neuropsychological assessment, diffusion tensor imaging, processing speed

INTRODUCTION

Temporal-lobe epilepsy (TLE) is the most common focal epilepsy syndrome and is often associated with cognitive comorbidity in particular for patients with mesial temporal sclerosis (MTS) (Hermann et al., 2009). Previous magnetic resonance imaging (MRI) volumetric studies have demonstrated that cognitive deficits in TLE are most strongly predicted by white matter volume (Hermann et al., 2002, 2003). Diffusion tensor imaging (DTI) permits the measurement of specific white matter tissue characteristics and thus has potential advantages over a non-specific technique like volumetric MRI (Basser et al., 1994). *In vivo* DTI of the fornix in TLE patients has shown histological correlates between fractional anisotropy (FA) and axonal membranes (Concha et al., 2010) thereby validating the technique as a non-invasive indicator of white matter micro-structural characteristics in human brain. Diffusion parameters of the uncinate fasciculus, inferior fronto-occipital fasciculus, arcuate fasciculus, and cingulum have been demonstrated to correlate with verbal memory, naming performance, and fluency in TLE patients (Flugel et al., 2006; Diehl et al., 2008; McDonald et al., 2008; Riley et al., 2010). In the present study, we focused on the fornix and cingulum, two prominent structures in the limbic white matter network, which have been demonstrated to be abnormal in TLE, albeit with differences between non-lesional TLE (nlTLE) and TLE with unilateral MTS (uTLE) (uTLE subjects have been demonstrated to have reduced FA of the fornix and cingulum while nlTLE have not) (Concha et al., 2005a,b, 2009). The purpose of this study was to assess correlations between white matter structure using DTI and cognitive function in a group of adult TLE patients.

Abbreviations: AVLT, Rey auditory verbal learning test recall score; CPMG, Carr Purcell Meibom Gill sequence; CVMT, continuous visual memory test total score; DTI, diffusion tensor imaging; FA, fractional anisotropy; MRI, magnetic resonance imaging; MTS, mesial temporal sclerosis; nlTLE, non-lesional temporal-lobe epilepsy; $r(p)'$, Spearman rho correlation.; ROI, region of interest; SD, standard deviation; TLE, temporal-lobe epilepsy; uTLE, temporal-lobe epilepsy with unilateral mesial temporal sclerosis; WAIS-III, Wechsler adult intelligence scale third edition.

MATERIALS AND METHODS

STANDARD PROTOCOL APPROVALS, REGISTRATIONS, AND PATIENT CONSENTS

Approval of the project was obtained from the University of Alberta Health Research Ethics Board and informed consent was obtained from all participants.

SUBJECTS

Twenty-one left hemisphere language dominant TLE patients were studied, including 7 nlTLE patients (3 left, 1 right, 3 bilateral) and 14 with uTLE (10 left, 4 right) (**Table 1**). No significant differences were observed between nlTLE and uTLE group means of age (nlTLE: 42, uTLE: 41, $p = 0.86$), onset age (nlTLE: 22, uTLE: 13, $p = 0.10$), or disease duration (nlTLE: 20, uTLE: 27, $p = 0.21$). The median number of prescribed anti-epileptic drugs per patient was two in both groups. Of note, a similar number of patients in each group were prescribed topiramate (nlTLE: 3, uTLE: 4), which has been shown to negatively impact cognitive ability, particularly verbal memory, and fluency (Thompson et al., 2000). TLE diagnosis

Table 1 | Demographic and clinical data for study patients.

Variable		nlTLE	uTLE
Epileptic focus	Left	3	10
	Right	1	4
	Bilateral	3	–
Sex	Male	3	4
	Female	4	10
Age (years)	Mean ± SD	42 ± 10	41 ± 10
	Range	30–59	20–59
Education (years)	Mean ± SD	12 ± 2	10 ± 3
	Range	7–14	4–15
Onset age (years)	Mean ± SD	22 ± 10	13 ± 11
	Range	11–37	1–33
Disease duration (years)	Mean ± SD	20 ± 13	27 ± 13
	Range	8–47	6–51
Processing Speed Index	Mean ± SD	88 ± 15	76 ± 14
	Range	70–112	55–105
Auditory Verbal Learning	Mean ± SD	34 ± 12	29 ± 10
Test score	Range	17–53	9–50
Continuous Visual Memory	Mean ± SD	28 ± 12	23 ± 20
Test score	Range	6–42	−11–63

No significant differences were observed between nlTLE and uTLE groups for age ($p = 0.83$), education ($p = 0.13$) onset age ($p = 0.09$), and disease duration ($p = 0.26$).

was based on ictal semiology of complex partial seizures, confined temporal-lobe interictal, and ictal electroencephalogram findings. Absence of structural lesions outside of the temporal-lobe was confirmed on clinical MRI. MTS was defined based on hippocampal T2 greater than two standard deviations of controls. Patients were considered non-lesional if hippocampal T2 was within two standard deviations of control values. Left hemisphere language dominance was confirmed by either dichotic listening or intracarotid sodium amytal tests. The patient group used in this analysis is a subset of the study group previously reported (Concha et al., 2009) exclusions were made for: insufficient neuropsychological test data, neuropsychological testing greater than 36 months from the time of research MRI, or atypical language dominance. The median length of time between research MRI and neuropsychological evaluation was 1 month (range 0–35 months), 14 patients having less than 6 months between MRI and neuropsychological evaluation. Additional patient information has been previously reported (Concha et al., 2009).

NEUROPSYCHOLOGICAL EVALUATION

The neuropsychological tests used were: Processing Speed Index (Digit Symbol and Symbol Search subtests of the WAIS-III) ($n = 19$), that has been reported to be sensitive to white matter abnormalities (Axelrod et al., 2001; Drew et al., 2009), the Rey Auditory Verbal Learning Test delayed recall score (AVLT) ($n = 21$) as a measure of verbal memory, and the Continuous Visual Memory Test total raw score (CVMT) as a measure of figural memory ($n = 21$). Standardized scores adjusted for both age and education were used.

IMAGE ACQUISITION

Cerebrospinal fluid-suppressed diffusion tensor images were acquired in 9:30 min using a 1.5 T Siemens Sonata MRI scanner (Siemens Medical Systems, Erlangen, Germany). The sequence consisted of 26 contiguous 2 mm thick axial slices positioned to provide coverage of the limbic tracts with an in-plane resolution of 2 mm × 2 mm (interpolated to 1 mm × 1 mm × 2 mm). Diffusion-sensitized images were acquired in six directions, with a b value of 1000 s/mm^2. Full details of the DTI protocol have been previously provided (Concha et al., 2005a,b). T2 images for the quantification of hippocampal T2 were obtained using a modified CPMG sequence with 32 echoes (TR = 4.43 s; $TE_1 = 9.1$ ms, echo spacing = 9.1 ms), producing 10 coronal 3 mm thick slices with a 3 mm interslice gap in 8:13 min (voxel size 1.2 mm × 1.2 mm × 3 mm interpolated to 0.6 mm × 0.6 mm × 3 mm).

IMAGE PROCESSING

Bilateral fornix and cingulum were investigated using deterministic tractography. By transferring DTI images to a personal computer running DTIstudio 2.5 (Johns Hopkins University, Baltimore, MD, USA), tracts were depicted using fiber assignment by continuous tracking algorithm. Placement of tract-selection regions of interest (ROI) for each fiber bundle was based on methods outlined previously (Mori et al., 1999; Wakana et al., 2004). The FA threshold was set at 0.3 for all tracts. The FA threshold of 0.3 is commonly used in the deterministic tractography literature and is the threshold that we have used in our previous tractography studies of the fornix and cingulum (Mori et al., 1999; Concha et al., 2005a,b, 2009). If more than one streamline for a tract passed through a voxel, repeated coordinates were discarded and the voxel was only included once in the analysis. Mean diffusion parameters for each white matter tract were calculated in each patient. For this study, the crus of the fornix and the temporal portion of the cingulum were analyzed between the axial levels of the mammillary bodies and the fusion of the crura of the fornices. The T2 signal decay was fitted to a mono-exponential curve by voxel across the multi-echo coronal images. T2 values for each hippocampus were calculated by averaging within ROIs manually drawn on two consecutive slices (Concha et al., 2005a,b).

STATISTICAL ANALYSIS

Statistical tests

Analyses were performed using SPSS 17.0 (SPSS Inc., Chicago, IL, USA). Spearman correlations were used to evaluate the relationship between FA of each tract and neuropsychological test scores. With a total of 12 tests performed for the primary analysis, Bonferroni correction sets a significance level of $p < 0.0042$.

Primary analysis

The primary analysis was made studying the entire group (nlTLE, uTLE, right, left, and bilateral TLE combined) based on the hypothesis that correlations would be observed between white matter measures and neuropsychological tests and that the previously reported differences in white matter DTI measures and neuropsychological tests seen in nlTLE and uTLE and right and left TLE would provide an adequate range of values to demonstrate significant correlations.

Secondary analysis

Where significant correlations were observed in the preliminary analysis, subsequent analysis was performed looking at the nlTLE and uTLE groups and right and left TLE groups separately. Correlations between hippocampal T2 and neuropsychological test scores were also assessed based on the hypothesis that changes in either white matter diffusion parameters or cognitive test scores could be secondary to mesial temporal pathology.

RESULTS

PATIENT NEUROPSYCHOLOGICAL TEST SCORES

After examining whole group summary statistics of neuropsychological test scores [Processing Speed: 80 ± 15 (55–112); AVLT: 32 ± 12 (9–57); CVMT: 23 ± 17 (−11–63)], differences between nlTLE and uTLE subgroups were also investigated (**Table 1**). When compared to the average processing speed standard score of 100 (SD 15), the nlTLE group mean of 88 is low average but still within normal limits, whereas the uTLE group score of 76 is mildly deficient. Considering AVLT, for which the mean standard score is 50 (SD 10), both groups are within normal limits for AVLT but nlTLE patients scored higher (54) than uTLE (42). Both groups were impaired (<first percentile) on the CVMT (nlTLE: 24, uTLE: 23) (**Table 1**).

PRIMARY ANALYSIS (ENTIRE TLE GROUP)

Higher FA values for the left fornix were associated with higher Processing Speed indices [$r(p)' = 0.62$, $p = 0.004$] (**Table 2**). No other correlations were observed between Processing Speed, AVLT, CVMT, and FA of the fornix and cingulum (**Table 2**).

SECONDARY ANALYSIS

nlTLE and uTLE groups

After splitting the TLE patients into subgroups (nlTLE $n = 7$, uTLE $n = 14$), other trends became evident. The correlation between FA of the left fornix and Processing Speed was explained by a strong correlation in the nlTLE group [$r(p)' = 0.90$, $p = 0.02$], whereas the uTLE group showed no correlation [$r(p)' = 0.40$, $p = 0.18$] (**Figure 1**).

Table 2 | Spearman rho correlations of neuropsychological test scores and fractional anisotropy (FA) of the fornix and cingulum in TLE patients.

	Processing Speed Index (PS)	Auditory Verbal Learning Test (AVLT)	Continuous Visual Memory Test (CVMT)
	***n* = 19**	***n* = 21**	***n* = 21**
Left fornix	0.62 (0.004)*	−0.10 (0.67)	0.33 (0.15)
Right fornix	0.25 (0.30)	−0.04 (0.87)	0.27 (0.25)
Left cingulum	0.32 (0.18)	−0.09 (0.71)	−0.02 (0.92)
Right cingulum	0.26 (0.28)	0.01 (0.97)	−0.05 (0.82)

*Displayed as 'Spearmans's r (p)'. *denotes significance with Bonferoni correction ($p < 0.0042$).*

Right and left TLE

Analysis of right TLE ($n = 5$) and left TLE ($n = 13$) demonstrated a positive correlation between FA of the left fornix and processing speed in left TLE [$r(p)' = 0.60$, $p = 0.04$].

Correlations between hippocampal T2 relaxometry and neuropsychology

Correlations were not observed between any of the neuropsychological test scores and left or right hippocampal T2 in the total patient group. As well, no correlation was seen between left hippocampal T2 and processing speed in the nlTLE group.

DISCUSSION

Quantitative MRI studies have shown white matter volume correlates with verbal and figural memory (Hermann et al., 2002, 2003). Recent DTI studies have demonstrated reduced FA in cerebral white matter in multiple brain regions and specific white matter tracts (Concha et al., 2005a,b, 2009; Gross et al., 2006; Focke et al., 2008; Schoene-Bake et al., 2009) with several reports demonstrating correlations between memory and DTI changes in TLE (Diehl et al., 2008; McDonald et al., 2008; Riley et al., 2010). While memory deficits are considered central to the clinical phenotype of TLE, broader cognitive measures such as intelligence, executive function and motor speed have also been demonstrated to be reduced (Hermann et al., 1997; Oyegbile et al., 2004).

The goal of this study was to investigate the relationship between limbic white matter microstructure and cognition in TLE. The primary observation of this study was that correlations were only observed between FA of the left fornix and processing speed for the TLE group as a whole with no correlations observed for the verbal (AVLT) and non-verbal (CVMT) memory tests nor for FA of the other tracts (right fornix and bilateral cingulum) and any of the cognitive measures.

It was observed that the Processing Speed Index, a WAIS-III measure that is most sensitive to brain disorders affecting white matter (Hawkins, 1998) such as traumatic brain injury (Axelrod et al., 2001) and multiple sclerosis (Drew et al., 2009), only correlated with left fornix FA whereas it is usually considered a measure of more widespread white matter function. Wernicke–Korsakoff syndrome, largely based in mammillary body pathology (Zubaran et al., 1997), has also been linked to deficits in one of the two subtests making up the Processing Speed Index, the Digit Symbol-Coding test, in addition to the expected deficit in memory test scores (Jacobson et al., 1990; Oscar-Berman et al., 2004). While there are no other specific references to the relationship between the left fornix specifically and Processing Speed, the link between Processing Speed and limbic structures both for Wernicke–Korsakoff as well as this study suggests an important role of the limbic system specifically in what has been considered a measure of more widespread white matter functioning. While the absence of correlations with other white matter structures suggests a unique role for the left fornix, given the limited sample size, false negative results cannot be ruled out, therefore, further work is required to better understand the relationship between Processing Speed and specific white matter tracts.

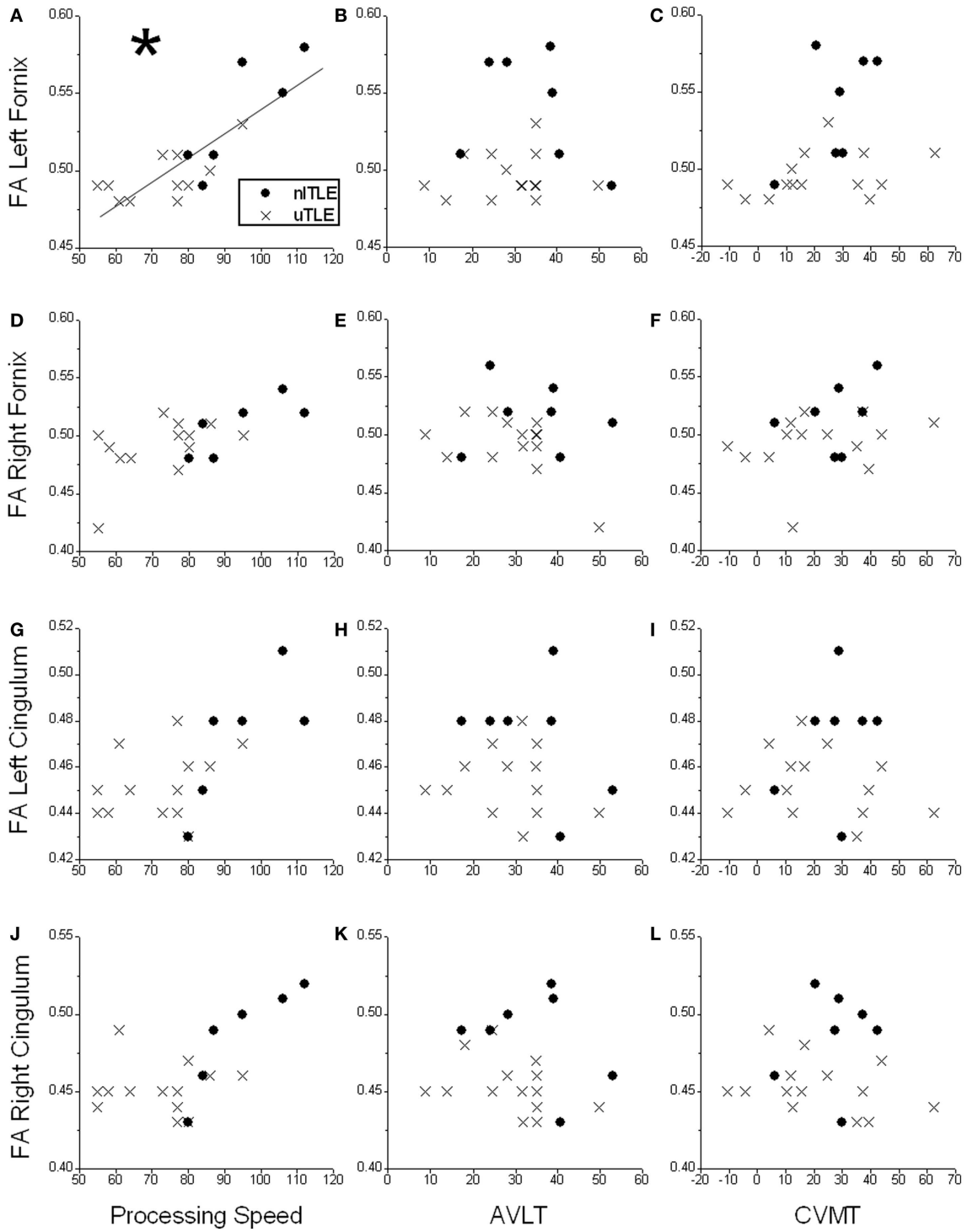

FIGURE 1 | Scatter plots displaying correlations of neuropsychological test scores [Processing Speed Index, Auditory Verbal Learning Test (AVLT), and Continuous Visual Memory Test (CVMT)] and fractional anisotropy (FA) of the left fornix (A–C), right fornix (D–F), left cingulum (G–I), and right cingulum (J–L) in patients with temporal-lobe epilepsy without mesial temporal sclerosis (nlTLE) and with mesial temporal sclerosis (uTLE). *A significant positive correlation is seen between Processing Speed and FA of the left fornix which is primarily driven by the nlTLE subjects. No other significant correlations were observed for the other comparisons.

While caution must be taken in drawing strong conclusions from the secondary analysis, in particular given the small sample size of some of the subgroups, several interesting findings are observed in particular when looking at the nlTLE and uTLE subgroups.

We observed that the association between left fornix FA and Processing Speed is unique to the nlTLE group despite the greater deficit in intelligence scores previously shown to be evident in uTLE patients (McMillan et al., 1987). Of note, we have previously reported correlations between FA of the fornix and disease duration in nlTLE (Concha et al., 2009). Together these observations, albeit preliminary, are consistent with fornix degeneration and progressive cognitive dysfunction being secondary to ongoing seizures in nlTLE. Of note, the absence of correlations between hippocampal T2 and cognition suggests that the observed correlations between the left fornix and Processing Speed are not a secondary effect (i.e., our findings are not consistent with the nlTLE subjects developing hippocampal degeneration which then leads to downstream degeneration of the fornix and subsequent to this reduced FA).

The dissociation of findings between subgroups suggests the potential for seizure-related white matter and cognitive deterioration being unique to the nlTLE group, supporting the distinctiveness of the nlTLE and uTLE disease states. This idea has also been suggested and supported in recent DTI research (Concha et al., 2009; Kim et al., 2010; Shon et al., 2010). The fact that no correlations were observed in uTLE patients despite greater neuropsychological impairment suggests factors other than fornix damage are responsible for cognitive deficits in this group.

There has been much investigation into the extent and severity of cognitive decline in chronic TLE. Verbal memory peaks earlier and declines faster in TLE patients, especially in left TLE (Helmstaedter and Elger, 2009). A recent prospective study has demonstrated abnormal 4 year trajectory for memory as well as executive function and motor speed in TLE which was associated with baseline MRI abnormalities, lower baseline intelligence, older age, and longer duration of epilepsy (Hermann et al., 2006). As well, general intelligence has been demonstrated to be significantly reduced in earlier onset TLE, including patients without MTS (Kaaden and Helmstaedter, 2009). The cross-sectional nature of our data makes it difficult to draw conclusions regarding whether structural (fornix) or functional (processing speed) changes are progressive. Longitudinal studies are required to evaluate the relationship between functional and structural changes seen in TLE and determine whether nlTLE and uTLE may follow different trajectories.

With respect to division of our TLE sample, an appealing avenue of analysis would be to study group differences between right and left epileptic foci, as has been previously reported (Diehl et al., 2008; McDonald et al., 2008). The primary objective of this study was to use a population of patients with TLE to look for correlations between limbic white matter structure and cognitive function. The study design intentionally included uTLE, nlTLE as well as TLE patients with both right and left epileptic foci as this design was expected to provide a range of both structural and functional abnormalities [i.e., based on the literature uTLE patients were expected to have reduced limbic white matter FA (Concha et al., 2009) and lower cognitive test scores compared to nlTLE (McMillan et al., 1987) and right and left TLE patients were expected to expand the range of scores in particular tests of verbal and figural memory] (Powell et al., 2007). While it remains interesting to look at right and left differences, unfortunately, due to limitations of sample size in particular for the right TLE group ($n = 5$), it is difficult to compare right and left TLE in this study. While the left TLE group did show a significant correlation between FA of the left fornix and processing speed, the absence of positive findings in the right TLE group is most likely explained by the low sample size.

CONCLUSION

In conclusion, our findings suggest that integrity of the left fornix specifically is an important anatomical correlate of cognitive function, in particular processing speed, in TLE patients. Furthermore, the differences in correlations of limbic white matter FA versus cognitive test scores in the subgroup analysis suggest that uTLE and nlTLE are distinctly different clinical and anatomical entities.

ACKNOWLEDGMENTS

Operating support provided by the Canadian Institutes of Health Research (DWG, Christian Beaulieu) as well as salary support by Alberta Innovates – Health Solutions (Christian Beaulieu).

REFERENCES

Axelrod, B. N., Fichtenberg, N. L., Liethen, P. C., Czarnota, M. A., and Stucky, K. (2001). Performance characteristics of postacute traumatic brain injury patients on the WAIS-III and WMS-III. *Clin. Neuropsychol.* 15, 516–520. doi:10.1076/clin.15.4.516.1884

Basser, P. J., Mattiello, J., and LeBihan, D. (1994). MR diffusion tensor spectroscopy and imaging. *Biophys. J.* 66, 259–267. doi:10.1016/S0006-3495(94)80775-1

Concha, L., Beaulieu, C., Collins, D. L., and Gross, D. W. (2009). White-matter diffusion abnormalities in temporal-lobe epilepsy with and without mesial temporal sclerosis. *J. Neurol. Neurosurg. Psychiatr.* 80, 312–319. doi:10.1136/jnnp.2007.139287

Concha, L., Beaulieu, C., and Gross, D. W. (2005a). Bilateral limbic diffusion abnormalities in unilateral temporal lobe epilepsy. *Ann. Neurol.* 57, 188–196. doi:10.1002/ana.20334

Concha, L., Gross, D. W., and Beaulieu, C. (2005b). Diffusion tensor tractography of the limbic system. *AJNR Am. J. Neuroradiol.* 26, 2267–2274.

Concha, L., Livy, D. J., Beaulieu, C., Wheatley, B. M., and Gross, D. W. (2010). In vivo diffusion tensor imaging and histopathology of the fimbria-fornix in temporal lobe epilepsy. *J. Neurosci.* 30, 996–1002. doi:10.1523/JNEUROSCI.1619-09.2010

Diehl, B., Busch, R. M., Duncan, J. S., Piao, Z., Tkach, J., and Luders, H. O. (2008). Abnormalities in diffusion tensor imaging of the uncinate fasciculus relate to reduced memory in temporal lobe epilepsy. *Epilepsia* 49, 1409–1418. doi:10.1111/j.1528-1167.2008.01596.x

Drew, M. A., Starkey, N. J., and Isler, R. B. (2009). Examining the link between information processing speed and executive functioning in multiple sclerosis. *Arch. Clin. Neuropsychol.* 24, 47–58. doi:10.1093/arclin/acp007

Flugel, D., Cercignani, M., Symms, M. R., O'Toole, A., Thompson, P. J., Koepp, M. J., et al. (2006). Diffusion tensor imaging findings and their correlation with neuropsychological deficits in patients with temporal lobe epilepsy and interictal psychosis. *Epilepsia* 47, 941–944. doi:10.1111/j.1528-1167.2006.00527.x

Focke, N. K., Thompson, P. J., and Duncan, J. S. (2008). Correlation of cognitive functions with voxel-based morphometry in patients with hippocampal sclerosis. *Epilepsy Behav.* 12, 472–476. doi:10.1016/j.yebeh.2007.12.011

Gross, D. W., Concha, L., and Beaulieu, C. (2006). Extratemporal white matter abnormalities in mesial temporal lobe epilepsy demonstrated with diffusion tensor imaging. *Epilepsia* 47, 1360–1363. doi:10.1111/j.1528-1167.2006.00603.x

Hawkins, K. A. (1998). Indicators of brain dysfunction derived from graphic representations of the WAIS-III/WMS-III Technical Manual clinical samples

data: a preliminary approach to clinical utility. *Clin Neuropsychol* 12, 535–551. doi:10.1076/clin.12.4.535.7236

Helmstaedter, C., and Elger, C. E. (2009). Chronic temporal lobe epilepsy: a neurodevelopmental or progressively dementing disease? *Brain* 132, 2822–2830. doi:10.1093/brain/awp182

Hermann, B., Seidenberg, M., Bell, B., Rutecki, P., Sheth, R., Ruggles, K., et al. (2002). The neurodevelopmental impact of childhood-onset temporal lobe epilepsy on brain structure and function. *Epilepsia* 43, 1062–1071. doi:10.1046/j.1528-1157.2002.49901.x

Hermann, B., Seidenberg, M., Bell, B., Rutecki, P., Sheth, R. D., Wendt, G., et al. (2003). Extratemporal quantitative MR volumetrics and neuropsychological status in temporal lobe epilepsy. *J. Int. Neuropsychol. Soc.* 9, 353–362. doi:10.1017/S1355617703930013

Hermann, B. P., Lin, J. J., Jones, J. E., and Seidenberg, M. (2009). The emerging architecture of neuropsychological impairment in epilepsy. *Neurol. Clin.* 27, 881–907. doi:10.1016/j.ncl.2009.08.001

Hermann, B. P., Seidenberg, M., Dow, C., Jones, J., Rutecki, P., Bhattacharya, A., et al. (2006). Cognitive prognosis in chronic temporal lobe epilepsy. *Ann. Neurol.* 60, 80–87. doi:10.1002/ana.20872

Hermann, B. P., Seidenberg, M., Schoenfeld, J., and Davies, K. (1997). Neuropsychological characteristics of the syndrome of mesial temporal lobe epilepsy. *Arch. Neurol.* 54, 369–376. doi:10.1001/archneur.1997.00550160019010

Jacobson, R. R., Acker, C. F., and Lishman, W. A. (1990). Patterns of neuropsychological deficit in alcoholic Korsakoff's syndrome. *Psychol. Med.* 20, 321–334. doi:10.1017/S0033291700017633

Kaaden, S., and Helmstaedter, C. (2009). Age at onset of epilepsy as a determinant of intellectual impairment in temporal lobe epilepsy. *Epilepsy Behav.* 15, 213–217. doi:10.1016/j.yebeh.2009.03.027

Kim, C. H., Koo, B. B., Chung, C. K., Lee, J. M., Kim, J. S., and Lee, S. K. (2010). Thalamic changes in temporal lobe epilepsy with and without hippocampal sclerosis: a diffusion tensor imaging study. *Epilepsy Res.* 90, 21–27. doi:10.1016/j.eplepsyres.2010.03.002

McDonald, C. R., Ahmadi, M. E., Hagler, D. J., Tecoma, E. S., Iragui, V. J., Gharapetian, L., et al. (2008). Diffusion tensor imaging correlates of memory and language impairments in temporal lobe epilepsy. *Neurology* 71, 1869–1876. doi:10.1212/01.wnl.0000327824.05348.3b

McMillan, T. M., Powell, G. E., Janota, I., and Polkey, C. E. (1987). Relationships between neuropathology and cognitive functioning in temporal lobectomy patients. *J. Neurol. Neurosurg. Psychiatr.* 50, 167–176. doi:10.1136/jnnp.50.2.167

Mori, S., Crain, B. J., Chacko, V. P., and van Zijl, P. C. (1999). Three-dimensional tracking of axonal projections in the brain by magnetic resonance imaging. *Ann. Neurol.* 45, 265–269. doi:10.1002/1531-8249(199902)45:2<265::AID-ANA21>3.0.CO;2-3

Oscar-Berman, M., Kirkley, S. M., Gansler, D. A., and Couture, A. (2004). Comparisons of Korsakoff and non-Korsakoff alcoholics on neuropsychological tests of prefrontal brain functioning. *Alcohol. Clin. Exp. Res.* 28, 667–675. doi:10.1097/01.ALC.0000122761.09179.B9

Oyegbile, T. O., Dow, C., Jones, J., Bell, B., Rutecki, P., Sheth, R., et al. (2004). The nature and course of neuropsychological morbidity in chronic temporal lobe epilepsy. *Neurology* 62, 1736–1742. doi:10.1212/01.WNL.0000125186.04867.34

Powell, H. W., Richardson, M. P., Symms, M. R., Boulby, P. A., Thompson, P. J., Duncan, J. S., et al. (2007). Reorganization of verbal and nonverbal memory in temporal lobe epilepsy due to unilateral hippocampal sclerosis. *Epilepsia* 48, 1512–1525. doi:10.1111/j.1528-1167.2007.01053.x

Riley, J. D., Franklin, D. L., Choi, V., Kim, R. C., Binder, D. K., Cramer, S. C., et al. (2010). Altered white matter integrity in temporal lobe epilepsy: association with cognitive and clinical profiles. *Epilepsia* 51, 536–545. doi:10.1111/j.1528-1167.2009.02508.x

Schoene-Bake, J. C., Faber, J., Trautner, P., Kaaden, S., Tittgemeyer, M., Elger, C. E., et al. (2009). Widespread affections of large fiber tracts in postoperative temporal lobe epilepsy. *Neuroimage* 46, 569–576. doi:10.1016/j.neuroimage.2009.03.013

Shon, Y. M., Kim, Y. I., Koo, B. B., Lee, J. M., Kim, H. J., Kim, W. J., et al. (2010). Group-specific regional white matter abnormality revealed in diffusion tensor imaging of medial temporal lobe epilepsy without hippocampal sclerosis. *Epilepsia* 51, 529–535. doi:10.1111/j.1528-1167.2009.02327.x

Thompson, P. J., Baxendale, S. A., Duncan, J. S., and Sander, J. W. (2000). Effects of topiramate on cognitive function. *J. Neurol. Neurosurg. Psychiatr.* 69, 636–641. doi:10.1136/jnnp.69.5.636

Wakana, S., Jiang, H., Nagae-Poetscher, L. M., van Zijl, P. C., and Mori, S. (2004). Fiber tract-based atlas of human white matter anatomy. *Radiology* 230, 77–87. doi:10.1148/radiol.2301021640

Zubaran, C., Fernandes, J. G., and Rodnight, R. (1997). Wernicke-Korsakoff syndrome. *Postgrad. Med. J.* 73, 27–31. doi:10.1136/pgmj.73.855.27

Conflict of Interest Statement: The authors declare that the research was conducted in the absence of any commercial or financial relationships that could be construed as a potential conflict of interest.

Received: 11 March 2014; accepted: 12 June 2014; published online: 30 June 2014.
*Citation: Alexander RPD, Concha L, Snyder TJ, Beaulieu C and Gross DW (2014) Correlations between limbic white matter and cognitive function in temporal-lobe epilepsy, preliminary findings. Front. Aging Neurosci. **6**:142. doi: 10.3389/fnagi.2014.00142*
This article was submitted to the journal Frontiers in Aging Neuroscience.

frontiers in
AGING NEUROSCIENCE

MINI REVIEW ARTICLE
published: 13 November 2014
doi: 10.3389/fnagi.2014.00316

Fractional anisotropy of the fornix and hippocampal atrophy in Alzheimer's disease

Kejal Kantarci*

Department of Radiology, Mayo Clinic, Rochester, MN, USA

Edited by:
Kenichi Oishi, Johns Hopkins University, USA

Reviewed by:
Roberta Brinton, University of Southern California, USA
Hui Wang, Children's National Medical Center, USA

****Correspondence:***
Kejal Kantarci, Department of Radiology, Mayo Clinic, 200 First Street SW, Rochester, MN 55905, USA
e-mail: kantarci.kejal@mayo.edu

Decrease in the directionality of water diffusion measured with fractional anisotropy (FA) on diffusion tensor imaging has been linked to loss of myelin and axons in the white matter. Fornix FA is consistently decreased in patients with mild cognitive impairment (MCI) and Alzheimer's disease (AD). Furthermore, decreased fornix FA is one of the earliest MRI abnormalities observed in cognitively normal individuals who are at an increased risk for AD, such as in pre-symptomatic carriers of familial AD mutations and in pre-clinical AD. Reductions of FA at these early stages, which predicted the decline in memory function. Fornix carries the efferent projections from the CA1 and CA3 pyramidal neurons of the hippocampus and subiculum, connecting these structures to the septal nuclei, anterior thalamic nucleus, mammillary bodies, and medial hypothalamus. Fornix also carries the afferent cholinergic and GABAergic projections from the medial septal nuclei and the adjacent diagonal band back to the medial temporal lobe, interconnecting the core limbic structures. Because fornix carries the axons projecting from the hippocampus, integrity of the fornix is in-part linked to the integrity of the hippocampus. In keeping with that, fornix FA is reduced in subjects with hippocampal atrophy, correlating with memory function. The literature on FA reductions in the fornix in the clinical spectrum of AD from pre-symptomatic carriers of familial AD mutations to pre-clinical AD, MCI, and dementia stages is reviewed.

Keywords: fornix, DTI, Alzheimer's disease, hippocampus, MRI imaging

ANATOMY OF THE HIPPOCAMPUS AND FORNIX CONNECTIONS

Hippocampal projections to the subcortical structures that form the fimbria are carried by the fornix bundle. The fornix has two major components that connect hippocampus and subcortical structures. These are the larger postcommissural component and the smaller precommissural component. A majority of the axonal projections in the fornix originate from the subiculum of the hippocampus and form the postcommissural fornix carrying subicular axons to the mammillary bodies, which then project to the anterior nucleus of the thalamus. A major axonal tract originating from the anterior thalamus projects to the posterior cingulate cortex, which connects back to hippocampus via the cingulum tract closing the "Papez Circuit" (Benarroch, 2006). In addition, the precommissural fornix caries axons originating from the CA1 and CA3 pyramidal neurons of the hippocampus to the lateral septal nucleus, which projects to the medial septum. The medial septum and the nucleus of the diagonal band send cholinergic and GABAergic projections back to the medial temporal lobe via the fornix.

Damage to fornix in monkeys produces deficits in learning about the places of objects and about the places where responses should be made. They are impaired in using information about their place in an environment. Furthermore, fornix lesions impair conditional left–right discrimination learning based on visual appearance of an object on either side (Rolls, 2014). Fornix transection in human beings has been reported to produce significant and persistent anterograde amnesia (D'Esposito et al., 1995).

Because majority of the axonal projections carried by the fornix originate from the subiculum and to a lesser extent from CA1 and CA3 pyramidal neurons of the hippocampus, neurodegenerative processes impacting these neuronal populations would also lead to degeneration of the axonal projections originating from these neurons. However, it is important to note that not all axons in the fornix originate from the hippocampus, as the cholinergic and GABAergic connections originating from the medial septum and the nucleus of the diagonal band project back to the medial temporal lobe via the fornix. Therefore, degeneration of neuronal populations in the hippocampus may not fully explain the axonal loss in the fornix.

NORMAL AGING AND THE HIPPOCAMPUS–FORNIX AXIS

In monkeys, number of myelinated nerve fibers in the fornix decrease with aging by 15–34%, but the loss of myelinated nerve fibers in the fornix is not disproportionately high or low compared to the rest of the white matter. However, it is not clear whether the myelinated nerve fiber loss from the fornix with age is due to loss of the parent neurons from the hippocampus, or due to age-related alterations that affect myelin sheaths, and alter the conduction velocities along nerve fibers resulting in degeneration in long projecting myelinated nerve fiber tracts. This loss of nerve fibers lead to a reduced subcortical connectivity of the hippocampus and may in-part be responsible for cognitive decline associated with normal aging even when the hippocampal neurons are intact (Peters et al., 2010).

Aging is associated with alterations in hippocampal dendritic morphology in the absence of neuronal loss, therefore

age-associated structural alterations in the fornix less likely to originate from hippocampal neuronal loss, and more likely be the consequence of demyelination and degeneration of fornix fibers with age (Hof and Morrison, 2004). While both hippocampal volumes (Jack et al., 1998), and white matter fractional anisotropy (FA) decreases during aging (Walhovd et al., 2010), a relationship between fornix FA and hippocampal volume remains even after controlling for age. Using a recursive regression procedure, to evaluate sequential relationships between the alterations of the hippocampus and fornix, Pelletier et al. showed that hippocampal atrophy in healthy aging could be mediated by a loss of fornix connections potentially through a retrograde process (Pelletier et al., 2013). Longitudinal change in hippocampal volumes and fornix FA over the adult lifespan may be useful in determining whether hippocampal volume loss or a decrease in fornix FA occur earlier during the aging process.

Sex differences in structural network connectivity across the life span have been observed in DTI studies, with women showing greater overall cortical connectivity and network organization and greater efficiency than men (Gong et al., 2009). However, it is unclear at this time whether there is a difference in structural connectivity across the hippocampus-fornix axis among men and women.

HIPPOCAMPUS-FORNIX AXIS IN PRODROMAL AND PRE-CLINICAL AD

There is converging evidence from longitudinal studies on clinically followed and autopsied cohorts that most people with the amnestic form of mild cognitive impairment (MCI) who progress to dementia in the future, develop Alzheimer's disease (AD) (Flicker et al., 1991; Bowen et al., 1997; Morris et al., 2001; Bennett et al., 2002; Meyer et al., 2002; Jicha et al., 2006; Petersen et al., 2006). In keeping with these findings, both hippocampal atrophy and a reduction in fornix FA are frequently observed in amnestic MCI (Liu et al., 2011; Zhuang et al., 2012, 2013; Zhang et al., 2013) and are associated with memory decline (Mielke et al., 2012) and the risk of progression to AD (Mielke et al., 2012; Douaud et al., 2013).

The relationship between the structural integrity of hippocampus and fornix has been demonstrated in MCI (Mielke et al., 2012; Zhuang et al., 2012). In a cohort of cognitively normal (CN) older adults ($n = 570$; median age = 78; interquartile range = 74-83) and MCI ($n = 131$; median age = 80; interquartile range = 77–86) from the community, both CN and MCI patients showed decreased fornix FA if they also had hippocampal atrophy or AD pattern of hypometabolism on ^{18}F Fluorodeoxyglucose (FDG) PET compared to the CN group with normal hippocampal volumes and metabolism on FDG PET. Having only a positive amyloid-β PET scan with Pittsburgh compound-B (PiB) was not responsible for a reduction in fornix FA in CN individuals, demonstrating that high amyloid load does not influence diffusion tensor imaging (DTI)-based measures of white matter integrity in the absence of co-existent gray matter neurodegeneration in non-demented older adults (**Figure 1**) (Kantarci et al., 2014). Although individuals with MCI and pre-clinical AD have reductions in fornix FA, it should be noted that a reduction in fornix FA by itself would be insufficient in classifying preclinical and prodromal AD. However, fornix FA can be combined with other imaging

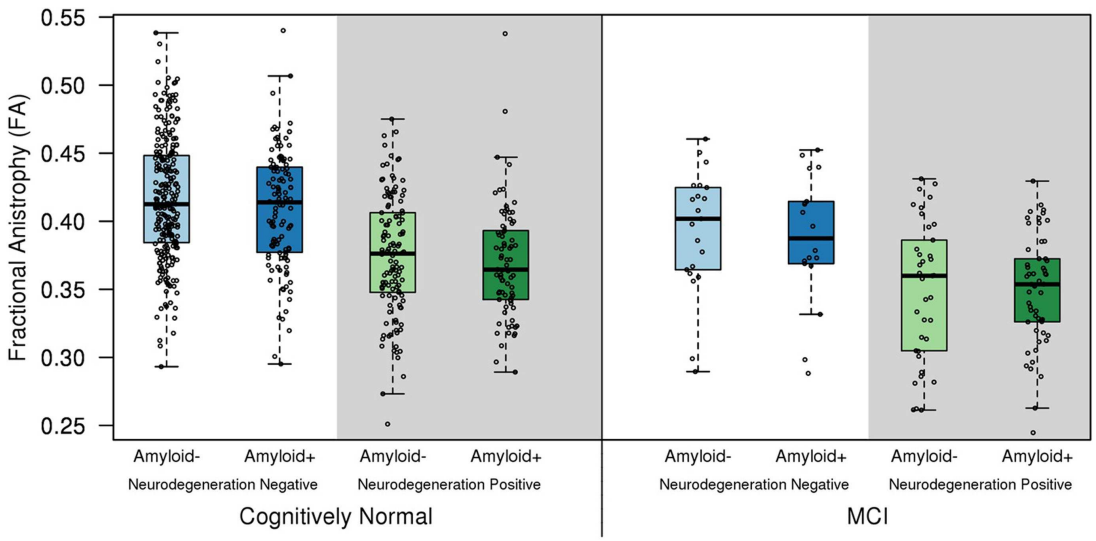

FIGURE 1 | Fractional anisotropy of the fornix in the cognitively normal (CN) and mild cognitive impairment (MCI) biomarker groups. Hippocampal atrophy on MRI and/or hypometabolism in the Alzheimer signature composite on FDG PET was used to classify subjects into the neurodegeneration-positive group, and high amyloid load on PET was used to classify subjects into the amyloid-positive group. Cut-points for amyloid positivity, hippocampal atrophy, and Alzheimer signature hypometabolism were determined from the 10th percentile of the measurement distributions in clinically diagnosed AD patients as previously described (Jack et al., 2012). Fornix FA was lower in the neurodegeneration positive CN and MCI patients compared to the cognitively normal group with normal imaging findings (amyloid and neurodegeneration negative; $p < 0.001$). A positive amyloid PET scan was not associated with a reduction in fornix FA, in the absence of co-existent neurodegeneration in cognitively normal individuals ($p = 0.19$) (Kantarci et al., 2014).

biomarkers such as hypometabolism on FDG PET, hippocampal atrophy, and amyloid-β PET for a more accurate classification of individuals at risk for AD, and predicting outcomes.

In carriers of the fully penetrant familial AD mutations (Ringman et al., 2007), a reduction in fornix FA was present in CN individuals who were destined to develop AD regardless of the cross-sectional area of the fornix, suggesting that the FA reduction in the fornix may precede hippocampal atrophy and clinical symptoms in AD. It is not possible to make inferences on whether FA reductions precede hippocampal atrophy on MRI in the course of AD based on findings from cross-sectional studies. Longitudinal investigations with serial DTI and structural MRI in pre-clinical AD and MCI may clarify the sequence of DTI and volumetric MRI findings in AD.

HIPPOCAMPUS-FORNIX AXIS IN ALZHEIMER'S DISEASE

There is a topographic concordance between gray and white matter diffusivity changes in AD (Kantarci et al., 2010), which implies that the disruption in white matter tracts is closely associated with the cortical pathology. Late-myelinating fibers in the brain such as the corticocortical association and the limbic pathways that are more vulnerable to degeneration related to AD than the early-myelinating fibers such as the corticospinal tracts, which do not show any DTI abnormalities in early AD (Stricker et al., 2009; Kantarci et al., 2010; Oishi et al., 2012).

Consistent with the findings in normal aging and MCI and pre-clinical AD, correlations between fornix FA and hippocampal atrophy has been observed in AD (Firbank et al., 2007; Pievani et al., 2010; Lee et al., 2012). In a sub-regional analysis of the hippocampus Lee et al. reported that the strongest associations between the structural changes in the hippocampus and fornix diffusivity is localized to the hippocampal CA1 and anteromedial subiculum (Lee et al., 2012). CA1 and subiculum are the subregions of the hippocampus that are vulnerable to AD-related neurodegeneration (Davies et al., 1992). Hippocampal efferent fibers that pass through the fornix are thought to originate from both of these subfields. The authors concluded that: "Cortical neuronal damage and subcortical axonal defects in AD are likely to be closely linked with each other, possibly reflecting a suggested pathogenic interaction between the two" (Lee et al., 2012). However, they also acknowledged that this hypothesis needs to be tested through longitudinal studies.

CONCLUSION

The association of microstructural alterations in the hippocampus and fornix continues throughout human lifespan and remains even when these structures are impacted by AD starting from the preclinical and prodromal stages. Prospective studies investigating the rates of structural alterations in these two structures may clarify the temporal sequence of the reductions in fornix FA and hippocampal volumes through preclinical, prodromal, and dementia stages of AD.

ACKNOWLEDGMENTS

Dr. Kantarci's research program is supported by the R01 AG40042, P50 AG16574/Project1, and P50 AG44170/Project 2

REFERENCES

Benarroch, E. (2006). *Basic Neurosciences with Clinical Applications.* Philadelphia, PA: Elsevier.

Bennett, D. A., Wilson, R. S., Schneider, J. A., Evans, D. A., Beckett, L. A., Aggarwal, N. T., et al. (2002). Natural history of mild cognitive impairment in older persons. *Neurology* 59, 198–205. doi:10.1212/WNL.59.2.198

Bowen, J., Teri, L., Kukull, W., McCormick, W., McCurry, S. M., and Larson, E. B. (1997). Progression to dementia in patients with isolated memory loss. *Lancet* 349, 763–765. doi:10.1016/S0140-6736(96)08256-6

Davies, D. C., Horwood, N., Isaacs, S. L., and Mann, D. M. (1992). The effect of age and Alzheimer's disease on pyramidal neuron density in the individual fields of the hippocampal formation. *Acta Neuropathol.* 83, 510–517. doi:10.1007/BF00310028

D'Esposito, M., Verfaellie, M., Alexander, M. P., and Katz, D. I. (1995). Amnesia following traumatic bilateral fornix transection. *Neurology* 45, 1546–1550. doi:10.1212/WNL.45.8.1546

Douaud, G., Menke, R. A., Gass, A., Monsch, A. U., Rao, A., Whitcher, B., et al. (2013). Brain microstructure reveals early abnormalities more than two years prior to clinical progression from mild cognitive impairment to Alzheimer's disease. *J. Neurosci.* 33, 2147–2155. doi:10.1523/JNEUROSCI.4437-12.2013

Firbank, M. J., Blamire, A. M., Krishnan, M. S., Teodorczuk, A., English, P., Gholkar, A., et al. (2007). Diffusion tensor imaging in dementia with Lewy bodies and Alzheimer's disease. *Psychiatry Res.* 155, 135–145. doi:10.1016/j.pscychresns.2007.01.001

Flicker, C., Ferris, S. H., and Reisberg, B. (1991). Mild cognitive impairment in the elderly: predictors of dementia. *Neurology* 41, 1006–1009. doi:10.1212/WNL.41.7.1006

Gong, G., Rosa-Neto, P., Carbonell, F., Chen, Z. J., He, Y., and Evans, A. C. (2009). Age- and gender-related differences in the cortical anatomical network. *J. Neurosci.* 29, 15684–15693. doi:10.1523/JNEUROSCI.2308-09.2009

Hof, P. R., and Morrison, J. H. (2004). The aging brain: morphomolecular senescence of cortical circuits. *Trends Neurosci.* 27, 607–613. doi:10.1016/j.tins.2004.07.013

Jack, C. R. Jr., Knopman, D. S., Weigand, S. D., Wiste, H. J., Vemuri, P., Lowe, V., et al. (2012). An operational approach to National Institute on Aging-Alzheimer's Association criteria for preclinical Alzheimer disease. *Ann. Neurol.* 71, 765–775. doi:10.1002/ana.22628

Jack, C. R. Jr., Petersen, R. C., Xu, Y., O'Brien, P. C., Smith, G. E., Ivnik, R. J., et al. (1998). Rate of medial temporal lobe atrophy in typical aging and Alzheimer's disease. *Neurology* 51, 993–999.

Jicha, G. A., Parisi, J. E., Dickson, D. W., Johnson, K., Cha, R., Ivnik, R. J., et al. (2006). Neuropathologic outcome of mild cognitive impairment following progression to clinical dementia. *Arch Neurol* 63, 674–681. doi:10.1001/archneur.63.5.674

Kantarci, K., Avula, R., Senjem, M. L., Samikoglu, A. R., Zhang, B., Weigand, S. D., et al. (2010). Dementia with Lewy bodies and Alzheimer disease: neurodegenerative patterns characterized by DTI. *Neurology* 74, 1814–1821. doi:10.1212/WNL.0b013e3181e0f7cf

Kantarci, K., Schwarz, C. G., Reid, R. I., Przybelski, S. A., Lesnick, T. G., Zuk, S. M., et al. (2014). White matter integrity on DTI, amyloid load, and neurodegeneration in non-demented elderly. *JAMA Neurol.* doi:10.1001/jamaneurol.2014.1482

Lee, D. Y., Fletcher, E., Carmichael, O. T., Singh, B., Mungas, D., Reed, B., et al. (2012). Sub-regional hippocampal injury is associated with fornix degeneration in Alzheimer's disease. *Front. Aging Neurosci.* 4:1. doi:10.3389/fnagi.2012.00001

Liu, Y., Spulber, G., Lehtimaki, K. K., Kononen, M., Hallikainen, I., Grohn, H., et al. (2011). Diffusion tensor imaging and tract-based spatial statistics in Alzheimer's disease and mild cognitive impairment. *Neurobiol. Aging.* 32, 1558–1571. doi:10.1016/j.neurobiolaging.2009.10.006

Meyer, J. S., Xu, G., Thornby, J., Chowdhury, M. H., and Quach, M. (2002). Is mild cognitive impairment prodromal for vascular dementia like Alzheimer's disease? *Stroke* 33, 1981–1985. doi:10.1161/01.STR.0000024432.34557.10

Mielke, M. M., Okonkwo, O. C., Oishi, K., Mori, S., Tighe, S., Miller, M. I., et al. (2012). Fornix integrity and hippocampal volume predict memory decline and progression to Alzheimer's disease. *Alzheimers Dement.* 8, 105–113. doi:10.1016/j.jalz.2011.05.2416

Morris, J. C., Storandt, M., Miller, J. P., McKeel, D. W., Price, J. L., Rubin, E. H., et al. (2001). Mild cognitive impairment represents early-stage Alzheimer disease. *Arch. Neurol.* 58, 397–405. doi:10.1001/archneur.58.3.397

Oishi, K., Mielke, M. M., Albert, M., Lyketsos, C. G., and Mori, S. (2012). The fornix sign: a potential sign for Alzheimer's disease based on diffusion tensor imaging. *J. Neuroimaging* 22, 365–374. doi:10.1111/j.1552-6569.2011.00633.x

Pelletier, A., Periot, O., Dilharreguy, B., Hiba, B., Bordessoules, M., Peres, K., et al. (2013). Structural hippocampal network alterations during healthy aging: a multi-modal MRI study. *Front. Aging Neurosci.* 5:84. doi:10.3389/fnagi.2013.00084

Peters, A., Sethares, C., and Moss, M. B. (2010). How the primate fornix is affected by age. *J. Comp. Neurol.* 518, 3962–3980. doi:10.1002/cne.22434

Petersen, R. C., Parisi, J. E., Dickson, D. W., Johnson, K. A., Knopman, D. S., Boeve, B. F., et al. (2006). Neuropathologic features of amnestic mild cognitive impairment. *Arch. Neurol.* 63, 665–672. doi:10.1001/archneur.63.5.665

Pievani, M., Agosta, F., Pagani, E., Canu, E., Sala, S., Absinta, M., et al. (2010). Assessment of white matter tract damage in mild cognitive impairment and Alzheimer's disease. *Hum. Brain Mapp.* 31, 1862–1875. doi:10.1002/hbm.20978

Ringman, J. M., O'Neill, J., Geschwind, D., Medina, L., Apostolova, L. G., Rodriguez, Y., et al. (2007). Diffusion tensor imaging in preclinical and presymptomatic carriers of familial Alzheimer's disease mutations. *Brain* 130, 1767–1776. doi:10.1093/brain/awm102

Rolls, E. T. (2014). Limbic systems for emotion and memory but no single limbic system. *Cortex*. doi:10.1016/j.cortex.2013.12.005

Stricker, N. H., Schweinsburg, B. C., Delano-Wood, L., Wierenga, C. E., Bangen, K. J., Haaland, K. Y., et al. (2009). Decreased white matter integrity in late-myelinating fiber pathways in Alzheimer's disease supports retrogenesis. *Neuroimage* 45, 10–16. doi:10.1016/j.neuroimage.2008.11.027

Walhovd, K. B., Westlye, L. T., Moe, V., Slinning, K., Due-Tonnessen, P., Bjornerud, A., et al. (2010). White matter characteristics and cognition in prenatally opiate- and polysubstance-exposed children: a diffusion tensor imaging study. *AJNR Am. J. Neuroradiol.* 31, 894–900. doi:10.3174/ajnr.A1957

Zhang, Y., Schuff, N., Camacho, M., Chao, L. L., Fletcher, T. P., Yaffe, K., et al. (2013). MRI markers for mild cognitive impairment: comparisons between white matter integrity and gray matter volume measurements. *PLoS ONE* 8:e66367. doi:10.1371/journal.pone.0066367

Zhuang, L., Sachdev, P. S., Trollor, J. N., Reppermund, S., Kochan, N. A., Brodaty, H., et al. (2013). Microstructural white matter changes, not hippocampal atrophy, detect early amnestic mild cognitive impairment. *PLoS ONE* 8:e58887. doi:10.1371/journal.pone.0058887

Zhuang, L., Wen, W., Trollor, J. N., Kochan, N. A., Reppermund, S., Brodaty, H., et al. (2012). Abnormalities of the fornix in mild cognitive impairment are related to episodic memory loss. *J Alzheimers Dis* 29, 629–639. doi:10.3233/JAD-2012-111766

Conflict of Interest Statement: The author declares that the research was conducted in the absence of any commercial or financial relationships that could be construed as a potential conflict of interest.

Received: 11 August 2014; paper pending published: 05 October 2014; accepted: 27 October 2014; published online: 13 November 2014.

*Citation: Kantarci K (2014) Fractional anisotropy of the fornix and hippocampal atrophy in Alzheimer's disease. Front. Aging Neurosci. **6**:316. doi: 10.3389/fnagi.2014.00316 This article was submitted to the journal Frontiers in Aging Neuroscience.*

frontiers in
AGING NEUROSCIENCE

MINI REVIEW ARTICLE
published: 21 January 2015
doi: 10.3389/fnagi.2015.00001

The fornix in mild cognitive impairment and Alzheimer's disease

Milap A. Nowrangi* and Paul B. Rosenberg

Department of Psychiatry and Behavioral Sciences, Johns Hopkins University School of Medicine, Baltimore, MD, USA

Edited by:
Fernanda Laezza, University of Texas Medical Branch, USA

Reviewed by:
Bogdan O. Popescu, Colentina Clinical Hospital, Romania
Shin Murakami, Touro University California, USA

****Correspondence:***
Milap A. Nowrangi, Department of Psychiatry, Johns Hopkins Bayview Medical Center, 5300 Alpha Commons Drive, 4th Floor, Baltimore, MD 21224, USA
e-mail: mnowran1@jhmi.edu

The fornix is an integral white matter bundle located in the medial diencephalon and is part of the limbic structures. It serves a vital role in memory functions and as such has become the subject of recent research emphasis in Alzheimer's disease (AD) and mild cognitive impairment (MCI). As the characteristic pathological processes of AD progress, structural and functional changes to the medial temporal lobes and other regions become evident years before clinical symptoms are present. Though gray matter atrophy has been the most studied, degradation of white matter structures especially the fornix may precede these and has become detectable with use of diffusion tensor imaging (DTI) and other complimentary imaging techniques. Recent research utilizing DTI measurement of the fornix has shown good discriminability of diagnostic groups, particularly early and preclinical, as well as predictive power for incident MCI and AD. Stimulating and modulating fornix function by the way of DBS has been an exciting new area as pharmacological therapeutics has been slow to develop.

Keywords: Alzheimer's, MCI, fornix, DTI, DBS

INTRODUCTION

Alzheimer's disease (AD) is the most common neurodegenerative condition in aging. AD is a growing public health problem that is projected to reach epidemic proportions if disease-modifying therapies are not found. The latest figures from the Alzheimer's Association indicate that there are an estimated 5.3 million Americans living with AD. By 2050, an estimated 11–16 million people are expected to be diagnosed in the United States alone (Thies et al., 2013). Establishing the diagnosis of Mild Cognitive Impairment (MCI) and AD has evolved over the last 25 years with the most recent iteration of the National Institute on Aging and Alzheimer's Association criteria (Mckhann et al., 1984, 2011). These criteria place a new emphasis on the use of biomarkers of AD pathophysiology whereas the original criteria were based solely on the clinical evaluation. Although the use of biomarkers to establish diagnosis or track progression is considered a step forward in the field, there is a need for continued development of complementary technologies utilizing biological, physical, cognitive, and behavioral substrates.

Broadly, the initial pathologic changes in AD have been shown to involve the medial temporal lobes with the accumulation of neurofibrillary tangles and senile beta amyloid plaques (Bancher et al., 1993; Braak and Braak, 1995; Xu et al., 2000; Braak et al., 2006). This region is thought to mediate the retrieval and learning of semantic and episodic memory – the most common early cognitive deficits in AD (Aggleton and Brown, 1999; Behl et al., 2005; Levy and Chelune, 2007; Baldwin and Farias, 2009). The accumulation of tangles and plaques is associated with progressive atrophy of the cortical gray matter as loss of large pyramidal neurons (layers III and IV) advances, particularly in cortical association regions (Braak and Braak, 1995). In addition to this, several white matter (WM) abnormalities have been described and are thought to reflect axonal disintegration, rarefaction, oligodendrocytosis, and astrocytosis (Xu et al., 2001; Roher et al., 2002; Shahani et al., 2002). Neuroimaging techniques, particularly magnetic resonance imaging (MRI), is a robust method used to visualize and detect subtle changes in structure and function of the substructures within the medial temporal lobe and related regions as important and perhaps early markers of disease and progression.

Though most volumetric imaging studies focused on atrophy of the entorhinal cortex and hippocampus, close inspection of the limbic structures has revealed significant volume reductions in patients with sporadic and familial AD (Decarli, 2001; Cash et al., 2013). The fornix is one structure within the limbic system that is receiving increasing attention recently in part because of its ease of detectability using MRI scanning as well as robust associations to cognitive changes, diagnostic group discrimination, and susceptibility to therapeutic intervention (Aggleton and Brown, 1999; Thomas et al., 2011). Because of the increasing interest in this structure, this brief review will serve as an updated survey of the key research over the last 10 years involving the fornix with hopes for continued and increasing efforts to better understand the use of this structure in the diagnosis, progression, and treatment of AD.

FORNIX – STRUCTURE AND FUNCTION

The fornix is a WM bundle belonging to the medial diencephalon, which also includes the hippocampus, mammillary bodies, and anterior and medial thalamus. Grossly, the fornix is found on the medial aspects of the cerebral hemispheres connecting the medial temporal lobes to the hypothalamus. It is formed at first from the output fibers of the hippocampus in the mesial temporal lobe, beneath the floor of the lateral ventricle. It courses along the curve of the corpus callosum forming its body. At the level of the foramen of Monro, the fornix divides and travels inferiorly and posteriorly

in the lateral wall of the third ventricle to end in the hypothalamus and basal forebrain. Though the left and right fornices travel separately along their course from the hippocampus to the hypothalamus, they merge at the level of the forniceal body to form an important commissural tract (Nolte, 1993; Aggleton and Brown, 1999; Brewer, 2003; Patestas Ma, 2006). See **Figures 1A,B**.

The fornix is but one structure within the "temporal lobe memory system" also termed the Papez circuit described by James Papez in 1937 (Papez, 1995). The fornix has been demonstrated as the link between the hippocampus, mammillary bodies of the hypothalamus, and the anterior thalamic nuclei (via the mammilothalamic tract) (Nolte, 1993; Yamada et al., 1998; Aggleton and Brown, 1999; Patestas Ma, 2006). Efferent projections from the hippocampus to the medial diencephalon, particularly the anterior thalamic nuclei, are thought to be essential for normal hippocampal activity and are directed by the fornix, which then forms the major cholinergic output tract for the hippocampus (Cassel et al., 1997; Aggleton and Brown, 1999). Some of the earliest research involving lesion studies of this system asserted that damage to this axis resulted in anterograde amnesia, which occurs as a result of faulty encoding of episodic information (Aggleton and Brown, 1999). Specifically, damage to the hippocampus, fornix, and other diencephalic structures result in the inability to form declarative (semantic and episodic) memories. Although selective damage of the fornices has been shown to result in anterograde amnesia, the damage to other structures within the Papez circuit result in similar deficits emphasizes that the integrity of the circuit rather than individual substructure is important.

FORNIX AS AN IMAGING BIOMARKER IN MCI AND AD

There has been increasing research in recent years on imaging the fornix as a biomarker for diagnosis, progression (or conversion), and cognition in MCI and AD. Some of the earliest research focused on fornix ultrastructure as a sign of MCI and AD. Much of this research employed MRI volumetric methods and showed atrophy (volume reduction) in many of the limbic lobe structures including the fornix. Early volumetric studies by Callen et al. (2001) showed that a number of structures within the Papez circuit (hippocampus, amygdala, anterior thalamus, hypothalamus, mammillary bodies, basal forebrain, septal area, fornix, orbitofrontal, and parahippocampal cortices) suffered significant atrophy with hippocampal and posterior cingulate regions being particularly affected. These early studies largely established complimentary findings to neuropathological observations of limbic atrophy in AD (Hopper and Vogel, 1976). The interest in establishing morphological changes in preclinical AD (MCI) as an early marker of disease was first undertaken by Copenhaver et al. (2006) who did not show significant atrophy of fornix or mammillary bodies in MCI as was initially hypothesized. The inability to show this difference was likely due to the relative insensitivity of volumetric methods used at the time even though imaging processes and analyses were improved upon compared to similar

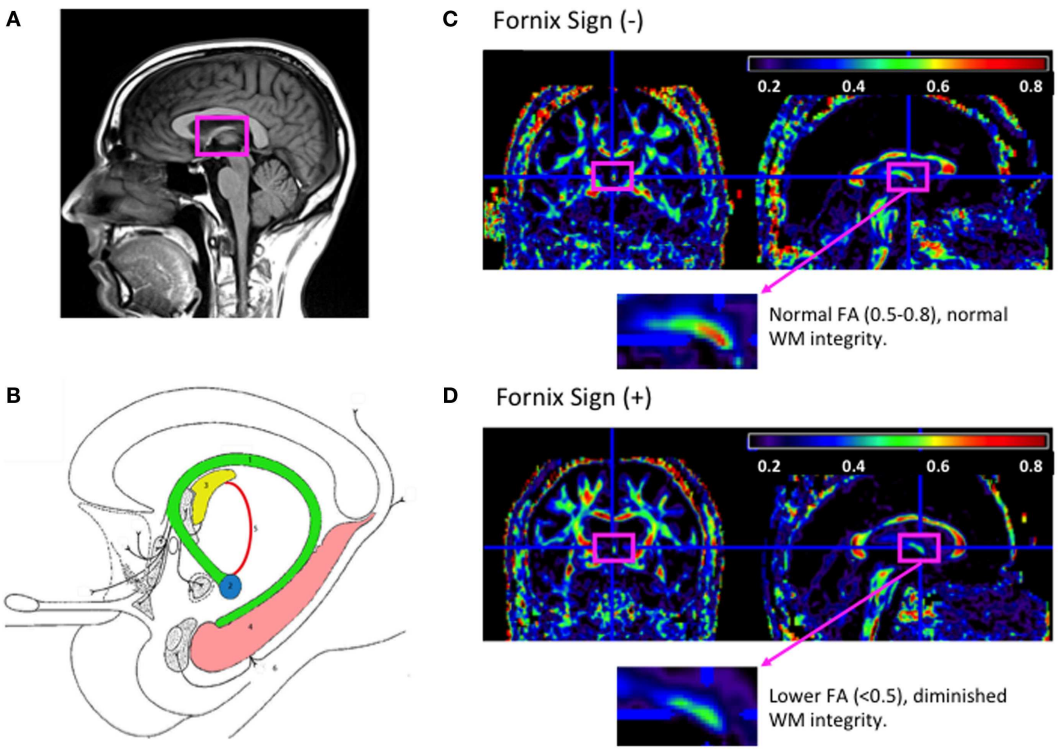

FIGURE 1 | The fornix anatomy and DTI fornix sign. **(A)** Normal neuroanatomy highlighting limbic structures. **(B)** 1. Fornix; 2. mammilary body; 3. anterior thalamic nucleus; 4. hippocampus; 5. mammillothalamic tract; and 6. entorhinal cortex. Adapted from Nieuwenhuys (2008). **(C)** FA map of cognitively normal 80-year-old woman without fornix sign. **(D)** FA map of 80-year-old woman with Alzheimer's disease with fornix sign. **(C,D)** FA maps shown with magnified view of the fornix (fuchsia rectangle), adapted from Oishi et al. (2011).

previous studies (Gale et al., 1993; Bilir et al., 1998; Kuzniecky et al., 1999; Callen et al., 2001). As a result, most recent research in the area has focused on fornix microstructure as the measurement of WM integrity. This renewed direction in imaging research of the fornix was based on the hypothesis that the earliest morphological changes occurred within medial temporal lobe gray matter, specifically the hippocampus and entorhinal structures with secondary effect to the efferent outflow tract through the fornix and mammillary bodies (Braak and Braak, 1995; Cassel et al., 1997; Aggleton and Brown, 1999). Needless to say, the underlying pathological processes affect an interconnected network of regions rather than single regions.

Diffusion tensor imaging has been the most commonly used *in vivo* MRI technique in studying the WM architecture of the fornix. Diffusion tensor imaging (DTI) is an indirect method of measuring WM integrity when conventional MRI lacks the contrast to delineate WM fiber tract organization (Beaulieu et al., 1996; Mori et al., 1999; Basser and Jones, 2002). Fractional anisotropy (FA) and mean diffusivity (MD) are two DTI measures used to quantify the integrity of WM microstructure by measuring the relative random motion of water in cerebral tissue. These measures are scalar values where higher values of FA and lower values of MD are thought to represent normal tissue cytoarchitecture where the random motion of water along a healthy axon, for example, is tightly constrained and restricted to movement along one direction (anisotropic). Two additional measures, axial diffusivity (DA) and radial diffusivity (DR) are associated with secondary degeneration of axons and breakdown of myelin and may provide additional detail into WM fiber integrity (Pierpaoli et al., 1996; Song et al., 2003, 2004).

Relating DTI measurement with other biomarkers that are considered more direct ways of detecting AD pathology has shown good correlation and has been a means of test validation. PET amyloid imaging is a well-established method of directly measuring AD pathology, β-amyloid (Aβ) deposition *in vivo,* but clinical application has been limited by convenience of use, invasiveness, and the half-life of radiotracers. When compared with DTI, several studies have shown positive correlation. A study by Chao et al. (2013) showed Aβ deposition as measured by Pittsburgh compound B (PiB) PET imaging was associated with reduced WM integrity (lower FA) in the fornix and splenium of the corpus callosum in subjects who ranged from normal to MCI. Similarly, Racine et al. (2014) showed a positive correlation between Aβ+ subjects and those with lower FA in the corpus callosum, hippocampal cingulum, and lateral fornix. Comparison with CSF markers of AD pathology $A\beta_{42}$ and p-Tau_{181} has also been an important area of research. A study by Gold et al. (2014) showed a positive correlation between these CSF markers and WM integrity (FA) in the fornix, a relationship that persisted after controlling for hippocampal and fornix volume in a cohort of 20 cognitively normal older adults. Lower FA in the fornix was also associated with reduced performance on several cognitive tests including a Digit Symbol Test. This study is particularly important because CSF changes are thought to precede neuroimaging alterations by several years (Jack et al., 2010). These studies strongly suggest that microstructural measurements are related to AD pathology.

As the interest in the field of identifying early markers of AD continued to grow, several studies aimed to identify WM changes in preclinical AD. One of the earlier studies by Ringman et al. (2007) found decreased FA in the columns of the fornix were associated (linear regression) with hippocampal atrophy ($p = 0.023$), WM volume ($p = 0.002$), and mutation status ($p = 0.032$) in asymptomatic familial AD. They concluded that decreased FA in the forniceal columns is a robust finding in early familial AD and may be a biomarker of early disease in sporadic AD. Since this important study, there have been a number of more recent DTI studies showing similar associations between the WM tracts of the fornix and earlier preclinical stage. Cross-sectional DTI analysis by Mielke et al. (2009) and longitudinal analysis of the same cohort by Nowrangi et al. (2013) showed significant differences between normal participants and those with MCI and AD in the fornix, anterior cingulum, and splenium cross-sectionally and longitudinally ($p < 0.01$). Decreases in FA cross-sectionally and increases in MD longitudinally were observed in the fornix and were thought to indicate early markers of disease and longitudinal disease progression. Studies by Huang et al. (2012) and Boespflug et al. (2013) offered full DTI characterization (FA, MD, DA, and DR) of region of interest and atlas-based approaches to WM analysis respectively in MCI and AD. Both studies showed selective disruption of WM integrity in limbic structures including the fornix with DR being most sensitive to changes in the fornix. These studies further highlight a robust association between loss of integrity within the limbic structures and decrease in cognitive performance as illustrated by neuropsychological tests of episodic memory. Taken together, these studies suggest that the limbic WM tracts are preferentially affected in the early stages of cognitive dysfunction and that microstructural degradation of the fornix may precede atrophy of the hippocampus as detected by MRI.

Identifying preclinical signs of AD have been complemented by other research identifying individuals who would go on to progress to AD or convert from MCI to AD. One of the first studies observing this was by Oishi et al. (2011) who identified the fornix on an FA-scaled DTI map. FA reductions in this region predicted conversion form normal to amnestic MCI (aMCI) with a specificity of 1.0 and sensitivity of 0.67 and conversion from aMCI to AD with a specificity of 0.94 and sensitivity of 0.83. This finding was termed "the fornix sign" and has shown promise as an early predictive imaging sign of AD (See **Figures 1C,D**). Two other studies similarly emphasized the use of fornix microstructure as a predictor of conversion. One study by Van Bruggen et al. (2012) retrospectively used DTI analysis to differentiate between a subgroup of aMCI who converted to AD and a subgroup that did not. They found that FA, DR, and DA changes within the fornix, cingulum, and the corpus callosum were able to significantly discriminate between the two diagnostic groups and therefore could be thought of as a predictor for conversion between MCI and AD. Another study by Douaud et al. (2013) compared two groups of MCI patients; one that converted to AD no earlier than from baseline scanning and another that remained stable without progression of symptoms for at least 3 years. Comparing both volumetric and microstructural variables including DTI anisotropy and diffusivity, they found significant group differences in the body of the fornix, left fimbria, and the superior longitudinal fasciculus. These studies emphasize

the importance of microstructural integrity of the limbic lobe and specifically the fornix in predicting the progression/conversion from preclinical to clinical AD.

Recently, the field has been quite interested in identifying cognitively normal individuals who might be at increased risk for developing AD. The well-known and well-regarded hypothesis by Jack et al. and others that imaging changes are evident before clinical symptoms arise and that the pathological changes in the brain begin even decades before those has prompted increased interest in identifying these individuals (Morris et al., 1996; Bennett et al., 2006; Jack et al., 2010, 2013). In line with previous hypotheses that microstructural change precedes gross atrophic changes, there has been increasing work in using DTI and complimentary imaging methods to examine this. One study by Fletcher et al. (2013) identified the fornix as a region of microstructural change in cognitively normal elders. They found that the fornix body volume and DA were highly significant predictors of cognitive decline from normal cognition [$r = =0.47$ (0.24–0.89), $p = 0.02$, and $r = =1.25$ (1.02–1.46), $p = 0.005$, respectively]. This is one of the first studies establishing fornix degeneration as a predictor of incipient cognitive decline among healthy elderly individuals. Two studies conducted by Zhuang et al. (2012, 2013) demonstrated that WM changes in the fornix were evident in preclinical AD. One study (Zhuang et al., 2013) showed that when compared to

Table 1 | Summary of key biomarker research of the fornix in cognitively normal (NC), MCI, and AD.

Study	Cohort	Regions of interest and imaging findings	Conclusion
Ringman et al. (2007)	2 AD 21 at-risk AD	FA for mean whole brain WM, forniceal columns, bilateral perforant pathways, left orbitofrontal lobe were decreased relative to non-carriers	FA is reduced in the fornix in persons carrying mutations for AD prior to symptoms of dementia and is a better predictor of mutation status than other regions
Mielke et al. (2009)	25 NC 25 MCI 25 AD	Lower FA in fornix, anterior cingulum bundle, splenium of the corpus collosum in AD vs. NC and AD vs. MCI	FA is decreased in specific fiber tracts including the fornix in NC, MCI, and AD and may be an indicator of progression over 3 months
Nowrangi et al. (2013)	25 NC 25 MCI 25 AD	Higher MD and lower FA in the fornix and splenium in AD vs. MCI or NC of 12 months	Higher MD in the fornix longitudinally was a better indicator of change than FA and may be an early indicator of progression
Huang et al. (2012)	24 NC 11 aMCI 26 AD	FA, MD, DR, DA of limbic, commissural, and association tracts are differentially associated with diagnostic group. Comparison between aMCI and NC show differences only in limbic structures	WM disruption of limbic tract structures is caused by neuronal damage in aMCI and indicates a progression pattern between WM tracts
Boespflug et al. (2013)	18 MCI	Lower DR, higher FA, and lower MD in the fornix associated with better paired associate learning	Disparate pathology of temporal stems and fornix WM is associated with early memory impairment in MCI
Oishi et al. (2011)	25 NC 24 aMCI 23 AD	Fornix sign differentiated AD vs. NC and predicted conversion from NC to aMCI and from aMCI to AD	The fornix sign may be a predictive biomarker sign of AD
Van Bruggen et al. (2012)	15 NC 17 MCI (8 stable, 9 converters) 15 AD	Significant differences in FA and DR in the fornix, corpus callosum, and cingulum in MCI who remained stable vs. converters	DTI changes in MCI converters vs. those who remained stable may be an early indicator of progression to AD
Douaud et al. (2013)	13 aMCI (converters) 22 aMCI (stable)	Significant group differences in volume and microstructure of left hippocampus, body of the fornix, left fibria, and superior longitudinal fasciculus	Microstructural changes in left hippocampus using DTI showed most substantial differences between two diagnostic groups and was best predictor of future progression to AD
Fletcher et al. (2013)	102 NC	Fornix body volume and DA were highly significant predictors of cognitive decline from normal cognition	Fornix degeneration in NC may be a predictor of incipient cognitive decline among healthy elderly individuals
Zhuang et al. (2012)	173 NC (stable) 20 aMCI (converted)	aMCI converters had substantial reduction in FA in precuneus, parahippocampal cingulum and gyrus, and fornix while gray matter structures intact	Microstructural WM changes are present in NC in the pre-aMCI stage and may be an imaging marker of early AD-related brain changes
Zhuang et al. (2013)	155 NC 27 "late" aMCI 39 "early" aMCI	Late aMCI had lower WM integrity in the fornix, parahippocampal cingulum, and uncinate fasciculus, early aMCI showed white matter damage in fornix	Limbic WM tracts preferentially affected in early stages of cognitive dysfunction particularly in the fornix, which may precede hippocampal atrophy

cognitively normal subjects and those with late MCI, early aMCI subjects had lower WM integrity in the fornix. In a second study (Zhuang et al., 2012), the same group showed that when compared to normal subjects who remained stable over 2 years, those who converted to aMCI had substantial reductions in WM integrity in the fornix, parahippocampal gyrus WM, and cingulum while gray matter structures remained relatively intact. FA was found to be a predictor of conversion from cognitively normal to aMCI. Taken together, these studies emphasize the continued importance of detecting earlier preclinical forms of AD even in normal subjects in order to identify patients who might benefit from interventional approaches. **Table 1** summarizes the key studies described above.

FORNIX AND CLINICAL TREATMENT IN AD

One of the most recent and exciting avenues of research has been directed at enhancing cognition by stimulating or modulating fornix function. Deep Brain Stimulation (DBS) has been thought of for some time now as having significant effect on mood and anxiety disorders such as major depression, obsessive compulsive disorder as well as Gilles de Tourette's syndrome, and other conditions. Similarly, it has been hypothesized that DBS may also play a role in enhancing memory functions. One of the first studies in this area by Hamani et al. (2008) used DBS to stimulate the fornix/hypothalamus area in a man with morbid obesity. In a case observation report, they also described that the procedure generated detailed autobiographical memory. In AD, this same concept has been hypothesized as being a potential therapeutic intervention for the treatment of amnesia and has just started being seriously studied. The first study of its kind, by Laxton et al. (2010), performed DBS stimulation of the fornix and hypothalamus in six AD patients. Though this was largely a safety study, the authors found that DBS triggered neural activity (increased metabolism) in some patients as seen through PET imaging (Laxton et al., 2010).

Later *in vivo* studies of DBS in patients with AD have been few and largely with relatively low *N*. Since 1985, there have been just two DBS studies targeting the stimulation of the fornix in patients with AD (Laxton et al., 2010; Fontaine et al., 2013). Found to over-all be safe, the clinical response has been rather modest with MMSE scores stabilizing rather than improving. However, reversal of AD-related hypometabolism has been observed in temporo-parietal-occipital regions as well as increased connectivity between similar regions representing distributed cognitive networks (Smith et al., 2012). Given the lack of success thus far in developing pharmacological therapies for AD and the slow pace of further developments, such novel treatments as DBS is a promising avenue for therapy in AD. Currently, the Advance DBS clinical trial has recently completed recruitment of 42 participants with mild AD. Half of the study participants will have the stimulators turned on at the start of the study and the other half 12 months later. All participants will be followed for 18 months to track progression of their cognitive impairment. More information of this study can be found at www.clinicaltrials.gov.

CONCLUSION

There is a small but growing body of research directed toward the structure and function of the fornix in MCI and AD. Because of its important role within the "temporal lobe memory system," understanding the microstructural integrity of the fornix in MCI and AD has become an important area of focus in the field as there is a growing priority for identifying individuals early in the disease process and those who are at increased risk for progression or conversion. Recent studies have shown DTI is able to indirectly measure microstructural changes of the fornix that may precede gross atrophic changes of gray matter structures such as the hippocampus and entorhinal cortex. These studies demonstrate that DTI measurements of the fornix can significantly discriminate between cognitively normal, MCI, and AD groups thereby serving as a robust biomarker of disease. Moreover, fornix measurements have been shown to be a reliable measure of conversion from preclinical disease to AD. As pharmacological interventions continue to develop, studies of stimulating the fornix through DBS to alleviate or even reverse cognitive impairment has shown some early promise in stabilizing cognitive decline and increasing neural network activity.

REFERENCES

Aggleton, J. P., and Brown, M. W. (1999). Episodic memory, amnesia, and the hippocampal-anterior thalamic axis. *Behav. Brain Sci.* 22, 425–444. doi:10.1017/S0140525X99002034 Discussion 444-489,

Baldwin, S., and Farias, S. T. (2009). Neuropsychological assessment in the diagnosis of Alzheimer's disease. *Curr. Protoc. Neurosci.* Chapter 10, Unit 10.3.

Bancher, C., Braak, H., Fischer, P., and Jellinger, K. A. (1993). Neuropathological staging of Alzheimer lesions and intellectual status in Alzheimer's and Parkinson's disease patients. *Neurosci. Lett.* 162, 179–182. doi:10.1016/0304-3940(93)90590-H

Basser, P. J., and Jones, D. K. (2002). Diffusion-tensor MRI: theory, experimental design and data analysis – a technical review. *NMR. Biomed.* 15, 456–467. doi:10.1002/nbm.783

Beaulieu, C., Does, M. D., Snyder, R. E., and Allen, P. S. (1996). Changes in water diffusion due to Wallerian degeneration in peripheral nerve. *Magn. Reson. Med.* 36, 627–631. doi:10.1002/mrm.1910360419

Behl, P., Stefurak, T. L., and Black, S. E. (2005). Progress in clinical neurosciences: cognitive markers of progression in Alzheimer's disease. *Can. J. Neurol. Sci.* 32, 140–151. doi:10.1017/S0317167100003917

Bennett, D. A., Schneider, J. A., Arvanitakis, Z., Kelly, J. F., Aggarwal, N. T., Shah, R. C., et al. (2006). Neuropathology of older persons without cognitive impairment from two community-based studies. *Neurology* 66, 1837–1844. doi:10.1212/01.wnl.0000219668.47116.e6

Bilir, E., Craven, W., Hugg, J., Gilliam, F., Martin, R., Faught, E., et al. (1998). Volumetric MRI of the limbic system: anatomic determinants. *Neuroradiology* 40, 138–144. doi:10.1007/s002340050554

Boespflug, E. L., Storrs, J., Sadat-Hossieny, S., Eliassen, J., Shidler, M., Norris, M., et al. (2013). Full diffusion characterization implicates regionally disparate neuropathology in mild cognitive impairment. *Brain Struct. Funct.* 219, 367–379. doi:10.1007/s00429-013-0506-x

Braak, H., Alafuzoff, I., Arzberger, T., Kretzschmar, H., and Del Tredici, K. (2006). Staging of Alzheimer disease-associated neurofibrillary pathology using paraffin sections and immunocytochemistry. *Acta Neuropathol.* 112, 389–404. doi:10.1007/s00401-006-0127-z

Braak, H., and Braak, E. (1995). Staging of Alzheimer's disease-related neurofibrillary changes. *Neurobiol. Aging* 16, 271–278. doi:10.1016/0197-4580(95)00021-6 Discussion 278–284.,

Brewer, J. B., Gabrielli, J. D., Preston, A. R., Vaidya, C. J., and Rosen, A. C. (2003). "Memory," in *Textbook of Clinical Neurology*, ed. C. G. Goetz (Philadelphia, PA: Saunders).

Callen, D. J., Black, S. E., Gao, F., Caldwell, C. B., and Szalai, J. P. (2001). Beyond the hippocampus: MRI volumetry confirms widespread limbic atrophy in AD. *Neurology* 57, 1669–1674.

Cash, D. M., Ridgway, G. R., Liang, Y., Ryan, N. S., Kinnunen, K. M., Yeatman, T., et al. (2013). The pattern of atrophy in familial Alzheimer disease: volumetric MRI results from the Dian study. *Neurology* 81, 1425–1433. doi:10.1212/WNL.0b013e3182a841c6

Cassel, J. C., Duconseille, E., Jeltsch, H., and Will, B. (1997). The fimbria-fornix/cingular bundle pathways: a review of neurochemical and behavioural approaches using lesions and transplantation techniques. *Prog. Neurobiol.* 51, 663–716. doi:10.1016/S0301-0082(97)00009-9

Chao, L. L., Decarli, C., Kriger, S., Truran, D., Zhang, Y., Laxamana, J., et al. (2013). Associations between white matter hyperintensities and β amyloid on integrity of projection, association, and limbic fiber tracts measured with diffusion tensor MRI. *PLoS ONE* 8:e65175. doi:10.1371/journal.pone.0065175

Copenhaver, B. R., Rabin, L. A., Saykin, A. J., Roth, R. M., Wishart, H. A., Flashman, L. A., et al. (2006). The fornix and mammillary bodies in older adults with Alzheimer's disease, mild cognitive impairment, and cognitive complaints: a volumetric MRI study. *Psychiatry Res.* 147, 93–103. doi:10.1016/j.pscychresns.2006.01.015

Decarli, C. (2001). The role of neuroimaging in dementia. *Clin. Geriatr. Med.* 17, 255–279. doi:10.1016/S0749-0690(05)70068-9

Douaud, G., Menke, R. A., Gass, A., Monsch, A. U., Rao, A., Whitcher, B., et al. (2013). Brain microstructure reveals early abnormalities more than two years prior to clinical progression from mild cognitive impairment to Alzheimer's disease. *J. Neurosci.* 33, 2147–2155. doi:10.1523/JNEUROSCI.4437-12.2013

Fletcher, E., Raman, M., Huebner, P., Liu, A., Mungas, D., Carmichael, O., et al. (2013). Loss of fornix white matter volume as a predictor of cognitive impairment in cognitively normal elderly individuals. *JAMA Neurol.* 70, 1389. doi:10.1001/jamaneurol.2013.3263

Fontaine, D., Deudon, A., Lemaire, J. J., Razzouk, M., Viau, P., Darcourt, J., et al. (2013). Symptomatic treatment of memory decline in Alzheimer's disease by deep brain stimulation: a feasibility study. *J. Alzheimers Dis.* 34, 315–323. doi:10.3233/JAD-121579

Gale, S. D., Burr, R. B., Bigler, E. D., and Blatter, D. (1993). Fornix degeneration and memory in traumatic brain injury. *Brain Res. Bull.* 32, 345–349. doi:10.1016/0361-9230(93)90198-K

Gold, B. T., Zhu, Z., Brown, C. A., Andersen, A. H., Ladu, M. J., Tai, L., et al. (2014). White matter integrity is associated with cerebrospinal fluid markers of Alzheimer's disease in normal adults. *Neurobiol. Aging* 35, 2263–2271. doi:10.1016/j.neurobiolaging.2014.04.030

Hamani, C., McAndrews, M. P., Cohn, M., Oh, M., Zumsteg, D., Shapiro, C. M., et al. (2008). Memory enhancement induced by hypothalamic/fornix deep brain stimulation. *Ann. Neurol.* 63, 119–123. doi:10.1002/ana.21295

Hopper, M. W., and Vogel, F. S. (1976). The limbic system in Alzheimer's disease. A neuropathologic investigation. *Am. J. Pathol.* 85, 1–20.

Huang, H., Fan, X., Weiner, M., Martin-Cook, K., Xiao, G., Davis, J., et al. (2012). Distinctive disruption patterns of white matter tracts in Alzheimer's disease with full diffusion tensor characterization. *Neurobiol. Aging* 33, 2029–2045. doi:10.1016/j.neurobiolaging.2011.06.027

Jack, C. R. Jr., Knopman, D. S., Jagust, W. J., Petersen, R. C., Weiner, M. W., Aisen, P. S., et al. (2013). Tracking pathophysiological processes in Alzheimer's disease: an updated hypothetical model of dynamic biomarkers. *Lancet Neurol.* 12, 207–216. doi:10.1016/S1474-4422(12)70291-0

Jack, C. R. Jr., Knopman, D. S., Jagust, W. J., Shaw, L. M., Aisen, P. S., Weiner, M. W., et al. (2010). Hypothetical model of dynamic biomarkers of the Alzheimer's pathological cascade. *Lancet Neurol.* 9, 119–128. doi:10.1016/S1474-4422(09)70299-6

Kuzniecky, R., Bilir, E., Gilliam, F., Faught, E., Martin, R., and Hugg, J. (1999). Quantitative MRI in temporal lobe epilepsy: evidence for fornix atrophy. *Neurology* 53, 496–501. doi:10.1212/WNL.53.3.496

Laxton, A. W., Tang-Wai, D. F., McAndrews, M. P., Zumsteg, D., Wennberg, R., Keren, R., et al. (2010). A phase I trial of deep brain stimulation of memory circuits in Alzheimer's disease. *Ann. Neurol.* 68, 521–534. doi:10.1002/ana.22089

Levy, J. A., and Chelune, G. J. (2007). Cognitive-behavioral profiles of neurodegenerative dementias: beyond Alzheimer's disease. *J. Geriatr. Psychiatry Neurol.* 20, 227–238. doi:10.1177/0891988707308806

McKhann, G., Drachman, D., Folstein, M., Katzman, R., Price, D., and Stadlan, E. M. (1984). Clinical diagnosis of Alzheimer's disease: report of the NINCDS-ADRDA work group under the auspices of department of health and human services task force on Alzheimer's disease. *Neurology* 34, 939–944. doi:10.1212/WNL.34.7.939

McKhann, G. M., Knopman, D. S., Chertkow, H., Hyman, B. T., Jack, C. R. Jr., Kawas, C. H., et al. (2011). The diagnosis of dementia due to Alzheimer's disease: recommendations from the national institute on aging-Alzheimer's association workgroups on diagnostic guidelines for Alzheimer's disease. *Alzheimers Dement.* 7, 263–269. doi:10.1016/j.jalz.2011.03.005

Mielke, M. M., Kozauer, N. A., Chan, K. C., George, M., Toroney, J., Zerrate, M., et al. (2009). Regionally-specific diffusion tensor imaging in mild cognitive impairment and Alzheimer's disease. *Neuroimage* 46, 47–55. doi:10.1016/j.neuroimage.2009.01.054

Mori, S., Crain, B. J., Chacko, V. P., and Van Zijl, P. C. (1999). Three-dimensional tracking of axonal projections in the brain by magnetic resonance imaging. *Ann. Neurol.* 45, 265–269. doi:10.1002/1531-8249(199902)45:2<265::AID-ANA21>3.0.CO;2-3

Morris, J. C., Storandt, M., McKeel, D. W. Jr., Rubin, E. H., Price, J. L., Grant, E. A., et al. (1996). Cerebral amyloid deposition and diffuse plaques in "normal" aging: evidence for presymptomatic and very mild Alzheimer's disease. *Neurology* 46, 707–719. doi:10.1212/WNL.46.3.707

Nieuwenhuys, R. (2008). "The human central nervous system," in *The Human Central Nervous System*, eds J. Voogd, C. Huijzen. 4th Edn (New York: Springer).

Nolte, J. (1993). "Origin and course of the fornix," in *The Human Brain*, 3rd Edn (St. Louis, MO: Mosby Yearbook).

Nowrangi, M. A., Lyketsos, C. G., Leoutsakos, J. M., Oishi, K., Albert, M., Mori, S., et al. (2013). Longitudinal, region-specific course of diffusion tensor imaging measures in mild cognitive impairment and Alzheimer's disease. *Alzheimers Dement.* 9, 519–528. doi:10.1016/j.jalz.2012.05.2186

Oishi, K., Mielke, M. M., Albert, M., Lyketsos, C. G., and Mori, S. (2011). The fornix sign: a potential sign for Alzheimer's disease based on diffusion tensor imaging. *J. Neuroimaging* 22, 365–374. doi:10.1111/j.1552-6569.2011.00633.x

Papez, J. W. (1995). A proposed mechanism of emotion. 1937. *J. Neuropsychiatry Clin. Neurosci.* 7, 103–112. doi:10.1176/jnp.7.1.103

Patestas Ma, G. L. (2006). "Limbic system," in *A Textbook of Neuroanatomy*, ed. L. P. Gartner (Oxford: Blackwell), 344–359.

Pierpaoli, C., Jezzard, P., Basser, P. J., Barnett, A., and Di Chiro, G. (1996). Diffusion tensor MR imaging of the human brain. *Radiology* 201, 637–648. doi:10.1148/radiology.201.3.8939209

Racine, A. M., Adluru, N., Alexander, A. L., Christian, B. T., Okonkwo, O. C., Oh, J., et al. (2014). Associations between white matter microstructure and amyloid burden in preclinical Alzheimer's disease: a multimodal imaging investigation. *Neuroimage Clin.* 4, 604–614. doi:10.1016/j.nicl.2014.02.001

Ringman, J. M., O'Neill, J., Geschwind, D., Medina, L., Apostolova, L. G., Rodriguez, Y., et al. (2007). Diffusion tensor imaging in preclinical and presymptomatic carriers of familial Alzheimer's disease mutations. *Brain* 130, 1767–1776. doi:10.1093/brain/awm102

Roher, A. E., Weiss, N., Kokjohn, T. A., Kuo, Y. M., Kalback, W., Anthony, J., et al. (2002). Increased A beta peptides and reduced cholesterol and myelin proteins characterize white matter degeneration in Alzheimer's disease. *Biochemistry* 41, 11080–11090. doi:10.1021/bi026173d

Shahani, S. K., Lingamaneni, R., and Hemmings, H. C. Jr. (2002). General anesthetic actions on norepinephrine, dopamine, and gamma-aminobutyric acid transporters in stably transfected cells. *Anesth. Analg.* 95, 893–899. doi:10.1097/00000539-200210000-00019

Smith, G. S., Laxton, A. W., Tang-Wai, D. F., McAndrews, M. P., Diaconescu, A. O., Workman, C. I., et al. (2012). Increased cerebral metabolism after 1 year of deep brain stimulation in Alzheimer disease. *Arch. Neurol.* 69, 1141–1148. doi:10.1001/archneurol.2012.590

Song, S. K., Kim, J. H., Lin, S. J., Brendza, R. P., and Holtzman, D. M. (2004). Diffusion tensor imaging detects age-dependent white matter changes in a transgenic mouse model with amyloid deposition. *Neurobiol. Dis.* 15, 640–647. doi:10.1016/j.nbd.2003.12.003

Song, S. K., Sun, S. W., Ju, W. K., Lin, S. J., Cross, A. H., and Neufeld, A. H. (2003). Diffusion tensor imaging detects and differentiates axon and myelin degeneration in mouse optic nerve after retinal ischemia. *Neuroimage* 20, 1714–1722. doi:10.1016/j.neuroimage.2003.07.005

Thies, W., Bleiler, L., and Alzheimer's, A. (2013). 2013 Alzheimer's disease facts and figures. *Alzheimers Dement.* 9, 208–245. doi:10.1016/j.jalz.2013.02.003

Thomas, A. G., Koumellis, P., and Dineen, R. A. (2011). The fornix in health and disease: an imaging review. *Radiographics* 31, 1107–1121. doi:10.1148/rg.314105729

Van Bruggen, T., Stieltjes, B., Thomann, P. A., Parzer, P., Meinzer, H. P., and Fritzsche, K. H. (2012). Do Alzheimer-specific microstructural changes in mild cognitive impairment predict conversion? *Psychiatry Res.* 203, 184–193. doi:10.1016/j.pscychresns.2011.12.003

Xu, J., Chen, S., Ahmed, S. H., Chen, H., Ku, G., Goldberg, M. P., et al. (2001). Amyloid-beta peptides are cytotoxic to oligodendrocytes. *J. Neurosci.* 21, Rc118.

Xu, Y., Jack, C. R. Jr., O'brien, P. C., Kokmen, E., Smith, G. E., Ivnik, R. J., et al. (2000). Usefulness of MRI measures of entorhinal cortex versus hippocampus in AD. *Neurology* 54, 1760–1767. doi:10.1212/WNL.54.9.1760

Yamada, K., Shrier, D. A., Rubio, A., Yoshiura, T., Iwanaga, S., Shibata, D. K., et al. (1998). MR imaging of the mamillothalamic tract. *Radiology* 207, 593–598. doi:10.1148/radiology.207.3.9609878

Zhuang, L., Sachdev, P. S., Trollor, J. N., Kochan, N. A., Reppermund, S., Brodaty, H., et al. (2012). Microstructural white matter changes in cognitively normal individuals at risk of amnestic MCI. *Neurology* 79, 748–754. doi:10.1212/WNL.0b013e3182661f4d

Zhuang, L., Sachdev, P. S., Trollor, J. N., Reppermund, S., Kochan, N. A., Brodaty, H., et al. (2013). Microstructural white matter changes, not hippocampal atrophy, detect early amnestic mild cognitive impairment. *PLoS ONE* 8:E58887. doi:10.1371/journal.pone.0058887

Conflict of Interest Statement: The authors declare that the research was conducted in the absence of any commercial or financial relationships that could be construed as a potential conflict of interest.

Received: 01 September 2014; accepted: 02 January 2015; published online: 21 January 2015.

Citation: Nowrangi MA and Rosenberg PB (2015) The fornix in mild cognitive impairment and Alzheimer's disease. Front. Aging Neurosci. ***7****:1. doi: 10.3389/fnagi.2015.00001*

This article was submitted to the journal Frontiers in Aging Neuroscience.

frontiers in
AGING NEUROSCIENCE

ORIGINAL RESEARCH ARTICLE
published: 28 May 2014
doi: 10.3389/fnagi.2014.00106

Early brain loss in circuits affected by Alzheimer's disease is predicted by fornix microstructure but may be independent of gray matter

Evan Fletcher[1]*, Owen Carmichael[1,2], Ofer Pasternak[3], Klaus H. Maier-Hein[4] and Charles DeCarli[1]

[1] *IDeA Laboratory, Department of Neurology, University of California Davis, Davis, CA, USA*
[2] *Department of Computer Science, University of California Davis, Davis, CA, USA*
[3] *Departments of Psychiatry and Radiology, Harvard University, Cambridge, MA, USA*
[4] *Medical Image Computing Group, German Cancer Research Center (DKFZ), Heidelberg, Germany*

Edited by:
Kenichi Oishi, Johns Hopkins University, USA

Reviewed by:
Claudia Metzler-Baddeley, Cardiff University, UK
Michelle M. Mielke, Mayo Clinic, USA

****Correspondence:***
Evan Fletcher, IDeA Laboratory, Center for Neuroscience, University of California Davis, 1544 Newton Court, Davis, California 95616, USA
e-mail: evanfletcher@gmail.com

In a cohort of community-recruited elderly subjects with normal cognition at initial evaluation, we found that baseline fornix white matter (WM) microstructure was significantly correlated with early volumetric longitudinal tissue change across a region of interest (called fornix significant ROI, fSROI), which overlaps circuits known to be selectively vulnerable to Alzheimer's dementia pathology. Other WM and gray matter regions had much weaker or non-existent associations with longitudinal tissue change. Tissue loss in fSROI was in turn a significant factor in a survival model of cognitive decline, as was baseline fornix microstructure. These findings suggest that WM deterioration in the fornix and tissue loss in fSROI may be the early beginnings of posterior limbic circuit and default mode network degeneration. We also found that gray matter baseline volumes in the entorhinal cortex and hippocampus predicted cognitive decline in survival models. But since GM regions did not also significantly predict brain-tissue loss, our results may imply a view in which early, prodromal deterioration appears as two quasi independent processes in white and gray matter regions of the limbic circuit crucial to memory.

Keywords: fornix diffusivity, longitudinal brain change, limbic circuit, default mode network, normal cognition

INTRODUCTION

Recent work has shown that the fornix (Oishi et al., 2012; Fletcher et al., 2013a) and other memory-related white matter (WM) tracts (Zhuang et al., 2012, 2013) are sensitive predictors of conversion from normal cognition to mild cognitive impairment (MCI) or Alzheimer's dementia. In these findings, the loss of WM volume or microstructural integrity, in key structures, appears to be measurable before gray matter differences. Similarly, in groups of subjects with and without subjective memory complaints, but scoring normally on all cognitive tests – thus encompassing very subtle differences – WM diffusivity of the posterior cingulate, retrosplenial cortex (RSC), and precuneus (Selnes et al., 2012) and parahippocampal WM (Wang et al., 2012) was significantly different for those with memory complaints, while gray matter thickness was not. Recent results such as these have been taken to suggest that early WM deterioration may be at least partially separate (Agosta et al., 2011; Selnes et al., 2012) from the β-amyloid and tau pathologies of gray matter, whose evolution is known to characterize Alzheimer's disease (AD) (Braak and Braak, 1996), and have even raised the question whether Alzheimer's should be considered a disease of the WM (Sachdev et al., 2013).

On the other hand, the progression of β-amyloid and tau pathologies has long been established (Braak and Braak, 1996) and remains the dominant paradigm of AD modeling (Jack et al., 2010; Sperling et al., 2011; Jack and Holtzman, 2013). In these models, gray matter changes due to an "amyloid cascade" and the tauopathy driven by it (Jack and Holtzman, 2013) underly brain atrophy and deterioration. The sequence of events consists of GM atrophy followed by WM disconnection and regional hypometabolism (Villain et al., 2008, 2010). This deterioration is best viewed as a network disconnection syndrome (Reid and Evans, 2013) in which specific networks – the Papez memory circuit (Villain et al., 2008; Acosta-Cabronero et al., 2010), also known as the limbic circuit (Nestor et al., 2003), together with the default mode network (DMN) (Greicius et al., 2004) – are selectively affected (Seeley et al., 2009). In recent biomarker models of AD progression (Jack and Holtzman, 2013), tauopathy may or may not arise before the amyloid cascade but increasing levels of β-amyloid, perhaps due to inadequate clearance from the brain, drive the trajectory of brain deterioration. Thus according to the "amyloid cascade hypothesis" (Jack and Holtzman, 2013), tauopathy is separate from amyloidopathy but dependent on it. When tauopathy progresses, it follows the well-known stereotypical pattern starting with the brainstem and transentorhinal cortex (Braak and Braak, 1996; Jack and Holtzman, 2013). The biomarker models (Jack et al., 2010; Jack and Holtzman, 2013) therefore picture an ordering of amyloid and tau pathologies followed eventually by macroscopic brain changes and measurable declines in memory and clinical function.

Thus, there may be an apparent contrast between amyloid models and recent results, among preclinical subjects, suggesting the importance of WM differences as early markers of decline. This has

raised the question whether the biomarker sequence of Jack and Holtzman (2013) should be modified to include measurable WM deterioration as one of the earliest events (Sachdev et al., 2013). It would therefore be useful to clarify the extent to which baseline white and gray matter measurements, in the prodromal phase preceding MCI and AD, are associated with longitudinal changes in the brain. This could help evaluate recent suggestions about the usefulness of key WM tracts as early biomarkers (Zhuang et al., 2012; Fletcher et al., 2013a; Sachdev et al., 2013) to supplement the CSF and brain biomarkers (Jack et al., 2010; Jack and Holtzman, 2013) of the amyloid models. And by comparing the sequencing of gray and WM changes, we may gain clues about whether white and gray matter processes are related or separate, thus advancing our knowledge of the ways in which the brain starts to change prior to measurable cognitive decline.

In this article, we investigate whether baseline measurements of cortical gray matter volume and WM microstructure, in regions of interests (ROIs) known to be associated with cognitive decline, are also predictors of early longitudinal brain changes in a cohort of clinically normal subjects. Our GM ROIs are the hippocampi, entorhinal cortical gray, and gray matter in the RSC and posterior cingulate – known sites of early and later AD pathology – as well as the anterior cingulate GM for comparison. WM ROIs include the fornix, which has been shown to be a predictor of earliest cognitive decline, along with the splenium and anterior and posterior cingulum, whose integrity is diminished in MCI or AD (Zhang et al., 2007; Mielke et al., 2009; Acosta-Cabronero et al., 2010). We also test the genu and corticospinal tract (CST) as WM tract controls. Our comparison of baseline WM with longitudinal change has some precedent. It is similar to the approach in an earlier study of middle-aged normal subjects (Ly et al., 2013), which found that baseline fractional anisotropy (FA) measurements in entorhinal WM, corpus callosum genu, and splenium were associated with tissue loss in the superior longitudinal fasciculus (SLF), corona radiata, and other regions. This indicated that baseline WM measurements may be predictive of WM tissue change even in relatively young subjects – 15 years before the lower age cutoff of our normal elderly cohort – and suggested that WM microstructure and tissue loss should be included in models of aging.

As in that study, we did not suppose an *a priori* hypothesis about *which* specific brain regions may be associated with baseline cortical GM thickness or microstructural features in the WM ROIs. But we did test the hypothesis that tissue loss in *some* brain area is associated with baseline measurements in one or more of these ROIs. And we analyzed these findings to attempt inferences about the nature and timing of brain processes preceding cognitive change in elderly normals.

MATERIALS AND METHODS

PARTICIPANTS

Subjects for this study consisted of cognitively normal individuals recruited into the Longitudinal Cohort of the Alzheimer's Disease Center of the University of California Davis (UCD ADC). Participants were recruited through community outreach using methods designed to enhance ethnic diversity (Hinton et al., 2010). All subjects provided informed consent before participating in this study.

CLINICAL EVALUATION

Each participant received multidisciplinary clinical evaluations at the UCD ADC at baseline and at approximately annual follow-up examinations. Evaluations included detailed medical history, with physical and neurological examinations. Diagnosis of cognitive syndromes – MCI or AD – was made according to standardized criteria (Mungas et al., 2011) by a consensus conference of clinicians. The clinical dementia rating sum of boxes score (CDRSum) (Morris, 1997) was assessed as a measure of clinically relevant functional impairment. Clinical "conversion" from normal cognition occurred when a subject with normal cognition at baseline was diagnosed as MCI or AD at a follow-up visit. The time to conversion was measured as the time from baseline to date of conversion.

MAGNETIC RESONANCE IMAGING

Each subject received at least two structural T1-weighted MRI scans, with the first one close to the date of the baseline clinical evaluation, as well as a diffusion MRI sequence at the same date as the first scan. All images were acquired at the University of California Davis, Imaging Research Center. The T1-weighted spoiled gradient recalled echo acquisition had the following parameters: TR 9.1 ms, flip angle 15°, field of view 24 cm, slice thickness 1.5 mm, and field strength 1.5 T. The 2D axial–oblique single-shot spin-echo planar imaging diffusion sequence had the following parameters: TE 9.4 ms, TR 8000 ms, flip angle 90°, field of view 24 cm, and slice thickness 5 mm. In-plane voxel dimensions were 1.875 mm in each direction. The B value was 1000 s/mm^2 with six gradient directions collected four times each (two times each in the plus and minus directions), plus two B0 images. In order to perform group statistical analysis, all subject T1 images at baseline were non-linearly deformed to a minimal deformation template (MDT) (Kochunov et al., 2001) using linear and non-linear B-spline transformation parameters (Rueckert et al., 2006). Diffusion images were corrected for eddy currents in native space using the FSL toolbox (Jenkinson et al., 2012). To account for the presence of extracellular free water contamination as partial voluming in the diffusion images, diffusion tensors were estimated by the free water elimination (FWE) algorithm (Pasternak et al., 2009). This algorithm estimates at each voxel the contributions to apparent diffusivity of separate tissue and free water compartments, returning both a voxel map of free water fractional volume (from 0 to 100%) and estimated diffusion tensors that represent tissue without free water. Scalar measures of FWE-corrected FA were calculated from the diffusion tensors. In addition to free water corrected maps, we previously calculated regular (uncorrected) FA maps that were warped to a template for group analysis. An FA–MDT was constructed as the average of 69 cognitively normal subject FA images, each linearly aligned to its corresponding native T1 image and then transformed to MDT space using the transformation parameters generated for its T1 image, after visual verification that the linear alignment between native FA and T1 was accurate. For the current study, native subject uncorrected FA baseline images were separately linearly aligned and B-spline deformed directly to the FA–MDT image that was already coincident with our MDT. The transformation parameters deforming native FA to FA–MDT were then used to deform individual subject

diffusivity images (FWE-corrected FA and Free water maps) into template space. In the remainder of this article, we refer to all FWE-corrected FA maps simply as FA.

LONGITUDINAL CHANGE ANALYSIS

Each normal subject received a T1-weighted structural scan at a date close to the baseline clinical evaluation and second scan at least a year later. Localized voxelwise longitudinal change between the two T1 images was computed using a tensor-based morphometry (TBM) algorithm designed to enhance sensitivity and specificity by incorporating knowledge of likely tissue boundary locations (Fletcher et al., 2013b). Brain change was quantified using log-Jacobians derived at each voxel from the TBM deformation field. In this analysis, the determinant of the 3×3 derivative matrix of the deformation field computes the local volume change factor indicated by the deformation. Determinants between 0 and 1 indicate volume shrinkage or loss, while determinants >1 indicate expansion. Thus, Jacobians represent multiplicative proportional volume changes from baseline. Performing a log transform then gives a distribution of values symmetric about 0, with negative logs indicating contraction, positive logs indicating expansion, and 0 indicating no volume change (Hua et al., 2008; Fletcher et al., 2013b). These will be referred to as the log-Jacobians. In longitudinal brain mapping of our elderly cohorts, log-Jacobians of CSF spaces like the ventricles and sulci are generally positive, while those located in tissue are negative, indicating patterns of tissue loss and CSF expansion. To perform group statistical analysis, native space log-Jacobian images were deformed into template space using the linear and B-spline parameters previously computed for native T1 images as described above. For valid group comparison, log-Jacobian images in template space were normalized to represent change over a 2-year period. This was done by multiplying each Jacobian image by a factor consisting of the ratio $2.0/\Delta T$, where ΔT was the interscan time interval for that subject's two T1 MRI scans. This normalization is justified by the assumption, verified empirically on sample subjects having several scan times, that brain-tissue change is roughly log-linear over time.

REGIONS OF INTEREST

Regions of interest were used to evaluate the correlations of baseline measurements in both white and gray matter with longitudinal changes. For WM measurements, template MDT space ROIs were used to examine the association of mean FA with voxelwise brain changes. For the fornix body we used an ROI generated in-house by an experienced neurologist, and previously used in publications from our lab (Lee et al., 2012; Fletcher et al., 2013a). The genu and splenium of the corpus callosum and the anterior and posterior cingulum ROIs were generated by the same neurologist. We tested baseline mean FA values in these regions for the existence of significant clusters of associated tissue change as measured by our log-Jacobians. We also ascertained which relevant WM structures overlapped our clusters of significantly associated log-Jacobian change. We calculated overlaps of the Jacobian clusters with our thalamus, splenium, and cingulum ROIs, Brodmann areas (BA) also generated in-house, together with ROIs in the Johns Hopkins WM atlas (Zhang et al., 2010), all warped to our own MDT. For GM measurements, ROI GM volume was ascertained in each subject's native space. BA template MDT ROIs were inversely transformed to native space structural T1 images via a process we have used in previous publications (Fletcher et al., 2013a,b). GM volumes were computed from these ROIs overlaid over the native space four-tissue segmented image. Tissue segmentation in the native T1 images was accomplished using a Bayesian maximal-likelihood algorithm enhanced for sensitivity at tissue boundaries (Fletcher et al., 2012). Hippocampal volumes were computed in native space by hand tracing methods that have been described previously (Carmichael et al., 2010; Lee et al., 2012). To test the hypothesis that baseline GM measurements were associated with longitudinal brain change, we used the hippocampi and BA ROIs that are known to be implicated in GM loss during the trajectory of cognitive decline – BA 28 and 34 (the ventral and dorsal bilateral entorhinal cortices).

STATISTICAL ANALYSIS

To assess the correlation of baseline ROI GM or WM measurements with longitudinal change, we used single linear regression models of ROI mean FA values or GM volumes and voxelwise log-Jacobian values, computing the Student's t-value at each voxel for the slope of the regression line. In these regressions, the slope of the regressions at brain-tissue voxels will generally be positive for ROI FA values, corresponding to the association between lower FA values (putative markers of impaired ROI microstructure) and more negative log-Jacobians (indicating more severe brain-tissue loss). Conversely, higher ROI FA values should correspond to less severe brain-tissue loss, computed by negative log-Jacobians of smaller magnitude. Similarly for GM ROIs, the associations should be positive in brain-tissue areas, corresponding to a smaller magnitude of local tissue loss associated with greater baseline GM volume. The t-value clusters were corrected for multiple comparisons (Nichols and Holmes, 2001). We did this by non-parametric permutation testing over 1000 iterations. We tested for size of contiguous voxel clusters all having regression t-value >3.5 for both the FA values and the GM volumes. Clusters with sizes in the top 95th percentile over all iterations were taken as regions of significant association ($p < 0.05$) between ROI FA or GM and longitudinal brain change.

To evaluate the significance of brain factors for cognitive conversion, we constructed Cox proportional hazards models (Cox, 1972). Each model contained demographic factors of age, gender, education, and ethnicity as covariates, together with a single brain measurement. A brain measurement was a significant factor in cognitive conversion if the probability of having a larger χ^2 than the one in the likelihood ratio test for that variable was <0.05.

RESULTS

SUBJECTS

Longitudinal analysis was based on a group of 68 community-recruited normal subjects with two structural MR scans, diffusion MRI taken at the baseline date, and clinical data gathered at or near the dates of the structural MRIs. This group contained 12 subjects who later converted to MCI or AD, and 56 who remained stable. Demographics of the subjects are displayed in **Table 1**. Except for information on clinical conversion, all other data in the table reflect baseline date evaluations.

LONGITUDINAL BRAIN-TISSUE LOSS ASSOCIATED WITH BASELINE WM AND GM ROIs

In the regression tests of ROI GM volume (including hippocampal volume) and voxelwise log-Jacobians, we found only one small significant cluster ($2\,cm^3$) log-Jacobian cluster for $t > 3.5$, corresponding to hippocampal volume. Other GM ROIs had no significant clusters.

For the correlations with WM ROIs, **Figure 1** displays raw t-values of log-Jacobians vs. FA in (left to right) the fornix body, splenium, and posterior cingulum. A consistent pattern of highly positive correlations is seen for the fornix (left panel) as compared to inconsistent and low magnitude associations for the other two ROIs in the middle and right panels. Sizes of significant clusters for all WM ROIs, corresponding to a threshold of $t > 3.5$, are given in **Table 2**. None of the anterior and posterior cingulate, the splenium, and genu ROIs had any significant clusters for t-values above this threshold. The CST had a very small cluster. The fornix body generated much larger ROI comprising components bilaterally in the posterior parietal, temporal, and frontal lobes, with small sections in the cerebellum. We will henceforth designate the ensemble of these clusters as *fornix significant ROI* (fSROI). Its tissue composition consisted of about 80% white and 20% gray matter. The fSROI is shown in **Figure 2**.

Table 1 | Demographics of normal cohort having DTI.

Characteristic	Converters ($N = 12$)	Non-converters ($N = 56$)
Gender (M/F)	3/9	15/41
Age*	76.7 (7.2)	72.1 (6.9)
Education (years)	11.7 (3.6)	11.4 (5.1)
Time to convert (years)	2.2 (1.1)	–
MMSE	27.4 (3.1)	28.5 (1.6)
Episodic memory (Z-score)*	−0.48 (0.75)	0.20 (0.78)
Executive (Z-score)*	−0.35 (0.55)	0.08 (0.55)
ApoE4 (%)	25%	22%
Ethnicity (W/H/AA/other)	1/8/1/2	21/30/3/2

For ethnicity designations: W means white, H means Hispanic, AA means African American. Starred variables are significantly different between converters and non-converters.

ANATOMICAL COMPOSITION OF THE fSROI

Table 3 shows the intersection of the fSROI with selected BA, regions of the corpus callosum, thalamus, longitudinal fasciculi, and WM tracts from the CC and thalamus to the parietal and occipital lobes. It indicates extensive overlap with the posterior cingulate cortex (PCC) (BA 23 and 31) and RSC (BA 26–29 and 30), as well as the thalamus. More generally, the fSROI heavily intersects the posterior portions of the corpus callosum, longitudinal fasciculi, and several of the WM tracts from thalamus or CC to posterior parietal or occipital gyri. Color-coded maps of intersections with ROIs listed in **Table 3** are shown in **Figure 3**. Green areas illustrate extensive overlap of BA; purple shows overlap with thalamus and its projections; and tan shows coverage of the splenium and projections from the corpus callosum.

BRAIN FACTORS AS PREDICTORS OF COGNITIVE CONVERSION

We tested the significance of the fSROI along with baseline brain measurements in Cox proportional hazards models for cognitive conversion from normal. Each model contained the multiple demographic variables described previously along with a single brain factor. Significant factors in the individual models, with their p-values and those of significant covariates, are summarized in **Table 4**. To facilitate effect comparisons amongst all brain variables and with age, hazard ratios for each brain factor are provided based on unit change in Z-score for brain factors and 1 year increase for age. Significant GM predictors of conversion were volumes in the ventral and dorsal entorhinal regions (BA 28, 34), the dorsal anterior cingulate (BA 32), and bilateral hippocampal volume. Age and ethnicity were also significant factors in the GM models. Fornix body FA and mean tissue change in fSROI were the other significant brain predictors of conversion. We note that in the GM models, age was highly significant and except for BA 28, it had a lower p-value than the accompanying brain factor. In the models of fornix FA and fSROI, by contrast, age was not significant.

INTERACTIONS BETWEEN GM, WM, AND fSROI TISSUE LOSS

To test for confounding effects of age or other demographic factors in association between baseline fornix FA and fSROI log-Jacobians,

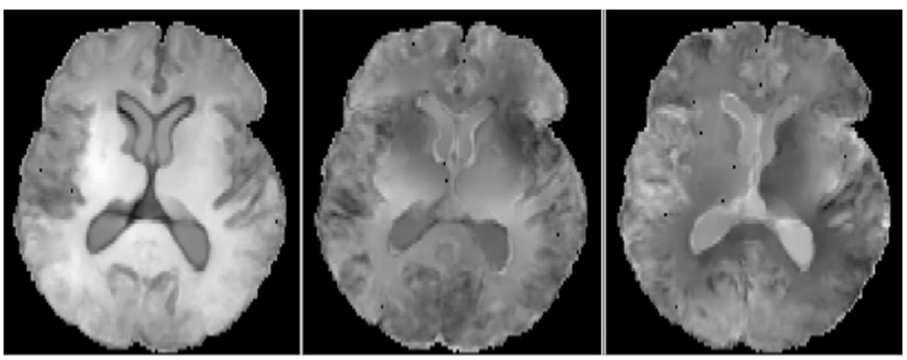

FIGURE 1 | Axial views of raw t-values from voxel regressions of log-Jacobians vs. FA. Left: regressions with fornix body FA. Middle: regressions with splenium. Right: regressions with posterior cingulate. Bright indicates positive t-values, reflecting correlation of high ROI FA with smaller brain tissue loss.

we modeled the mean fSROI values as outcome of a multi-regression including independent variables of age, gender, education, ethnicity, and fornix FA. The overall model produced a strong fit ($R^2 = 0.52$) with significance of the independent variables as follows: fornix FA, $p = 0.0008$; age, $p = 0.016$; education, $p = 0.17$; gender, $p = 0.23$; and ethnicity $p = 0.69$. Thus, fornix FA and age were the only significant correlates of tissue change in fSROI, with FA being much stronger than age.

To test for GM contributions to fSROI outcomes, we performed multiple regression modeling of mean fSROI log-Jacobians vs. baseline hippocampal, BA 28 or BA 34 gray volumes, one per regression model, together with the demographic factors of age, education, gender, and ethnicity. In each of these models, the overall fit was not as good as for the fornix FA (R^2 was about 0.36 in each case) and no brain factor was significant, while age was significant in each model.

Finally, to test the mutual interaction of the brain variables, we examined the correlation matrix of components including the fSROI log-Jacobians, fornix FA, and GM volumes from BA 28, 34, and bilateral hippocampus. The matrix is given in **Table 5**.

DISCUSSION

In this study, an analysis of the relation between baseline ROI FA measurements and longitudinal brain change has indicated that fornix body microstructure is significantly associated with a large region of tissue loss (fSROI) primarily in the WM of the posterior frontal, parietal, and temporal lobes. Similar correlation analyses of WM in the CST, anterior and posterior cingulate, genu, and splenium, showed small or non-existent effects. Baseline GM values for the entorhinal cortex and hippocampus also failed to show strong associations with longitudinal brain change. The fornix has already been identified as a sensitive predictor of early cognitive change in normals (Oishi et al., 2012; Zhuang et al., 2012; Fletcher et al., 2013a) – a result corroborated in our present study – and our current findings now also link it with longitudinal change in posterior brain structures known to be affected by AD pathology (**Table 3**; **Figure 3**). Our regressions incorporating age as a covariate have indicated that these associations are not merely dependent on age. And the tissue losses in the fSROI are themselves significant predictors of conversion, in Cox survival models that included age as a covariate. The picture is nuanced, however, because GM regions in the limbic circuit also predicted cognitive conversion (**Table 4**) but not longitudinal brain change. In this section, we discuss these findings in relation to previous work, and attempt to draw some inferences about the nature and timing of early brain changes associated with cognitive decline.

Table 2 | Volumes of significant clusters in regression of ROI FA values with voxel log-Jacobians, for $t > 3.5$.

WM FA ROIs	Log-Jacobian significant cluster (cc brain-tissue loss) for $t > 3.5$
CST	0.76
Anterior cingulate	0
Posterior cingulate	0
CC genu	0
CC splenium	0
Fornix body	83.20

There were no significant clusters for any GM ROI corresponding to threshold $t > 3.5$ except for the hippocampi, with cluster volume 2 cm^3.

fSROI, LIMBIC CIRCUIT, AND PRIOR RESULTS CHARACTERIZING EARLY AD

Table 3 and **Figure 3** outline the intersection of the fSROI with other brain regions. The fSROI has relatively large overlaps with the thalamus; projections of the thalamus to precuneus; the superior parietal gyrus (including precuneus) and underlying WM; the RSC (BA 26, 29, and 30); the posterior cingulum (BA 23 and 31); and the splenium of the corpus callosum. Most of these are components of the circuit of Papez or limbic circuit (Nestor et al., 2003), considered to be important in the formation and consolidation of memory (Thomas et al., 2011). The fSROI is similar to the ROI found in a previous study investigating disconnection of the hippocampus and PCC in a cohort of early AD subjects (Villain et al., 2008). Their ROI of correlations between WM and hippocampal GM Z-scores ($p < 0.05$ uncorrected) included most of the cingulum bundle from frontal to parahippocampal fibers. They reported a correlation between gray matter Z-scores of the hippocampus and damage to the retrosplenial BA 29, 30, together with WM disruption of the posterior cingulum bundle. Cingulum bundle

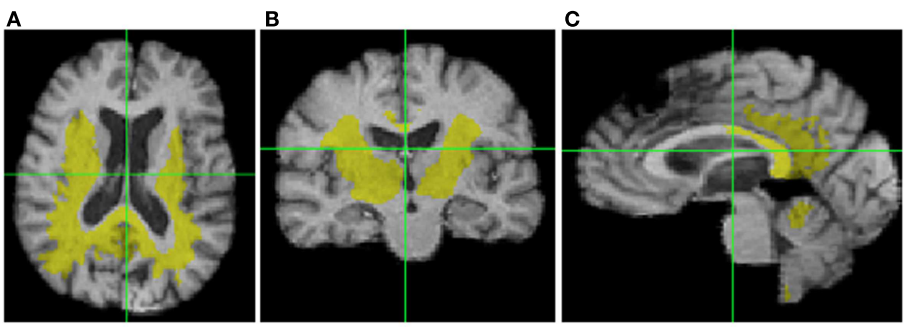

FIGURE 2 | Significant cluster of association (fSROI) between fornix body FA mean and negative log-Jacobians ($t > 3.5$). Views from left to right: **(A)** axial, **(B)** coronal, and **(C)** sagittal.

Table 3 | Component brain regions, which overlap with the whole fornix significant association ROI (fSROI).

(A)	
Brodmann ROIs	**fSROI overlap (% of ROI)**
BA 39 (angular gyrus)	20
BA 31 (dorsal PCC)	27
BA 30 (part of RSC)	41
BA 23 (ventral PCC)	61
BA 41 (auditory)	45
BA 26–29 (part of RSC)	78
(B)	
Corpus callosum ROIs	**fSROI overlap (% of ROI)**
CC MOG (middle occipital gyrus)	30
CC SOG (sup occipital gyrus)	43
CC SPG (sup parietal gyrus)	47
CC PrCU (precuneus)	50
CC Cu (cuneus)	55
Splenium	65
(C)	
Thalamus ROIs	**fSROI overlap (% of ROI)**
TH PrCu (precuneus)	51
Thalamus	51
TH SPG (sup parietal gyrus)	49
TH SOG (sup occipital gyrus)	58
TH MOG (middle occipital gyrus)	56
(D)	
Longitudinal fasciculi ROIs	**fSROI overlap (% of ROI)**
IFOF	22
ILF	22
SLF	34

Right column shows what percentage of the given ROI is intersected by fSROI. (A) Brodmann areas intersecting fSROI. (B) Corpus callosum (CC) and tracts originating in CC. (C) Thalamus (TH) and tracts originating there. (D) Longitudinal fasciculi; CC_SOG, white matter tract from CC to superior occipital gyrus, etc.; IFOF, inferior frontal occipital fasciculus; TH_PrCu, thalamo-precuneus tract, etc.; ILF, inferior longitudinal fasciculus; SLF, superior longitudinal fasciculus; SPG, superior parietal gyrus (encompasses precuneus and connections from CC and thalamus); RSC, retrosplenial cortex and underlying white matter (encompasses Brodmann areas 26, 29, and 30).

atrophy was in turn found to be correlated with glucose hypometabolism of the thalamus, mammillary bodies, middle cingulum, parahippocampal cingulum, and hippocampus – again components of the Papez circuit. The difference from our study was that in their early AD subjects the ROI arose from correlations of hippocampal and WM disruption, whereas our similar fSROI was correlated with fornix microstructural integrity at baseline. We shall discuss this below.

Another study (Acosta-Cabronero et al., 2010) examined the degeneration of WM tracts in early AD, using axial and radial diffusivities and mean diffusivity (MD). It found degeneration of tracts in the Papez circuit including the fornix, splenium, posterior cingulum, parahippocampal gyrus, and adjacent tracts of the temporo-parietal cortex as compared with normal controls. Anterior WM tracts were relatively spared. An important conclusion, according to that paper, is that this limbic circuit is preferentially vulnerable to degeneration in AD. This echoes an earlier proposal, based on the study of hypometabolism in MCI and AD subjects, that damage to the limbic circuit is the earliest significant event in the progression of AD (Nestor et al., 2003).

To summarize, then, previous studies both of hypometabolism and WM tract disruption among MCI and AD cohorts have found degeneration in regions which our fSROI extensively overlaps and in fact resembles. This is consistent with the possibility that the fSROI represents early longitudinal tissue changes, predicted by baseline fornix FA, which precede and eventually result in the effects described in those studies. This possibility is strengthened by our finding that brain-tissue losses in the fSROI are themselves significantly associated with cognitive conversion in survival models (**Table 4**).

fSROI AND THE DEFAULT MODE NETWORK

Table 3 and **Figure 3** show that the fSROI extensively overlaps the RSC. The RSC has been identified with the one of the main nodes, the PCC/RSC node (Greicius et al., 2009) of the DMN (Greicius et al., 2003), which is connected to a second principal node, the medial prefrontal cortex, by the cingulum bundles (Greicius et al., 2009). The RSC is also connected more ventrally to the medial temporal lobes probably by fibers in the descending (parahippocampal) cingulum (Thomas et al., 2011). In AD subjects, the DMN has diminished resting state activity in the PCC (Greicius et al., 2004), probably resulting from disrupted connectivity between the hippocampus and posterior cingulum, and DMN activity may be a sensitive biomarker for incipient AD. Further, among five distinct functional connectivity networks of the brain selectively targeted by differing neurodegenerative diseases, the DMN is the one specifically characterized by vulnerability to AD (Seeley et al., 2009). Because the fSROI extensively overlaps the RSC and posterior cingulum, it appears that the fSROI contains early tissue loss in principal posterior components of the DMN, thereby presaging the later loss of connectivity and decreased activity. And the strong association of the fSROI with fornix FA therefore suggests that fornix microstructure in cognitively normal subjects may be a very early marker of future disconnection in the DMN.

INFERENCES ABOUT EARLY BRAIN PROCESSES OF DEGENERATION

The fornix and the rest of the limbic circuit, along with the DMN, are all selectively vulnerable to early Alzheimer's pathology (Nestor et al., 2003; Seeley et al., 2009; Acosta-Cabronero et al., 2010). And degeneration in the limbic circuit has been proposed as the first significant event in the progression of AD (Nestor et al., 2003). If our identification of the fSROI with major components of the limbic circuit and DMN is correct, then we may have traced the trajectory of tissue losses in these circuits farther backwards toward their origins than has been done heretofore. In this early phase, the changes are associated with baseline fornix WM but

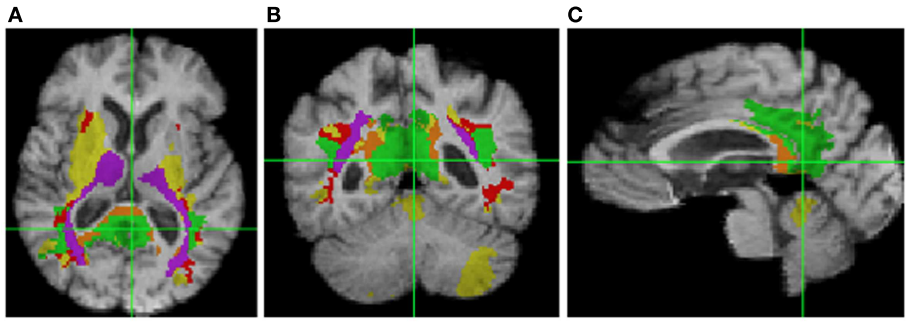

FIGURE 3 | Intersection of fSROI with ROIs in Table 3. Warm colors: Tan, splenium, and projections from corpus callosum; red, longitudinal fasciculi. Cool colors: green, Brodmann areas; purple, thalamus and projections from thalamus. Yellow: fSROI regions not intersecting any of these ROIs. Left to right: **(A)** axial, **(B)** coronal, and **(C)** sagittal.

Table 4 | Statistically significant factors for cognitive conversion (decline from normal) in Cox proportional hazards models.

Brain factor in survival model	Brain factor *p*-value	Brain factor hazard ratio per unit *Z* increase	Age hazard ratio per year increase	Other significant factors (*p*-value)
BA 28 (ventral ER) GM	0.001*	0.34 (0.16–0.63)	1.15 (1.04–1.31)	Age (0.008), ethnicity (0.01)
BA 32 (dorsal AC) GM	0.03*	0.46 (0.23–0.92)	1.16 (1.04–1.32)	Age (0.006), ethnicity (0.02)
BA 34 (dorsal ER) GM	0.02*	0.47 (0.26–0.86)	1.17 (1.05–1.33)	Age (0.005), ethnicity (0.05)
Hippo volume	0.04*	0.47 (0.21–0.95)	1.22 (1.08–1.41)	Age (0.001), ethnicity (0.03)
Fornix body FA	0.015*	0.38 (0.16–0.83)	1.11 (1.00–1.26)	Ethnicity (0.037)
fSROI log-Jacobian	0.045*	0.45 (0.20–0.98)	1.11 (0.99–1.25)	Ethnicity (0.03)

Each model contained age, gender, education, and ethnicity together with one brain factor. p-Values refer to the probability of the χ^2 value being larger than computed for a given variable in likelihood ratio test. All brain factor values were converted to Z-scores prior to analysis in order to enable meaningful comparisons of hazard ratios. The hazard ratio columns show change in conversion risk per unit Z-score change (in brain factors) or year (age). Values in parentheses for these columns are the lower and upper 95% confidence interval endpoints. GM regions BA 26–29, 23, 31 are not shown because not significant; nor were the FA white matter regions in anterior and posterior cingulate, genu, and splenium; BA, Brodmann area; AC, anterior cingulate; ER, entorhinal cortex; fSROI, fornix significant ROI.

Table 5 | Correlation matrix for factor interaction analysis of GM, fornix FA, and fSROI variables.

	fSROI	Fornix FA	BA 28 GM	BA 34 GM	Hippo volume
fSROI	1.00	0.60	0.17	0.20	0.29
Fornix FA		1.00	0.38	0.45	0.31
BA 28 GM			1.00	0.58	0.35
BA 34 GM				1.00	0.38
Hippo volume					1.00

From the table, fSROI is strongly correlated (0.60) with fornix FA but with no GM factor or the hippocampus. But fornix FA, while being most strongly correlated with fSROI, is also correlated with BA 28 and 34 (0.38 and 0.45, respectively). And BA 28 and 34 are strongly correlated with each other, and less so with hippocampal volume.

not strongly with temporal gray matter. Tissue losses in fSROI are greater than due to aging alone, since their correlation with fornix FA was much stronger than with age. On the other hand, baseline GM measurements in the hippocampus and entorhinal cortices (also components of the limbic circuit) were significant predictors of cognitive decline but not of any brain-tissue loss. Analysis of these components (**Table 5**) showed that entorhinal areas were correlated with each other and with fornix FA but not strongly with fSROI. This may support the inference of two processes in early deterioration. One process may contribute most heavily to fornix WM and fSROI changes, underlying that strong correlation. The other may contribute to GM in the temporal lobe ROIs and also to fornix WM, but little to fSROI. Thus early deterioration in the posterior limbic circuit may be at least partly separate from gray matter processes in the entorhinal cortex or hippocampi. This inference does not necessarily contradict previous findings relating fornix and hippocampus (Lee et al., 2012) in MCI and AD, or cingulate WM and hippocampus (Villain et al., 2008, 2010) in early AD, because in the later stages, gray matter atrophy is more advanced and may contribute to circuit deterioration. Furthermore, a previous study has suggested (Sexton et al., 2010) that though fornix and gray matter pathologies may not be independent, the relationship may be complex, involving factors of Wallerian degeneration as well as separate WM disruptive processes. And another study (Douaud et al., 2013) has found that more than 2 years prior to conversion, WM microstructural differences in the fornix, left fimbria, and SLF characterized MCI patients who converted to probable dementia, when compared

with other stable MCI subjects. Those findings appear to be consistent with the suggestions put forth here, that in the prodromal phase, fornix microstructure, and tissue loss in the limbic circuit overlain by fSROI may have a component independent of gray matter change.

LIMITATIONS

We must note several limitations of our study. The first limitation is the small size of our normal cohort. This may have restricted our statistical power, for example in seeing relationships between GM ROIs and longitudinal brain change. The second limitation is the low resolution of our diffusion MRI data and the uncertainty of using it to make inferences about a structure as small as the fornix. It is evident from recent studies (Metzler-Baddeley et al., 2012; Berlot et al., 2014) that caution is required when interpreting diffusivity measurements, because of free water contamination to WM tracts generally and particularly in the fornix, due to its small size and proximity to the ventricles. But FWE (Pasternak et al., 2009) seems to improve FA's distinctions between groups and the robustness of inferences about WM change (Metzler-Baddeley et al., 2012). In our experiments, FWE improved the statistical power of FA correlations with longitudinal brain change, enabling us to see a more clear contrast between the effects of the fornix and other WM tracts (**Figure 1**), while dampening diffusivities such as MD and their apparent statistical power (data not shown). Lastly, we were unable in this project to explore hypotheses about the possible origins of WM changes in the fornix and the associated tissue loss in the fSROI, and whether such changes are related to gray matter changes by some underlying mechanism. A likely candidate for such exploration would be brain levels of β-amyloid accumulation.

CONCLUSION

In a cohort of normal subjects, baseline fornix WM microstructure significantly correlates with early longitudinal tissue change across an fSROI intersecting the posterior DMN and limbic circuits. These circuits are known to be selectively vulnerable to AD pathology. Baseline fornix WM microstructure, longitudinal tissue loss in the fSROI, and baseline GM volumes in the entorhinal cortices and hippocampus all are significantly associated with cognitive conversion from normal. But only fornix WM is associated with brain-tissue loss in the fSROI. Thus, WM deterioration in the fornix and tissue loss in fSROI may be the early beginnings of posterior limbic circuit and DMN degeneration. This early degeneration appears to be partly separate from gray matter atrophy. Future research may either identify separate mechanisms for early GM and WM change, or else show a common underlying process, which at the early stages manifests itself more strongly in the fornix–fSROI association.

ACKNOWLEDGMENTS

Thanks to Anna Lam and Evan Hamaguchi for data collection and quality control and discussion of experimental approaches in this article.

REFERENCES

Acosta-Cabronero, J., Williams, G. B., Pengas, G., and Nestor, P. J. (2010). Absolute diffusivities define the landscape of white matter degeneration in Alzheimer's disease. *Brain* 133(Pt 2), 529–539. doi:10.1093/brain/awp257

Agosta, F., Pievani, M., Sala, S., and Geroldi, C. (2011). White matter damage in Alzheimer disease and its relationship to gray matter atrophy. *Radiology* 258, 853–863. doi:10.1148/radiol.10101284

Berlot, R., Metzler-Baddeley, C., Jones, D. K., and O'Sullivan, M. J. (2014). CSF contamination contributes to apparent microstructural alterations in mild cognitive impairment. *Neuroimage* 92, 27–35. doi:10.1016/j.neuroimage.2014.01.031

Braak, H., and Braak, E. (1996). Evolution of the neuropathology of Alzheimer's disease. *Acta Neurol. Scand.* 94, 3–12. doi:10.1111/j.1600-0404.1996.tb05866.x

Carmichael, O., Mungas, D., Beckett, L., Harvey, D., Tomaszewski Farias, S., Reed, B., et al. (2010). MRI predictors of cognitive change in a diverse and carefully characterized elderly population. *Neurobiol. Aging* 33, 83–95. doi:10.1016/j.neurobiolaging.2010.01.021

Cox, D. (1972). Regression models and life-tables. *J. R. Stat. Soc. Ser. B* 34, 187–220.

Douaud, G., Menke, R. A. L., Gass, A., Monsch, A. U., Rao, A., Whitcher, B., et al. (2013). Brain microstructure reveals early abnormalities more than two years prior to clinical progression from mild cognitive impairment to Alzheimer's disease. *J. Neurosci.* 33, 2147–2155. doi:10.1523/JNEUROSCI.4437-12.2013

Fletcher, E., Raman, M., Huebner, P., Liu, A., Mungas, D., Carmichael, O., et al. (2013a). Loss of fornix white matter volume as a predictor of cognitive impairment in cognitively normal elderly individuals. *JAMA Neurol.* 95616, 1–7. doi:10.1001/jamaneurol.2013.3263

Fletcher, E., Knaack, A., Singh, B., Lloyd, E., Wu, E., Carmichael, O., et al. (2013b). Combining boundary-based methods with tensor-based morphometry in the measurement of longitudinal brain change. *IEEE Trans. Med. Imaging* 32, 223–236. doi:10.1109/TMI.2012.2220153

Fletcher, E., Singh, B., Harvey, D., Carmichael, O., DeCarli, C., Maximum, A., et al. (2012). Adaptive image segmentation for robust measurement of longitudinal brain tissue change. *Conf. Proc. IEEE Eng. Med. Biol. Soc.* 2012, 5319–5322. doi:10.1109/EMBC.2012.6347195

Greicius, M., Srivastava, G., Reiss, A., and Menon, V. (2004). Default-mode network activity distinguishes Alzheimer's disease from healthy aging: evidence from functional MRI. *Proc. Natl. Acad. Sci. U.S.A.* 101, 4637–4642. doi:10.1073/pnas.0308627101

Greicius, M. D., Krasnow, B., Reiss, A. L., and Menon, V. (2003). Functional connectivity in the resting brain: a network analysis of the default mode hypothesis. *Proc. Natl. Acad. Sci. U.S.A.* 100, 253–258. doi:10.1073/pnas.0135058100

Greicius, M. D., Supekar, K., Menon, V., and Dougherty, R. F. (2009). Resting-state functional connectivity reflects structural connectivity in the default mode network. *Cereb. Cortex* 19, 72–78. doi:10.1093/cercor/bhn059

Hinton, L., Carter, K., Reed, B. R., Beckett, L., Lara, E., DeCarli, C., et al. (2010). Recruitment of a community-based cohort for research on diversity and risk of dementia. *Alzheimer Dis. Assoc. Disord.* 24, 234–241. doi:10.1097/WAD.0b013e3181c1ee01

Hua, X., Leow, A. D., Parikshak, N., Lee, S., Chiang, M.-C., Toga, A. W., et al. (2008). Tensor-based morphometry as a neuroimaging biomarker for Alzheimer's disease: an MRI study of 676 AD, MCI, and normal subjects. *Neuroimage* 43, 458–469. doi:10.1016/j.neuroimage.2008.07.013

Jack, C., Knopman, D. S., Jagust, W. J., Shaw, L. M., Aisen, P. S., Weiner, M. W., et al. (2010). Hypothetical model of dynamic biomarkers of the Alzheimer's pathological cascade. *Lancet Neurol.* 9, 119–128. doi:10.1016/S1474-4422(09)70299-6

Jack, C. R., and Holtzman, D. M. (2013). Biomarker modeling of Alzheimer's disease. *Neuron* 80, 1347–1358. doi:10.1016/j.neuron.2013.12.003

Jenkinson, M., Beckmann, C. F., Behrens, T. E. J., Woolrich, M. W., and Smith, S. M. (2012). Fsl. *Neuroimage* 62, 782–790. doi:10.1016/j.neuroimage.2011.09.015

Kochunov, P., Lancaster, J. L., Thompson, P., Woods, R., Mazziotta, J., Hardies, J., et al. (2001). Regional spatial normalization: toward and optimal target. *J. Comput. Assist. Tomogr.* 25, 805–816. doi:10.1097/00004728-200109000-00023

Lee, D. D. Y., Fletcher, E., Carmichael, O. T., Singh, B., Mungas, D., Reed, B. R., et al. (2012). Sub-regional hippocampal injury is associated with fornix degeneration in Alzheimer's disease. *Front. Aging Neurosci.* 4:1. doi:10.3389/fnagi.2012.00001

Ly, M., Canu, E., Xu, G., Oh, J., McLaren, D. G., Dowling, N. M., et al. (2013). Midlife measurements of white matter microstructure predict subsequent regional white matter atrophy in healthy adults. *Hum. Brain Mapp.* 1–11. doi:10.1002/hbm.22311

Metzler-Baddeley, C., O'Sullivan, M. J., Bells, S., Pasternak, O., and Jones, D. K. (2012). How and how not to correct for CSF-contamination in diffusion MRI. *Neuroimage* 59, 1394–1403. doi:10.1016/j.neuroimage.2011.08.043

Mielke, M. M., Kozauer, N. A., Chan, K. C. G., George, M., Toroney, J., Zerrate, M., et al. (2009). Regionally-specific diffusion tensor imaging in mild cognitive impairment and Alzheimer's disease. *Neuroimage* 46, 47–55. doi:10.1016/j.neuroimage.2009.01.054

Morris, J. C. (1997). Clinical dementia rating: a reliable and valid diagnostic and staging measure for dementia of the Alzheimer type. *Int. Psychogeriatr.* 9, 173–176. doi:10.1017/S1041610297004870

Mungas, D., Beckett, L., Harvey, D., Farias, S. T., Carmichael, O., Olichney, J., et al. (2011). Heterogeneity of cognitive trajectories in diverse older person. *Psychol. Aging* 25, 606–619. doi:10.1037/a0019502

Nestor, P. J., Fryer, T. D., Smielewski, P., and Hodges, J. R. (2003). Limbic hypometabolism in Alzheimer's disease and mild cognitive impairment. *Ann. Neurol.* 54, 343–351. doi:10.1002/ana.10669

Nichols, T., and Holmes, A. P. (2001). Nonparametric permutation tests for functional neuroimaging: a primer with examples. *Hum. Brain Mapp.* 15, 1–25. doi:10.1002/hbm.1058

Oishi, K., Mielke, M. M., Albert, M., Lyketsos, C. G., and Mori, S. (2012). The fornix sign: a potential sign for Alzheimer's disease based on diffusion tensor imaging. *J. Neuroimaging* 22, 365–374. doi:10.1111/j.1552-6569.2011.00633.x

Pasternak, O., Sochen, N., Gur, Y., Intrator, N., and Assaf, Y. (2009). Free water elimination and mapping from diffusion MRI. *Magn. Reson. Med.* 62, 717–730. doi:10.1002/mrm.22055

Reid, A. T., and Evans, A. C. (2013). Structural networks in Alzheimer's disease. *Eur. Neuropsychopharmacol.* 23, 63–77. doi:10.1016/j.euroneuro.2012.11.010

Rueckert, D., Aljabar, P., Heckemann, R. A., Hajnal, J. V., Hammers, A., Larsen, R., et al. (2006). Diffeomorphic registration using b-splines. *Med. Image Comput. Comput. Assist. Interv.* 4191, 702–709. doi:10.1007/11866763_86

Sachdev, P. S., Zhuang, L., Braidy, N., and Wen, W. (2013). Is Alzheimer's a disease of the white matter? *Curr. Opin. Psychiatry* 26, 244–251. doi:10.1097/YCO.0b013e32835ed6e8

Seeley, W. W., Crawford, R. K., Zhou, J., Miller, B. L., and Greicius, M. D. (2009). Neurodegenerative diseases target large-scale human brain networks. *Neuron* 62, 42–52. doi:10.1016/j.neuron.2009.03.024

Selnes, P., Fjell, A. M., Gjerstad, L., Bjørnerud, A., Wallin, A., Due-Tønnessen, P., et al. (2012). White matter imaging changes in subjective and mild cognitive impairment. *Alzheimers Dement.* 8(5 Suppl.), S112–S121. doi:10.1016/j.jalz.2011.07.001

Sexton, C. E., Mackay, C. E., Lonie, J. A., Bastin, M. E., Terrière, E., O'Carroll, R. E., et al. (2010). MRI correlates of episodic memory in Alzheimer's disease, mild cognitive impairment, and healthy aging. *Psychiatry Res.* 184, 57–62. doi:10.1016/j.pscychresns.2010.07.005

Sperling, R. A., Aisen, P. S., Beckett, L. A., Bennett, D. A., Craft, S., Fagan, A. M., et al. (2011). Toward defining the preclinical stages of Alzheimer's disease: recommendations from the National Institute on Aging-Alzheimer's Association workgroups on diagnostic guidelines for Alzheimer's disease. *Alzheimers Dement.* 7, 280–292. doi:10.1016/j.jalz.2011.03.003

Thomas, A. G., Koumellis, P., and Dineen, R. A. (2011). The fornix in health and disease: an imaging review. *Radiographics* 31, 1107–1121. doi:10.1148/rg.314105729

Villain, N., Desgranges, B., Viader, F., de la Sayette, V., Mézenge, F., Landeau, B., et al. (2008). Relationships between hippocampal atrophy, white matter disruption, and gray matter hypometabolism in Alzheimer's disease. *J. Neurosci.* 28, 6174–6181. doi:10.1523/JNEUROSCI.1392-08.2008

Villain, N., Fouquet, M., Baron, J.-C., Mézenge, F., Landeau, B., de La Sayette, V., et al. (2010). Sequential relationships between grey matter and white matter atrophy and brain metabolic abnormalities in early Alzheimer's disease. *Brain* 133, 3301–3314. doi:10.1093/brain/awq203

Wang, Y., West, J. D., Flashman, L. A., Wishart, H. A., Santulli, R. B., Rabin, L. A., et al. (2012). Selective changes in white matter integrity in MCI and older adults with cognitive complaints. *Biochim. Biophys. Acta* 1822, 423–430. doi:10.1016/j.bbadis.2011.08.002

Zhang, Y., Schuff, N., Jahng, G.-H., Bayne, W., Mori, S., Schad, L., et al. (2007). Diffusion tensor imaging of cingulum fibers in mild cognitive impairment and Alzheimer disease. *Neurology* 68, 13–19. doi:10.1212/01.wnl.0000250326.77323.01

Zhang, Y., Zhang, J., Oishi, K., Faria, A. V., Jiang, H., Li, X., et al. (2010). Atlas-guided tract reconstruction for automated and comprehensive examination of the white matter anatomy. *Neuroimage* 52, 1289–1301. doi:10.1016/j.neuroimage.2010.05.049

Zhuang, L., Sachdev, P. S., Trollor, J. N., Kochan, N. A., Reppermund, S., Brodaty, H., et al. (2012). Microstructural white matter changes in cognitively normal individuals at risk of amnestic MCI. *Neurology* 79, 748–754. doi:10.1212/WNL.0b013e3182661f4d

Zhuang, L., Sachdev, P. S., Trollor, J. N., Reppermund, S., Kochan, N. A., Brodaty, H., et al. (2013). Microstructural white matter changes, not hippocampal atrophy, detect early amnestic mild cognitive impairment. *PLoS ONE* 8:e58887. doi:10.1371/journal.pone.0058887

Conflict of Interest Statement: The authors declare that the research was conducted in the absence of any commercial or financial relationships that could be construed as a potential conflict of interest.

Received: 30 January 2014; accepted: 15 May 2014; published online: 28 May 2014.
Citation: Fletcher E, Carmichael O, Pasternak O, Maier-Hein KH and DeCarli C (2014) Early brain loss in circuits affected by Alzheimer's disease is predicted by fornix microstructure but may be independent of gray matter. Front. Aging Neurosci. ***6****:106. doi: 10.3389/fnagi.2014.00106*
This article was submitted to the journal Frontiers in Aging Neuroscience.

frontiers in
AGING NEUROSCIENCE

REVIEW ARTICLE
published: 02 October 2014
doi: 10.3389/fnagi.2014.00266

Diffusion tensor imaging in Alzheimer's disease: insights into the limbic-diencephalic network and methodological considerations

Julio Acosta-Cabronero* and Peter J. Nestor

Brain Plasticity and Neurodegeneration Group, German Center for Neurodegenerative Diseases (DZNE), Magdeburg, Germany

Edited by:
Kenichi Oishi, Johns Hopkins University, USA

Reviewed by:
Marco Bozzali, Fondazione Santa Lucia, Italy
Paul Gerson Unschuld, University of Zürich, Switzerland

****Correspondence:***
Julio Acosta-Cabronero, Deutsches Zentrum für Neurodegenerative Erkrankungen (DZNE), Universitätsklinikum Magdeburg, Leipziger Strasse 44, Haus 64, 39120 Magdeburg, Deutschland
e-mail: julio.acosta@dzne.de

Glucose hypometabolism and gray matter atrophy are well known consequences of Alzheimer's disease (AD). Studies using these measures have shown that the earliest clinical stages, in which memory impairment is a relatively isolated feature, are associated with degeneration in an apparently remote group of areas—mesial temporal lobe (MTL), diencephalic structures such as anterior thalamus and mammillary bodies, and posterior cingulate. These sites are thought to be strongly anatomically inter-connected via a limbic-diencephalic network. Diffusion tensor imaging or DTI—an imaging technique capable of probing white matter tissue microstructure—has recently confirmed degeneration of the white matter connections of the limbic-diencephalic network in AD by way of an unbiased analysis strategy known as tract-based spatial statistics (TBSS). The present review contextualizes the relevance of these findings, in which the fornix is likely to play a fundamental role in linking MTL and diencephalon. An interesting by-product of this work has been in showing that alterations in diffusion behavior are complex in AD—while early studies tended to focus on fractional anisotropy, recent work has highlighted that this measure is not the most sensitive to early changes. Finally, this review will discuss in detail several technical aspects of DTI both in terms of image acquisition and TBSS analysis as both of these factors have important implications to ensure reliable observations are made that inform understanding of neurodegenerative diseases.

Keywords: neurodegenerative diseases, Alzheimer's disease neurobiology, axonal loss, *circuit of Papez*, long association tracts, splenium, DTI criteria, Alzheimer's disease biomarkers

INTRODUCTION

Alzheimer's disease (AD) is characterized, histopathologically, by amyloid deposition and neurofibrillary tangles (composed of hyperphosphorylated tau); these features occur in somewhat topographically distinct distributions in the brain. The ultimate outcome of AD is neuronal loss though exactly how histopathological features interact with each other and how they relate, in turn, to neuronal degeneration remains rather unclear. It seems reasonable to assume, nonetheless, that neuronal—and synaptic—loss is critical to the development of cognitive impairment. To date, therapeutic attempts to slow the course of AD have targeted the histopathology. A possible alternative, or even complimentary approach, might be to understand what makes some neuronal populations in the central nervous system more vulnerable to degeneration than others with a view to finding ways to make neurons less vulnerable to pathological insult—regardless of what that pathological insult might be. Such an approach requires a precise understanding of the spread of neurodegeneration and this can only be achieved by studies in humans rather than disease models.

Historically, *in vivo* work to understand the landscape of neurodegeneration in AD has focused on atrophy detection using T_1-weighted magnetic resonance imaging (MRI) and metabolic studies using (^{18}F)-2-fluoro-deoxy-D-glucose positron emission tomography (FDG-PET)—the latter being primarily a marker for synaptic loss. Both of these modalities typically focus on changes in gray matter (GM) and have tended to show what, at first glance, appear to be different profiles of degeneration (Ishii et al., 2005). Structural MRI has been good at highlighting mesial temporal lobe (MTL) atrophy (Du et al., 2001; Jack et al., 2002, 2004), while FDG-PET has typically highlighted early changes in posterior association cortex (Minoshima et al., 1995) with the posterior cingulate region in particular appearing as the first hypometabolic region in very early symptomatic AD (Minoshima et al., 1997; Nestor et al., 2003a). This apparent discrepancy between structural MRI and FDG-PET may well, however, be technical. For instance, much of the work on MTL atrophy derives from region-of-interest (ROI) studies that did not examine for atrophy elsewhere. Where whole brain analyses were conducted, most used the voxel-based morphometry (VBM) technique (Ashburner and Friston, 2000) though recent evidence highlights that although this method is good at identifying MTL atrophy, it is relatively insensitive to atrophy in the isocortical ribbon (Diaz-De-Grenu et al., 2014); in contrast,

using the Freesurfer's cortical thickness method (Dale et al., 1999; Fischl et al., 1999), atrophy of the cortical ribbon in posterior association cortex emerges in a pattern highly reminiscent of that seen with FDG-PET (Diaz-De-Grenu et al., 2014). Similarly, although ROI studies in the cortical ribbon are rare, manual volumetry of the posterior cingulate region in MCI-stage AD has confirmed comparable degrees of atrophy to that seen in the hippocampus (Choo et al., 2010; Pengas et al., 2010). Looking at the apparent discrepancy in these imaging modalities from the FDG-PET side, voxel-based analysis (VBA) appears relatively insensitive to MTL changes in early AD; however, using MRI-derived ROIs to calculate cerebral metabolic rates (i.e., quantified imaging), FDG-PET identified significant hypometabolism not only in the posterior cingulate but also the MTL, as well as anterior thalamus and mammillary bodies (Nestor et al., 2003b). This "limbic-diencephalic" network, therefore, appears to be the correlate of very early symptomatic AD when memory impairment is a relatively isolated feature. It is interesting, therefore, that these network structures—MTL, posterior cingulate, anterior thalamus and mammillary bodies—which are connected through the *circuit of Papez* (Papez, 1937), have all been individually implicated from focal lesions in human amnesia.

The hypothesis that these structures are degenerating in concert predicts that white matter (WM) projections between these areas—such as, for instance the fornix, which links the MTL with the diencephalon—should also show signs of degeneration. To test such hypotheses as well as to understand how degeneration in AD may impact on areas remote from GM degeneration more generally, the relatively more recent technique of diffusion tensor MRI offers considerable promise. Diffusion MRI enables mapping of WM microstructure alterations in development, aging and neurological disorders, and has therefore become an important tool in the study neurodegeneration. Parenchymal WM is composed of bundles of axons (or fiber tracts) that interconnect GM areas. The diameter of neuronal fibers is well below MRI resolution but the technique can be sensitized to measure the displacement of water molecules as a surrogate marker of tract integrity. Axonal membranes, myelin sheaths and cytoskeletal constituents such as microtubules and neurofilaments are long structures that may hinder water diffusion preferentially perpendicular to their length; this phenomenon enables MRI to detect abnormalities caused by neurodegenerative diseases such as loss of fibers, demyelination, damage within fibers or to support tissue around them (Beaulieu, 2002). The technique remains fairly new and there has been a relatively steep learning curve in terms of understanding and interpreting diffusion tensor imaging (DTI) (Alger, 2012; Winston, 2012); this learning process is far from over. What is clear at this time is that technical factors—both in terms of acquisition parameters and analysis methods—play a more important role in terms of generating spurious findings compared to older modalities such as structural T_1-weighted imaging and FDG-PET. The outcome being that the DTI literature in AD can come across as a confusing jumble of inconsistent abnormalities—an unsurprising observation considering DTI's vulnerability to spurious results when suboptimal experimental designs are employed. The prescription of DTI acquisitions with fewer-than-recommended diffusion-encoding directions, low *b*-values or thick slices; the study of mild cognitive impairment (MCI) cohorts without clinical outcome and the detrimental effect of Gaussian smoothing in post-processing pipelines are the most likely contributors to such inconsistencies.

It is crucial therefore that clinicians and researchers have some understanding of the pitfalls that can arise from inadequate methods in order to interpret what have often been rather contradictory results in DTI studies. This review will focus on what we have learned from DTI in AD to date, but also will go into some detail in explaining the methodological issues that can cause problems for DTI studies.

THE PHYSICAL BASIS OF DTI

The present section is not intended as a comprehensive description of DTI theory—for that, extensive reviews can be found elsewhere (Kingsley, 2006a,b,c). It aims, however, to provide an intuitive understanding of the method and an appreciation of the possible tensor dynamics that can arise with neurodegeneration; these are important theoretical considerations because diffusion, as measured with the "single tensor" model (Basser et al., 1994b), is based on a number of assumptions that lead to certain limitations; limitations that have been extensively discussed in the diffusion MRI literature (Jones and Cercignani, 2010; Jones et al., 2013b), but that are often overlooked in clinical studies. Nevertheless, DTI is a powerful technique to study neurodegenerative diseases; thus, an overview of its theoretical foundations will also enable a more clear understanding of the discoveries that have been made to date in AD. The theoretical underpinning of DTI can, however, seem impenetrable for non-specialists even when most of the background mathematics is omitted, as is the case in this section. For readers, therefore, who might find the physics described in this section too daunting, we suggest simply focusing on the Figures and their captions; and with a brief understanding of what a diffusion tensor means, one can then skip on to the following section "Technical considerations for clinical DTI studies" for a discussion of the factors that influence the suitability of DTI scans for clinical studies.

Brownian motion, also known as "self-diffusion," is a physical phenomenon arising from matter's intrinsic thermal energy that leads to pseudo-random kinetic fluctuations. Such molecular thermal motion is named after Robert Brown—a Scottish botanist—who first observed such behavior in grains of pollen suspended in water (Brown, 1828). A full mathematical description emerged a few decades later when Adolf Fick—a physiologist studying mass transport in saline solutions—proposed that microscopic motion could be seen as a probability density function (*pdf*) of a particle's location in space and time, i.e., as the likelihood of finding a particle in a certain place at a certain time, and then went on to predict that self-diffusion must be governed by such time-dependent probabilistic behavior (Fick, 1855). Soon after the turn of the 20th century, Albert Einstein solved the general case of Fickian diffusion to provide an analytical answer to the practical question: *how far do "free particles" travel "in average" during a time interval?* Einstein proposed a simple "random walk" model comprising a series of discrete, unrestricted, independent and uncorrelated steps, which led him to discover that for such boundary conditions, Fick's *pdf* is a Gaussian distribution

whose width—a measure of average molecular displacement—is modulated by two factors: time and a parameter dependent on fluid viscosity and temperature; he figured the latter must be a self-diffusion coefficient, *D* (Einstein, 1905) (see **Figure 1A**).

Since the inception of "spin echoes" in 1950, the MR signal has been known to be sensitive to molecular thermal motion (Hahn, 1950; Carr and Purcell, 1954; Torrey, 1956), which hereafter will be assumed to be that of hydrogen protons in water molecules within human brain tissue. Applying Einstein's relationship, it was determined that "free diffusion" under the effect of a steady magnetic field "gradient" attenuates the MR signal. This was first observed because field gradients (i.e., gradual increments or decrements in magnetic field strength) occur naturally when an experimental sample is introduced into the uniform magnetic field of a magnet and disturbs it. Magnetic field gradients, however, can be applied artificially to vary the main field gradually along one direction; such gradual field change, in essence, labels protons according to their spatial position. Stronger gradients, therefore, have the capability of giving a wider range of spatial signatures that result in higher image resolutions (if we refer to imaging gradients) or finer sensitivity to motion (if we refer to diffusion MRI). It was soon realized, however, that measuring self-diffusion through the application of sustained gradients was inconvenient and largely ineffective. Then in 1965, Stejskal and Tanner proposed that the amount of diffusion weighting in the MR signal could be finely controlled with a pair of identical, short-lived, magnetic field gradients (Stejskal and Tanner, 1965) (see **Figure 1B**). Pulsed gradients sequentially label, and then unlabel, protons according to their position; with the result that if a proton moves to a different location after a "diffusion time"—i.e., when the second gradient is applied—, the proton gets assigned a wrong label and returns less signal according to how far it has moved. This principle—the basis for most diffusion MRI acquisitions today—results in an overall signal intensity attenuation due to free diffusion that depends on the self-diffusion coefficient, *D*, and the gradient characteristics. For simplicity, and

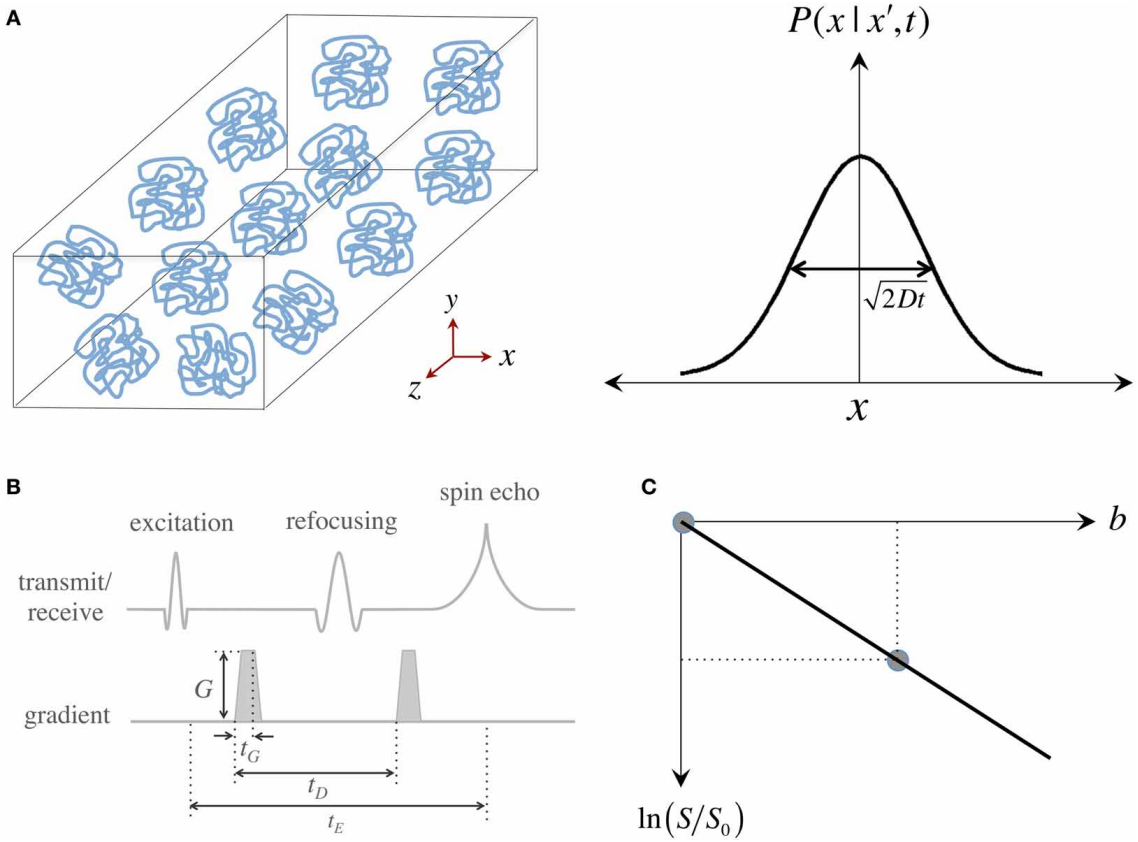

FIGURE 1 | Measurement of the "self-diffusion" coefficient with magnetic resonance. (A) Self-diffusion is a special case of diffusion that describes the relentless motion of microscopic particles in a substance. Such motion is random—it can be described by a "Gaussian" distribution whose width determines how far particles travel on average after some time; the important thing to remember is that only time, the "diffusion time," and the "self-diffusion coefficient," *D*, modulate this width. **(B)** Illustration of a magnetic resonance pulse sequence that is sensitive to self-diffusion: (i) an "excitation pulse" gives some energy to water protons; (ii) then the first "gradient" *encodes* where they are; (iii) and some (diffusion) time later, a second gradient *decodes* their position by giving them a "signal penalty" according to how far they have moved away from their original position; (iv) as a result of this penalty, protons that have moved furthest, return the least signal. The overall signal attenuation is a function of *D* and the gradient characteristics—i.e., intensity (*G*), duration (t_G) and diffusion time (t_D)—usually conglomerated into a single term known as the "*b*-value." **(C)** Visual representation of the linear fit required to quantify *D* using two signals: a diffusion weighted measurement (i.e., with a non-zero *b*-value), *S*, that must be normalized by a measurement without diffusion weighting, S_0 (also often called b_0); *D* can be inferred as the "negative" of the slope.

because in MRI there is a complex interaction between diffusion and imaging gradients, the overall effect of motion-sensitizing gradients is often synthesized into a so-called "*b*-value." This is convenient because the signal attenuation due to diffusion can be expressed simply by an exponential function of D and b, i.e., $S \propto \exp(-bD)$. As in any spin echo experiment, however, the signal also decays due to transverse relaxation (T_2) effects; thus, for the signal to depend only on the effects of water mobility, it must be normalized by a reference measurement without diffusion weighting, S_0, also known in DTI jargon as a "b_0 scan." Two measurements, therefore, are sufficient to infer a diffusion coefficient as: $D = -\ln(S/S_0)/b$; or in visual representation terms, that D is the negative of the slope connecting the two data points in **Figure 1C**.

The information that a Stejskal-Tanner experiment provides, however, is limited because the positions of resonant protons can only be encoded along the direction of the applied field gradient; thus, D only reflects the effect of self-diffusion along that specific spatial dimension. This is enough to characterize an isotropic medium, e.g., if measuring water's self-diffusion in a bucket, because diffusion measured in a given dimension will be same as that of every other dimension, but to probe a complex system with multiple, rotationally variant diffusion behaviors such as biological tissue one needs, in theory, an infinite number of observations with sensitizing gradients along an infinite number of diffusion orientations.

In an attempt to capture such directional dependency while keeping experimental requirements feasible, Basser et al. proposed the generalization of Einstein's equation by extending the Gaussian *pdf* idea to a second order, symmetric, definite-positive covariance matrix, **D**, and this is the diffusion tensor (Basser et al., 1994a):

$$\mathbf{D} = \begin{pmatrix} D_{xx} & D_{xy} & D_{xz} \\ D_{yx} & D_{yy} & D_{yz} \\ D_{zx} & D_{zy} & D_{zz} \end{pmatrix} \quad (1)$$

D is a reciprocal matrix with $D_{xy} = D_{yx}$, *etc*—i.e., it only has six "independent" scalar elements: D_{xx}, D_{xy}, D_{xz}, D_{yy}, D_{yz}, and D_{zz}; thus, in order to reconstruct a diffusion tensor, the minimum requirements are one S_0 ($b = 0$ s/mm^2 or b_0) measurement and six diffusion measurements applying gradients along six non-collinear orientations (see **Figure 2A**)—i.e., N_d, the number of diffusion gradient directions, must be at least 6, though N_d can be larger with obvious benefits (see **Figure 2B**). The single tensor model proposed by Basser et al. requires that all diffusion directions (b-vectors), b-values and b_0 information (which can also be provided through multiple scans to improve stability) must be stored as a **B**-matrix, leading to a linear system of equations that can be solved for the six independent terms of **D** and for S_0 efficiently across an entire imaging volume.

Another convenient feature of the diffusion tensor is that it can be expressed in its quadratic form as an ellipsoidal surface that characterizes the water displacement probability at a given diffusion time, i.e., an ellipsoid that visualizes the 3D character of water mobility; though in the present form, i.e., that in

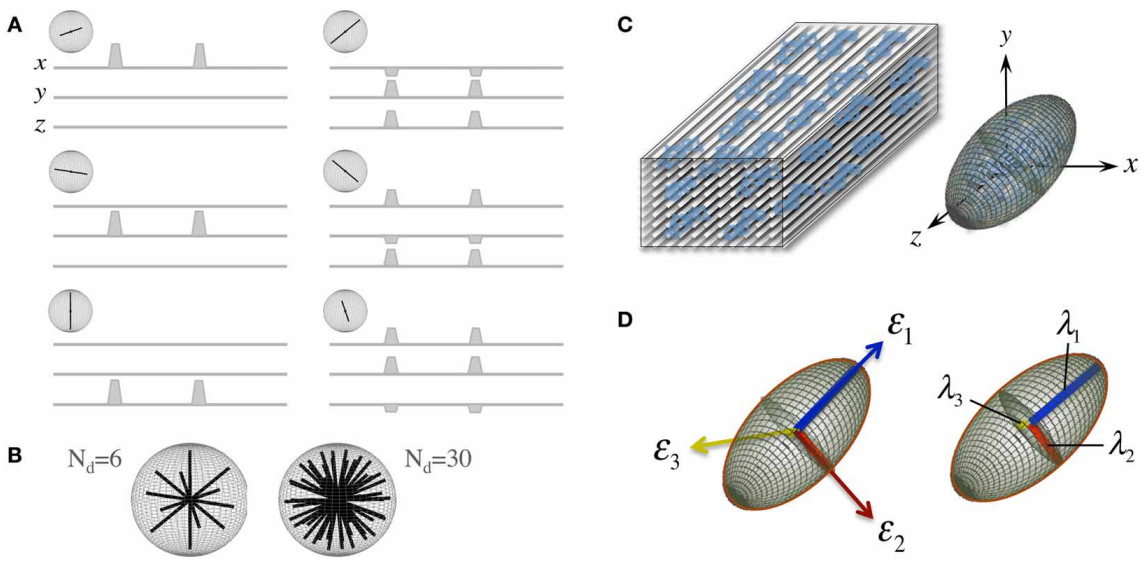

FIGURE 2 | The "diffusion tensor." (A) Six combinations of gradients applied with different intensities along three orthogonal orientations (*x*, *y*, and *z*), and a measurement without diffusion weighting, are the minimum requirements to probe diffusion in a 3D space; each non-collinear combination is called a "diffusion direction." **(B)** A larger number of diffusion directions, N_d, can estimate the directional dependence of microstructural restrictions to water diffusion with greater precision. **(C)** Basser et al. (1994b) proposed the formulation of a diffusion tensor (represented by an ellipsoid) to capture diffusion behaviors in 3D with a finite N_d. **(D)** The tensor can be rotated to match the principal direction of diffusion, i.e., in white matter, the first eigenvector (ε_1) matches the predominant fiber tract orientation; thus, the largest eigenvalue (λ_1, known as "axial diffusivity") quantifies water mobility along this orientation. Analogously, ε_2 and ε_3 define the plane perpendicular to the axonal arrangement so that λ_2 and λ_3 can be averaged as a "radial diffusivity" (RD). In addition, all three eigenvalues can be averaged to estimate the "mean square displacement" of water molecules—that is, the "mean diffusivity" (MD).

Equation (1), **D** is still rotationally variant because it depends on the principal diffusion orientation relative to the *x*, *y*, and *z* axes of the scanner or to whatever coordinate system the b-vectors were in (see **Figure 2C**). **D**, however, is positive and symmetric regardless of such orientation; thus, using linear algebra, it can be easily made diagonal for a specific orientation—i.e., it can be decomposed into a set of orthonormal eigenvectors and related eigenvalues (see **Figure 2D**):

$$\mathbf{D} = \begin{pmatrix} \varepsilon_1 \\ \varepsilon_2 \\ \varepsilon_3 \end{pmatrix} \begin{pmatrix} \lambda_1 & 0 & 0 \\ 0 & \lambda_2 & 0 \\ 0 & 0 & \lambda_3 \end{pmatrix} \begin{pmatrix} \varepsilon_1 & \varepsilon_2 & \varepsilon_3 \end{pmatrix}. \quad (2)$$

In essence, the diagonalization step in Equation (2) rotates the principal axes of **D** to match the principal directions of diffusivity, leading, as a result, to a diffusion tensor that is rotationally invariant for each imaging "voxel."

A number of metrics can be derived from the diffusion tensor; for example, the 3D "mean square displacement" of water molecules during a diffusion time can be derived by averaging the three tensor eigenvalues to form a DTI metric known as "mean diffusivity": $MD = (\lambda_1 + \lambda_2 + \lambda_3)/3$. In addition, the rotational invariance of the diffusion tensor has clear advantages because water molecules can be generally assumed to "diffuse" due to their thermal energy more readily along the length of a uniaxial environment than perpendicular to it. It is, thus, commonly assumed when referring to, e.g., parenchymal WM, that the eigenvector, ε_1, associated with the largest eigenvalue, λ_1—known as "axial diffusivity"—maps the principal orientation of a fiber tract. Similarly, diffusivities along ε_2 and ε_3—typically averaged to form "radial diffusivity," i.e., $RD = (\lambda_2 + \lambda_3)/2$—reflects the diffusion behavior transverse to an axonal path. Therefore, the inter-relationship between eigenvalues—i.e., between axial and radial diffusivities—contains relevant information about the geometry of the restricting microstructure. For example, in a scenario where axons are tightly packed together such as, e.g., the mid-sagittal corpus callosum, water molecules are more restricted perpendicular to the axons, hence $\lambda_1 >> \lambda_2 \geq \lambda_3$, or $\lambda_1 >>$ RD—i.e., it can be represented as a cigar-shaped diffusion ellipsoid with the long axis parallel to the axons (see **Figure 3**). In other regions, however, where, e.g., two tightly packed WM bundles cross, water molecules in the extra-cellular space might travel more freely across a plane, $\lambda_1 \geq \lambda_2 >> \lambda_3$, hence $\lambda_1 >$ RD—i.e., the ellipsoid adopts a planar geometry; whereas in WM areas where multiple fiber bundles cross, or in GM or cerebrospinal fluid (CSF), where water diffusion does not exhibit a preferential orientation because obstacles are randomly distributed in space or because there are no restrictions at all, the ellipsoid is largely "isotropic," i.e., $\lambda_1 \approx \lambda_2 \approx \lambda_3$, thus $\lambda_1 \approx$ RD. The eccentricity of the diffusion ellipsoid, therefore, is an important property that can provide useful information about the biological tissue under investigation. This property is typically measured using the "second moment" of the diffusion tensor, because of its robust noise properties, by a metric known as fractional anisotropy (FA): $FA = \sqrt{3/2}\sqrt{\left[(\lambda_1 - MD)^2 + (\lambda_2 - MD)^2 + (\lambda_3 - MD)^2\right]/\left(\lambda_1{}^2 + \lambda_2{}^2 + \lambda_3{}^2\right)}$ (Basser and Pierpaoli, 1996). FA can be seen as the relative ratio between axial and radial diffusivities, where its boundary situations are: (i) $FA = 0$ for a perfectly "ergodic" or "isotropic" behavior, i.e., when $\lambda_1 =$ RD, and (ii) $FA = 1$ for 1D molecular displacements in a 3D space, i.e., when RD is infinitesimally small relative to λ_1. The latter behavior is the extreme case for "anisotropic" diffusion. In graphical terms (**Figure 3**), isotropic diffusion ($FA = 0$) is a perfect sphere because it means water can travel equally in all directions, whereas if water mobility is restricted disproportionally along one or two dimensions in space, FA moves away from zero.

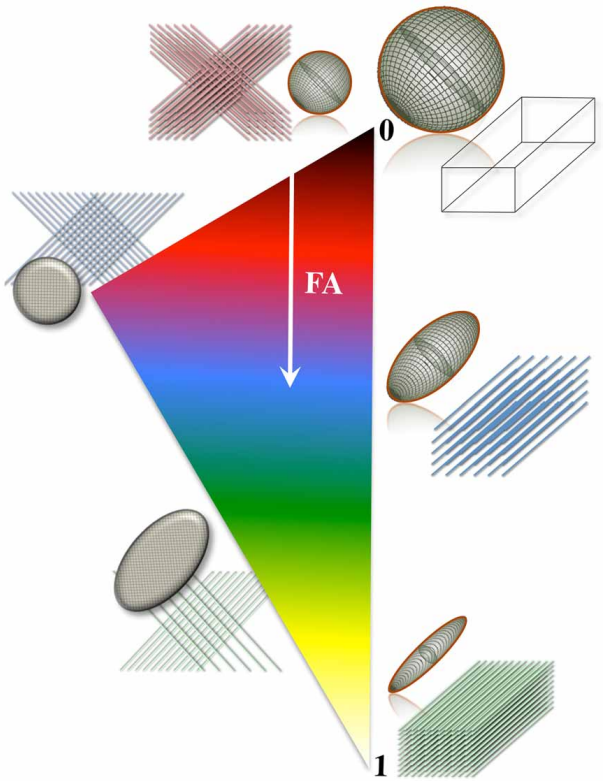

FIGURE 3 | Differential tensor behaviors in white matter. Cell membranes are thought to be the main restricting boundary to water mobility in white matter. As such, the ratio of axial to radial diffusivities, commonly described by a metric known as "fractional anisotropy" (FA), can reflect the coherence (sometimes thus the integrity) of packed axons in white matter. FA approaches one in well-organized tracts, where the diffusion ellipsoid is elongated along the principal tract orientation; and tends to zero, in less coherent environments—i.e., in heterogeneous areas of many crossing fibers, and in gray matter or cerebrospinal fluid—, where the ellipsoid resembles a sphere. In the full complexity of white matter microstructure, however, the ellipsoid can take a wider range of geometries from that of a rugby ball to that of surfboard or a dish—with the degree of sphericity and planarity dictated primarily—but not only—by axon packing density, degree of myelination and/or the geometrical arrangement of crossing, kissing and/or splaying fiber populations.

The pseudo-random (Gaussian) nature of unrestricted diffusional motion is, in turn, the theoretical basis supporting the single tensor model in DTI (Basser et al., 1994b); this highlights, however, one of DTI's major limitations—it is based on an idealization. As already discussed, in WM, cytoarchitectural barriers

hinder and physically restrict water mobility (see **Figure 4A**); such nuisances to self-diffusion, therefore, impose a different set of boundary conditions to Fick's equation, making "walks" no longer random. Instead, they become correlated and dependent on the geometry of the restricting boundaries; thus leading to *pdf* departures (narrowing) from the ideal Gaussian behavior (see **Figure 4A**). In such scenarios, the diffusion tensor proposed by Basser et al. does not contain enough terms to account for the higher order effects in non-Gaussian molecular displacement distributions; thus, they lead to the violation of DTI's basic assumption that the signal decay due to diffusion follows a single exponential behavior. Consequently, the single tensor model must be regarded as an approximation (**Figure 4B**); and the three tensor-eigenvalues—if they describe restricted water motion—are not true self-diffusion coefficients, but "apparent" measures of diffusion or "diffusivities."

A further caveat is that most DTI experimental designs assume that tensor behaviors are independent of diffusion time—i.e., that the brain parenchyma is a restricted environment in a "pseudo-Gaussian" state, where diffusion time is long relative to the time needed for water molecules to be hindered/restricted by cellular membranes or other microstructural components. Note that the former are thought to be the primary microstructural restrictions to water diffusion in white matter (Beaulieu and Allen, 1994). This can be generally assumed to be valid because in typical clinical situations, diffusion times range between 30 and 50 ms, which translate to *in vivo* 1D molecular displacements of 13–17 μm. Such displacements are an order of magnitude greater than, for example, the typical axon diameter in the corpus callosum of young individuals, which is approximately 1 μm (Aboitiz et al., 1992)—though axons can also be much larger. In lay terms, the reason this is important is that in order to know that restrictions of water diffusion due to barriers in neural tissue are present, one must measure long enough "diffusion paths" to ensure water molecules have had a chance to "bounce off" some barriers. **Figure 5A** illustrates this scenario, where such paths are long relative to the distance between physical obstacles, enabling DTI to sense differential bulk behaviors parallel and perpendicular to white matter tracts. In patients with neurodegenerative diseases, however, cellular membranes may become more permeable; or the extra-cellular space might be greater due to axonal loss, demyelination, and/or glial pathology. Such effects—alone or in combination—may result in local environments where, during a given diffusion time, water molecules interact only partially with microstructural boundaries. **Figure 5C** illustrates such a scenario where some paths (e.g., the blue path) do not encounter any obstacle during a given diffusion time, i.e., they behave as if they were in an unrestricted medium. In theory, during disease progression the loss of large myelinated axons, or clumps of adjacent tracts, may result in diffusion paths that cannot capture the full extent of such "voidage." This is the so-called "quasi-restricted" regime, in which measurements depend on diffusion time—i.e., if water molecules were allowed to diffuse twice as far by doubling the diffusion time, microstructural boundaries would be sensed again, resulting in smaller radial diffusivity relative to axial diffusivity, hence leading to a more anisotropic tensor. Such behavior may inadvertently compromise whole brain assessments because the same neurodegenerative process, e.g., axonal loss, could impact diffusivities differentially across WM tract environments with different axon size distributions, packing arrangements or degrees of myelination. Suppose, for instance, an enlargement of the extra-cellular space of 20% due to axonal loss; its impact on RD would be different, for example, in a scenario where axons are lost sparsely than if a small bundle of large myelinated axons degenerate together. In the latter case, if molecular displacements were small relative to the "new" boundaries, FA would be underestimated as a result. It may be desirable to detect such diffusion-time dependencies (Baron and Beaulieu, 2014); but they imply that whole brain analyses would be biased toward such phenomena if they were proven to be present in some

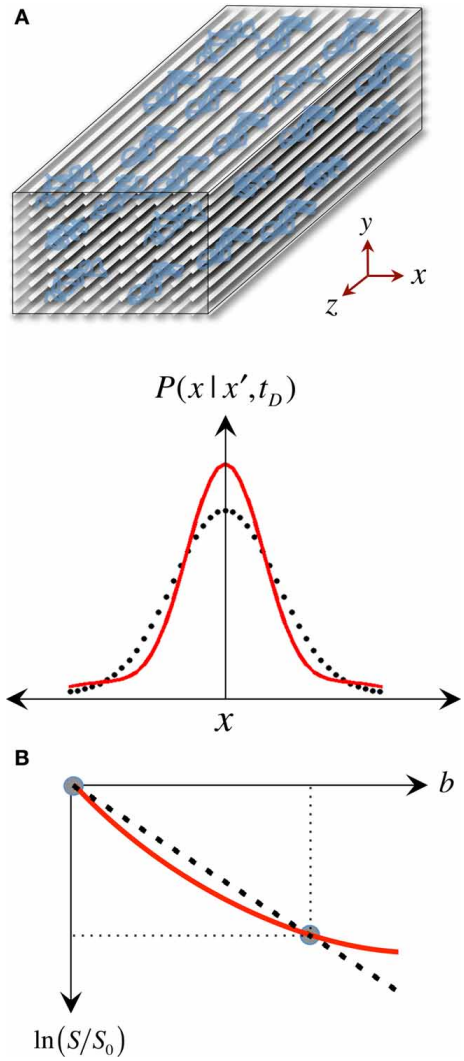

FIGURE 4 | The approximate nature of the "single tensor" model. (A) "Restricted" diffusion processes such as those in white matter result in displacement probabilities that are no longer accurately described by a Gaussian "bell." **(B)** Therefore, the assumption that the signal attenuation must have a linear relationship in a logarithmic scale with the *b*-value is no longer valid, resulting in tensor diffusivities that are "apparent" (i.e., model approximations) rather than "true" measures of restricted self-diffusion.

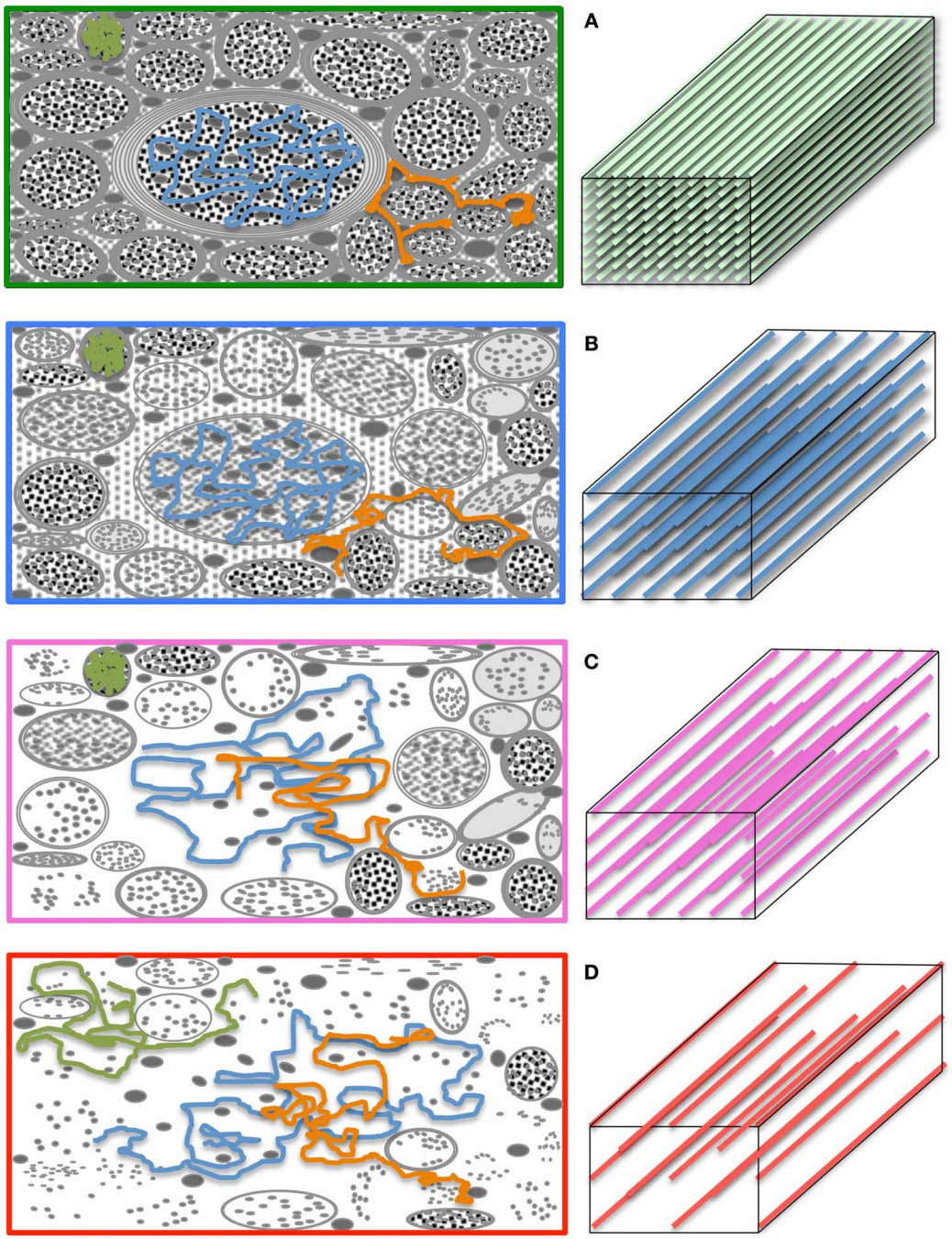

FIGURE 5 | The "diffusion regimes." (A) White matter is a complex—but relatively ordered— microstructure primarily composed of nerve fibers (axons) and glial cells. Axons are bundled together; their main role is to transport substances intra-cellularly through microtubules and conduct electricity to enable inter-communication between cells. The myelin sheath—a "fatty" insulating layer around the axons—facilitates such conduction. In the healthy brain, such microstructure exerts restrictive boundary conditions to water diffusion. **(B)** The exact mechanism by which microstructural damage occurs in neurodegenerative diseases is unknown but it is conceivable that, after a period of instability, demyelinative and other axon degeneration processes will lead to longer "diffusion paths." If therefore, the diffusion time is sufficiently long and the gradients sufficiently strong, such diffusion behavior will yield a change in signal attenuation that will be reflected in tensor diffusivities. **(C)** If, however, some diffusing molecules cease to interact with microstructural barriers during a given diffusion time, the axial to radial relationship would be dependent on the local geometry leading to heterogeneous tensor behaviors across the brain. **(D)** In the extreme case, where the diffusion time is too short for molecular displacements to be hindered, tensor diffusivity measures would be unable to detect further change. Large *b*-values—enabling long diffusion times and strong gradients—make the diffusion measurement with magnetic resonance both more sensitive to subtle microstructural alterations in highly restricted environments, and less prone to diffusion-time dependencies.

diseased regions but not in others. Furthermore, there might be scenarios of extreme degeneration, or CSF contamination in a voxel, where the majority of water molecules behave as in an unrestricted medium; under such circumstances, further loss of microstructural integrity would lie largely undetected with DTI because water mobility would not reflect the presence of any boundary (as in **Figure 5D**).

While these important theoretical considerations and limitations should not be ignored, DTI can be very useful to probe abnormal tissue microstructure. For instance, in a pseudo-Gaussian scenario where several fiber tracts are damaged as a consequence of a disease, diffusion hindrance would be reduced (see **Figure 5B**), i.e., *pdf*s would approximate more readily to a Gaussian distribution, and would return greater diffusivity values closer to the intrinsic unrestricted self-diffusion coefficient; it is this change in diffusivity pattern that can indicate abnormality in degenerative disease states. In addition, because the tensor model yields three rotationally invariant—and orthogonal—diffusivities (λ_1, λ_2, and λ_3), a disproportionate diffusivity change along a particular orientation will impact on absolute (axial and radial) diffusivities, or composite measures of diffusion anisotropy such as FA as illustrated in **Figure 3**.

It is presently unknown whether diffusion-time dependencies might be a confounding force in the study of neurodegenerative diseases; for now, they remind us that caution must be at the forefront in DTI interpretations. Unfortunately, DTI studies in neurodegenerative diseases have often been guilty of over-interpreting results, particularly when such interpretations are based on consistency with prior knowledge rather than offering a proof of a given mechanism. Mechanisms underpinning DTI changes in clinical cohorts are often inferred by citing homology with controlled animal experiments or computer simulations, where processes such as myelin loss, fiber reorganization, changes in membrane permeability, *etc*, are modeled in isolation—for a extended review see Beaulieu (2002). Reductionist approaches such as animal experiments are important in that they can highlight the types of neural changes that are possible to detect with DTI but there is a potentially serious error in logic when such observations are exported directly to explain changes observed in human neurodegeneration. For instance, if a given DTI change has been observed in an animal model of demyelination and then the same DTI change is observed in a degenerative disease, one will often read that the mechanism in the latter is also demyelination. The error in logic is that there are only a finite number of ways in which the diffusion tensor can change, and for any given change, it is incorrect to assume that only one mechanism might be the explanation—there may be many different types of pathological change that could cause the same diffusion tensor alteration. Using a clinical analogy, this is the same error in logic as stating that because sub-arachnoid hemorrhage can cause headache, any person with a headache must have a sub-arachnoid hemorrhage. Furthermore, it seems highly unlikely that a single mechanism will dominate the diffusion weighted MR signal because fiber degradation processes such as Wallerian degeneration—which typically involve the complex combination of cytoskeleton dissolution, contraction, fragmentation, disintegration of myelin and glial disposal (Coleman and Freeman, 2010)—are unlikely to occur simultaneously across all cells in a single measurement voxel. Such complexity, worsened by the diffusion regime uncertainty, suggests that DTI results should not be interpreted beyond their canonical form—i.e., that increased (or reduced) diffusivities are caused by less (or more) restrictive barriers to water diffusion, and that diffusion anisotropy alterations are driven by orientation dependent changes in the configuration of such microstructural arrangement. What these exactly represent in neurobiological terms can only be speculated. Nevertheless, DTI-derived diffusivity and anisotropy measurements can offer important mechanistic insights toward understanding the sequence of events that lead to neurodegeneration by highlighting tracts that are diverging from normality, even if diffusion MRI, at present, cannot precisely state what the underlying pathology driving such divergence might be.

TECHNICAL CONSIDERATIONS FOR CLINICAL DTI STUDIES

Historically, T_1-weighting has been the MRI contrast of choice to study structural abnormalities in the human brain. It is clear that imaging parameter discrepancies or different field strengths result in differential method sensitivity, but overall they tend to be relatively concordant if the same processing steps are used. This is because structural MRI post-processing methods typically concentrate on resolving and standardizing different types of tissue using large amounts of prior anatomical knowledge; this makes such analysis strategies relatively immune to differences, e.g., in signal-to-noise ratio (SNR). Unlike structural MRI, however, DTI relies on *quantitative* information to yield meaningful assessments; thus, DTI sensitivity and stability strongly depend on how robustly the signals have been acquired. Therefore, additional precaution must be taken when reviewing the literature because the ability of diffusion MRI to accurately reconstruct tensorial information strongly depends on measurement SNR, which varies throughout the brain, between subjects and across studies. It is likely that when non-specialists read an imaging study, acquisition details—which may seem an impenetrable paragraph of technical jargon—are skipped over. Such information though is critical to DTI because some acquisition protocols that have been applied in clinical studies are simply not fit for purpose. It is beyond the scope of the present manuscript to discuss in detail every relevant factor—for a more specialized review, see e.g., Jones and Cercignani (2010)—but to help readers to critically evaluate the literature in this ever-growing field, a number of the most clinically relevant technical considerations will be briefly discussed:

THE DTI ACQUISITION SCHEME

The "*b*-value" is the parameter that tunes how much microstructural information the diffusion MR signal can carry. Relatively large *b*-values are needed to ensure both (i) that strong diffusion gradients sensitize water motion in complex, highly restricted environments, and (ii) that the diffusion time is sufficiently long to enable "meandering" diffusion paths to probe less restricted (or diseased) microstructure. Early computer simulations suggested that for a single non-zero *b*-value experiment, $b = 1250\,\mathrm{s/mm^2}$ minimizes fitting errors for a mean diffusivity of $0.7 \times 10^{-3}\,\mathrm{mm^2/s}$, i.e., approximately that of brain parenchyma

(Xing et al., 1997). More recent simulations have demonstrated that even taking the simplification that the human brain is constituted by single-orientation fiber populations, i.e., that crossing fibers are not present, the *b*-value—if interested in MD and FA—should not be lower than $b = 900$ s/mm^2 (Alexander and Barker, 2005). Such results highlight a pitfall with a large number of studies—particularly at 1.5 Tesla (T)—that used a maximum *b*-value of 700 s/mm^2. Capturing high order signal decays reflecting non-Gaussian restricted diffusion with a smaller-than-optimal single non-zero *b*-value translates to inaccurate "fits," which, as illustrated in **Figure 4B**, may lead to tensor reconstructions that do not accurately reflect the true diffusion process, and hence, the underlying microstructure. The use of larger *b*-values—closer to optimal for tensor estimation in WM—can help reduce such residual errors, but high *b*-values further attenuate the MR signal; thus, in order to ensure that diffusion-weighted signals are well above the "noise floor," a common practice is to take advantage of the higher baseline SNR at stronger magnetic fields (e.g., 3T MRI). It should be noted, however, that stronger fields are not always favorable for DTI because the diffusion-weighted signal is also T_2 dependent, and T_2 is shorter for stronger fields, which, in turn, translates to faster signal decays. This is undesirable, and poses a serious challenge, particularly at ultra-high field (7T and above), because whole brain DTI acquisitions typically consist of a single-shot echo planar imaging (EPI) pulse sequence with long-lasting diffusion and readout gradients resulting in long delays before the signal can be acquired, i.e., long echo time. At 3T, however, the gain in baseline SNR usually overcomes the T_2 penalty; that is why presently 3T MRI is the platform of choice for diffusion tensor neuroimaging. It is noteworthy, looking to the future, that low SNRs will become less of a problem for clinical studies with the advent of high performance gradient systems capable of stronger field gradients with shorter switching times, which enable the use of higher *b*-values with shorter echo times.

Returning to the present, it is important to avoid low SNR because the noise floor may damp signal decay, resulting in artefactually reduced diffusivities; this effect is orientation dependent in the WM because faster signal decays—caused by greater diffusivities along tracts—are more vulnerable to this effect, resulting in artefactual reductions of diffusion anisotropy. This is critically important because if one is attempting to map the distribution of WM change in degenerative brain disease it is possible to miss changes in affected areas where the local fiber orientations were more vulnerable to the effects of low SNR. Signal levels are modulated by the magnetic field strength, the type of radio-frequency coil used and imaging parameters such as the echo time (TE); number of *b*-values (N_b); number of repeat excitations (NEX); receiver bandwidth or parallel imaging acceleration, e.g., GRAPPA (Griswold et al., 2002) or SENSE (Pruessmann et al., 1999). Unfortunately, however, SNRs are not usually reported in the literature. In addition, details about the number of channels available in phased-array coils, acceleration factor or receiver bandwidth are also often not reported in clinical studies, making comparisons between works hard to interpret from methods sections.

The influence of suboptimal gradient sampling schemes is also an important factor to consider when scrutinizing the literature. Diffusion weighting along six unique orientations (see **Figures 2A,B**) and the acquisition of a reference non-diffusion weighted (or b_0) image are the minimum requirements to reconstruct DTI parametric maps; but to ensure primary diffusivities are independent of fiber orientation—i.e., to ensure DTI metrics are rotationally invariant –, one has to probe diffusion behaviors evenly and at a high spatial frequency. This is because tensor eigenvalues, hence diffusivities and anisotropy estimates, are more robust when WM tracts are collinear with one of the motion-sensitizing gradients (Jones, 2004). It is, therefore, essential that large numbers of diffusion-encoding orientations (N_d) are used for accurate DTI measurements in whole brain studies. In fact, the minimum number for robust tensor reconstruction has been estimated to range between $N_d = 20$ (Papadakis et al., 2000) and $N_d = 30$ directions (Batchelor et al., 2003; Jones, 2004), though a recent computer simulation has shown that a number of directions as low as $N_d = 12$ can yield accurate MD estimates if the number of *b*-values is sufficiently large, e.g., $N_b = 5$ (Correia et al., 2009). Interestingly, such robust behavior with respect to noise could not be replicated using repeat measures (NEX = 5) with a single *b*-value. This work, therefore, highlights the importance of collecting more than one *b*-value—untrue for NEX > 1—both to sensitize the DTI measurement to a wider range of diffusivities—i.e., microstructural environments—and to reduce the measurement bias due to noise. In clinical research practice, however, the number of measurements, N_m, is typically limited to 60–70 for a total scan time of 10 min; hence an optimal compromise between N_d and N_b must be achieved. Correia et al.'s DTI simulation revealed that for $N_m = 60$ measurements, if the interest is in MD, $N_d = 12 \times N_b = 5$ is the optimal set-up—i.e., a large number of *b*-values is preferred. For FA estimation, however, a larger number of directions—$N_d \geq 30$ (as in Batchelor et al., 2003; Jones, 2004)—is needed to establish accurate axial-to-radial diffusivity relationships, whereas little gain was observed for $N_b > 2$. Therefore, an important outcome of these studies is that $N_d = 30 \times N_b = 2$ appears to be a good compromise to ensure that tensor reconstructions are reliable; leading to the notion that the majority of clinical studies—typically sensitized with a single *b*-value and often, $N_d \leq 15$ with NEX ≥ 2—may have led to poor measurement stability.

An additional factor that may play a role in DTI robustness is the accurate estimation of S_0 through multiple b_0 scans (N_{b0}). To our knowledge, this has not been systematically investigated, though in theory its impact will depend on SNR (TE, parallel acceleration factor, *etc*), and on the prescribed number of *b*-values—becoming less relevant with increasing N_b. It is conceivable, however, that a large N_{b0} can help stabilize the measurements for little additional scan time—particularly in single *b*-value experiments.

Figure 6 illustrates the choice of *b*-value, N_b and N_{b0} dependence on DTI reconstructions. All maps were inferred from subsets (or the complete dataset) of a single acquisition with $N_d = 30$, two non-zero *b*-values ($b = 700$ and 1000 s/mm^2) and $N_{b0} = 12$—i.e., $N_m = 72$. Notable improvement in the calculation of diffusivities and anisotropy can be observed with the increase in *b*-value from 700 to 1000 s/mm^2. As would be expected, further improvements are noticeable when using the

information from both *b*-values in combination; though the highest diffusivity-to-noise ratios are returned by the complete dataset with a larger number of b_0 scans. It is, therefore, clear that they all contribute to improving DTI measurement stability.

Correia et al. (2009) showed that measurements from suboptimal schemes quickly deviate from true simulated values with decreasing SNR; but SNR is not only dictated by the factors enumerated above, but also by image resolution. One finds a plethora of voxel sizes in the published DTI literature. In the best case scenario, images are composed of isometric $2 \times 2 \times 2\,mm^3$ voxels, but a large number of studies—particularly early research at 1.5T—used slices more than twice as thick as in-plane resolution to ensure sufficient measurement SNR. Non-isometric voxels, however, are undesirable for volumetric analyses because they encourage volume averaging along the slice direction, which translates to spurious direction-dependent error biases (Oouchi et al., 2007). An alternative would be to encode smaller matrices with larger isotropic voxels, which is common practice, but

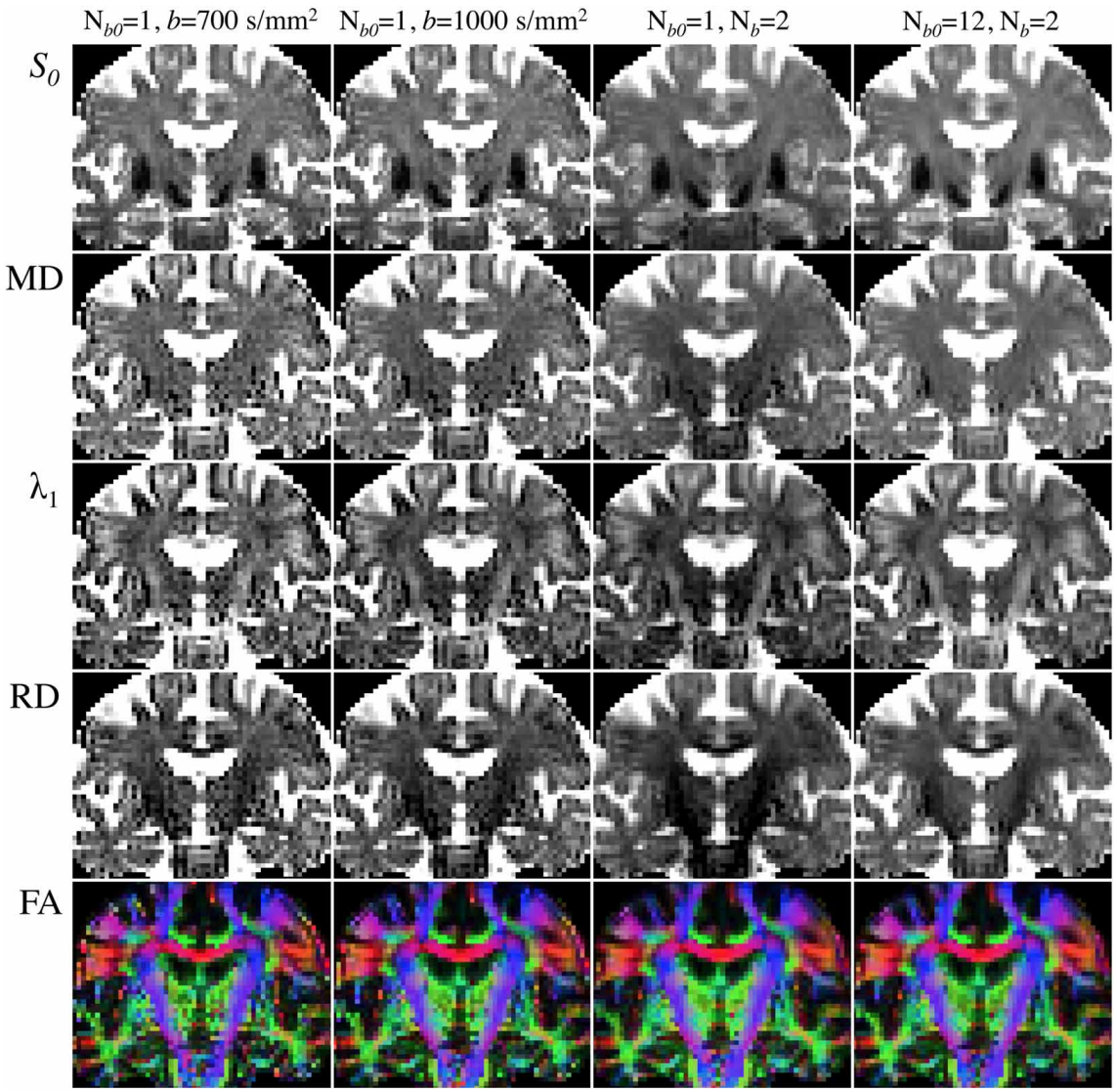

FIGURE 6 | Comparison of DTI parametric maps with different *b*-value, number of *b*-values (N_b) and number of b_0 scans (N_{b0}). MRI measurements were performed on a Siemens Verio 3T system (Siemens Medical Systems, Erlangen, Germany)—gradient coils capable of 45 mT/m and 200 T/m/s slew rate—with a 32-channel phased-array head-coil. Diffusion volumes were acquired using a standard twice-refocused, single-shot EPI pulse sequence: repetition/echo time = 9000/94 ms; matrix, 120 × 120; 63 contiguous slices aligned parallel to the anterior commissure/posterior commissure line; voxel size: $2 \times 2 \times 2\,mm^3$; 7/8-phase partial Fourier; bandwidth of 1667 Hz/pixel and echo spacing of 0.68 ms. Diffusion gradients were applied along $N_d = 30$ non-collinear directions (Siemens default vectors) with $N_b = 2$ non-zero *b*-values ($b = 700$ and $1000\,s/mm^2$), and $N_{b0} = 12$ reference scans. Parallel imaging was enabled (GRAPPA, acceleration factor = 2 and 38 reference lines), leading to a total scan time of 11 min and 15 s. DTI maps were computed with standard tools from FSL's diffusion toolbox. (Left to right columns): (i) $N_b = 1$ ($b = 700\,s/mm^2$), $N_{b0} = 1$ (5:06); (ii) $N_b = 1$ ($b = 1000\,s/mm^2$), $N_{b0} = 1$ (5:06); (iii) $N_b = 2$ ($b = 700$ and $1000\,s/mm^2$), $N_{b0} = 1$ (9:36); (iv) $N_b = 2$ ($b = 700$ and $1000\,s/mm^2$), $N_{b0} = 12$ (11:15).

one should not ignore that partial volume effects caused by large measurement voxels can also be highly detrimental in DTI due to GM and/or CSF contamination. This, in turn, can lead to systematic errors in patient populations because typically patients have more brain atrophy than controls, and therefore, DTI alterations may reflect CSF inclusions rather than true microstructural changes. It should be noted that the WM tract of interest in the present Research Topic—the fornix—due to its close vicinity to ventricular CSF is particularly vulnerable to this phenomenon as illustrated in **Figure 7**.

In conclusion, although DTI is becoming a mature technique, there is not yet a universal agreement on the minimum requirements for a reliable DTI acquisition, or on an optimal image acquisition scheme for a given scan time, so we must reconcile with the fact that different DTI studies to date may have sensitized their acquisitions very differently.

THE POST-PROCESSING METHODOLOGY

Post-processing methods are also highly relevant to interpreting DTI literature. To date, a number of analysis strategies have been used including region-average, histogram or voxel-/cluster-based. No method, however, has demonstrated systematic superiority in every scenario; though it is widely accepted that for unbiased whole-brain assessments, the tract-based spatial statistics (TBSS) approach (Smith et al., 2006) has advantages and is the most desirable technique for volumetric DTI analysis at present (see **Figure 8**). TBSS—part of FMRIB's software library or FSL (Smith et al., 2004)—enables whole brain assessment of WM tract integrity in neurodegenerative diseases using DTI data without the need for *a priori* hypotheses about the spatial location of degenerative involvement. TBSS circumvents the lack of anatomical landmarks in WM, which is a limiting factor for manual tracing of tracts of interest in native space. TBSS deals with this problem by automatically co-registering all DTI parametric maps to a standard template; also, unlike histogram analyses, it can resolve the specific location of abnormal clusters; it is not biased by the dependency issues known to affect tractography based regional analysis (Besseling et al., 2012); and finally, TBSS does not require convolution with a smoothing kernel, as is used in standard VBA methods, due to the introduction of a skeletonisation step. The skeleton is derived from averaging FA images across all subjects and subsequent identification of tract centers;

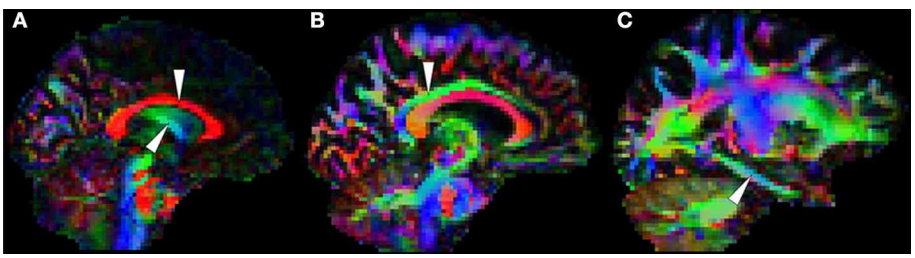

FIGURE 7 | White matter tracts that are usually prone to measurement error. (A) The body of the corpus callosum (top arrow) and the body of the fornix (bottom arrow) are often problematic because they are adjacent to cerebrospinal fluid. The cingulum bundle, **(B)** which is typically less vulnerable at the level of the posterior cingulate, **(C)** is sometimes prone to partial volume contamination and other types of measurement error in the parahippocampal region due to its thinner physical appearance (Jones et al., 2013a) and its closer proximity to rostral temporal areas known to be affected by magnetic susceptibility artifacts. Note in addition that orbitofrontal white matter is also vulnerable to such artifacts.

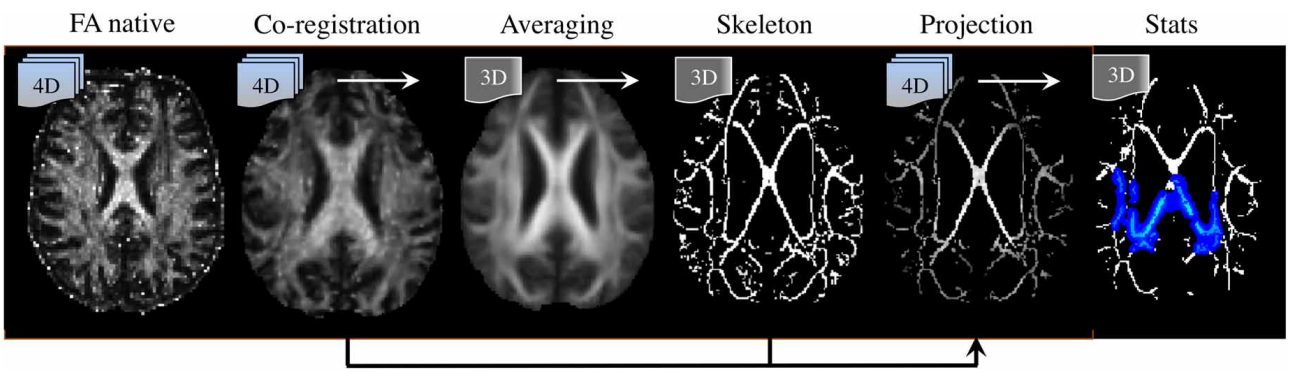

FIGURE 8 | Tract-based spatial statistics (TBSS) processing pipeline. (Left to right) DTI-derived fractional anisotropy (FA) images are co-registered to a template; they are then averaged, from which a "skeleton" containing all major tract centers common to all subjects is derived. Skeleton voxels with low *FA*-values (typically $FA < 0.2$) are excluded to ensure only white matter is present. Next, spatially normalized FA images are projected to the skeleton. In this step, the center of each tract is identified for each individual FA image, and projection vectors to their analogous location in the skeleton are computed and applied. Transformation fields (to template space) and projection vectors (to the skeleton) are then also applied to the additional DTI parametric maps (i.e., MD, λ_1, RD). Finally, non-parametric, permutation based, statistical testing of the null-hypothesis is performed.

this ensures the analysis is carried out exclusively on definite WM. But the main advantage of projecting DTI data to a WM skeleton is that it corrects, to some extent, co-registration inaccuracies, rendering the data more comparable than in VBA. In addition, performing statistics only along the center of major WM bundles minimizes the effects of partial volume contamination and reduces the number of statistical tests. Furthermore, TBSS' non-parametric statistical method does not require normally distributed data and, as for any randomization approach, it is inherently robust against Type-I errors (Winkler et al., 2014).

The default TBSS processing pipeline, however, suffers from its own sources of inaccuracy and limitations: it fails to rotate the **B**-matrix after realigning all images to account for motion and eddy-current effects (Leemans and Jones, 2009); it implements a fast—but oversimplified—tensor fitting routine (Jones and Cercignani, 2010) that assumes single fiber populations in each voxel, hence leading to potential miscalculations in areas of crossing and kissing fibers (Jbabdi et al., 2010); its non-linear co-registration algorithm, FNIRT, performs moderately relative to other *state-of-the-art* methods (Klein et al., 2009); assessments are spatially restricted to WM tract centers only—ignoring, therefore, a large amount of WM[1]; and finally, it suffers from spatial- and orientation-dependent statistical sensitivity (Edden and Jones, 2011). That is, TBSS is not completely unbiased. Such limitations should not be ignored; in fact, they suggest that in certain scenarios other methods might be preferable. For example, the fornix is often excluded from the WM skeleton due to the perennial issue of image misregistration (Keihaninejad et al., 2012) or does not survive correction for multiple comparisons at the cluster level due to its small physical size (Acosta-Cabronero et al., 2012; Schwarz et al., 2014). The fornix, however, has clear boundaries in FA maps (at least through the midline), and more advanced co-registration methods exist; thus, although FNIRT-based TBSS studies in AD will be the focus here to homogenize the potential confounding error introduced by different post-processing routines and because, to date, it is the most widely used method of whole-brain DTI analysis, it should be highlighted that manual tracing or automated regional extraction using high-performing, tensor-orientation enabled (Zhang et al., 2006) or intensity-based, diffeomorphic image registration algorithms (Avants et al., 2008) might be better suited to study structures such as the fornix.

Turning to the issue of image misregistration with standard FSL tools, a recent study has compared the warping performance for a number of co-registration strategies, including the standard TBSS procedure of warping each subject to the FMRIB's FA template (ST-TBSS), the previously recommended method of using the most representative subject as an intermediate registration step (RS-TBSS), and building study-specific (SS-TBSS) or group-wise templates (GW-TBSS)—all in the context of AD (Keihaninejad et al., 2012). The lack of ground truth makes the visual assessment of TBSS results in AD hard to interpret; however, using inter-subject variability and a proxy-measure of false positive rate as indicators of overall warping performance, Keihaninejad et al.'s results suggest that RS-TBSS is substantially inferior to the other methods, and that the use of the GW-TBSS approach might be beneficial.

THE SUBJECT COHORT

An important factor that must be considered is the nature of the patient cohort under investigation. Many studies focus on the prodromal stages of AD—typically patients diagnosed with subjective or mild cognitive impairment (SCI/MCI), genetically at risk (e.g., carriers of the apolipoprotein E ε4 allele), and/or those who are positive for an AD biomarker, e.g., CSF analysis or amyloid-ligand PET. It is noteworthy, however, that not all risk indicators are equivalent; while amyloid-PET is an unambiguous marker of AD neuropathology (Clark et al., 2012), CSF markers are not as robust due to inconsistent standardization (Verwey et al., 2009). In addition, genetic risk profiles (for sporadic AD) are problematic because they are only risk factors. Most troublesome, though, are studies that report cross-sectional cohorts of SCI or MCI with neither biomarker nor longitudinal outcome data to confirm symptoms were due to early AD. Cohorts without such information are impossible to interpret because of the potentially large number of false positive cases meeting such inclusion criteria (Jicha et al., 2006). This problem can be further compounded if imaging studies stratify MCI into amnestic (aMCI), non-amnestic (naMCI) and multi-domain (mdMCI), or, into "early" and "late" MCI without outcome or biomarker data. Individuals belonging to an mdMCI or late MCI group, being more cognitively impaired, have a higher probability of having AD, while naMCI has a lower probability (Mitchell et al., 2009). These are, however, only probabilities and do not indicate the pathology of each individual in a group. If the aim is to study the neurobiology—as it should be in an imaging study—of prodromal AD, a subject with naMCI due to AD is an appropriate inclusion whereas one with mdMCI that is not due to AD pathology is not. The present review, therefore, will not discuss such studies unless outcome data through clinical follow-up, or amyloid-PET/CSF analysis, confirmed that subjects in these pre-dementia stages were likely to have had incipient AD. It should be noted that meeting established criteria for probable AD (McKhann et al., 1984) does not completely predict AD neuropathology at autopsy, but the risk of including false positive cases is far lower than for SCI/MCI.

A further confounding effect that must always be considered is the comorbidity of WM hyperintensities. Studies typically deal with this by excluding cases with such lesions through visual inspection of T_2-weighted images; this can also be supported by semi-quantitative measures using the Fazekas visual rating scale (Fazekas et al., 1987). It should be highlighted, however, that there is no consensus on what constitutes an unacceptable level of lesion burden for a DTI analysis in dementia although such information is very relevant given the extremely high prevalence of WM hyperintensities in the target population. This would be an interesting topic for further research, as would more automated

[1]In practical terms, however, this is not a problem for neurodegenerative diseases in which degeneration involves large-scale networks as opposed to tiny focal lesions. Visual inspection of a skeleton typically demonstrates that TBSS does not systematically miss any large chunks of the brain. In fact it can be desirable, particularly in neurodegenerative diseases, where the data reduction step to tract centers eliminates to a greater extent the vulnerability to partial volume contamination due to focal lesions.

and quantifiable measures of lesion load. For instance, it seems reasonable that subjects with negligible amounts of WM signal change would still be appropriate for inclusion in a DTI study, but this immediately raises the question of how one defines "negligible." More objective scales and a consensus on an acceptable threshold would, therefore, be desirable.

MULTI-CENTER STUDY DESIGNS

Multi-site designs are becoming increasingly common in AD research, particularly with the advent of the Alzheimer's Disease Neuroimaging Initiative (ADNI) and related spin-offs (Jack et al., 2010). Whilst such initiatives incorporate a pilot stage to estimate measurement stability across centers, a systematic assessment of inter-site DTI variability has not yet been carried out within the ADNI framework. An independent European initiative, however, performed such measurements and found significant FA variations across scanners, leading to the conclusion that FA variability cannot be fully controlled by the use of identical scanner type and acquisition parameters (Teipel et al., 2011). This result highlights that, at least until full cross-validations confirm otherwise, multi-center studies should account for potentially confounding scanner effects—a practice that is not commonly carried out. It should be noted, therefore, that multi-center studies in the present review have been included only to confirm widely reproduced observations, but little emphasis has been given to idiosyncratic results generated from such datasets.

LITERATURE SYNTHESIS: INCLUSION CRITERIA

In an effort to evaluate the DTI literature to date in AD, studies meeting the "essential" criteria for this review (**Table 1**) were selected. **Table 2** illustrates the iterative process that led to identification of 13 publications in which an acceptable acquisition and analysis protocol was employed; and in which patients had either clinically probable AD, MCI-stage AD where longitudinal follow-up or biomarkers were used to define probable AD status, or patients with autosomally inherited known gene mutations for AD (Acosta-Cabronero et al., 2010, 2012; Douaud et al., 2011; Bosch et al., 2012; Huang et al., 2012; Canu et al., 2013; Fieremans et al., 2013; Mahoney et al., 2013; Nir et al., 2013; Rowley et al., 2013; Ryan et al., 2013; Lim et al., 2014; Molinuevo et al., 2014). It should be stressed that **Table 2** highlights the order of iterations by which studies were excluded; it should not be read to mean that for each criterion the number of excluded studies equals that number of studies in total that failed on that specific criterion because many studies failed on multiple criteria. **Table 1** also includes a list of proposals of additional criteria for future studies based on current knowledge.

Details of the 13 studies that were identified from the literature review can be found in the Supplementary Table. It should also be noted that several of the studies (Douaud et al., 2011; Bosch et al., 2012; Huang et al., 2012; Nir et al., 2013; Rowley et al., 2013) included both AD and MCI groups where the latter did not

Table 1 | Selection criteria for DTI studies in Alzheimer's disease included in the present review and additional guidelines for future studies.

Essential (inclusion criteria for this review)
DTI ACQUISITION
✓ Number of diffusion-encoding directions equal to or greater than 30
✓ Quasi-isometric voxels—ratio between in-plane resolution and slice thickness greater than 0.75, i.e., the geometry of $1.875 \times 1.875 \times 2.5\,mm^3$ voxels is at the lower limit
✓ Voxels smaller than $20\,mm^3$, i.e., image resolution $2.7 \times 2.7 \times 2.7\,mm^3$ is at the upper limit
✓ Maximum *b*-value equal to or greater than $900\,s/mm^2$
STUDY COHORT
✓ (i) Clinical diagnosis of probable AD (at acquisition or through clinical follow-up), (ii) positive CSF analysis for AD (iii) positive amyloid-PET, or (iv) autosomal dominantly inherited mutation carriers
✓ Number of subjects equal or greater than $N = 10$ in each group
DATA ANALYSIS
✓ Voxel-/cluster-wise (or region-average) whole-brain TBSS
✓ Show results for both FA and MD (at least)
✓ Demonstrate results are robust against multiple testing effects
Desirable (additional suggested criteria for future studies)
DTI ACQUISITION
+ Studies performed on a single scanner
+ Use of multiple *b*-values, i.e., $N_b \geq 2$
+ If $N_b = 1$, total number of measurements greater than 60, i.e., $N_m > 60$
+ Ensure stable S_0 measurement, i.e., $N_{b0} \geq 5$
+ Voxels equal to or smaller than $8\,mm^3$, i.e., image resolution $2 \times 2 \times 2\,mm^3$ or finer
+ Perfect voxel symmetry (or within 90%)
DATA ANALYSIS
+ Avoidance of RS-TBSS pipelines

Table 2 | Summary of the hierarchical iterative steps leading to the selection of 13 DTI studies in Alzheimer's disease.

	# of studies	Remaining
1. PubMed search ("diffusion tensor" OR DTI) AND (Alzheimer's) on 5/8/2014	476	
2. Not relevant (i.e., tractography based structural/functional connectivity studies, DTI works with marginal reference to AD, *etc*)	285	191
3. Not TBSS (i.e., VBA, ROI, atlas-based, *etc*)	118	73
4. TBSS in MCI or ApoE4 carriers without clinical outcome or additional biomarker	27	46
5. TBSS in AD using images with unacceptably thick scan slices	11	35
6. TBSS in AD using an insufficient number of diffusion-encoding directions (i.e., $N_d < 30$)	10	25
7. TBSS in AD using low maximum *b*-value (i.e., $b_{max} < 900\,s/mm^2$)	4	21
8. TBSS in non-representative groups (i.e., $N < 10$ AD subjects)	2	19
9. TBSS to study AD-related aspects not directly relevant to this comparison (e.g., investigation of neural correlates)	2	17
10. TBSS in AD with a non-conventional statistical approach	1	16
11. TBSS in AD where no contrast against controls was shown	1	15
12. TBSS in AD where only the FA contrast was shown	2	13
Selected TBSS studies in AD	13	

meet entry criteria for the present review. Only data from the AD groups is included from such studies.

TBSS IN AD: FINDINGS FROM THE LITERATURE OVERVIEW

After careful literature filtering for potential technical problems in past studies, a number of consistent TBSS behaviors were identified; it would be wrong to assume, however, that such results provide a definitive understanding of WM changes in AD because, as discussed, alterations in structures that are prone to error may lie undetected for technical reasons. In contrast, prominent DTI effects that have been reproduced in a number of methodologically sound studies are evidence of real phenomena and that may, thus, be interpreted with scientific rigor as disease-related processes.

WHAT DOES THE DISTRIBUTION OF DIFFUSION TENSOR ALTERATIONS TELL ABOUT AD?

The selection process identified TBSS studies in AD that generally had a consistent common denominator—i.e., widespread and confluent tensor abnormalities in parietal, temporal and pre-frontal WM—specifically involving long association fibers (including limbic tracts) and inter-hemispheric connections through the corpus callosum. Generally speaking changes were more apparent in posterior areas compared to frontal areas as would be expected from prior knowledge of cortical atrophy studies and FDG-PET. **Figure 9** exemplifies such a distribution in a mild AD cohort (Acosta-Cabronero et al., 2012), where the posterior corpus callosum, cingulum bundle at the level of the posterior cingulate gyrus, superior longitudinal fasciculus and sagittal stratum (including the inferior longitudinal fasciculus, fronto-occipital fasciculus, and posterior thalamic radiation) were affected. Additional involvement is also commonly found in superior temporo-parietal WM at the level of the corona radiata and centrum semiovale—composed of intertwined long/short association and projection tracts.

Two exceptions, however, were found; the studies by Ryan et al. (2013) and Lim et al. (2014) did not find any cross-sectional differences in pre-symptomatic, autosomal dominant (PSEN1) mutation carriers and a group of MCI-stage AD patients defined by CSF biomarkers, respectively. The group reported by Ryan et al. (2013) were estimated to be a mean of 5.6 years from symptom onset so it simply may be that the group was too early to have major changes in WM; to this end it was notable that as a group there was also no significant hippocampal atrophy. The group only comprised $N = 10$ mutation carriers which also suggests it may have been underpowered to detect subtle changes with whole brain TBSS analysis; finally, the control group used was significantly older than the PSEN1 group which may have also masked abnormalities. The cohort in Lim et al. (2014) were $N = 16$ early MCI-stage AD subjects scanned under the umbrella of the ADNI2 framework, i.e., on 14 different scanners, which may, thus, have contributed to the lack of sensitivity. Though one might be tempted, in light of these results, to conclude that DTI is unable to detect WM changes in such early stages, the *post-hoc* regional study carried out by Ryan et al. (2013); the TBSS study by Molinuevo et al. (2014) in a group of cognitively normal and SCI subjects (positive for CSF biomarkers); and an atlas-based regional study (with suitable methods) in cognitively normal (amyloid-PET positive) subjects (Racine et al., 2014) suggest otherwise, as these reported DTI alterations that were consistent with the distribution in **Figure 9**.

The results from Canu et al. (2013) are also worthy of further discussion. The study examined two AD cohorts with different onset ages, but matched otherwise for disease severity, with two appropriately age-matched control groups. The early-onset group showed very widespread abnormalities highly concordant with **Figure 9**, but that spread slightly more anteriorly along association tracts and the genu of the corpus callosum. These were moderately impaired cohorts, i.e., average mini-mental cognitive examination (MMSE) score (Folstein et al., 1975) around 20/30; thus it would be reasonable to expect that changes had extended more extensively into frontal areas. Interestingly, however, the result in the late-onset cohort was relatively insensitive. Whilst differences were found in posterior areas largely overlapping the

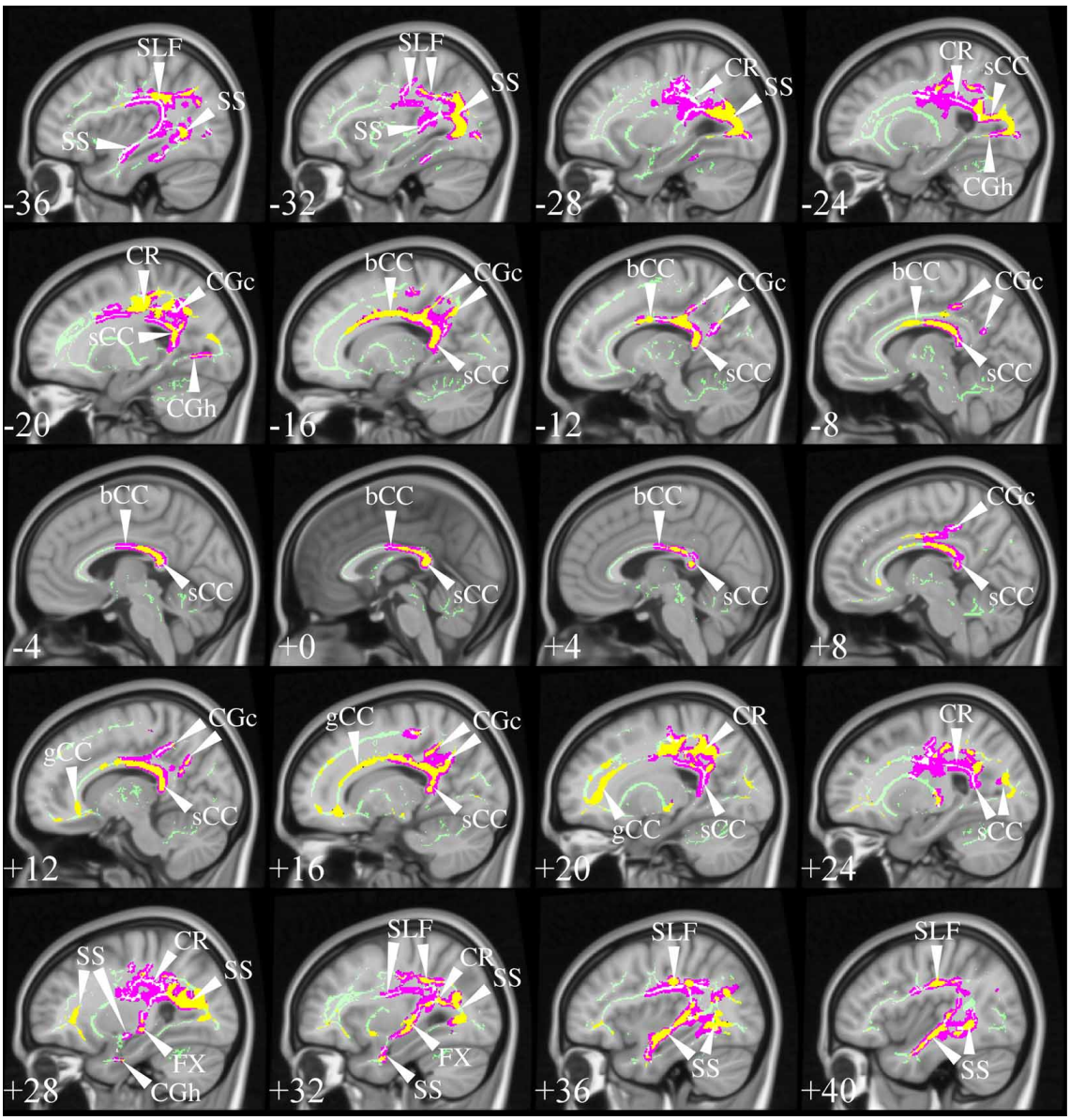

FIGURE 9 | TBSS in AD. TBSS results for $N = 43$ early-stage AD patients (age: 70 ± 6, <MMSE>= 24 ± 4) vs. $N = 26$ matched controls (age: 68 ± 6) (Acosta-Cabronero et al., 2012). Pink clusters denote increased MD in patients, whereas those in yellow represent FA reductions at $P < 0.05$ enabling threshold free cluster enhancement (TFCE) (Smith and Nichols, 2009) and controlling the family-wise error (FWE) rate. Thresholded statistical maps are overlaid onto the TBSS skeleton and MNI152 template. Sagittal MNI coordinates are given in millimeter where $x < 0$ is left. Abbreviations: [SLF] superior longitudinal fasciculus; [SS] sagittal stratum; [CR] corona radiata; [s/b/gCC] splenium/body/genu of the corpus callosum; [CGc/h] cingulum at the level of the posterior cingulate/parahippocampus; and [FX] fornix.

clusters in **Figure 9**, the distribution was markedly less extensive, which was interpreted as less severe damage than in the earlier-onset group of patients. While this might be true, the study highlights another potentially important confound; that is, the age of the control group. The mean age of controls for the contrast with "late-onset" AD was 73 years but at this age one would expect around one third of a control population to be amyloid positive, i.e., in the pre-clinical stage of AD (Villemagne et al., 2011). In contrast, the control group for the early-onset AD cohort had a mean age of 59 years—an age at which one would expect negligible, if any, contamination from pre-clinical AD. In other words, older control subjects are probabilistically more likely to introduce undesirable variability into group comparisons, which may explain some of the differences in sensitivity across studies. This suggests that when targeting "late-onset" AD, it would be desirable in future that the control group was defined by being amyloid-negative, in addition to being cognitively intact, to ensure that this possible confound was not attenuating sensitivity.

Studies in symptomatic, young PSEN1 carriers (Ryan et al., 2013), or in relatively young sporadic AD cohorts (age: 63 ± 5,

Mahoney et al.), where control groups were young and abnormalities, very extensive—with posterior predilection but spreading toward anterior areas—also support the notion that control age might be a contributing factor affecting analysis sensitivity. However, extensive abnormalities are not a unique feature of young cohorts, a number of studies in older groups have also shown a similar behavior, e.g., mild AD in Fieremans et al. (2013), mild AD in Acosta-Cabronero et al. (2012), mild AD in Douaud et al. (2011), mild AD (ADNI data) in Rowley et al. (2013) and mild AD (ADNI data) in Nir et al. (2013). In such studies, the posterior parietal and superior temporal regions highlighted in **Figure 9** were key features, but abnormalities also spread more anteriorly along association tracts and also included extensively the anterior corpus callosum, corticocortical association fibers running through the external capsule and the anterior limb of the internal capsule. Disentangling whether more, or less, widespread distributions across studies are the result of subtle technical factors, differences in disease severity, in control variability, or in cohort size, is impossible to disambiguate, but it should be highlighted that from the selected studies, cohorts with the most widespread abnormality patterns had, in general, more advanced disease stages than the cohort displayed in **Figure 9**, suggesting disease severity is a dominant factor in result sensitivity. A recent study in two age-matched AD cohorts with different disease severity that controlled for all the above factors using the same acquisition, the same control cohort and the same number of subjects in each patient group, showed evidence indicating a posterior first, then more anterior distribution in more advanced disease stages (Acosta-Cabronero et al., 2012)—matching the expected progression of degeneration as would be measured by cerebral glucose metabolism (Minoshima et al., 1997; Nestor et al., 2003b). In summary, although a number of additional factors might have contributed to variability in result sensitivity across studies, disease staging appears to drive the overall distribution of WM abnormalities in AD.

Focusing on the earliest DTI changes in AD specifically, Molinuevo et al. (2014) studied a combined cohort of cognitively normal subjects and SCI with a CSF profile consistent with AD, while Acosta-Cabronero et al. (2012) reported on patients with MCI-stage AD confirmed through longitudinal follow-up. The two studies showed a consistent picture of the affected neural network in incipient stages of AD. Both results highlighted involvement of parietal and superior temporal WM bilaterally—spatial distributions that are also in close agreement with the expected landscape of WM involvement that can be inferred from the pattern of glucose hypometabolism in very mild AD (Nestor et al., 2003b, 2006).

DIFFERENTIAL DIFFUSION METRIC SENSITIVITY DURING THE COURSE OF AD

An interesting by-product of TBSS analyses in AD has been in showing that alterations in diffusion behavior are complex—while early (and some recent) studies tended to focus only on FA—often leading to largely insensitive results (Damoiseaux et al., 2009; Zarei et al., 2009; Balachandar et al., 2014)—, more extensive abnormality distributions for MD have been a consistent finding across studies (Acosta-Cabronero et al., 2010, 2012; Douaud et al., 2011; Huang et al., 2012; Fieremans et al., 2013; Mahoney et al., 2013; Nir et al., 2013; Rowley et al., 2013; Ryan et al., 2013). What this behavior represents in neurobiological terms, however, is unknown because, as discussed already, DTI offers limited information about the geometry of the underlying damaged microstructure. In contrast, what DTI enables us to infer from such behavior is that WM degeneration in AD results in alterations to WM tissue that are not grossly driven along any preferential direction (Acosta-Cabronero et al., 2010). Subtle orientation dependent behaviors missed by FA can be explored by dissecting the apparent diffusion coefficient encapsulated in MD into its primary components, i.e., λ_1 (also commonly referred to in the literature as AxD or DA) and RD. A superficial reading of studies examining these primary components appear not to provide a clear picture—a number of studies such as those in very mild AD by Acosta-Cabronero et al. (2012) and in CSF-positive SCI by Molinuevo et al. (2014) indicate that λ_1 might be the dominant source of DTI abnormalities; whereas other studies such as those in mild AD by Mahoney et al. (2013) and Bosch et al. (2012), and in moderately impaired AD by Ryan et al. (2013) show greater RD effects. Douaud et al. (2011) proposed that the λ_1 increase could be explained as an artifact of loss of one fiber population in areas of crossing fibers (see **Figure 3**). This would be a plausible theory if increased λ_1 were restricted to areas of crossing fibers (e.g., centrum semiovale), however increased λ_1 in AD is not limited to such regions: the same phenomenon is observed in the midline corpus callosum and fornix where crossing tracts are not present. This indicates that increased λ_1 in AD must be due to another mechanism but what that might be in biological terms is, at present, unclear[2].

The patient cohorts in Mahoney et al. (2013); Bosch et al. (2012) and the symptomatic cohort in Ryan et al. (2013), which all reported increased RD, had more advanced dementia (MMSE < 23) than those outlined with extensive λ_1 changes, suggesting that on closer inspection of the literature, individual component metrics of the diffusion tensor may evolve along different trajectories with disease progression. This implies that different metrics may be more or less sensitive to different disease stages. This hypothesis was tested on two—very mildly (MCI-stage) and mildly impaired—AD groups using the same MR acquisition and post-processing methods (Acosta-Cabronero et al., 2012). The distribution of increased λ_1 involving posterior temporo-parietal WM—largely consistent with Molinuevo et al. (2014)—was identified as the first sign of change. In the more advanced group, however, increased RD—which, in turn, drove FA reductions—emerged in these regions that had shown increased λ_1 in the very mild group. As degeneration spread to new areas—notably frontal and left temporal WM—increased λ_1

[2]One possible situation where loss of crossing fibers may explain increased λ_1 was a study that examined the neural substrate of topographical memory impairment in AD (Pengas et al., 2012). The study in question found correlations between increasing λ_1 and decreasing task performance; interestingly the regions that correlated were all in close proximity to the cortical ribbon—in other words, in the U-fiber layer. It is tempting, therefore, to speculate that local degeneration of GM, in turn meaning less axons entering adjacent WM, might lead to a simplification of the adjacent U-fiber layer—i.e., less crossing fibers—making increased λ_1 correlate significantly.

was again the first abnormality to appear. These results suggested that while λ_1 increase is the first sign of change in a given location, RD is relatively insensitive at the earliest disease stages but becomes progressively more abnormal as the disease progresses. Confirming this theory, a subset of AD patients in the same study, who were scanned serially, revealed that RD/FA changes emerged at follow up in areas where increased λ_1 had been seen at baseline. Interestingly, λ_1 increases did not progressively worsen over time with longitudinal follow-up. There was, furthermore, no evidence for progressive worsening of λ_1 between the two severity stages in the cross-sectional cohorts when investigating the midline splenium in isolation. In fact, if anything there was a slight tendency for the increase in λ_1 to lessen with advancing disease (Acosta-Cabronero et al., 2012); in other words suggesting that when a WM region first becomes affected in AD, there is a sharp increase in λ_1, that may possibly attenuate with further disease progression.

In summary, RD progressively increases (and therefore FA progressively decreases) as a function of disease severity—as defined by degree of cognitive impairment—whereas λ_1 does not

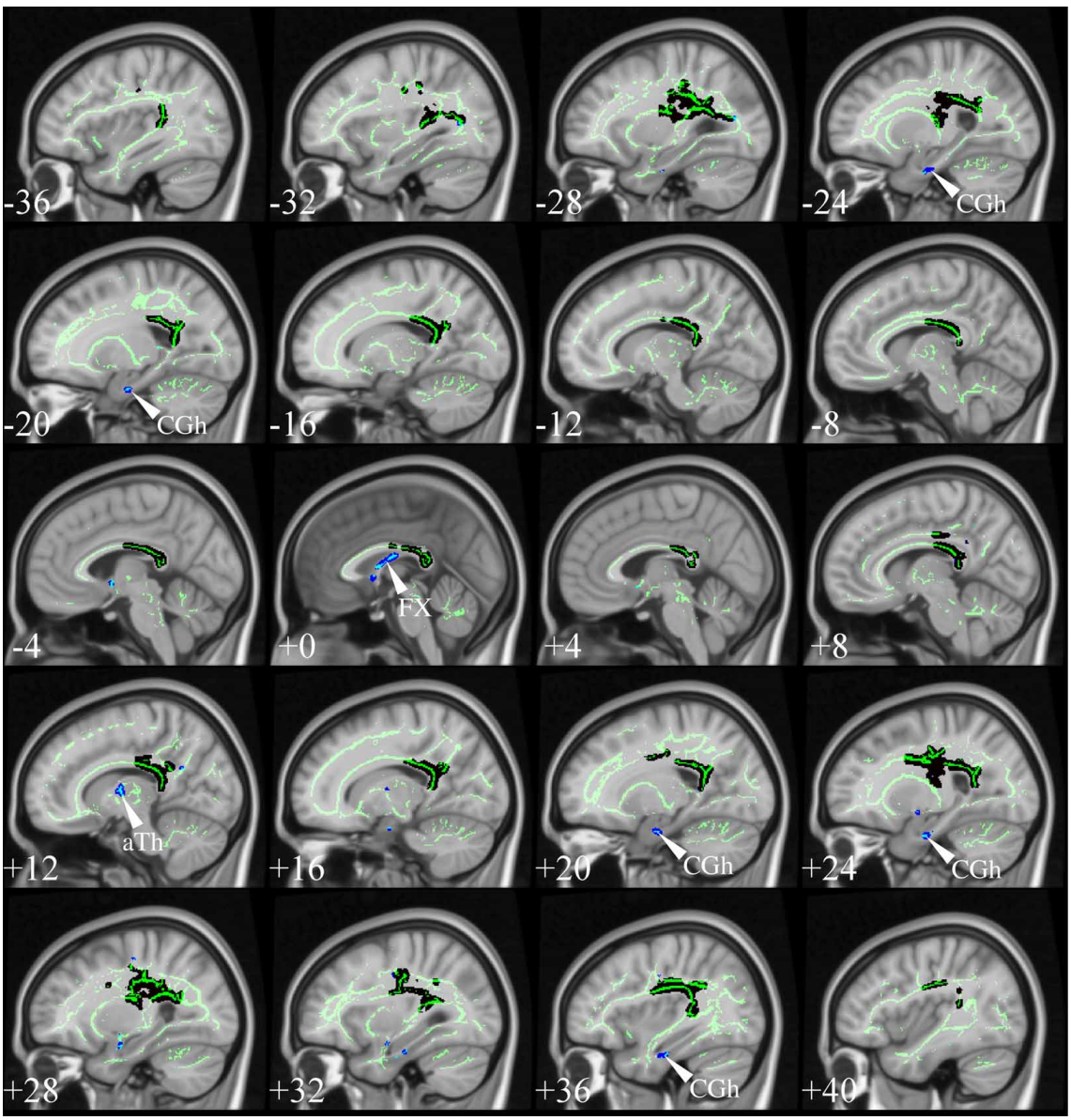

FIGURE 10 | TBSS in very mild AD. TBSS results for $N = 21$ very mild AD patients (age: 72 ± 5, <MMSE>= 26 ± 2) vs. $N = 26$ matched controls (age: 68 ± 6) (Acosta-Cabronero et al., 2012). The patient group included $N = 16$ subjects who were scanned with a diagnosis of mild cognitive impairment but were subsequently shown to have probable AD with longitudinal follow-up. Black clusters denote increased λ_1 in patients at $P_{FWE} < 0.05$, whereas those in blue represent changes with *post-hoc* control over the false discovery rate (FDR) at $q < 0.05$. Thresholded statistical maps are overlaid onto the TBSS skeleton and MNI152 template. Sagittal coordinates are given in millimeter ($x < 0$ is left). Abbreviations: [aTh] anterior thalamic white matter; [CGh] cingulum at the level of the hippocampus; and [FX] fornix.

progressively increase. That increasing λ_1 is not a function of disease severity, at least in the midline splenium, suggests that the early λ_1 increase in AD may be capturing an upstream event to axonal degeneration, whereas processes more directly related to neuronal loss might dominate RD/FA dynamics—implying thus that, whilst λ_1 in the splenium could act as a state-specific marker in prodromal disease stages, the spatial distribution of RD/FA changes may be a more suitable staging biomarker.

FORNIX CHANGES IN AD

Although atlas-based approaches consistently find strong effects in the fornix (Keihaninejad et al., 2013; Racine et al., 2014), this was not, however, a universal feature of the TBSS studies reviewed above. Such tracts are often excessively penalized due to their small size by the strictness of non-parametric statistics controlling for family-wise error (FWE) rate. Using, however, the more lenient false-discovery rate (FDR) correction (Benjamini and Hochberg, 1995) to show abnormalities that are less prominent at the cluster level—yet statistically robust—fornix changes emerge also with TBSS analysis. **Figure 10** illustrates the impact of this slight statistical modification, resulting in "new" λ_1 abnormalities in the fornix, parahippocampal WM and anterior thalamus (possibly capturing change in the mammillo-thalamic tract). These structures are not just random new blobs—they precisely target major WM connections in the limbic-diencephalic network that has been highlighted as the early hypometabolic landscape of AD (Nestor et al., 2003b, 2006). For a focused review on the specific role of the fornix in this network, including the possibility of it being therapeutic target for deep brain stimulation in AD, see the review in this Research Topic (Oishi and Lyketsos, 2014).

The notion that limbic tracts and the corpus callosum—particularly the splenium—are key features in early stages of AD has now a solid body of evidence. The theory that these regions should show the most advanced degeneration in the course of AD (and therefore be the first to show RD/FA changes) when other areas, being less advanced in the course of disease, would only show λ_1 changes is strongly supported by the regional TBSS analysis in mild AD carried out by Huang et al. (2012). These authors found λ_1 increase in association and projection tracts and RD/FA effects in the corpus callosum, cingulum and fornix, precisely suggesting that the latter were at a more advanced stage of degeneration compared to the former. In a similarly impaired cohort extracted from the ADNI dataset, Nir et al.'s regional TBSS study also found strong RD/FA alterations for such structures. In addition, a prospective study—targeting specifically the corpus callosum, fornix and cingulum—found significant cross-sectional and longitudinal tensor differences for all three structures (Keihaninejad et al., 2013). The common aspect in these studies is that—consistent with all the selected works—absolute diffusivities were increased in AD relative to controls, whereas FA was reduced.

CONCLUSION

In summary, the existing literature supports the theory that a bilateral neural network that involves preferentially the cingulum bundle, fornix and corpus callosum is vulnerable to early disease processes triggered by the Alzheimer's disease neuropathological cascade. This suggests that the nodes that this network interconnects—i.e., the mesial temporal lobe, mammillary bodies, thalamus, and posterior cingulate—degenerate as a network, rather than in isolation.

To conclude with a note of caution and a window to future research directions. While much effort was made to rationalize published DTI studies in AD for this review, it remains possible that a large number of technical factors including suboptimal acquisitions, poor tensor reconstruction routines, poor image co-registration performance, or intrinsic DTI limitations, to name a few, might still have resulted in some systematically incorrect results across the literature, in turn, leading to incompletely valid interpretations in this review. A number of technical developments, however, should hopefully soon help confirm, or reject, the above theories: stronger gradient systems enabling larger *b*-values, shorter echo times and smaller voxels; improved image quality through multiband acquisitions (Frost et al., 2014); the prescription of multiple *b*-values; the implementation into standard tensor reconstruction pipelines of distortion correction, **B**-matrix rotation and multi-component fitting routines with a free-water component (Pasternak et al., 2009); the application of advanced diffusion models beyond the single tensor such as diffusion kurtosis imaging (Jensen et al., 2005), NODDI (Zhang et al., 2012), CHARMED (Assaf and Basser, 2005), or q-space approaches such as q-ball reconstruction (Tuch, 2004) or diffusion spectrum imaging (Wedeen et al., 2005); the use of *state-of-the-art* co-registration methods (Zhang et al., 2006; Avants et al., 2008); and a long *et cetera*.

ACKNOWLEDGMENT

We gratefully acknowledge the support from our patients, their relatives and healthy volunteers, without whom our past research reviewed here would have not been possible.

SUPPLEMENTARY MATERIAL

The Supplementary Material for this article can be found online at: http://www.frontiersin.org/journal/10.3389/fnagi.2014.00266/abstract

REFERENCES

Aboitiz, F., Scheibel, A. B., Fisher, R. S., and Zaidel, E. (1992). Fiber composition of the human corpus callosum. *Brain Res.* 598, 143–153. doi: 10.1016/0006-8993(92)90178-C

Acosta-Cabronero, J., Alley, S., Williams, G. B., Pengas, G., and Nestor, P. J. (2012). Diffusion tensor metrics as biomarkers in Alzheimer's disease. *PLoS ONE* 7:e49072. doi: 10.1371/journal.pone.0049072

Acosta-Cabronero, J., Williams, G. B., Pengas, G., and Nestor, P. J. (2010). Absolute diffusivities define the landscape of white matter degeneration in Alzheimer's disease. *Brain* 133, 529–539. doi: 10.1093/brain/awp257

Alexander, D. C., and Barker, G. J. (2005). Optimal imaging parameters for fiber-orientation estimation in diffusion MRI. *Neuroimage* 27, 357–367. doi: 10.1016/j.neuroimage.2005.04.008

Alger, J. R. (2012). The diffusion tensor imaging toolbox. *J. Neurosci.* 32, 7418–7428. doi: 10.1523/JNEUROSCI.4687-11.2012

Ashburner, J., and Friston, K. J. (2000). Voxel-based morphometry—the methods. *Neuroimage* 11, 805–821. doi: 10.1006/nimg.2000.0582

Assaf, Y., and Basser, P. J. (2005). Composite hindered and restricted model of diffusion (CHARMED) MR imaging of the human brain. *Neuroimage* 27, 48–58. doi: 10.1016/j.neuroimage.2005.03.042

Avants, B. B., Epstein, C. L., Grossman, M., and Gee, J. C. (2008). Symmetric diffeomorphic image registration with cross-correlation: evaluating automated

labeling of elderly and neurodegenerative brain. *Med. Image Anal.* 12, 26–41. doi: 10.1016/j.media.2007.06.004

Balachandar, R., John, J. P., Saini, J., Kumar, K. J., Joshi, H., Sadanand, S., et al. (2014). A study of structural and functional connectivity in early Alzheimer's disease using rest fMRI and diffusion tensor imaging. *Int. J. Geriatr. Psychiatry*. doi: 10.1002/gps.4168. [Epub ahead of print].

Baron, C. A., and Beaulieu, C. (2014). Oscillating Gradient Spin-Echo (OGSE) diffusion tensor imaging of the human brain. *Magn. Reson. Med.* 72, 726–736. doi: 10.1002/mrm.24987

Basser, P. J., Mattiello, J., and Lebihan, D. (1994a). Estimation of the effective self-diffusion tensor from the NMR spin echo. *J. Magn. Reson. B* 103, 247–254. doi: 10.1006/jmrb.1994.1037

Basser, P. J., Mattiello, J., and Lebihan, D. (1994b). MR diffusion tensor spectroscopy and imaging. *Biophys. J.* 66, 259–267. doi: 10.1016/S0006-3495(94)80775-1

Basser, P. J., and Pierpaoli, C. (1996). Microstructural and physiological features of tissues elucidated by quantitative-diffusion-tensor MRI. *J. Magn. Reson. B* 111, 209–219. doi: 10.1006/jmrb.1996.0086

Batchelor, P. G., Atkinson, D., Hill, D. L., Calamante, F., and Connelly, A. (2003). Anisotropic noise propagation in diffusion tensor MRI sampling schemes. *Magn. Reson. Med.* 49, 1143–1151. doi: 10.1002/mrm.10491

Beaulieu, C. (2002). The basis of anisotropic water diffusion in the nervous system—a technical review. *NMR Biomed.* 15, 435–455. doi: 10.1002/nbm.782

Beaulieu, C., and Allen, P. S. (1994). Water diffusion in the giant axon of the squid: implications for diffusion-weighted MRI of the nervous system. *Magn. Reson. Med.* 32, 579–583. doi: 10.1002/mrm.1910320506

Benjamini, Y., and Hochberg, Y. (1995). Controlling the false discovery rate: a practical and powerful approach to multiple testing. *J. R. Stat. Soc. Series. B Stat. Methodol.* 57, 289–300.

Besseling, R. M., Jansen, J. F., Overvliet, G. M., Vaessen, M. J., Braakman, H. M., Hofman, P. A., et al. (2012). Tract specific reproducibility of tractography based morphology and diffusion metrics. *PLoS ONE* 7:e34125. doi: 10.1371/journal.pone.0034125

Bosch, B., Arenaza-Urquijo, E. M., Rami, L., Sala-Llonch, R., Junque, C., Sole-Padulles, C., et al. (2012). Multiple DTI index analysis in normal aging, amnestic MCI and AD. Relationship with neuropsychological performance. *Neurobiol. Aging* 33, 61–74. doi: 10.1016/j.neurobiolaging.2010.02.004

Brown, R. (1828). Microscopical observations of active molecules. *Edinburgh New Philos. J.*, 358–371.

Canu, E., Agosta, F., Spinelli, E. G., Magnani, G., Marcone, A., Scola, E., et al. (2013). White matter microstructural damage in Alzheimer's disease at different ages of onset. *Neurobiol. Aging* 34, 2331–2340. doi: 10.1016/j.neurobiolaging.2013.03.026

Carr, H. Y., and Purcell, E. M. (1954). Effects of diffusion on free precession in nuclear magnetic resonance experiments. *Phys. Rev.* 94, 630–638. doi: 10.1103/PhysRev.94.630

Choo, I. H., Lee, D. Y., Oh, J. S., Lee, J. S., Lee, D. S., Song, I. C., et al. (2010). Posterior cingulate cortex atrophy and regional cingulum disruption in mild cognitive impairment and Alzheimer's disease. *Neurobiol. Aging* 31, 772–779. doi: 10.1016/j.neurobiolaging.2008.06.015

Clark, C. M., Pontecorvo, M. J., Beach, T. G., Bedell, B. J., Coleman, R. E., Doraiswamy, P. M., et al. (2012). Cerebral PET with florbetapir compared with neuropathology at autopsy for detection of neuritic amyloid-beta plaques: a prospective cohort study. *Lancet Neurol.* 11, 669–678. doi: 10.1016/S1474-4422(12)70142-4

Coleman, M. P., and Freeman, M. R. (2010). Wallerian degeneration, wld(s), and nmnat. *Annu. Rev. Neurosci.* 33, 245–267. doi: 10.1146/annurev-neuro-060909-153248

Correia, M. M., Carpenter, T. A., and Williams, G. B. (2009). Looking for the optimal DTI acquisition scheme given a maximum scan time: are more b-values a waste of time? *Magn. Reson. Imaging* 27, 163–175. doi: 10.1016/j.mri.2008.06.011

Dale, A. M., Fischl, B., and Sereno, M. I. (1999). Cortical surface-based analysis. I. Segmentation and surface reconstruction. *Neuroimage* 9, 179–194. doi: 10.1006/nimg.1998.0395

Damoiseaux, J. S., Smith, S. M., Witter, M. P., Sanz-Arigita, E. J., Barkhof, F., Scheltens, P., et al. (2009). White matter tract integrity in aging and Alzheimer's disease. *Hum. Brain. Mapp.* 30, 1051–1059. doi: 10.1002/hbm.20563

Diaz-De-Grenu, L. Z., Acosta-Cabronero, J., Chong, Y. F., Pereira, J. M., Sajjadi, S. A., Williams, G. B., et al. (2014). A brief history of voxel-based grey matter analysis in Alzheimer's disease. *J. Alzheimers Dis.* 38, 647–659. doi: 10.3233/JAD-130362

Douaud, G., Jbabdi, S., Behrens, T. E., Menke, R. A., Gass, A., Monsch, A. U., et al. (2011). DTI measures in crossing-fibre areas: increased diffusion anisotropy reveals early white matter alteration in MCI and mild Alzheimer's disease. *Neuroimage* 55, 880–890. doi: 10.1016/j.neuroimage.2010.12.008

Du, A. T., Schuff, N., Amend, D., Laakso, M. P., Hsu, Y. Y., Jagust, W. J., et al. (2001). Magnetic resonance imaging of the entorhinal cortex and hippocampus in mild cognitive impairment and Alzheimer's disease. *J. Neurol. Neurosurg. Psychiatry* 71, 441–447. doi: 10.1136/jnnp.71.4.441

Edden, R. A., and Jones, D. K. (2011). Spatial and orientational heterogeneity in the statistical sensitivity of skeleton-based analyses of diffusion tensor MR imaging data. *J. Neurosci. Methods* 201, 213–219. doi: 10.1016/j.jneumeth.2011.07.025

Einstein, A. (1905). Über die von der molekularkinetischen Theorie der Wärme geforderte Bewegung von in ruhenden Flüssigkeiten suspendierten Teilchen. *Ann. Phys.* 322, 549–560. doi: 10.1002/andp.19053220806

Fazekas, F., Chawluk, J. B., Alavi, A., Hurtig, H. I., and Zimmerman, R. A. (1987). MR signal abnormalities at 1.5 T in Alzheimer's dementia and normal aging. *Am. J. Roentgenol.* 149, 351–356. doi: 10.2214/ajr.149.2.351

Fick, A. (1855). Ueber Diffusion. *Ann. Phys.* 170, 59–86. doi: 10.1002/andp.18551700105

Fieremans, E., Benitez, A., Jensen, J. H., Falangola, M. F., Tabesh, A., Deardorff, R. L., et al. (2013). Novel white matter tract integrity metrics sensitive to Alzheimer disease progression. *Am. J. Neuroradiol.* 34, 2105–2112. doi: 10.3174/ajnr.A3553

Fischl, B., Sereno, M. I., and Dale, A. M. (1999). Cortical surface-based analysis. II: Inflation, flattening, and a surface-based coordinate system. *Neuroimage* 9, 195–207. doi: 10.1006/nimg.1998.0396

Folstein, M. F., Folstein, S. E., and McHugh, P. R. (1975). "Mini-mental state." A practical method for grading the cognitive state of patients for the clinician. *J. Psychiatr. Res.* 12, 189–198. doi: 10.1016/0022-3956(75)90026-6

Frost, R., Jezzard, P., Douaud, G., Clare, S., Porter, D. A., and Miller, K. L. (2014). Scan time reduction for readout-segmented EPI using simultaneous multislice acceleration: diffusion-weighted imaging at 3 and 7 Tesla. *Magn. Reson. Med.* doi: 10.1002/mrm.25391. [Epub ahead of print].

Griswold, M. A., Jakob, P. M., Heidemann, R. M., Nittka, M., Jellus, V., Wang, J., et al. (2002). Generalized autocalibrating partially parallel acquisitions (GRAPPA). *Magn. Reson. Med.* 47, 1202–1210. doi: 10.1002/mrm.10171

Hahn, E. L. (1950). Spin echoes. *Phys. Rev.* 80, 580–594. doi: 10.1103/PhysRev.80.580

Huang, H., Fan, X., Weiner, M., Martin-Cook, K., Xiao, G., Davis, J., et al. (2012). Distinctive disruption patterns of white matter tracts in Alzheimer's disease with full diffusion tensor characterization. *Neurobiol. Aging* 33, 2029–2045. doi: 10.1016/j.neurobiolaging.2011.06.027

Ishii, K., Sasaki, H., Kono, A. K., Miyamoto, N., Fukuda, T., and Mori, E. (2005). Comparison of gray matter and metabolic reduction in mild Alzheimer's disease using FDG-PET and voxel-based morphometric MR studies. *Eur. J. Nucl. Med. Mol. Imaging* 32, 959–963. doi: 10.1007/s00259-004-1740-5

Jack, C. R. Jr., Bernstein, M. A., Borowski, B. J., Gunter, J. L., Fox, N. C., Thompson, P. M., et al. (2010). Update on the magnetic resonance imaging core of the Alzheimer's disease neuroimaging initiative. *Alzheimers Dement.* 6, 212–220. doi: 10.1016/j.jalz.2010.03.004

Jack, C. R. Jr., Dickson, D. W., Parisi, J. E., Xu, Y. C., Cha, R. H., O'brien, P. C., et al. (2002). Antemortem MRI findings correlate with hippocampal neuropathology in typical aging and dementia. *Neurology* 58, 750–757. doi: 10.1212/WNL.58.5.750

Jack, C. R. Jr., Shiung, M. M., Gunter, J. L., O'brien, P. C., Weigand, S. D., Knopman, D. S., et al. (2004). Comparison of different MRI brain atrophy rate measures with clinical disease progression in AD. *Neurology* 62, 591–600. doi: 10.1212/01.WNL.0000110315.26026.EF

Jbabdi, S., Behrens, T. E., and Smith, S. M. (2010). Crossing fibres in tract-based spatial statistics. *Neuroimage* 49, 249–256. doi: 10.1016/j.neuroimage.2009.08.039

Jensen, J. H., Helpern, J. A., Ramani, A., Lu, H., and Kaczynski, K. (2005). Diffusional kurtosis imaging: the quantification of non-gaussian water diffusion by means of magnetic resonance imaging. *Magn. Reson. Med.* 53, 1432–1440. doi: 10.1002/mrm.20508

Jicha, G. A., Parisi, J. E., Dickson, D. W., Johnson, K., Cha, R., Ivnik, R. J., et al. (2006). Neuropathologic outcome of mild cognitive impairment following progression to clinical dementia. *Arch. Neurol.* 63, 674–681. doi: 10.1001/archneur.63.5.674

Jones, D. K. (2004). The effect of gradient sampling schemes on measures derived from diffusion tensor MRI: a Monte Carlo study. *Magn. Reson. Med.* 51, 807–815. doi: 10.1002/mrm.20033

Jones, D. K., and Cercignani, M. (2010). Twenty-five pitfalls in the analysis of diffusion MRI data. *NMR Biomed.* 23, 803–820. doi: 10.1002/nbm.1543

Jones, D. K., Christiansen, K. F., Chapman, R. J., and Aggleton, J. P. (2013a). Distinct subdivisions of the cingulum bundle revealed by diffusion MRI fibre tracking: implications for neuropsychological investigations. *Neuropsychologia* 51, 67–78. doi: 10.1016/j.neuropsychologia.2012.11.018

Jones, D. K., Knosche, T. R., and Turner, R. (2013b). White matter integrity, fiber count, and other fallacies: the do's and don'ts of diffusion MRI. *Neuroimage* 73, 239–254. doi: 10.1016/j.neuroimage.2012.06.081

Keihaninejad, S., Ryan, N. S., Malone, I. B., Modat, M., Cash, D., Ridgway, G. R., et al. (2012). The importance of group-wise registration in tract based spatial statistics study of neurodegeneration: a simulation study in Alzheimer's disease. *PLoS ONE* 7:e45996. doi: 10.1371/journal.pone.0045996

Keihaninejad, S., Zhang, H., Ryan, N. S., Malone, I. B., Modat, M., Cardoso, M. J., et al. (2013). An unbiased longitudinal analysis framework for tracking white matter changes using diffusion tensor imaging with application to Alzheimer's disease. *Neuroimage* 72, 153–163. doi: 10.1016/j.neuroimage.2013.01.044

Kingsley, P. B. (2006a). Introduction to diffusion tensor imaging mathematics: Part I. Tensors, rotations, and eigenvectors. *Concept. Magn. Reson. A* 28A, 101–122. doi: 10.1002/cmr.a.20048

Kingsley, P. B. (2006b). Introduction to diffusion tensor imaging mathematics: Part II. Anisotropy, diffusion-weighting factors, and gradient encoding schemes. *Concept. Magn. Reson. A* 28A, 123–154. doi: 10.1002/cmr.a.20049

Kingsley, P. B. (2006c). Introduction to diffusion tensor imaging mathematics: Part III. Tensor calculation, noise, simulations, and optimization. *Concept. Magn. Reson. A* 28A, 155–179. doi: 10.1002/cmr.a.20050

Klein, A., Andersson, J., Ardekani, B. A., Ashburner, J., Avants, B., Chiang, M. C., et al. (2009). Evaluation of 14 nonlinear deformation algorithms applied to human brain MRI registration. *Neuroimage* 46, 786–802. doi: 10.1016/j.neuroimage.2008.12.037

Leemans, A., and Jones, D. K. (2009). The B-matrix must be rotated when correcting for subject motion in DTI data. *Magn. Reson. Med.* 61, 1336–1349. doi: 10.1002/mrm.21890

Lim, J. S., Park, Y. H., Jang, J. W., Park, S. Y., Kim, S., and Alzheimer's Disease Neuroimaging, I. (2014). Differential white matter connectivity in early mild cognitive impairment according to CSF biomarkers. *PLoS ONE* 9:e91400. doi: 10.1371/journal.pone.0091400

Mahoney, C. J., Malone, I. B., Ridgway, G. R., Buckley, A. H., Downey, L. E., Golden, H. L., et al. (2013). White matter tract signatures of the progressive aphasias. *Neurobiol. Aging* 34, 1687–1699. doi: 10.1016/j.neurobiolaging.2012.12.002

McKhann, G., Drachman, D., Folstein, M., Katzman, R., Price, D., and Stadlan, E. M. (1984). Clinical diagnosis of Alzheimer's disease: report of the NINCDS-ADRDA Work Group under the auspices of Department of Health and Human Services Task Force on Alzheimer's Disease. *Neurology* 34, 939–944. doi: 10.1212/WNL.34.7.939

Minoshima, S., Frey, K. A., Koeppe, R. A., Foster, N. L., and Kuhl, D. E. (1995). A diagnostic approach in Alzheimer's disease using three-dimensional stereotactic surface projections of fluorine-18-FDG PET. *J. Nucl. Med.* 36, 1238–1248.

Minoshima, S., Giordani, B., Berent, S., Frey, K. A., Foster, N. L., and Kuhl, D. E. (1997). Metabolic reduction in the posterior cingulate cortex in very early Alzheimer's disease. *Ann. Neurol.* 42, 85–94. doi: 10.1002/ana.410420114

Mitchell, J., Arnold, R., Dawson, K., Nestor, P. J., and Hodges, J. R. (2009). Outcome in subgroups of mild cognitive impairment (MCI) is highly predictable using a simple algorithm. *J. Neurol.* 256, 1500–1509. doi: 10.1007/s00415-009-5152-0

Molinuevo, J. L., Ripolles, P., Simo, M., Llado, A., Olives, J., Balasa, M., et al. (2014). White matter changes in preclinical Alzheimer's disease: a magnetic resonance imaging-diffusion tensor imaging study on cognitively normal older people with positive amyloid beta protein 42 levels. *Neurobiol. Aging*. doi: 10.1016/j.neurobiolaging.2014.05.027. [Epub ahead of print].

Nestor, P. J., Fryer, T. D., and Hodges, J. R. (2006). Declarative memory impairments in Alzheimer's disease and semantic dementia. *Neuroimage* 30, 1010–1020. doi: 10.1016/j.neuroimage.2005.10.008

Nestor, P. J., Fryer, T. D., Ikeda, M., and Hodges, J. R. (2003a). Retrosplenial cortex (BA 29/30) hypometabolism in mild cognitive impairment (prodromal Alzheimer's disease). *Eur. J. Neurosci.* 18, 2663–2667. doi: 10.1046/j.1460-9568.2003.02999.x

Nestor, P. J., Fryer, T. D., Smielewski, P., and Hodges, J. R. (2003b). Limbic hypometabolism in Alzheimer's disease and mild cognitive impairment. *Ann. Neurol.* 54, 343–351. doi: 10.1002/ana.10669

Nir, T. M., Jahanshad, N., Villalon-Reina, J. E., Toga, A. W., Jack, C. R., Weiner, M. W., et al. (2013). Effectiveness of regional DTI measures in distinguishing Alzheimer's disease, MCI, and normal aging. *Neuroimage Clin.* 3, 180–195. doi: 10.1016/j.nicl.2013.07.006

Oishi, K., and Lyketsos, C. (2014). Alzheimer's disease and the fornix. *Front. Aging Neurosci.* 6:241. doi: 10.3389/fnagi.2014.00241

Oouchi, H., Yamada, K., Sakai, K., Kizu, O., Kubota, T., Ito, H., et al. (2007). Diffusion anisotropy measurement of brain white matter is affected by voxel size: underestimation occurs in areas with crossing fibers. *Am. J. Neuroradiol.* 28, 1102–1106. doi: 10.3174/ajnr.A0488

Papadakis, N. G., Murrills, C. D., Hall, L. D., Huang, C. L., and Carpenter, A. T. (2000). Minimal gradient encoding for robust estimation of diffusion anisotropy. *Magn. Reson. Imaging* 18, 671–679. doi: 10.1016/S0730-725X(00)00151-X

Papez, J. W. (1937). A proposed mechanism of emotion. *Arch. Neurol. Psychiatry* 38, 725–743. doi: 10.1001/archneurpsyc.1937.02260220069003

Pasternak, O., Sochen, N., Gur, Y., Intrator, N., and Assaf, Y. (2009). Free water elimination and mapping from diffusion MRI. *Magn. Reson. Med.* 62, 717–730. doi: 10.1002/mrm.22055

Pengas, G., Hodges, J. R., Watson, P., and Nestor, P. J. (2010). Focal posterior cingulate atrophy in incipient Alzheimer's disease. *Neurobiol. Aging* 31, 25–33. doi: 10.1016/j.neurobiolaging.2008.03.014

Pengas, G., Williams, G. B., Acosta-Cabronero, J., Ash, T. W., Hong, Y. T., Izquierdo-Garcia, D., et al. (2012). The relationship of topographical memory performance to regional neurodegeneration in Alzheimer's disease. *Front. Aging Neurosci.* 4:17. doi: 10.3389/fnagi.2012.00017

Pruessmann, K. P., Weiger, M., Scheidegger, M. B., and Boesiger, P. (1999). SENSE: sensitivity encoding for fast MRI. *Magn. Reson. Med.* 42, 952–962.

Racine, A. M., Adluru, N., Alexander, A. L., Christian, B. T., Okonkwo, O. C., Oh, J., et al. (2014). Associations between white matter microstructure and amyloid burden in preclinical Alzheimer's disease: a multimodal imaging investigation. *Neuroimage Clin.* 4, 604–614. doi: 10.1016/j.nicl.2014.02.001

Rowley, J., Fonov, V., Wu, O., Eskildsen, S. F., Schoemaker, D., Wu, L., et al. (2013). White matter abnormalities and structural hippocampal disconnections in amnestic mild cognitive impairment and Alzheimer's disease. *PLoS ONE* 8:e74776. doi: 10.1371/annotation/c1e8aa6c-5e8a-4938-a0ed-1a7dc5ead757

Ryan, N. S., Keihaninejad, S., Shakespeare, T. J., Lehmann, M., Crutch, S. J., Malone, I. B., et al. (2013). Magnetic resonance imaging evidence for presymptomatic change in thalamus and caudate in familial Alzheimer's disease. *Brain* 136, 1399–1414. doi: 10.1093/brain/awt065

Schwarz, C. G., Reid, R. I., Gunter, J. L., Senjem, M. L., Przybelski, S. A., Zuk, S. M., et al. (2014). Improved DTI registration allows voxel-based analysis that outperforms tract-based spatial statistics. *Neuroimage* 94, 65–78. doi: 10.1016/j.neuroimage.2014.03.026

Smith, S. M., Jenkinson, M., Johansen-Berg, H., Rueckert, D., Nichols, T. E., Mackay, C. E., et al. (2006). Tract-based spatial statistics: voxelwise analysis of multi-subject diffusion data. *Neuroimage* 31, 1487–1505. doi: 10.1016/j.neuroimage.2006.02.024

Smith, S. M., Jenkinson, M., Woolrich, M. W., Beckmann, C. F., Behrens, T. E., Johansen-Berg, H., et al. (2004). Advances in functional and structural MR image analysis and implementation as FSL. *Neuroimage* 23(Suppl. 1), S208–S219. doi: 10.1016/j.neuroimage.2004.07.051

Smith, S. M., and Nichols, T. E. (2009). Threshold-free cluster enhancement: addressing problems of smoothing, threshold dependence and localisation in cluster inference. *Neuroimage* 44, 83–98. doi: 10.1016/j.neuroimage.2008.03.061

Stejskal, E. O., and Tanner, J. E. (1965). Spin diffusion measurements: spin echoes in the presence of a time−dependent field gradient. *J. Chem. Phys.* 42, 288–292. doi: 10.1063/1.1695690

Teipel, S. J., Reuter, S., Stieltjes, B., Acosta-Cabronero, J., Ernemann, U., Fellgiebel, A., et al. (2011). Multicenter stability of diffusion tensor imaging measures: a European clinical and physical phantom study. *Psychiatry Res.* 194, 363–371. doi: 10.1016/j.pscychresns.2011.05.012

Torrey, H. C. (1956). Bloch equations with diffusion terms. *Phys. Rev.* 104, 563–565. doi: 10.1103/PhysRev.104.563

Tuch, D. S. (2004). Q-ball imaging. *Magn. Reson. Med.* 52, 1358–1372. doi: 10.1002/mrm.20279

Verwey, N. A., Van Der Flier, W. M., Blennow, K., Clark, C., Sokolow, S., De Deyn, P. P., et al. (2009). A worldwide multicentre comparison of assays for cerebrospinal fluid biomarkers in Alzheimer's disease. *Ann. Clin. Biochem.* 46, 235–240. doi: 10.1258/acb.2009.008232

Villemagne, V. L., Pike, K. E., Chételat, G., Ellis, K. A., Mulligan, R. S., Bourgeat, P., et al. (2011). Longitudinal assessment of Aβ and cognition in aging and Alzheimer disease. *Ann. Neurol.* 69, 181–192. doi: 10.1002/ana.22248

Wedeen, V. J., Hagmann, P., Tseng, W. Y., Reese, T. G., and Weisskoff, R. M. (2005). Mapping complex tissue architecture with diffusion spectrum magnetic resonance imaging. *Magn. Reson. Med.* 54, 1377–1386. doi: 10.1002/mrm.20642

Winkler, A. M., Ridgway, G. R., Webster, M. A., Smith, S. M., and Nichols, T. E. (2014). Permutation inference for the general linear model. *Neuroimage* 92, 381–397. doi: 10.1016/j.neuroimage.2014.01.060

Winston, G. P. (2012). The physical and biological basis of quantitative parameters derived from diffusion MRI. *Quant. Imaging Med. Surg.* 2, 254–265. doi: 10.3978/j.issn.2223-4292.2012.12.05

Xing, D., Papadakis, N. G., Huang, C. L., Lee, V. M., Carpenter, T. A., and Hall, L. D. (1997). Optimised diffusion-weighting for measurement of apparent diffusion coefficient (ADC) in human brain. *Magn. Reson. Imaging* 15, 771–784. doi: 10.1016/S0730-725X(97)00037-4

Zarei, M., Damoiseaux, J. S., Morgese, C., Beckmann, C. F., Smith, S. M., Matthews, P. M., et al. (2009). Regional white matter integrity differentiates between vascular dementia and Alzheimer disease. *Stroke* 40, 773–779. doi: 10.1161/STROKEAHA.108.530832

Zhang, H., Schneider, T., Wheeler-Kingshott, C. A., and Alexander, D. C. (2012). NODDI: practical *in vivo* neurite orientation dispersion and density imaging of the human brain. *Neuroimage* 61, 1000–1016. doi: 10.1016/j.neuroimage.2012.03.072

Zhang, H., Yushkevich, P. A., Alexander, D. C., and Gee, J. C. (2006). Deformable registration of diffusion tensor MR images with explicit orientation optimization. *Med. Image Anal.* 10, 764–785. doi: 10.1016/j.media.2006.06.004

Conflict of Interest Statement: The authors declare that the research was conducted in the absence of any commercial or financial relationships that could be construed as a potential conflict of interest.

Received: 10 August 2014; accepted: 15 September 2014; published online: 02 October 2014.

*Citation: Acosta-Cabronero J and Nestor PJ (2014) Diffusion tensor imaging in Alzheimer's disease: insights into the limbic-diencephalic network and methodological considerations. Front. Aging Neurosci. **6**:266. doi: 10.3389/fnagi.2014.00266*

This article was submitted to the journal Frontiers in Aging Neuroscience.

frontiers in
AGING NEUROSCIENCE

MINI REVIEW ARTICLE
published: 11 September 2014
doi: 10.3389/fnagi.2014.00241

Alzheimer's disease and the fornix

Kenichi Oishi*[1] ***and Constantine G. Lyketsos*[2]**

[1] The Russell H. Morgan Department of Radiology and Radiological Science, School of Medicine, Johns Hopkins University, Baltimore, MD, USA
[2] Department of Psychiatry and Behavioral Sciences, Johns Hopkins Bayview and Johns Hopkins Medicine, Baltimore, MD, USA

Edited by:
P. Hemachandra Reddy, Oregen Health and Science University, USA

Reviewed by:
Mario Parra, University of Edinburgh, UK
Russell H. Swerdlow, University of Kansas Medical Center, USA

****Correspondence:***
Kenichi Oishi, The Russell H. Morgan Department of Radiology and Radiological Science, School of Medicine, Johns Hopkins University, 217 Traylor Building, 720 Rutland Avenue, Baltimore, MD 21205, USA
e-mail: koishi@mri.jhu.edu

Alzheimer's disease (AD) is the most common form of neurodegenerative dementia. Researchers have long been focused on the cortical pathology of AD, since the most important pathologic features are the senile plaques found in the cortex, and the neurofibrillary tangles and neuronal loss that begin in the entorhinal cortex and the hippocampus. In addition to these gray matter (GM) structures, histopathological studies indicate that the white matter (WM) is also a good target for both the early diagnosis of AD and for monitoring disease progression. The fornix is a WM bundle that constitutes a core element of the limbic circuits, and is one of the most important anatomical structures related to memory. Functional and anatomical features of the fornix have naturally captured researchers' attention as possible diagnostic and prognostic markers of AD. Indeed, neurodegeneration of the fornix has been histologically observed in AD, and growing evidence indicates that the alterations seen in the fornix are potentially a good marker to predict future conversion from mild cognitive impairment (MCI) to AD, and even from cognitively normal individuals to AD. The degree of alteration is correlated with the degree of memory impairment, indicating the potential for the use of the fornix as a functional marker. Moreover, there have been attempts to stimulate the fornix using deep brain stimulation (DBS) to augment cognitive function in AD, and ongoing research has suggested positive effects of DBS on brain glucose metabolism in AD patients. On the other hand, disease specificity for fornix degeneration, methodologies to evaluate fornix degeneration, and the clinical significance of the fornix DBS, especially for the long-term impact on the quality of life, are mostly unknown and need to be elucidated.

Keywords: Alzheimer's disease, mild cognitive impairment, diffusion tensor imaging, deep brain stimulation, fornix, limbic system, magnetic resonance imaging, white matter

INTRODUCTION

Alzheimer's disease (AD) research has targeted beta-amyloid and tau pathologies as diagnostic or progression markers. White matter (WM) shows less pathologic evidence of beta-amyloid or tau protein; nonetheless, alterations are seen in WM as well. Among WM bundles reportedly abnormal in AD, the fornix is especially interesting because robust and consistent alterations have been demonstrated. These could predict future gray matter (GM) atrophy and conversion from mild cognitive impairment (MCI) to AD, and even from cognitively normalcy to AD. Moreover, there are ongoing efforts to impact the biologic processes of AD by stimulating the fornix using deep brain stimulation (DBS). This review focuses on the fornix as a potential alternative diagnostic and prognostic marker, as well as a potential therapeutic target in AD.

WM ALTERATIONS SEEN IN AD

Histopathological studies have revealed various types of WM alterations in AD. Symmetrical WM changes compatible with incomplete infarction, independent of the GM changes, have been reported. These WM changes are partly explained by co-existing small vessel disease (Brun and Englund, 1986; Englund et al., 1988). WM changes are also related to cerebral amyloid angiopathy of AD, supporting a vascular contribution to the WM alterations (Haglund and Englund, 2002). Chronic hypoxia caused by vascular alterations might induce oxidative stress that could damage axonal membranes and myelin, and the reactivity of oligodendroglia to such damage (Back et al., 2011). However, in preclinical AD, WM alterations are independent of vascular alterations (de la Monte, 1989). In addition, degeneration of the WM was more obvious than that of the GM in early stages (de la Monte, 1989), suggesting that WM alteration precedes GM pathology. Indeed, the earliest disease-related anatomical changes have been observed in the axons and dendrites of AD animal model (Gunawardena and Goldstein, 2001; Pigino et al., 2003; Stokin et al., 2005; Chevalier-Larsen and Holzbaur, 2006). Therefore, mechanisms that cause the early pathological changes, aside from vascular alterations, might exist. According to the updated amyloid cascade hypothesis (Hardy and Selkoe, 2002), one of the high upstream events is production of soluble beta-amyloid oligomers, been discovered to be toxic to WM structure and function (Lue et al., 1999; Xu et al., 2001; Lee et al., 2004). This could be a major cause of the primary WM alterations in

AD (Roher et al., 2002; Chalmers et al., 2005) at least in early stages.

In addition to widespread WM alterations, structure-specific WM alterations have been observed, especially in limbic structures (Damoiseaux et al., 2009; Acosta-Cabronero et al., 2010; Smith et al., 2010; Liu et al., 2011). This might at least partly be explained by aberrant axonal transport due to misregulation of tau seen in early disease stage (Alonso et al., 1994; Ebneth et al., 1998; Dawson et al., 2010), with resultant tau aggregation that is closely related to neurodegeneration (Braak and Braak, 1995). Since the neurodegeneration of AD usually propagates systematically from the transentorhinal area to limbic structures, to neocortex at the most advanced stage, associated Wallerian-like degeneration (Bossy-Wetzel et al., 2004; Coleman, 2005) likely follows the same order, which might explain structure-specific WM alterations in AD (Bramblett et al., 1992).

Congruent with histopathological findings, WM alteration has been observed *in vivo* using various imaging modalities. Among these, diffusion tensor imaging (DTI) is one of the most effective modalities for the investigation of the WM anatomy since DTI has the ability to visualize WM fibers, based on directionality, and has the capability to provide detailed information about microscopic organization of the fibers. A meta-analysis of DTI studies indicated that WM alterations in AD are widespread throughout the brain (Sexton et al., 2011), particularly in limbic fibers, direct connections to the medial temporal lobe and the most vulnerable WM structures (Rose et al., 2000; Kantarci et al., 2001; Medina et al., 2006; Ringman et al., 2007; Stahl et al., 2007; Zhang et al., 2007; Zhou et al., 2008; Damoiseaux et al., 2009; Mielke et al., 2009; Salat et al., 2010). WM damage quantified by DTI has been correlated with atrophy in anatomically connected GM areas in AD patients, but the correlation was not robust in patients with amnestic MCI (Agosta et al., 2011). These findings support the histopathological observation that primary WM alterations may precede both GM degeneration, as well as secondary degenerative processes of the WM after neuronal loss. Based on the evidence about WM pathology in AD, Sachdev et al. proposed incorporating WM alterations into the model (Jack et al., 2010) of the pathophysiological cascade in AD (Sachdev et al., 2013).

WHY IS THE FORNIX IMPORTANT?

The fornices are WM bundles that originate from the bilateral hippocampi, merge at the midline of the brain, again divide into the left and right side, then into precommissural and postcommissural fibers, terminating at the septal nuclei, nucleus accumbens (precommissural fornix), and hypothalamus (postcommissural fornix). The fornix constitutes a core element of the limbic circuit that is vulnerable in AD, and one of the most important anatomical structures related to episodic memory, impairment of which is an initial symptom of AD (Hopper and Vogel, 1976; Mehraein and Rothemund, 1976). The fornix is also related to the cholinergic dysfunction characteristic of AD (Milner and Amaral, 1984; Wenk et al., 1987; Ransmayr et al., 1989; Sara, 1989; Schegg et al., 1989; Bunce et al., 2003; Colom et al., 2010). These functional and anatomical features have naturally captured researcher attention seeking diagnostic and prognostic markers of AD. Indeed, alterations of the fornix, such as demyelination or axonal loss, were reported as early as in 1976 (Hopper and Vogel, 1976) and have been consistently identified in AD (Ringman et al., 2007; Teipel et al., 2007; Mielke et al., 2009; Acosta-Cabronero et al., 2010; Salat et al., 2010; Liu et al., 2011; Douaud et al., 2013).

The other important anatomical feature of the fornix, compared to other WM areas, is its location. The body of the fornix is readily identifiable in the mid-sagittal plane of a brain MRI, without other WM structures adjacent to it. For research using brain MRI, this feature is particularly important. The thickness of the fornix can be easily measured on structural MRI, using T1- and T2-weighted images. Generally, identification of the boundaries of WM structures on structural MRI is not easy because the boundaries between adjacent WM structures are often invisible: the fornix is one of several exceptions. DTI is a good choice with which to identify the boundaries of WM bundles. Although a drawback of DTI is susceptibility to B0 distortion, especially for areas close to air cavities (e.g., nasal and oral cavities, frontal, ethmoid, sphenoid, and maxillary sinuses, and mastoid antrum), the fornix is less affected because there is a sufficient distance from the fornix to these air cavities. The anatomical location is also attractive from a neurosurgical point of view, since the fornix is surgically accessible for implanting electrodes for DBS (see Section Treatment), while other limbic structures are not easily accessible.

IMAGING STUDY OF THE FORNIX IN AD

REGION-OF-INTEREST STUDIES

Atrophy of the fornix measured using T1-weighted MRI has often been reported in AD (Callen et al., 2001; Copenhaver et al., 2006), although the onset of this atrophy has been a subject of debate. Fletcher et al. (2013) reported that atrophy of the fornix is a strong predictor of conversion from normal cognition to MCI or AD, suggesting that atrophy is present in the fornix at an early disease stage, before clinical manifestations. Abnormalities in the fornix have also been identified using DTI. A reduction of fractional anisotropy (FA) and an increase in diffusivity in the fornix is a robust and consistent finding in AD as demonstrated with manual ROI- analysis (Ringman et al., 2007; Mielke et al., 2009; Oishi et al., 2012), and the extent of the changes in DTI-derived parameters have been correlated with cognitive decline (Mielke et al., 2009; Oishi et al., 2012). Notably, FA reduction was already present in an asymptomatic gene carrier of familial AD who went on to develop AD in the future (Ringman et al., 2007). Longitudinal observation of cognitively normal elderly or individuals with amnestic MCI indicated that reduced fornix FA predicts conversion from normal cognition to amnestic MCI and from amnestic MCI to AD (Oishi et al., 2012). Moreover, lower fornix FA predicted later cognitive decline and hippocampal atrophy (Mielke et al., 2012). These studies suggest that volume loss and FA reduction of the fornix is one of the earliest anatomical changes in AD that happens before clinical manifestations.

WHOLE-BRAIN STUDIES

While region-of-interest analysis is a good choice when there are specific hypotheses (e.g., the fornix is affected in AD), the

drawback is the hypothesis dependency. To evaluate the spatial specificity of these findings, whole-brain analysis is a good choice. Voxel-based analysis is one of the most widely used approaches for whole-brain analysis, and has been used to evaluate regional abnormalities in WM volume (Li et al., 2008; Balthazar et al., 2009; Guo et al., 2010; Serra et al., 2010; Yoon et al., 2011) or in DTI-derived parameters, such as anisotropy and diffusivity (Head et al., 2004; Medina et al., 2006; Xie et al., 2006; Teipel et al., 2007; Zhang et al., 2009). Although cross-sectional group comparisons have identified widespread WM abnormalities in AD, the above studies failed to identify reduced volume or FA in the fornix, except for a study that used multivariate analysis (Teipel et al., 2007). The main explanation is probably inaccuracy in image normalization: the accuracy of automated non-linear registration used in these studies was limited for thin structures like the fornix, in which only a few pixels of misregistration cause significant loss of sensitivity to detect differences between groups (Oishi et al., 2009). A common approach to solve this problem is to apply Tract-Based Spatial Statistics (TBSS; Smith et al., 2006), in which WM tracts are "skeletonized" to summarize the anatomy of WM structures, from which statistics are calculated. Since the scalar values perpendicular to the skeleton are projected onto the skeleton, the effect of WM misregistration is largely ameliorated. Most of the whole brain TBSS studies applied to AD have, indeed, identified an FA reduction in the fornix, as well as in other limbic fibers, even in early-symptomatic patients or in individuals at high risk for developing AD (Damoiseaux et al., 2009; Honea et al., 2009; Stricker et al., 2009; Zarei et al., 2009; Acosta-Cabronero et al., 2010; Bosch et al., 2010; Smith et al., 2010; Liu et al., 2011; Douaud et al., 2013).

Application of large deformation diffeomorphic metric mapping (LDDMM) to DTI is another way to increase the sensitivity of whole-brain analysis, by which registration accuracy of the WM bundles could be increased. By using LDDMM, significant volume loss, FA reduction, and increases in mean diffusivity (MD) and radial diffusivity were detected in the fornix of individuals with AD (Oishi et al., 2011a,b). **Figure 1** is an example of such an analysis, designed to find brain areas with AD-specific WM alterations. This analysis indicates significant FA reduction in the fornix, the splenium of the corpus callosum, as well as in several small areas in superficial WM in the frontal lobes. To further increase sensitivity, multivariate models (Ashburner and Kloppel, 2011), such as principal component analysis (PCA; Teipel et al., 2007), or to apply voxel-grouping methods, such as atlas-based analysis (ABA; Oishi et al., 2009), were applied: all of these detected abnormalities in the fornix in AD. These whole-brain studies using sophisticated approaches consistently indicate the fornix as the "hotspot", in which the earliest anatomical changes begin ("Fornix First" (Landhuis, 2013)), and where the most robust changes are seen in AD.

PITFALLS AND ISSUES IN FORNIX IMAGE ANALYSIS

Misregistration

As mentioned previously, TBSS is currently a standard method by which to ameliorate WM tract misregistration. However, in patients with ventricular enlargement, like AD, the fornix is strongly deformed by the elevated and stretched corpus callosum, which results in uncorrectable misregistration, even with TBSS (Hattori et al., 2012). Therefore, careful interpretation is needed for AD studies. An inverse-projection of TBSS results onto original images is a simple method with which to identify invalid results caused by misregistration.

One solution to reduce the impact of erroneous mapping of voxels, and the consequent mis-parcellation of target structures, is to adopt multi-atlas approaches. Rather than using a single atlas for anatomical labeling, this approach uses multiple atlases to compute the likelihoods of labels, which are then fused to create an anatomical parcellation map for each image. This approach, which accounts for variations in brain anatomy, has been adapted to parcellate WM structures in DTI (Tang et al., 2014) with high accuracy even for individuals with ventricular enlargement. Applicability of the multi-atlas label fusion method to accurately define the fornix is a promising approach, which needs to be developed in the future with automated image analysis of AD.

Contamination of signal from cerebrospinal fluid

The fornix is prone to partial volume effects caused by contamination of signal from the cerebrospinal fluid (CSF), since it is a thin bundle that runs through the lateral ventricles that are filled with CSF. The effect is especially seen in individuals with AD because of atrophy, and thus, increased CSF signal in each voxel (Pfefferbaum and Sullivan, 2003; Metzler-Baddeley et al., 2012; Berlot et al., 2014). The greater diffusivity in CSF relative to the WM structures leads to false elevation of diffusivity values and a false reduction in FA values (Alexander et al., 2001; Vos et al., 2011). Therefore, reduced FA or increased diffusivity identified in the DTI studies of AD probably reflects pathological alterations of the fornix itself plus the partial volume effects caused by atrophy. Although this dual effect (atrophy + microstructural change) on the DTI parameters might make DTI a sensitive tool with which to detect early anatomical changes related to AD, it complicates inferences about the underlying anatomical changes. There have been several attempts to ameliorate the effects of CSF contamination in order to draw inferences about the microstructural changes in the WM structures, such as CSF-suppressed diffusion imaging (Kwong et al., 1991), or the free water elimination and mapping method that is applicable at the post-acquisition stage (Pasternak et al., 2009), both of which could detect alteration of the fornix in AD (Kantarci et al., 2010; Fletcher et al., 2014). Investigations of underlying changes in WM structures seem to suggest a good indication for the use these advanced methods (Metzler-Baddeley et al., 2012).

Cause of fornix degeneration and DTI parameters of choice

Since the contribution of each factor (see WM alterations seen in AD) to the degeneration of the fornix might vary depending on the degree of disease progression, longitudinal observation of the histopathology, from the preclinical to the advanced stages, is especially important. Use of the AD model in animals is an option for such longitudinal observation. A reduced size of the fornix is seen in the PDAPP mice (Gonzalez-Lima et al., 2001) and transgenic APP/PS1 mice (Delatour et al., 2006), and

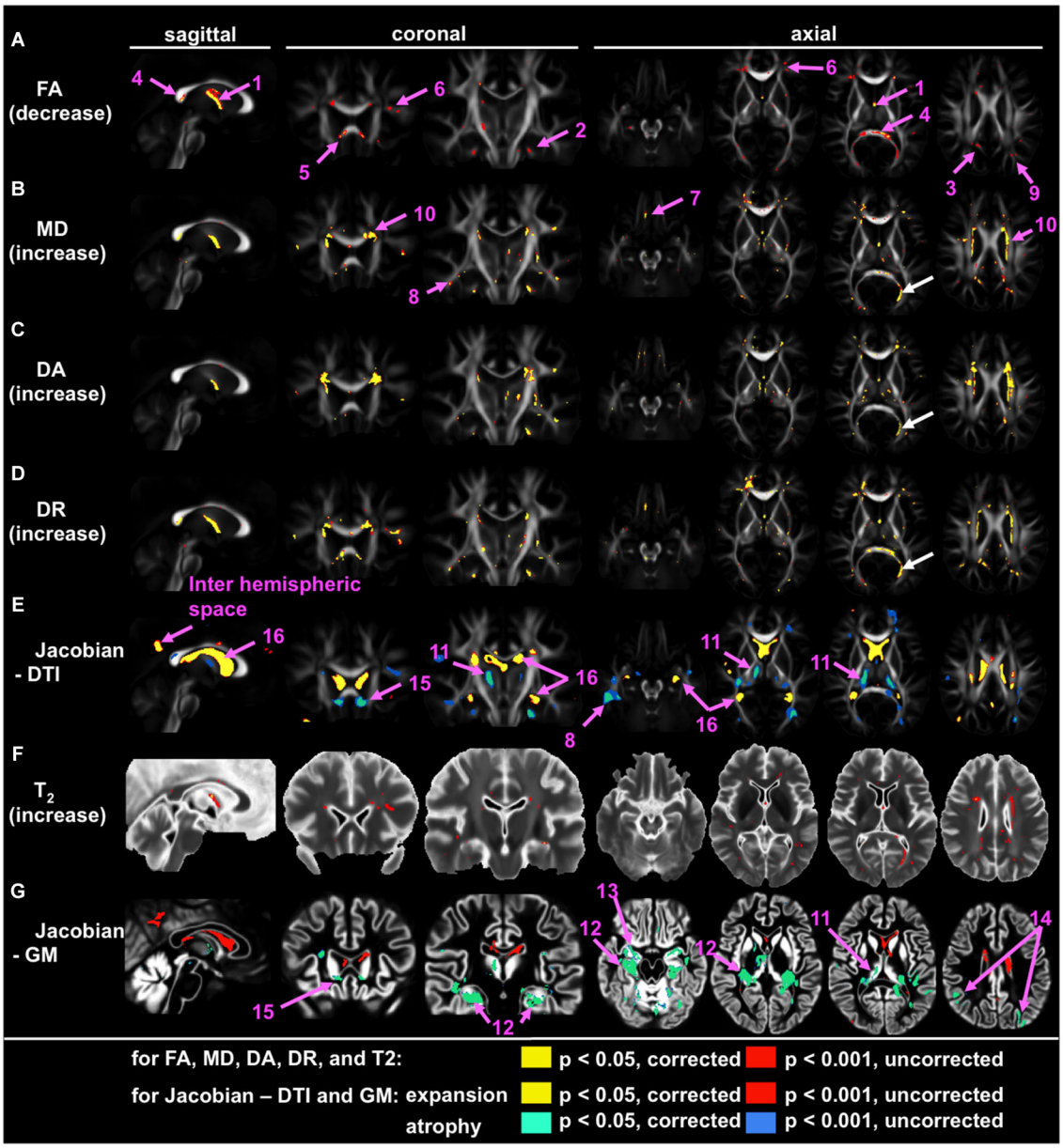

FIGURE 1 | Voxel-based group comparison between 19 AD and 22 cognitively normal age-matched control participants (NC), indicating the fornix as the hotspot. Areas with signal or volume alterations in AD compared to NC are shown as colored maps, overlaid on an averaged FA map **(A–E)**, an averaged T_2 map **(F)**, and an averaged GM segmentation map **(G)**. **(A)** Areas with reduced FA. **(B)** Areas with increased MD. **(C)** Areas with increased $\lambda_{\parallel}$. **(D)** Areas with increased $\lambda_{\perp}$. **(E)** Areas with an increased and decreased Jacobian, which was calculated from a transformation matrix obtained from the normalization of DTI. **(F)** Area with increased T_2. **(G)** Areas with increased and decreased Jacobian, which were calculated from a transformation matrix obtained from the normalization of a GM segmentation map. Pink arrows with numbers indicate: 1 = the fornix; 2 = the cingulum; 3 = the posterior cingulate gyrus white matter; 4 = splenium of the corpus callosum; 5 = genu of the corpus callosum; 6 = the prefrontal white matter; 7 = the orbitofrontal white matter; the temporal white matter; 9 = the parietal white matter; 10 = the periventricular area; 11 = the thalamus; 12 = the hippocampus; 13 = the entorhinal area; 14 = the parietal cortex; 15 = the area between the caudate head and the gyrus rectus; 16 = the lateral ventricle. White arrows show the misregistration seen in the left posterior horn of the lateral ventricle (From Oishi et al., 2011a; with permission).

immunohistochemistry shows the presence of increasing amyloidosis and related microgliosis and astrogliosis (Maheswaran et al., 2009). However, longitudinal changes in the size of the fornix differ depending on the type of AD model mice. Since type and variations in gene mutation are relevant to the pathophysiology of AD model animals, and considerable differences are seen between human AD and AD model animals, human *in vivo* neuroimaging studies are important to understand the pathophysiological underpinnings. For early AD, diffusion measures (MD and axial and radial diffusivities) could detect the widespread pathology

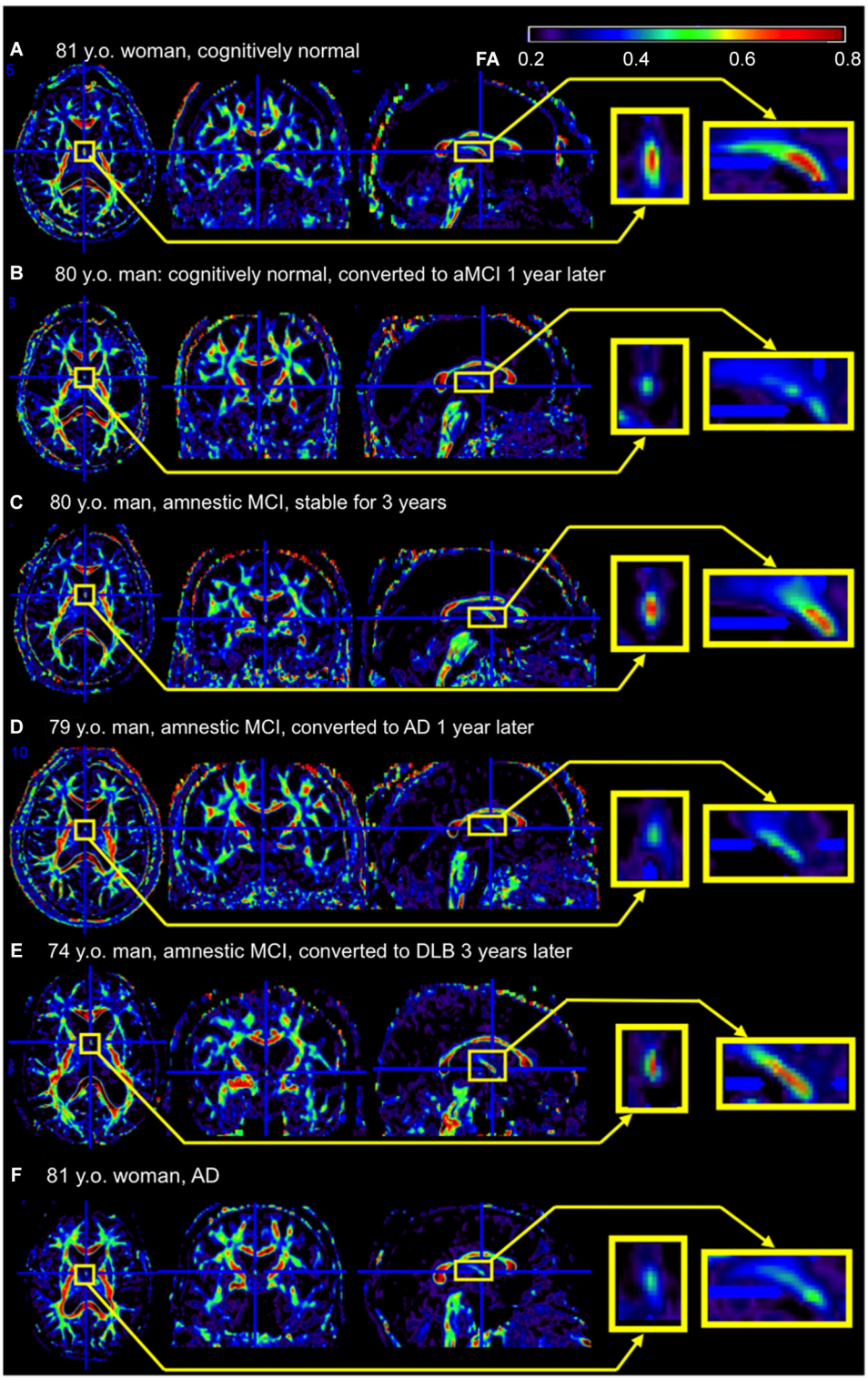

FIGURE 2 | Example of the fornix sign. The axial (left), coronal (middle), and sagittal (right) slices of the color-scaled FA map are shown with the magnified view of the fornix (yellow rectangle). **(A)** A cognitively normal 81-year-old woman without the fornix sign. The core part of the fornix appears yellow to red (FA 0.5–0.8). **(B)** A cognitively normal 80-year-old man with the fornix sign. The fornix appears green (FA < 0.5). He converted to amnestic MCI (aMCI) 1 year after the scan. **(C)** An 80-year-old man with aMCI without the fornix sign. He was stable during 3 years observation period after the scan. **(D)** A 79-year-old man with aMCI with the fornix sign. He converted to AD 1 year after the scan. **(E)** A 74-year-old man with aMCI without the fornix sign. He converted to dementia with Lewy bodies 3 years after the scan. **(F)** An 81-year-old woman with AD with the fornix sign. FA, fractional anisotropy.

of AD more sensitively than FA (Acosta-Cabronero et al., 2010; Oishi et al., 2011a). However, for the fornix, there seems to be a tendency that a decrease in FA is more sensitive than an increase in diffusivity measures. Whether there is a difference in pathophysiology between the fornix and other WM areas remains to be elucidated.

CLINICAL APPLICATIONS OF THE FINDINGS SEEN IN THE FORNIX

DIAGNOSIS AND PREDICTION

There are several hurdles when applying research findings to clinical practice. Research studies are based on selected participants with strict inclusion and exclusion criteria, and usually age- and gender-matched participants are recruited as controls. However, routine image-based diagnosis is almost exclusively performed by qualitative visual inspection, which is applied to each individual for clinical decision-making. Although numerous publications link AD to degeneration in the fornix, volume or the diffusivity are not quantified in daily practice because of the time-consuming nature of this process, and the inconsistent quantification methods used in research. The fornix sign, a discoloration of the fornix observed on color-coded FA maps of AD (Oishi et al., 2012), is one attempt to define qualitative image signs applicable to clinical images (**Figure 2**). Although sensitivity was limited, specificity was high. The positive likelihood ratio differentiating AD from controls and hence the ability to predict conversion of cognitively normal individuals to amnestic MCI, or from amnestic MCI to AD, was strong. However, further efforts are needed to identify appropriate scan parameters, cut-off values for the diagnosis and prediction, as well as to investigate degeneration in the fornix seen in other types of dementia.

Given that individuals with different types of memory complaints visit clinics, and physicians need to identify the etiology of the memory complaint for medical decision-making, the value of imaging signs that can separate AD from individuals with normal cognition are limited. Rather, clinically relevant imaging signs must provide clues that can be used to separate AD from other diseases that cause memory impairment. Indeed, the fornix might be affected by tumors, infections, inflammations (Yamamoto et al., 1990), metabolic abnormalities, vascular diseases (Molino et al., 2014), malformations, trauma, and hydrocephalus (Hattori et al., 2012) (for review, Thomas et al., 2011). Psychiatric diseases, such as schizophrenia and bipolar affective disorder (Oertel-Knöchel et al., 2014), or medical conditions, such as heart failure (Wu et al., 2007), also cause damage in the fornix. Less is known about the involvement of the fornix in other neurodegenerative dementias, such as frontotemporal dementia (FTD), dementia with Lewy bodies (DLB), and corticobasal degeneration (CBD). A study indicated substantial FA reduction in the fornix of the behavioral variant FTD that correlated with memory decline (Hornberger et al., 2012), and other studies have indicated that the fornix is affected in Pick's disease, FTD with tau mutation, or TAR-DNA-binding protein-43 type C pathology, but not for FTD caused by a progranulin mutation or with fused-in-sarcoma protein accumulation (Rohrer et al., 2011; Hornberger et al., 2012). Changes in the fornix were not detected by group comparison between DLB and control groups (Kantarci et al., 2010), or between CBD and control groups (Rohrer et al., 2011), but other research has reported reduced FA in the fornix of some DLB patients, especially for those with hippocampal atrophy (Firbank et al., 2011). The appropriate clinical use of imaging modalities for the evaluation of the fornix is, therefore, an important future direction.

TREATMENT

Inspired by neuroimaging evidence about early impairment of the limbic circuit seen in AD, and an unexpected augmentation of recollection during the hypothalamic/fornix DBS performed on a patient with obesity (Hamani et al., 2008), DBS of the fornix has been proposed as a novel therapy for AD to improve the neuronal circuitry involved in memory (Laxton et al., 2010). Based on the hypothesis that an important aspect of AD is that it is a system-level disorder affecting several integrated pathways related to memory and cognition (Lyketsos et al., 2012), and supported by rodent studies indicating that DBS improved memory and produced hippocampal neurogenesis (Toda et al., 2008; Hamani et al., 2011), a clinical trial evaluating the effect of DBS targeting the fornix is ongoing. Electrodes are placed adjacent to the fornix for high frequency electronic stimulation, with the hope of an immediate effect (direct effects of stimulating the fornix) and a disease-modifying effect (neurogenesis). Although its number of participants was small, the earlier Phase 1 trial suggested improved glucose metabolism in the posterior cortical areas, especially in cognitively improved participants after fornix DBS (Laxton et al., 2010; Smith et al., 2012). The assessment of long-term impact on cognitive function, activities of daily living, quality of life, and mortality is an important future direction.

ACKNOWLEDGMENTS

The authors thank Ms. Mary McAllister for help with manuscript editing. This study was supported by NIH grants, R01AG031348, R01AG042165 (Constantine G. Lyketsos), R21AG033774, P50AG 005146, and R01HD065955 (Kenichi Oishi). Its contents are solely the responsibility of the authors and do not necessarily represent the official view of NIA, NICHD, or NIH.

REFERENCES

Acosta-Cabronero, J., Williams, G. B., Pengas, G., and Nestor, P. J. (2010). Absolute diffusivities define the landscape of white matter degeneration in Alzheimer's disease. *Brain* 133, 529–539. doi: 10.1093/brain/awp257

Agosta, F., Pievani, M., Sala, S., Geroldi, C., Galluzzi, S., Frisoni, G. B., et al. (2011). White matter damage in Alzheimer disease and its relationship to gray matter atrophy. *Radiology* 258, 853–863. doi: 10.1148/radiol.10101284

Alexander, A. L., Hasan, K. M., Lazar, M., Tsuruda, J. S., and Parker, D. L. (2001). Analysis of partial volume effects in diffusion-tensor MRI. *Magn. Reson. Med.* 45, 770–780. doi: 10.1002/mrm.1105

Alonso, A. C., Zaidi, T., Grundke-Iqbal, I., and Iqbal, K. (1994). Role of abnormally phosphorylated tau in the breakdown of microtubules in Alzheimer disease. *Proc. Natl. Acad. Sci. U S A* 91, 5562–5566. doi: 10.1016/0197-4580(94)92603-4

Ashburner, J., and Kloppel, S. (2011). Multivariate models of inter-subject anatomical variability. *Neuroimage.* 56, 422–439. doi: 10.1016/j.neuroimage.2010.03.059

Back, S. A., Kroenke, C. D., Sherman, L. S., Lawrence, G., Gong, X., Taber, E. N., et al. (2011). White matter lesions defined by diffusion tensor imaging in older adults. *Ann. Neurol.* 70, 465–476. doi: 10.1002/ana.22484

Balthazar, M. L., Yasuda, C. L., Pereira, F. R., Pedro, T., Damasceno, B. P., and Cendes, F. (2009). Differences in grey and white matter atrophy in amnestic mild cognitive impairment and mild Alzheimer's disease. *Eur. J. Neurol.* 16, 468–474. doi: 10.1111/j.1468-1331.2008.02408.x

Berlot, R., Metzler-Baddeley, C., Jones, D. K., and O'sullivan, M. J. (2014). CSF contamination contributes to apparent microstructural alterations in mild cognitive impairment. *Neuroimage* 92, 27–35. doi: 10.1016/j.neuroimage.2014.01.031

Bosch, B., Arenaza-Urquijo, E. M., Rami, L., Sala-Llonch, R., Junqué, C., Solé-Padullés, C., et al. (2010). Multiple DTI index analysis in normal aging, amnestic MCI and AD. Relationship with neuropsychological performance. *Neurobiol. Aging* 33, 61–74. doi: 10.1016/j.neurobiolaging.2010.02.004

Bossy-Wetzel, E., Schwarzenbacher, R., and Lipton, S. A. (2004). Molecular pathways to neurodegeneration. *Nat. Med.* 10(Suppl.), S2–S9. doi: 10.1038/nm1067

Braak, H., and Braak, E. (1995). Staging of Alzheimer's disease-related neurofibrillary changes. *Neurobiol. Aging* 16, 271–278; discussion 278–284. doi: 10.1016/0197-4580(95)00021-6

Bramblett, G. T., Trojanowski, J. Q., and Lee, V. M. (1992). Regions with abundant neurofibrillary pathology in human brain exhibit a selective reduction in levels of binding-competent tau and accumulation of abnormal tau-isoforms (A68 proteins). *Lab. Invest.* 66, 212–222.

Brun, A., and Englund, E. (1986). A white matter disorder in dementia of the Alzheimer type: a pathoanatomical study. *Ann. Neurol.* 19, 253–262. doi: 10.1002/ana.410190306

Bunce, J. G., Sabolek, H. R., and Chrobak, J. J. (2003). Intraseptal infusion of oxotremorine impairs memory in a delayed-non-match-to-sample radial maze task. *Neuroscience* 121, 259–267. doi: 10.1016/s0306-4522(03)00462-7

Callen, D. J., Black, S. E., Gao, F., Caldwell, C. B., and Szalai, J. P. (2001). Beyond the hippocampus: MRI volumetry confirms widespread limbic atrophy in AD. *Neurology* 57, 1669–1674. doi: 10.1212/wnl.57.9.1669

Chalmers, K., Wilcock, G., and Love, S. (2005). Contributors to white matter damage in the frontal lobe in Alzheimer's disease. *Neuropathol. Appl. Neurobiol.* 31, 623–631. doi: 10.1111/j.1365-2990.2005.00678.x

Chevalier-Larsen, E., and Holzbaur, E. L. (2006). Axonal transport and neurodegenerative disease. *Biochim. Biophys. Acta* 1762, 1094–1108. doi: 10.1016/j.bbadis.2006.04.002

Coleman, M. (2005). Axon degeneration mechanisms: commonality amid diversity. *Nat. Rev. Neurosci.* 6, 889–898. doi: 10.1038/nrn1788

Colom, L. V., Castañeda, M. T., Bañuelos, C., Puras, G., García-Hernández, A., Hernandez, S., et al. (2010). Medial septal beta-amyloid 1-40 injections alter septo-hippocampal anatomy and function. *Neurobiol. Aging* 31, 46–57. doi: 10.1016/j.neurobiolaging.2008.05.006

Copenhaver, B. R., Rabin, L. A., Saykin, A. J., Roth, R. M., Wishart, H. A., Flashman, L. A., et al. (2006). The fornix and mammillary bodies in older adults with Alzheimer's disease, mild cognitive impairment and cognitive complaints: a volumetric MRI study. *Psychiatry Res.* 147, 93–103. doi: 10.1016/j.pscychresns.2006.01.015

Damoiseaux, J. S., Smith, S. M., Witter, M. P., Sanz-Arigita, E. J., Barkhof, F., Scheltens, P., et al. (2009). White matter tract integrity in aging and Alzheimer's disease. *Hum. Brain Mapp.* 30, 1051–1059. doi: 10.1002/hbm.20563

Dawson, H. N., Cantillana, V., Jansen, M., Wang, H., Vitek, M. P., Wilcock, D. M., et al. (2010). Loss of tau elicits axonal degeneration in a mouse model of Alzheimer's disease. *Neuroscience* 169, 516–531. doi: 10.1016/j.neuroscience.2010.04.037

de la Monte, S. M. (1989). Quantitation of cerebral atrophy in preclinical and end-stage Alzheimer's disease. *Ann. Neurol.* 25, 450–459. doi: 10.1002/ana.410250506

Delatour, B., Guégan, M., Volk, A., and Dhenain, M. (2006). In vivo MRI and histological evaluation of brain atrophy in APP/PS1 transgenic mice. *Neurobiol. Aging* 27, 835–847. doi: 10.1016/j.neurobiolaging.2005.04.011

Douaud, G., Menke, R. A., Gass, A., Monsch, A. U., Rao, A., Whitcher, B., et al. (2013). Brain microstructure reveals early abnormalities more than two years prior to clinical progression from mild cognitive impairment to Alzheimer's disease. *J. Neurosci.* 33, 2147–2155. doi: 10.1523/jneurosci.4437-12.2013

Ebneth, A., Godemann, R., Stamer, K., Illenberger, S., Trinczek, B., and Mandelkow, E. (1998). Overexpression of tau protein inhibits kinesin-dependent trafficking of vesicles, mitochondria and endoplasmic reticulum: implications for Alzheimer's disease. *J. Cell Biol.* 143, 777–794. doi: 10.1083/jcb.143.3.777

Englund, E., Brun, A., and Alling, C. (1988). White matter changes in dementia of Alzheimer's type. Biochemical and neuropathological correlates. *Brain* 111(Pt. 6), 1425–1439. doi: 10.1093/brain/111.6.1425

Firbank, M. J., Blamire, A. M., Teodorczuk, A., Teper, E., Mitra, D., and O'brien, J. T. (2011). Diffusion tensor imaging in Alzheimer's disease and dementia with Lewy bodies. *Psychiatry Res.* 194, 176–183. doi: 10.1016/j.pscychresns.2011.08.002

Fletcher, E., Carmichael, O., Pasternak, O., Maier-Hein, K. H., and Decarli, C. (2014). Early brain loss in circuits affected by Alzheimer's disease is predicted by fornix microstructure but may be independent of gray matter. *Front. Aging Neurosci.* 6:106. doi: 10.3389/fnagi.2014.00106

Fletcher, E., Raman, M., Huebner, P., Liu, A., Mungas, D., Carmichael, O., et al. (2013). Loss of fornix white matter volume as a predictor of cognitive impairment in cognitively normal elderly individuals. *JAMA Neurol.* 70, 1389–1395. doi: 10.1001/jamaneurol.2013.3263

Gonzalez-Lima, F., Berndt, J. D., Valla, J. E., Games, D., and Reiman, E. M. (2001). Reduced corpus callosum, fornix and hippocampus in PDAPP transgenic mouse model of Alzheimer's disease. *Neuroreport* 12, 2375–2379. doi: 10.1097/00001756-200108080-00018

Gunawardena, S., and Goldstein, L. S. (2001). Disruption of axonal transport and neuronal viability by amyloid precursor protein mutations in Drosophila. *Neuron* 32, 389–401. doi: 10.1016/s0896-6273(01)00496-2

Guo, X., Wang, Z., Li, K., Li, Z., Qi, Z., Jin, Z., et al. (2010). Voxel-based assessment of gray and white matter volumes in Alzheimer's disease. *Neurosci. Lett.* 468, 146–150. doi: 10.1016/j.neulet.2009.10.086

Haglund, M., and Englund, E. (2002). Cerebral amyloid angiopathy, white matter lesions and Alzheimer encephalopathy - a histopathological assessment. *Dement. Geriatr. Cogn. Disord.* 14, 161–166. doi: 10.1159/000063606

Hamani, C., Mcandrews, M. P., Cohn, M., Oh, M., Zumsteg, D., Shapiro, C. M., et al. (2008). Memory enhancement induced by hypothalamic/fornix deep brain stimulation. *Ann. Neurol.* 63, 119–123. doi: 10.1002/ana.21295

Hamani, C., Stone, S. S., Garten, A., Lozano, A. M., and Winocur, G. (2011). Memory rescue and enhanced neurogenesis following electrical stimulation of the anterior thalamus in rats treated with corticosterone. *Exp. Neurol.* 232, 100–104. doi: 10.1016/j.expneurol.2011.08.023

Hardy, J., and Selkoe, D. J. (2002). The amyloid hypothesis of Alzheimer's disease: progress and problems on the road to therapeutics. *Science* 297, 353–356. doi: 10.1126/science.1072994

Hattori, T., Ito, K., Aoki, S., Yuasa, T., Sato, R., Ishikawa, M., et al. (2012). White matter alteration in idiopathic normal pressure hydrocephalus: tract-based spatial statistics study. *AJNR Am. J. Neuroradiol.* 33, 97–103. doi: 10.3174/ajnr.a2706

Head, D., Buckner, R. L., Shimony, J. S., Williams, L. E., Akbudak, E., Conturo, T. E., et al. (2004). Differential vulnerability of anterior white matter in nondemented aging with minimal acceleration in dementia of the Alzheimer type: evidence from diffusion tensor imaging. *Cereb. Cortex* 14, 410–423. doi: 10.1093/cercor/bhh003

Honea, R. A., Vidoni, E., Harsha, A., and Burns, J. M. (2009). Impact of APOE on the healthy aging brain: a voxel-based MRI and DTI study. *J. Alzheimers Dis.* 18, 553–564. doi: 10.3233/JAD-2009-1163

Hopper, M. W., and Vogel, F. S. (1976). The limbic system in Alzheimer's disease. A neuropathologic investigation. *Am. J. Pathol.* 85, 1–20.

Hornberger, M., Wong, S., Tan, R., Irish, M., Piguet, O., Kril, J., et al. (2012). In vivo and post-mortem memory circuit integrity in frontotemporal dementia and Alzheimer's disease. *Brain* 135, 3015–3025. doi: 10.1093/brain/aws239

Jack, C. R. Jr., Knopman, D. S., Jagust, W. J., Shaw, L. M., Aisen, P. S., Weiner, M. W., et al. (2010). Hypothetical model of dynamic biomarkers of the Alzheimer's pathological cascade. *Lancet Neurol.* 9, 119–128. doi: 10.1016/s1474-4422(09)70299-6

Kantarci, K., Avula, R., Senjem, M. L., Samikoglu, A. R., Zhang, B., Weigand, S. D., et al. (2010). Dementia with Lewy bodies and Alzheimer disease: neurodegenerative patterns characterized by DTI. *Neurology* 74, 1814–1821. doi: 10.1212/wnl.0b013e3181e0f7cf

Kantarci, K., Jack, C. R. Jr., Xu, Y. C., Campeau, N. G., O'brien, P. C., Smith, G. E., et al. (2001). Mild cognitive impairment and Alzheimer disease: regional diffusivity of water. *Radiology* 219, 101–107. doi: 10.1148/radiology.219.1.r01ap14101

Kwong, K. K., Mckinstry, R. C., Chien, D., Crawley, A. P., Pearlman, J. D., and Rosen, B. R. (1991). CSF-suppressed quantitative single-shot diffusion imaging. *Magn. Reson. Med.* 21, 157–163. doi: 10.1002/mrm.1910210120

Landhuis, E. (2013). *Fornix First—Atrophy Foreshadows Decline in Normal Aging?* Available online at: http://www.alzforum.org/news/research-news/fornix-first-atrophy-foreshadows-decline-normal-aging. Accessed on June 19 2014.

Laxton, A. W., Tang-Wai, D. F., Mcandrews, M. P., Zumsteg, D., Wennberg, R., Keren, R., et al. (2010). A phase I trial of deep brain stimulation of memory circuits in Alzheimer's disease. *Ann. Neurol.* 68, 521–534. doi: 10.1002/ana.22089

Lee, J. T., Xu, J., Lee, J. M., Ku, G., Han, X., Yang, D. I., et al. (2004). Amyloid-beta peptide induces oligodendrocyte death by activating the neutral sphingomyelinase-ceramide pathway. *J. Cell Biol.* 164, 123–131. doi: 10.1083/jcb.200307017

Li, S., Pu, F., Shi, F., Xie, S., Wang, Y., and Jiang, T. (2008). Regional white matter decreases in Alzheimer's disease using optimized voxel-based morphometry. *Acta Radiol.* 49, 84–90. doi: 10.1080/02841850701627181

Liu, Y., Spulber, G., Lehtimäki, K. K., Könönen, M., Hallikainen, I., Gröhn, H., et al. (2011). Diffusion tensor imaging and tract-based spatial statistics in Alzheimer's disease and mild cognitive impairment. *Neurobiol. Aging* 32, 1558–1571. doi: 10.1016/j.neurobiolaging.2009.10.006

Lue, L. F., Kuo, Y. M., Roher, A. E., Brachova, L., Shen, Y., Sue, L., et al. (1999). Soluble amyloid beta peptide concentration as a predictor of synaptic change in Alzheimer's disease. *Am. J. Pathol.* 155, 853–862. doi: 10.1016/s0002-9440(10)65184-x

Lyketsos, C. G., Targum, S. D., Pendergrass, J. C., and Lozano, A. M. (2012). Deep brain stimulation: a novel strategy for treating Alzheimer's disease. *Innov. Clin. Neurosci.* 9, 10–17.

Maheswaran, S., Barjat, H., Rueckert, D., Bate, S. T., Howlett, D. R., Tilling, L., et al. (2009). Longitudinal regional brain volume changes quantified in normal aging and Alzheimer's APP x PS1 mice using MRI. *Brain Res.* 1270, 19–32. doi: 10.1016/j.brainres.2009.02.045

Medina, D., Detoledo-Morrell, L., Urresta, F., Gabrieli, J. D., Moseley, M., Fleischman, D., et al. (2006). White matter changes in mild cognitive impairment and AD: a diffusion tensor imaging study. *Neurobiol. Aging* 27, 663–672. doi: 10.1016/j.neurobiolaging.2005.03.026

Mehraein, P., and Rothemund, E. (1976). [Neuroanatomical correlates of the amnestic syndrome (author's transl)]. *Arch. Psychiatr. Nervenkr.* 222, 153–176.

Metzler-Baddeley, C., O'sullivan, M. J., Bells, S., Pasternak, O., and Jones, D. K. (2012). How and how not to correct for CSF-contamination in diffusion MRI. *Neuroimage* 59, 1394–1403. doi: 10.1016/j.neuroimage.2011.08.043

Mielke, M. M., Kozauer, N. A., Chan, K. C., George, M., Toroney, J., Zerrate, M., et al. (2009). Regionally-specific diffusion tensor imaging in mild cognitive impairment and Alzheimer's disease. *Neuroimage* 46, 47–55. doi: 10.1016/j.neuroimage.2009.01.054

Mielke, M. M., Okonkwo, O. C., Oishi, K., Mori, S., Tighe, S., Miller, M. I., et al. (2012). Fornix integrity and hippocampal volume predict memory decline and progression to Alzheimer's disease. *Alzheimers Dement.* 8, 105–113. doi: 10.1016/j.jalz.2011.05.2416

Milner, T. A., and Amaral, D. G. (1984). Evidence for a ventral septal projection to the hippocampal formation of the rat. *Exp. Brain Res.* 55, 579–585. doi: 10.1007/bf00235290

Molino, I., Cavaliere, C., Salvatore, E., Quarantelli, M., Colucci, L., and Fasanaro, A. M. (2014). Is anterior communicating artery syndrome related to fornix lesions? *J. Alzheimers Dis.* 42, S199–S204. doi: 10.3233/JAD-132648

Oertel-Knöchel, V., Reinke, B., Alves, G., Jurcoane, A., Wenzler, S., Prvulovic, D., et al. (2014). Frontal white matter alterations are associated with executive cognitive function in euthymic bipolar patients. *J. Affect. Disord.* 155, 223–233. doi: 10.1016/j.jad.2013.11.004

Oishi, K., Akhter, K., Mielke, M., Ceritoglu, C., Zhang, J., Jiang, H., et al. (2011a). Multi-modal MRI analysis with disease-specific spatial filtering: initial testing to predict mild cognitive impairment patients who convert to Alzheimer's disease. *Front. Neurol.* 2:54. doi: 10.3389/fneur.2011.00054

Oishi, K., Faria, A., Jiang, H., Li, X., Akhter, K., Zhang, J., et al. (2009). Atlas-based whole brain white matter analysis using large deformation diffeomorphic metric mapping: application to normal elderly and Alzheimer's disease participantstlas. *Neuroimage* 46, 486–499. doi: 10.1016/j.neuroimage.2009.01.002

Oishi, K., Mielke, M. M., Albert, M., Lyketsos, C. G., and Mori, S. (2011b). DTI analyses and clinical applications in Alzheimer's disease. *J. Alzheimers Dis.* 26(Suppl. 3), 287–296. doi: 10.3233/JAD-2011-0007

Oishi, K., Mielke, M. M., Albert, M., Lyketsos, C. G., and Mori, S. (2012). The fornix sign: a potential sign for Alzheimer's disease based on diffusion tensor imaging. *J. Neuroimaging* 22, 365–374. doi: 10.1111/j.1552-6569.2011.00633.x

Pasternak, O., Sochen, N., Gur, Y., Intrator, N., and Assaf, Y. (2009). Free water elimination and mapping from diffusion MRI. *Magn. Reson. Med.* 62, 717–730. doi: 10.1002/mrm.22055

Pfefferbaum, A., and Sullivan, E. V. (2003). Increased brain white matter diffusivity in normal adult aging: relationship to anisotropy and partial voluming. *Magn. Reson. Med.* 49, 953–961. doi: 10.1002/mrm.10452

Pigino, G., Morfini, G., Pelsman, A., Mattson, M. P., Brady, S. T., and Busciglio, J. (2003). Alzheimer's presenilin 1 mutations impair kinesin-based axonal transport. *J. Neurosci.* 23, 4499–4508.

Ransmayr, G., Cervera, P., Hirsch, E., Ruberg, M., Hersh, L. B., Duyckaerts, C., et al. (1989). Choline acetyltransferase-like immunoreactivity in the hippocampal formation of control subjects and patients with Alzheimer's disease. *Neuroscience* 32, 701–714. doi: 10.1016/0306-4522(89)90291-1

Ringman, J. M., O'neill, J., Geschwind, D., Medina, L., Apostolova, L. G., Rodriguez, Y., et al. (2007). Diffusion tensor imaging in preclinical and presymptomatic carriers of familial Alzheimer's disease mutations. *Brain* 130, 1767–1776. doi: 10.1093/brain/awm102

Roher, A. E., Weiss, N., Kokjohn, T. A., Kuo, Y. M., Kalback, W., Anthony, J., et al. (2002). Increased A beta peptides and reduced cholesterol and myelin proteins characterize white matter degeneration in Alzheimer's disease. *Biochemistry* 41, 11080–11090. doi: 10.1021/bi026173d

Rohrer, J. D., Lashley, T., Schott, J. M., Warren, J. E., Mead, S., Isaacs, A. M., et al. (2011). Clinical and neuroanatomical signatures of tissue pathology in frontotemporal lobar degeneration. *Brain* 134, 2565–2581. doi: 10.1093/brain/awr198

Rose, S. E., Chen, F., Chalk, J. B., Zelaya, F. O., Strugnell, W. E., Benson, M., et al. (2000). Loss of connectivity in Alzheimer's disease: an evaluation of white matter tract integrity with colour coded MR diffusion tensor imaging. *J. Neurol. Neurosurg. Psychiatry* 69, 528–530. doi: 10.1136/jnnp.69.4.528

Sachdev, P. S., Zhuang, L., Braidy, N., and Wen, W. (2013). Is Alzheimer's a disease of the white matter? *Curr. Opin. Psychiatry* 26, 244–251. doi: 10.1097/YCO.0b013e32835ed6e8

Salat, D. H., Tuch, D. S., Van Der Kouwe, A. J., Greve, D. N., Pappu, V., Lee, S. Y., et al. (2010). White matter pathology isolates the hippocampal formation in Alzheimer's disease. *Neurobiol. Aging* 31, 244–256. doi: 10.1016/j.neurobiolaging.2008.03.013

Sara, S. J. (1989). Noradrenergic-cholinergic interaction: its possible role in memory dysfunction associated with senile dementia. *Arch. Gerontol. Geriatr. Suppl.* 1, 99–108.

Schegg, K. M., Nielsen, S., Zweig, R. M., and Peacock, J. H. (1989). Decrease in membrane-bound G4 form of acetylcholinesterase in postmortem Alzheimer brain. *Prog. Clin. Biol. Res.* 317, 437–452.

Serra, L., Cercignani, M., Lenzi, D., Perri, R., Fadda, L., Caltagirone, C., et al. (2010). Grey and white matter changes at different stages of Alzheimer's disease. *J. Alzheimers Dis.* 19, 147–159. doi: 10.3233/JAD-2010-1223

Sexton, C. E., Kalu, U. G., Filippini, N., Mackay, C. E., and Ebmeier, K. P. (2011). A meta-analysis of diffusion tensor imaging in mild cognitive impairment and Alzheimer's disease. *Neurobiol. Aging* 32, 2322.e5–2322.e18. doi: 10.1016/j.neurobiolaging.2010.05.019

Smith, C. D., Chebrolu, H., Andersen, A. H., Powell, D. A., Lovell, M. A., Xiong, S., et al. (2010). White matter diffusion alterations in normal women at risk of Alzheimer's disease. *Neurobiol. Aging* 31, 1122–1131. doi: 10.1016/j.neurobiolaging.2008.08.006

Smith, S. M., Jenkinson, M., Johansen-Berg, H., Rueckert, D., Nichols, T. E., Mackay, C. E., et al. (2006). Tract-based spatial statistics: voxelwise analysis of multi-subject diffusion data. *Neuroimage* 31, 1487–1505. doi: 10.1016/j.neuroimage.2006.02.024

Smith, G. S., Laxton, A. W., Tang-Wai, D. F., Mcandrews, M. P., Diaconescu, A. O., Workman, C. I., et al. (2012). Increased cerebral metabolism after 1 year of deep brain stimulation in Alzheimer disease. *Arch. Neurol.* 69, 1141–1148. doi: 10.1001/archneurol.2012.590

Stahl, R., Dietrich, O., Teipel, S. J., Hampel, H., Reiser, M. F., and Schoenberg, S. O. (2007). White matter damage in Alzheimer disease and mild cognitive impairment: assessment with diffusion-tensor MR imaging and parallel imaging techniques. *Radiology* 243, 483–492. doi: 10.1148/radiol.2432051714

Stokin, G. B., Lillo, C., Falzone, T. L., Brusch, R. G., Rockenstein, E., Mount, S. L., et al. (2005). Axonopathy and transport deficits early in the pathogenesis of Alzheimer's disease. *Science* 307, 1282–1288. doi: 10.1126/science.1105681

Stricker, N. H., Schweinsburg, B. C., Delano-Wood, L., Wierenga, C. E., Bangen, K. J., Haaland, K. Y., et al. (2009). Decreased white matter integrity in late-myelinating fiber pathways in Alzheimer's disease supports retrogenesis. *Neuroimage* 45, 10–16. doi: 10.1016/j.neuroimage.2008.11.027

Tang, X., Yoshida, S., Hsu, J., Huisman, T. A., Faria, A. V., Oishi, K., et al. (2014). Multi-contrast multi-atlas parcellation of diffusion tensor imaging of the human brain. *PLoS One* 9:e96985. doi: 10.1371/journal.pone.0096985

Teipel, S. J., Stahl, R., Dietrich, O., Schoenberg, S. O., Perneczky, R., Bokde, A. L., et al. (2007). Multivariate network analysis of fiber tract integrity in Alzheimer's disease. *Neuroimage* 34, 985–995. doi: 10.1016/j.neuroimage.2006.07.047

Thomas, A. G., Koumellis, P., and Dineen, R. A. (2011). The fornix in health and disease: an imaging review. *Radiographics* 31, 1107–1121. doi: 10.1148/rg.314105729

Toda, H., Hamani, C., Fawcett, A. P., Hutchison, W. D., and Lozano, A. M. (2008). The regulation of adult rodent hippocampal neurogenesis by deep brain stimulation. *J. Neurosurg.* 108, 132–138. doi: 10.3171/jns/2008/108/01/0132

Vos, S. B., Jones, D. K., Viergever, M. A., and Leemans, A. (2011). Partial volume effect as a hidden covariate in DTI analyses. *Neuroimage* 55, 1566–1576. doi: 10.1016/j.neuroimage.2011.01.048

Wenk, G., Hughey, D., Boundy, V., Kim, A., Walker, L., and Olton, D. (1987). Neurotransmitters and memory: role of cholinergic, serotonergic and noradrenergic systems. *Behav. Neurosci.* 101, 325–332. doi: 10.1037//0735-7044.101.3.325

Wu, M., Rosano, C., Lopez-Garcia, P., Carter, C. S., and Aizenstein, H. J. (2007). Optimum template selection for atlas-based segmentation. *Neuroimage* 34, 1612–1618. doi: 10.1016/j.neuroimage.2006.07.050

Xie, S., Xiao, J. X., Gong, G. L., Zang, Y. F., Wang, Y. H., Wu, H. K., et al. (2006). Voxel-based detection of white matter abnormalities in mild Alzheimer disease. *Neurology* 66, 1845–1849. doi: 10.1212/01.wnl.0000219625.77625.aa

Xu, J., Chen, S., Ahmed, S. H., Chen, H., Ku, G., Goldberg, M. P., et al. (2001). Amyloid-beta peptides are cytotoxic to oligodendrocytes. *J. Neurosci.* 21: RC118.

Yamamoto, T., Kurobe, H., Kawamura, J., Hashimoto, S., and Nakamura, M. (1990). Subacute dementia with necrotising encephalitis selectively involving the fornix and splenium. Retrograde development of Alzheimer's neurofibrillar tangles in the subiculum. *J. Neurol. Sci.* 96, 159–172. doi: 10.1016/0022-510x(90)90129-b

Yoon, B., Shim, Y. S., Hong, Y. J., Koo, B. B., Kim, Y. D., Lee, K. O., et al. (2011). Comparison of diffusion tensor imaging and voxel-based morphometry to detect white matter damage in Alzheimer's disease. *J. Neurol. Sci.* 302, 89–95. doi: 10.1016/j.jns.2010.11.012

Zarei, M., Damoiseaux, J. S., Morgese, C., Beckmann, C. F., Smith, S. M., Matthews, P. M., et al. (2009). Regional white matter integrity differentiates between vascular dementia and Alzheimer disease. *Stroke* 40, 773–779. doi: 10.1161/strokeaha.108.530832

Zhang, Y., Schuff, N., Du, A. T., Rosen, H. J., Kramer, J. H., Gorno-Tempini, M. L., et al. (2009). White matter damage in frontotemporal dementia and Alzheimer's disease measured by diffusion MRI. *Brain* 132, 2579–2592. doi: 10.1093/brain/awp071

Zhang, Y., Schuff, N., Jahng, G. H., Bayne, W., Mori, S., Schad, L., et al. (2007). Diffusion tensor imaging of cingulum fibers in mild cognitive impairment and Alzheimer disease. *Neurology* 68, 13–19. doi: 10.1212/01.wnl.0000250326.77323.01

Zhou, Y., Dougherty, J. H. Jr., Hubner, K. F., Bai, B., Cannon, R. L., and Hutson, R. K. (2008). Abnormal connectivity in the posterior cingulate and hippocampus in early Alzheimer's disease and mild cognitive impairment. *Alzheimers Dement.* 4, 265–270. doi: 10.1016/j.jalz.2008.04.006

Conflict of Interest Statement: Constantine G. Lyketsos has received support from the following organizations: Associated Jewish Federation of Baltimore, Weinberg Foundation, Forest, Glaxo-Smith-Kline, Eisai, Pfizer, Astra-Zeneca, Lilly, Ortho-McNeil, Bristol-Myers, and Novartis. Constantine G. Lyketsos has served as a consultant/advisor for Astra-Zeneca, Glaxo-Smith-Kline, Eisai, Novartis, Forest, Supernus, Adlyfe, Takeda, Wyeth, Lundbeck, Merz, Lilly, and Genentech. Constantine G. Lyketsos has received honorarium or travel support from Pfizer, Forest, Glaxo-Smith-Kline, and Health Monitor. This arrangement has been approved by the Johns Hopkins University in accordance with its conflict of interest policies.

Received: 02 July 2014; accepted: 22 August 2014; published online: 11 September 2014.
*Citation: Oishi K and Lyketsos CG (2014) Alzheimer's disease and the fornix. Front. Aging Neurosci. **6**:241. doi: 10.3389/fnagi.2014.00241*
This article was submitted to the journal Frontiers in Aging Neuroscience.

Advantages of publishing in Frontiers

OPEN ACCESS
Articles are free to read, for greatest visibility

COLLABORATIVE PEER-REVIEW
Designed to be rigorous – yet also collaborative, fair and constructive

FAST PUBLICATION
Average 85 days from submission to publication (across all journals)

COPYRIGHT TO AUTHORS
No limit to article distribution and re-use

TRANSPARENT
Editors and reviewers acknowledged by name on published articles

SUPPORT
By our Swiss-based editorial team

IMPACT METRICS
Advanced metrics track your article's impact

GLOBAL SPREAD
5'100'000+ monthly article views and downloads

LOOP RESEARCH NETWORK
Our network increases readership for your article

Frontiers
EPFL Innovation Park, Building I • 1015 Lausanne • Switzerland
Tel +41 21 510 17 00 • Fax +41 21 510 17 01 • info@frontiersin.org
www.frontiersin.org

Find us on